PREPARATIVE PROTEIN PRECIPITATION

STRATEGIES FOR PROCESS DEVELOPMENT, INTEGRATION, AND MONITORING

zur Erlangung des akademischen Grades eines
DOKTORS DER INGENIEURWISSENSCHAFTEN (Dr.-Ing.)

von der KIT-Fakultät für Chemieingenieurwesen und Verfahrenstechnik des
Karlsruher Instituts für Technologie (KIT)
genehmigte

DISSERTATION

von
M.Sc. Steffen Großhans
geboren in Böblingen

Tag der mündlichen Prüfung: 07.10.2019
Referent: Prof. Dr. Jürgen Hubbuch
Korreferent: Prof. Dr.-Ing. Matthias Kind

Danksagung

Während der letzten Jahre haben mich zahlreiche Menschen begleitet, unterstützt und diese Arbeit möglich gemacht, denen ich an dieser Stelle danken möchte.

Zuallererst möchte ich Prof. Jürgen Hubbuch für die Möglichkeit danken, meine Promotion an seinem Lehrstuhl durchzuführen zu können. Vielen Dank für die Beratung und Unterstützung, auch in schwierigen Situationen.

Bei der Europäischen Union bedanke ich mich für die Finanzierung meiner Forschung im Rahmen des Horizon 2020 Projektes. Dem Team des Next Biopharm DSP Projektes danke ich für die gute Zusammenarbeit, die interessanten Treffen und tollen Einsichten in die biopharmazeutische Industrie.

Der gesamten Arbeitsgruppe des MABs danke ich für die tolle Zeit und die großartige Atmosphäre. Eure Anmerkungen und Verbesserungsvorschläge haben mir oft weitergeholfen den richtigen Weg einzuschlagen und die richtigen Entscheidungen zu treffen.

Bei meinen Kollegen und Kooperationspartnern Kai Baumgartner, Juliane Schütz, Gang Wang, Matthias Rüdt, Adrian Sanden, Nina Brestrich, Josefine Morgenstern, Stefan Heissler und Susanna Suhm möchte ich mich für die Zusammenarbeit und die tolle Kooperation bei verschiedenen Projekten bedanken.

Ganz herzlich möchte ich mich bei meinen Studenten Adrian Sanden, Christian Fischer, Roxana Disela, Marius Meier und Konstantin Petry für euren Einsatz, die fleißige Arbeit im Labor und die Unterstützung bei meiner Arbeit zu bedanken.

Pascal Baumann, Frank Hämmerling und Josefine Morgenstern möchte ich für die ausführliche und hilfreiche Beratung und das Korrekturlesen meiner Manuskripte danken.

Bei Sebastian Andris und Philipp Vormittag, ein riesiges Dankeschön für die angenehme und lustige Atmosphäre, sowie die hilfreichen fachlichen und interessanten fachfremden Gespräche im Experimental Office.

Meine Eltern und meine Schwester haben mich in schwierigen Situationen immer unterstützt, aufgebaut, mich in allem bestärkt und immer bedingungslos an mich geglaubt. Dafür

möchte ich mich von Herzen bedanken.

Zuletzt möchte ich mich bei meiner Freundin Susanna bedanken. Vielen Dank für die Unterstützung, die Gespräche, die Motivation und deine unglaubliche Geduld. Du hast es immer geschafft mir meine Selbstzweifel zu nehmen, mich zu beraten und mir klar zu machen, dass sich alles doch lohnt und am Ende alles gut wird.

Success is not final, failure is not
fatal: it is the courage to continue that counts.

Winston Churchill

Zusammenfassung

Diese Dissertation trägt zum Bereich der biopharmazeutischen Prozessentwicklung und Produktion bei. In der Pharmaindustrie gewinnen biopharmazeutische, meist proteinbasierte Medikamente, im Vergleich zu klassischen, niedermolekularen Medikamenten immer mehr an Bedeutung. Durch ihre hohe Spezifität sind proteinbasierte Medikamente in der Lage zielgerichtet an Zellen oder Rezeptoren zu binden und dadurch einen komplexen Wirkmechanismus auszulösen. Dadurch erreichen sie oft eine höhere Wirksamkeit bei gleichzeitiger Reduzierung der Nebenwirkungen. Die komplexe Wirkungsweise eröffnet zudem die Möglichkeit neue Krankheiten und solche, die aktuell noch nicht therapierbar sind, zu behandeln. In den letzten Jahren konnte der Bereich der Krebsimmuntherapie das größte Wachstum im biopharmazeutischen Markt aufweisen. Vor dem Hintergrund einer alternden Gesellschaft wird die Herausforderung Krebs zu bekämpfen stetig weiter wachsen. Darüber hinaus wird auch die Nachfrage nach Behandlungen von Autoimmunerkrankungen, Diabetes oder Alzheimer weiter steigen. Eine Gemeinsamkeit aller biopharmazeutischen Produkte sind die hohen Entwicklungs- und Produktionskosten. Der steigenden Nachfrage nach neuen Produkten und höheren Produktionskapazitäten stehen die immer knapper werdenden Gesundheitsbudgets gegenüber. Durch die Zulassung der ersten Biosimilars, generischen Versionen des Originalpräparats, nimmt der wirtschaftliche Druck auf den biopharmazeutischen Sektor weiter zu. Während für die erste Generation der biopharmazeutischen Blockbuster kaum eine Verbindung zwischen Produktionskosten und Verkaufspreisen bestand, erhöht die Entwicklung von Biosimilars den ökonomischen Druck auf die Produzenten und dadurch auch den Bedarf an einer schnelleren Prozessentwicklung, sowie an wirtschaftlicheren Prozessen.

Die Entwicklung von Biopharmazeutika lässt sich grob in Upstream-Prozessentwicklung (USP), der Produktexpression in lebenden Zellen, und Downstream-Prozessentwicklung (DSP), der Aufreinigung des hergestellten Produktes, unterteilen. In der Vergangenheit wurden bereits große Erfolge bei der Entwicklung einer effizienteren USP erzielt. Insbesondere erhöhte Zellkultur-Titer führten zu höheren Produktkonzentrationen. Um mit diesen USP Entwicklungen Schritt zu halten, werden neue und kostengünstige Alternativen zu den bisherigen Aufreinigungsprozessen benötigt. Heutzutage basiert die DSP von biopharmazeutischen Produkten hauptsächlich auf chromatographischen Auftrennungsschritten. Durch die hohe Selektivität der Chromatographie kann eine hohe Produktreinheit erziehlt werden. Jedoch sind diese Vorteile mit hohen Adsorberkosten und einem langsamen volumetrischen Durchsatz verbunden. Somit verursachen chromatographische

Aufreinigungsschritte die meisten Kosten der DSP. Dennoch basiert die Entwicklung eines Aufreinigungsprozesses großteils auf chromatographischen Schritten, da dafür bereits Plattformprozesse zur Verfügung stehen. Für monoklonale Antikörper (mAb) beispielsweise basiert diese Aufreinigungsplattform auf der Protein A Affinitätschromatographie als Capture Schritt. Dieser Schritt ist für alle mAbs generisch, da die Bindung mit dem Adsorber einer Interaktion mit der Fc-Region zugeschrieben wird, die in allen mAbs vorhanden ist. Folglich sind, in Abhängigkeit der verwendeten mAbs, nur geringfügige Anpassungen des Prozesses erforderlich. Dies macht die Prozessentwicklung einfacher, schneller und effizienter, führt schlussendlich aber auch zu einem Verlust an Flexibilität. Für neue Biopharmazeutika, wie alternative mAbs, virusähnliche Partikel (VLP) oder Nukleinsäuren werden die bestehenden Plattformen nicht geeignet sein. Infolgedessen müssen Alternativen zu den komfortablen, aber teuren Verfahren entwickelt werden. In der Forschung hat die präparative Proteinpräzipitation bereits gezeigt, dass sie eine einfach anwendbare und kostengünstige Alternative sein kann. Neben der salz- oder ethanolinduzierten Präzipitation hat sich Polyethylenglycol (PEG) als wirksames Präzipitationsmittel für die Reinigung von Proteinen bewährt. PEG ist vergleichsweise günstig, nicht brennbar, ungiftig und als Hilfsstoff bereits in vielen Medikamenten zugelassen. Allerdings müssen noch einige Hindernisse überwunden werden, um eine industrielle Anwendung zu ermöglichen.

Um die Akzeptanz der präparativen Proteinpräzipitation in der biopharmazeutischen Industrie zu erhöhen, sind ein tieferes Verständnis des Mechanismus, neue Entwicklungsstrategien und eine verbesserte Prozessüberwachung notwendig. Prozesskenntnis ist sowohl für eine erfolgreiche Prozessentwicklung wie auch für die erfolgreiche Genehmigung durch die zuständigen Behörden von großer Bedeutung. Obwohl auf dem Gebiet der Proteinstabilität viel Forschung betrieben wird, sind die dabei wirkenden Interaktionen nicht vollständig verstanden. Die Kenntnis des Mechanismus kann nicht nur dabei helfen die Proteinpräzipitation zu verstehen, sondern auch die Prozessentwicklung zu verbessern. Heutzutage wird DSP oft expertenbasiert, vor dem Hintergrund eines Plattformprozesses, durchgeführt. Um bestehende Plattformprozesse zu ersetzen, fehlt es an flexiblen, schnellen und materialsparenden Prozessentwicklungsstrategien. Darüber hinaus wird bei der Entwicklung eines Fällungsschrittes dieser Prozessschritt oft eigenständig optimiert, während ein Konzept zur Integration in den gesamten Produktionsprozess, einschließlich USP und der nachfolgenden Aufarbeitungsschritte, fehlt. Zudem wird in einem präparativen Fällungsschritt der Phasenübergang gezielt induziert. Dies führt zu einer Trübung der Lösung, was die Überwachung des Prozesschrittes erschwert, da gängige Transmissionsmessungen nicht durchgeführt werden können. Außerdem müssen der Lösung Fällungsmittel zugesetzt werden, die im folgenden Aufreinigungsschritt unter Überwachung vollständig abgereichert werden müssen. Die Tatsache, dass diese Komponenten oft nicht UV/Vis aktiv sind, macht bestehende Prozessüberwachungsmethoden nicht anwendbar.

Das übergeordnete Ziel dieser Arbeit war es, Probleme aus den Bereichen Prozessentwicklung, Prozessintegration und Prozessüberwachung zu definieren und zu lösen. Die Rolle hydrophober Wechselwirkungen auf den Phasenzustand von Proteinen sollte untersucht werden. Mit den gewonnenen Erkenntnissen über den Präzipitationsmechanismus sollte

eine mathematische Beschreibung gefunden werden, die eine modellbasierte Prozessentwicklung ermöglicht. Für die Prozessentwicklung eines Präzipitationsschrittes komplexer mAb-Lösungen sollte eine Entwicklungsplattform erarbeitet werden. Dabei sollte der Einfluss der vorhergehenden wie nachfolgenden Produktionsschritte berücksichtigt werden. Schließlich sollte eine in-line Überwachungsstrategie entwickelt werden, die in der Lage ist, das Produkt und die Verunreinigungen, einschließlich der zugesetzten Fällungsmittel, zu detektieren.

Im dritten Kapitel dieser Arbeit wurde der Einfluss des hydrophoben Effekts auf das Retentionsverhalten bei der hydrophoben Interaktionschromatographie (HIC), das Kristallisationsverhalten sowie die thermische Stabilität des Modellproteins Glukose-Isomerase untersucht [1]. Zu diesem Zweck wurde eine Hochdurchsatz-Screening-Plattform im Mikrobatchmaßstab eingesetzt, die es ermöglichte, ein Proteinphasendiagramm mit Variation der Salzkonzentration mit gleichzeitiger Änderung des pH-Wertes darzustellen. Das HIC-Retentionsverhalten konnte erfolgreich mit der Kristallgröße und -form von Glukose-Isomerase korreliert werden. Die thermische Stabilität wurde verwendet um Informationen über die Proteinstabilität zu erhalten. Durch eine Kombination aus HIC-Retentionsverhalten und thermischer Stabilität konnte das Phasenverhalten für die verschiedenen untersuchten Salzarten, Salzkonzentrationen und pH-Werte erfolgreich erklärt und vorhergesagt werden. Mit Hilfe von HIC wurde ein tieferes Verständnis des Einflusses hydrophober Wechselwirkungen während der Protein-Protein-Interaktion gewonnen.

Aufbauend darauf wurde in Kapitel vier die Erkenntnisse über den Mechanismus der hydrophoben Wechselwirkungen während des Präzipitationsprozesses genutzt, um ein mechanistisches Modell abzuleiten [2]. Die Grundannahme des neuen Modells basiert auf einer bestehenden Isotherme für HIC. Es wurde angenommen, dass sowohl die Adsorption an einen hydrophoben Liganden als auch die Proteinpräzipitation hauptsächlich durch eine Reduzierung der hydrophoben Bereiche auf der Proteinoberfläche verursacht werden. Weiterhin wurde angenommen, dass die treibende Kraft in diesem Prozess eine Veränderung der Wasserstruktur ist. Folglich wurde Wasser als zusätzliche Komponente in den Präzipitationsprozess eingeführt und ein Gleichgewicht zwischen strukturiertem und weniger geordnetem Wasser angenommen. Mit Hilfe einer Hochdurchsatz-Plattform wurden Präzipitationskurven für Proteine unterschiedlicher Größe, Oberflächenladung oder Hydrophobizität erzeugt. Die Isotherme konnte die Menge an ausgefälltem Protein in Abhängigkeit der Ausgangsprotein- und PEG-Konzentration beschreiben. Über den gesamten Untersuchungsbereich war das Modell in der Lage, die Präzipizationskurve exakt zu beschreiben. Zusammen mit der Fähigkeit, das Präzipitationsverhalten kleiner Proteine zu beschreiben, ist es bestehenden Modellen, wie der weit verbreiteten Cohn-Gleichung, überlegen. Da die Isotherme eine mechanistische Grundlage besitzt, ist es zudem möglich, Daten außerhalb des Kalibrierbereichs zu beschreiben. Dies wurde mithilfe von Validierungsdaten, die nicht für die Modellbildung verwendet wurden, demonstriert.

Während sich die vorhergehenden Studien vor allem mit Reinsystemen beschäftigten, konzentrierten sich die Untersuchungen in Kapitel fünf auf den Einfluss der komplexen Pro-

teinlösungen und des Zellkulturmediums auf das Präzipitationsverhalten von Proteinen [3]. Dafür wurde das Präzipitationsverhalten von zwei verschiedenen mAbs untersucht. In Hochdurchsatz-Experimenten wurden Präzipitationskurven von reinen mAb-Lösungen mit Lösungen verglichen, die vor der Präzipitation mit Verunreinigungen versetzt wurden. In den Lösungen, welche Kontaminanten enthielten, wurde eine Destabilisierung der mAbs und der Kontaminanten beobachtet. Dies führte zu einer theoretischen Reduktion der Reinheit, aber auch zu einer Fällung bei niedrigeren PEG-Konzentrationen. Um anschließend den Einfluss der unterschiedlichen Kontaminanten genauer zu untersuchen, wurden die Verunreinigungen vor Zugabe zu den mAbs umgepuffert. Dabei wurden kleine Moleküle abgereichert während Makromoleküle, wie Wirtszellproteine (HCP) oder DNA, in der Lösung verblieben. Mit diesem Versuchsaufbau konnte die Destabilisierung auf mAb-makromolekulare Wechselwirkungen zurückgeführt werden. Andererseits konnte eine Stabilisierung der mAbs und auch der Verunreinigungen, kleinen Molekülen im Zellkulturmedium zugeordnet werden. Dies führte zu höheren Reinheiten, gleichzeitig war aber eine größere Menge PEG notwendig, um für einen Aufreinigungsschritt akzeptable Ausbeuten zu erzielen. Diese Ergebnisse zeigten, wie wichtig es ist, den Bedarf der Prozessentwicklung des nachgelagerten Fällungsschrittes bereits während der USP zu berücksichtigen.

In Kapitel sechs wurde eine Prozessentwicklungsstrategie und die entsprechende Entwicklungsplattform für einen integrierten Präzipitations- und Ionenaustauschschritt (IEX) entwickelt [4]. Durch selektive Präzipitation und selektive Rücklösung wurden prozessbedingte Verunreinigungen wie HCP und DNA reduziert. Der nachfolgende Kationenaustauschchromatographie Schritt (CEX) wurde angewendet, um produktbezogene Verunreinigungen, beispielsweise mAb-Aggregate, abzureichern. Darüber hinaus wurde CEX als Produktkonzentrationsschritt eingesetzt. Durch die Kombination aus Hochdurchsatz-Prozessentwicklung, empirischer und mechanistischer Modellierung wurde eine schnelle, flexible und materialsparende Entwicklungsplattform entwickelt. In einer Fallstudie wurde ein Verfahren zur Aufreinigung eines komplexen mAb-Ausgangsmaterials entwickelt. Es wurde gezeigt, dass der entwickelte Prozess eine geeignete Alternative zur konventionellen Protein A Affinitätschromatographie darstellt. Mit der vorgestellten Prozessentwicklungsstrategie ist es möglich, einen traditionellen Batch-Prozess zu entwickeln. Darüber hinaus wurde das kalibrierte mechanistische Chromatographie-Modell für eine *in silico* Optimierung einer periodischen Gegenstromchromatographie (PCCC) verwendet. Dadurch wurde die Machbarkeit der Entwicklung eines kontinuierlichen Prozesses mit Hilfe der entwickelten Plattform gezeigt.

Während sich die bisherigen Kapitel mit dem Prozessverständnis und neuen Entwicklungsstrategien beschäftigten, war der letzte Teil der Arbeit neuen Kontrollstrategien, zur Erfüllung der Anforderungen an einen auf Proteinfällung basierenden Prozess, gewidmet. Im siebten Kapitel wurde die Fourier-Transformations-Infrarot-Spektroskopie (FTIR) als in-line prozessanalytische Technologie (PAT) zur Überwachung chromatographischer Prozesse implementiert [5]. In drei Fallstudien wurde das Potenzial der FTIR-Spektroskopie demonstriert. Die erste Fallstudie zeigte die Möglichkeit, zwei verschiedene Proteine durch Unterschiede in ihrer Sekundärstruktur zu differenzieren. Mit Hilfe eines Regressionsmo-

dells der partiellen kleinsten Quadraten (PLS) war es möglich, während der CEX-Elution zwischen mAb und Lysozym zu unterscheiden. In einer zweiten Fallstudie wurde ein Prozess, der unterschiedlich PEGylierte Lysozymspezies mittels CEX auftrennt, mit Hilfe der FTIR-Spektroskopie überwacht. Dies belegt die Möglichkeit, nicht UV/Vis aktive Moleküle wie PEG nachzuweisen. Im Rahmen eines PEG-induzierten Präzipitationsprozesses ist dies von großer Bedeutung, da PEG dem Prozess hinzugefügt wird und eine spätere Abreicherung gewährleistet sein muss. In der letzten Fallstudie wurden die typischen prozessbedingten Verunreinigungen und die ebenfalls nicht UV/Vis aktive Komponente Triton X-100 selektiv aus dem FTIR 3D-Feld quantifiziert.

Zusammenfassend liefert diese Arbeit Lösungen für die Entwicklung von neuen, flexibleren und kostengünstigeren Alternativen zu häufig verwendeten chromatographischen Methoden. Der Schwerpunkt lag auf der Etablierung von Präzipitationsprozessen im Hinblick auf die aktuellen Bedürfnisse der DSP. Durch die Untersuchung hydrophober Wechselwirkungen wurden neue Erkenntnisse über den Präzipitationsschritt gewonnen. Mit Hilfe dieser konnte ein mechanistisches Präzipitationsmodell entwickelt werden. Dies zeigte die Möglichkeit, die Prozessentwicklung zu vereinfachen und gleichzeitig den Materialverbrauch zu senken. Die generierte Prozessentwicklungsplattform ermöglicht eine einfache Prozessentwicklung in Bezug auf die vorhergehenden und nachfolgenden Prozessschritte. Der entwickelte Prozess zeigte vergleichbare Ergebnisse in Bezug auf Ausbeute, Reinheit und Aggregatreduktion im Vergleich zum Industriestandard Protein A Affinitätschromatographie. Mit der Entwicklung eines in-line-Sensors auf Basis von FTIR-Spektroskopie wurden Strategien entwickelt um sowohl das Produkt, als auch Additive wie PEG in den nachfolgenden Reinigungsschritten zu überwachen. Diese ermöglichen die Kontrolle der erfolgreichen Abreicherung.

Abstract

This PhD thesis contributes to the field of biopharmaceutical process development and production. In the pharmaceutical industry biopharmaceuticals, mostly protein-based drugs, are gaining more and more importance compared to classical, small molecule drugs. They often bind more specifically to the target or receptor. At the same time they trigger a complex mode of action. This often leads to higher efficacy, while at the same time side effects are reduced. The complex mode of action also opens up the possibility of treating new diseases or those for which there is currently no therapy available. In the past, the biggest growth in the biopharmaceutical market has taken place in the field of cancer immunotherapy. Against the background of an aging society, the challenge of fighting cancer will continue to grow. In addition, the demand for therapies for the treatment of autoimmune diseases, diabetes, and Alzheimer's disease will continue to rise as well. All biopharmaceutical products have high development and production costs in common. The increasing demand for new products and higher production capacities stands in contrast to the ever scarcer healthcare budgets. With the approval of the first biosimilars, generic versions of the originator drug, the economic pressure on the biopharmaceutical sector increases further. While for the first generation of biopharmaceutical blockbusters was hardly a link between production costs and sales prices, the development of biosimilars also increases the need for faster process development and more economical processes.

The development of biopharmaceuticals can be roughly divided into the expression of the product in living cells, the upstream process development (USP) and the purification of the produced molecule, the downstream process development (DSP). In the past, great success has been achieved in the development of a more efficient USP. In particular, higher cell culture titers led to higher product concentrations. In order to keep pace with these developments, new, and cost-effective alternatives for the purification process are needed. Today, the DSP of biopharmaceutical products is mainly based on chromatographic purification steps. These have a high selectivity, which leads to a high purity after the unit operation. Unfortunately, these advantages are associated with the disadvantage of high resin costs, and a slow volumetric throughput. Consequently, chromatographic steps contribute most to the cost of DSP. However, the development of a purification process is mostly based on chromatographic steps, as platform processes are available. For monoclonal antibodies (mAb) this purification platform is based on Protein A affinity chromatography as a capture step. This step is generic for all mAbs since the binding to the adsorber is attributed to an interaction with the Fc-region present in all mAbs.

Therefore, depending on the used mAb, only minor adjustments to the process are required. This makes process development easier, faster, and more efficient. Consequently, this also leads to a loss of flexibility. New biopharmaceuticals, such as alternative mAbs, virus-like particles (VLP), or nucleic acids will not fit into existing platforms. As a result, alternatives to the convenient but expensive methods have to be developed. In academia, preparative protein precipitation has already shown that it can be an easy-to-use and cost-effective alternative. In addition to salt-, or ethanol-induced precipitation, polyethylene glycol (PEG) has proven its suitability as effective precipitating agent for the purification of proteins. PEG is comparatively cheap, non-flammable, non-toxic, and already approved as an excipient in many drugs. However, several obstacles still have to be overcome in order to make industrial application possible.

In order to increase the acceptance of preparative protein precipitation in the biopharmaceutical industry, deeper knowledge of the mechanism, new development strategies and an improved monitoring of the process are necessary. Knowledge of the process is of great importance for a successful process development, and also for a successful approval by the relevant authorities. Although much research has been done in the field of protein stability, the involved interactions are not fully understood. Knowledge of the mechanism can not only help to understand protein precipitation, but also to improve process development. Today, DSP is often performed expert based, with the background of a platform process. To replace existing platform processes, flexible, fast, and material-saving process development strategies for preparative protein precipitation are missing. Furthermore, when developing a precipitation step, the purification step is often optimized as a stand-alone operation, while a concept for integrating the unit operation into the overall production process, including USP, and other polishing steps, is missing. In a preparative precipitation step, the phase transition is intentionally induced. This leads to a turbidity in the solution that makes the process step difficult to monitor. In addition, precipitants are added to the solution to cause this phase transition. In the following purification step, the complete degradation of these components must be ensured and monitored. The fact that these components are often not UV/Vis active makes common techniques inapplicable.

The overall aim of this work was to define and solve problems in the area of process development, process integration, and process monitoring. The role of hydrophobic interactions on the phase state of proteins should be investigated. With the knowledge gained about the precipitation mechanism, a mathematical description that enables model-based process development should be found. For the process development of a precipitation step for complex mAb solutions, a development platform should be generated. The influence of the previous and subsequent production steps should be taken into account. Finally, an in-line monitoring strategy should be developed that is capable of detecting the product and impurities, including the added precipitants.

In the third chapter the influence of the hydrophobic effect on the retention behavior during hydrophobic interaction chromatography (HIC), the crystallization behavior, and the thermal stability of the model protein glucose isomerase were investigated [1]. For this

purpose, a high-throughput screening platform in microbatch scale was used, which made it possible to produce a protein phase diagram with variation of the salt concentration and simultaneous change of the pH value. The HIC retention behavior could successfully be correlated to the crystal size and shape of glucose isomerase. The thermal stability was used to obtain information on the protein stability. Using a combination of HIC retention behavior and thermal stability, it was possible to successfully explain and estimate the phase behavior for glucose isomerase for the different investigated salt types, salt concentrations, and pH values. With the help of HIC, a deeper understanding of the influence of hydropbobic interactions during protein-protein interaction was obtained.

Based on these findings, in chapter four the mechanism of hydrophobic interaction during the precipitation process was used to derive a mechanistic model for preparative protein precipiation [2]. The new model is based on an existing isotherm for HIC. It was assumed that both, adsorption to a hydrophobic ligand, and protein precipitation are mainly caused by a reduction of the hydrophobic area on the protein surface. Furthermore, it was assumed that this was due to a change in the water structure. Consequently, water was introduced as an additional component into the precipitation process, and an equilibrium between well-ordered and bulk-like ordered water was assumed. A high-throughput platform was used to generate precipitation curves for proteins of different size, surface charge, or hydrophobicity. The isotherm could describe the amount of precipitated protein as a function of the initial protein and PEG concentrations. The model was able to accurately describe the precipitation curve over the entire investigated range. Together with the ability to describe the precipitation behavior of small proteins, it is superior to existing models, such as the widely used Cohn-equation. Since the isotherm has a mechanistic foundation it is also possible to describe data beyond the calibration range. This was demonstrated with validation data that were not included into the model building.

While the previous studies mainly dealt with with pure proteins solutions, the investigations presented in chapter five concentrated on the influence of complex protein solutions and the cell culture medium on the precipitation behavior of proteins [3]. Therefore, the precipitation behavior of two different mAbs was investigated. Using high-throughput experiments, precipitation curves of pure mAb solutions were compared to solutions, which were spiked with impurities prior to precipitation. In solutions containing contaminants, a destabilization of mAbs and the impurities was observed. This led to a reduction of the purity, but at the same time to an increase of the yield, respectively precipitation at lower PEG concentrations. In order to investigate the influence of the different components present in the complex solution, the contaminant solution was re-buffered before spiking. Thereby, small molecules were depleted while macromolecules, such as host cell proteins (HCP), or DNA, were still present. Using this experimental setup, destabilization could be attributed to mAb-macromolecular interactions. On the other hand, a stabilization of the mAbs, and also of the impurities, could be assigned to small molecules, present in the cell culture medium. This led to higher purities, but at the same time more PEG was necessary to achieve acceptable yields. The results showed how important it is to consider the process development needs of the downstream precipitation step already during the

USP.

In chapter six, a process development strategy, and the corresponding development platform for an integrated precipitation and ion exchange (IEX) step was developed [4]. By means of selective precipitation and selective resolubilisation, process-related impurities such as HCP and DNA were reduced. The subsequent cation exchange chromatography (CEX) step was used to remove product-related impurities such as mAb aggregates. In addition, CEX was used as product concentration step. By combining high-throughput process development, empirical, and mechanistic modeling, a fast, flexible, and material-saving development platform was designed. In a case study, a process for the purification of a complex mAb feedstock was developed. It was shown that the developed process is a suitable alternative to conventional Protein A affinity chromatography. With the presented process development strategy it is possible to develop a traditional batch process. In addition, the calibrated mechanistic chromatography model was used for *in silico* optimization of periodic counter-current chromatography (PCCC). Thus, the feasibility of developing a continuous process, using the developed platform, was demonstrated.

While the previous chapters dealt with process understanding, and new development strategies, the last part of the work was dedicated to new monitoring strategies to meet the requirements of a protein precipitation based process. In chapter seven, Fourier-transform infrared (FTIR) spectroscopy was implemented as in-line process analytical technology (PAT) for monitoring chromatographic processes [5]. The potential of FTIR spectroscopy was demonstrated in three case studies. The first showed the possibility to distinguish two different proteins by differences in their secondary structure. Using a partial least squares (PLS) regression model, it was possible to distinguish between mAb and lysozyme during CEX elution. In a second case study, a process that separates different types of PEGylated lysozyme with CEX was monitored by FTIR spectroscopy. This also showed the possibility to detect the non UV/Vis active molecule PEG. In the context of a PEG-induced precipitation process this is of great interest, as PEG is added to the process and therefore a later depletion must be guaranteed and monitored. In the last case study, the typical process-related impurities and also the non UV/Vis active component Triton X-100 were selectively quantified from the FTIR 3D field.

In summary, this dissertation provides solutions for the development of new, flexible, and cost-effective alternatives to frequently used chromatographic based methods. The focus was set on the establishment of precipitation processes with respect to the current needs of DSP. By the investigation of the role of hydrophobic interactions, new insights into the precipitation step were gained. With the help of this, a mechanistic precipitation model could be developed. This showed the possibility to simplify the process development and to reduce material consumption at the same time. The generated process development platform enables a simple process development with regard to the previous and subsequent process steps. The developed process showed comparable results in yield, purity and aggregate reduction compared to the industrial standard, Protein A affinity chromatography. With the development of an in-line sensor based on FTIR spectroscopy strategies were developed

to monitor both the product and additives such as PEG, in the subsequent purification steps.

Contents

1. Introduction

Biotechnology is defined as application of natural or engineered biological organisms for the use of technical and industrial processes [6]. One of the most important achievements was the decoding of deoxyribonucleic acid (DNA) by Watson and Crick in 1953 [7]. These findings enabled the development and application of recombinant DNA technology. Thereby, targeted manipulation of DNA allows the inserting of specific genes to the cell, and thus, using the cell as biochemical factory for the production of proteins [8].

With the availability of recombinant proteins, the number of biopharmaceuticals increased. The term biopharmaceutical refers to pharmaceutical products manufactured by microbiological methods [9]. This definition includes products expressed in living cells, but can also be applied to the entire living cell as a product, or small molecules produced or modified by biological systems. Small molecules are defined as drugs with a molecular weight of less than 500 Da, which have usually an oral bioavailability. In contrast, biopharmaceuticals are typically larger than 5000 Da, and have to be administered by injection. Among therapeutic proteins, insulin was the first recombinant drug to be approved in 1982 [10]. The first monoclonal antibody (mAb) product was launched in 1986. Since that time, mAbs have become the most important drug class on the market. In 2016, approximately 65.6 % of therapeutic protein sales, were achieved with mAbs [11]. Other approved protein-based drugs are anticoagulants, blood factors, bone morphogenetic proteins, artificial protein scaffolds, enzymes, growth factors, hormones, interferons, interleukins, and thrombolytics [12].

Biopharmaceuticals have the advantage to bind specifically to a cell or a receptor. This makes it possible to address a more complex mode of action, compared to small molecule drugs, leading to a higher efficacy of the biopharmaceutical drug. At the same time often fewer side effects occur. However, the complex mode of action is usually prone to changes of the molecule. Small variations can lead to a loss of efficacy, or even raise the immunogenicity of the drug [13]. This can be a serious problem since biopharmaceuticals usually tend to be unstable. Changes in temperature, ionic strength, pH value of the surrounding medium, or concentration of the various molecules involved, may result in changes, or loss of the product [11]. In addition, the expression of the product in living cells leads to a high number of impurities. Furthermore, the complexity of the product leads to several versions of the same protein with only minor variations. Consequently, the product is never a single molecule, but always a defined profile of several ones. The task of downstream process development (DSP) is to ensure a high product purity, to meet the

predefined composition of the different protein variants, and to reach an acceptable yield to ensure an economic process[10].

The complexity of the products and the associated demands on the processes lead to high development and production costs. However, in the past, there was hardly any direct correlation between manufacturing costs and selling prices [14]. Starting in 2010, several biopharmaceutical blockbusters will lose their patent protection in subsequent years. The phenomenon, known as "patent cliff", has the potential to change the market and increase economic pressure on the biopharmaceutical industry [15]. One result of the expiration of many patents is the development of biosimilars. Biosimilars are generic versions of the originator drug, based on the same DNA sequence [16]. As there is no need to search for the lead candidate development times, risks, and costs are reduced. The new competition will also increase the need for new, and more economical downstream processes. In contrast to the simple copying of an already developed drug, the development of biobetters is another trend in the biopharmaceutical industry. Biobetters are modifications of existing drugs, which have superior properties in drug delivery, pharmacokinetics, or pharmacodynamics [17]. Examples for this are PEGylated proteins, recombinant fusion proteins, antibody drug conjugates (ADC), or engineered mAbs [18]. A higher efficacy of biobetters may result in a lower amount of required drug, and consequently a lower production capacity. Beside mAbs, or mAb-like products, vaccines, gene therapies, and personalized medicine have a growing impact on the biopharmaceutical market [19]. For all these products, traditional downstream platform processes are either not efficient or not applicable at all.

Traditional downstream processes are usually based on a sequence of several chromatographic steps. With these, high resolutions can be achieved, but this is associated with high adsorber costs, and a slow volumetric throughput. In order to meet the requirements for more economical, and flexible downstream processes, alternative purification steps, operating modes, and new integrated process development strategies are necessary [20]. Alternative downstream methods such as preparative protein precipitation, preparative protein crystallization, aqueous two-phase systems (ATPS), or membrane technology have the potential to overcome these limitations [21–24]. During crystallization and precipitation, a phase transition of the protein from the liquid to the solid phase is used to purify the target protein. The difference between crystallization and precipitation refers to the morphology of the product. Precipitates often have a poorly defined amorphous structure, whereas crystals are well-defined large particles formed in a secondary nucleation process [25]. In particular, the successful applicability of preparative protein precipitation as capture step has already been demonstrated [26, 27]. However, purities achieved after chromatographic polishing steps are hardly achievable with alternative methods. Hence, meaningful process integration is necessary. To develop such processes, the combination of high-throughput screening (HTS), Design of Experiment (DoE), and model-based approaches have shown the potential to save development time, cost, and material [28–31]. These methods can also help to transfer the production process from traditional batch production to a continuous mode. Continuous production has shown the potential to shorten process times, lead

to higher productivity, and lower costs for equipment, and consumables. Thereby, new continuous applications have been developed for classical chromatographic steps, but also for alternative separation methods [32]. In order to monitor such continuous processes, and to ensure product quality and safety, academia and industry have focused on the development of process analytical technologies (PAT). The implementation of multivariate data analysis (MVDA) in combination with new in-line sensors can help to control processes, and thus make them more efficient [33, 34].

In order to give an overview of the current state of research, the following chapters deal with theoretical fundamentals which are necessary for this thesis. Chapter 1.1 introduces the most relevant intermolecular forces for the understanding of protein phase behavior and stability. Chapter 1.2 deals with the factors that affect the protein phase behavior, while chapter 1.3 discusses the basics of downstream process development of biopharmaceuticals. Chapter 1.4 describes the principles of in-line process monitoring and FTIR spectroscopy.

1.1. Intermolecular Protein Interactions

In downstream process development, various differences of the physical properties between the product and the impurities are used to purify the target protein. To understand the mechanism of the protein phase behavior, as well as adsorption phenomena, the acting forces between the proteins and their environment need to be understood. At a molecular level, the interactions of proteins with surfaces, adsorber ligands, other proteins, or solvents are mainly influenced by weak, non-covalent forces. Therefore, the most important intermolecular forces and their properties are listed below.

1.1.1. Van-der-Waals Forces

Van-der-Waals (VdW) forces are short-range intermolecular interactions with a weak binding energy of 0.08 to 42.00 kJ/mol [35]. In general, VdW forces act between all molecules. In particular, they contribute to the interaction of proteins with other molecules and with surfaces [36]. The attracting influence results from interactions between fixed or induced dipoles. These dipoles are caused by short-term electrostatic polarization of the molecules [37] . The electrostatic potential Ψ and the resulting force F are related to the distance between two particles z according to Eq. 1.1.

$$\Psi \approx \frac{1}{z^6} \quad F = \frac{-\partial \Psi}{\partial z} \tag{1.1}$$

1.1.2. Electrostatic Interactions

As described above, VdW forces have an electrostatic character resulting from dipole moments. In addition, most molecules found in biotechnological systems, such as salts, nucleic acids, or proteins, carry discrete surface charges. Even in pure water one finds the charged ions OH^- and H^+. During the separation of biomolecules, charged ligands bound to chromatographic resins are used to separate, and purify biomolecules [38].

The attractive or repulsive character of stationary charges is defined by Coulomb's law (Eq. 1.2). The force F is defined by the signed magnitudes of the charges q_p1, and q_p2, the distance between the charges z, and the Coulomb constant k_e. An attracting force results when the charges have an opposite sign and a repulsive force when they are like-signed [35].

$$F = k_e \frac{(q_p 1 q_p 2)}{z^2} \tag{1.2}$$

If proteins are considered as point charges q_p, and they are not disturbed by other charges, the electrostatic potential Ψ_p^{id}, follows Eq. 1.3, depending on the distance between two charges z, and the permittivity of the medium ε.

$$\Psi_p^{id}(z) = \frac{q_p}{4\pi\varepsilon z} \tag{1.3}$$

The electrostatic potential decreases slowly with the distance, correlating with z^{-1}. Therefore fixed charges are classified as long-range forces. In contrast, VdW forces are classified as short-range forces. As described in chap. 1.1.1., the strength of VdW forces correlates to the distance with z^{-6} [38]. The combination of the long-range repulsive electrostatic double layer, and attractive short-range VdW forces is explained in the DLVO theory, named after their founders Derjaguin, Landau, Verwey, and Overbeek [39]. According to the DLVO theory the attractive VdW forces are superimposed by the repulsive electrostatic double layer, resulting in attraction on very short distances and a repulsion on longer distances. Unfortunately, the DLVO theory is an oversimplification for proteins. For example, hydrophobic effects of Hofmeister ions, or hydration forces are not considered [40].

1.1.3. Hydrogen Bonds

Similar to VdW forces, hydrogen bonds are induced by dipoles. Hydrogen bonds are formed when a hydrogen atom, bound to an electronegative atom, especially oxygen, nitrogen, and fluorine, interacts with an neighboring electronegative atom (Fig. 1.1.). Hydrogen

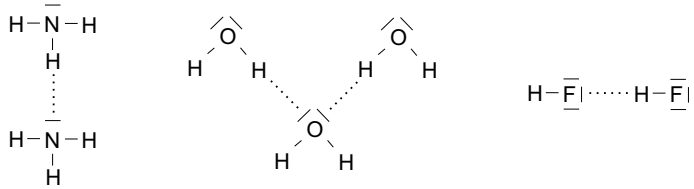

Figure 1.1.: Hydrogen bonds between the molecules NH_3, H_2O and HF. Illustration adapted from [41].

bonds are much stronger compared to VdW forces, but have only about 5-10 % of the bond energy of covalent bonds [41]. Theoretically, a water molecule can form up to four hydrogen bonds. Usually, a water molecule in liquid water is part of one to three bonds, in frozen water of three to four bonds. Since most protein chemistry takes place in aqueous solutions, the formation of hydrogen bonds plays an important role in the solution process of proteins. Thereby, the interaction of charged groups of the protein with the water via hydrogen bonds enables solvation. The interaction of water molecules with each other via hydrogen bonds is the source of hydrophobic interaction. The adsorption process towards a hydrophobic ligand, or a hydrophobic surface, is driven by changes in the water structure. The same effect explains the aggregation of proteins via hydrophobic patches on the protein surface. The hydrophobic effect is described in more detail in the following chapter.

1.1.4. Hydrophobic Interactions

Originally, the hydrophobic effect describes the low solubility of nonpolar solvents in water [42]. It was extended to also explain the poor water solubility of hydrophobic molecules or the repulsion of hydrophobic surfaces by the solvent water. Thereby, hydrophobic interaction is not a real force, but is fundamentally caused by the formation of hydrogen bonds between water molecules [43]. An important example of the effect of hydrophobic interactions is the formation of high-order biological structures, such as the formation of membranes, or the spontaneous folding of proteins [44]. Solvation behavior and aggregation tendency of proteins can be explained by changes in the Gibbs' free energy G (Eq. 1.4). Systems always show a tendency to minimize free Gibbs energy. The two terms ΔH and ΔS describe the enthalpic and entropic changes that occur during solvation or aggregation [45].

$$\Delta G = \Delta H - T\Delta S \tag{1.4}$$

During an aggregation process of proteins, changes of the intermolecular interaction, like the formation or solving of bonds, can lead to an increase or a decrease of the enthalpy H. This term alone would not successfully explain the formation of high-ordered structures. However, the consideration of water molecules provides an explanation for the spontaneous formation of complex structures, or the aggregation of proteins. Hydrophobic surface groups can hardly be solvated, as they cannot form hydrogen bonds with the solvent water. Therefore, the water molecules can only interact, respectively, form hydrogen bonds with each other. This leads to a higher-ordered water structure around hydrophobic surfaces. When two hydrophobic surfaces merge, this leads to a rearrangement of the water molecules. The change of the water structure, from a higher order to a bulk-like water structure, leads to an increase of the entropy S, and therefore, an overall decrease of Gibbs free energy. Following changes in the entropy have to be the driving force for the hydrophobic effect [45, 46].

1.2. Influencing Factors on Protein Phase Behavior

To understand the precipitation process, the nature of the proteins, the forces acting at the molecular level, and the precipitation mechanism have to be considered. Protein solubility can be influenced by intrinsic factors, such as protein structure (1.2.1), and extrinsic factors, such as pH value (1.2.2), ionic strength, or other added components. In this thesis the influence of inorganic salts as precipitant (chapter 3), respectively as contaminant (chapter 5) are investigated. Hence, chapter 1.2.3 introduces the fundamentals of salt induced precipitation. The developed monoclonal antibody (mAb) capture step (chapter 6) is based on polymer induced precipitation. The fundamentals are explained in chapter 1.2.4. A methodology for displaying protein phase behavior in the form of protein phase diagrams is presented in Chapter 1.2.5.

1.2.1. Protein Structure

Proteins are well-ordered bio-polymers, consisting of amino acids as subunits. Linked by peptide bonds, the amino acid sequence forms the primary structure. In particular, the different residues of the amino acids used define the protein character. They influence both the formation of structural elements of the secondary structure and the folding into the defined three-dimensional tertiary structure [47].

The residues of amino acids can be divided into three groups: charged; uncharged and hydrophilic; and hydrophobic. These different properties not only influence protein folding, but also define protein surface properties. They influence charge distribution, and the formation of hydrophilic, or hydrophobic patches on the protein surface. Therefore, they also have a strong influence on protein solubility. In addition to the amino acid sequence, posttranslational modifications influence the protein character, and solubility. Especially proteins produced in eukaryotic cells are subject to these changes, such as proteolytic cleavages, formation of disulfide bonds, or glycosylation [48]. Together they are referred to as intrinsic factors of protein stability.

Extrinsic factors can also influence the surface character of proteins. During a biopharmaceutical process in general, and during a preparative precipitation step in particular, extrinsic factors are altered, and a phase transition is induced [49]. In the following, the most important extrinsic factors for native protein precipitation or crystallization are listed.

1.2.2. Influence of Solution pH

For the surface net charge of biomolecules such as proteins, or DNA, the pH value of the solvent plays a significant role. Thereby, the surface net charge of the proteins is defined by the charge of the amino acid residues, or more precisely, by the pKa of the corresponding acid or base. At low pH values, the acids and bases are neutral, respectively positively charged. With increasing pH value the residues are deprotonated and the total surface net charge of the biomolecules becomes negative. Fig. 1.2. (a) gives a schematic overview of the surface net charge of DNA, host cell proteins (HCP), and a monoclonal antibody (mAb). For DNA, an isoelectric point (pI) around pH 2.0-3.0 is reported. Proteins have a wide range of pIs from pH 3.5 to pH 11.0 [50]. For example, it is reported that the majority of HCPs have an pI around the pH 5.0, while the mAb used in this paper has an pI of pH 8.5 [51, 52].

Long-range electrostatic forces between equal charged particles are reported to stabilize molecules, by preventing attraction [53]. Therefore, proteins have the lowest solubility at their pI, where the total surface net charge is neutral [54]. The influence of surface net charge on the solubility of biomolecules is shown in Fig. 1.2. (b). The stabilization

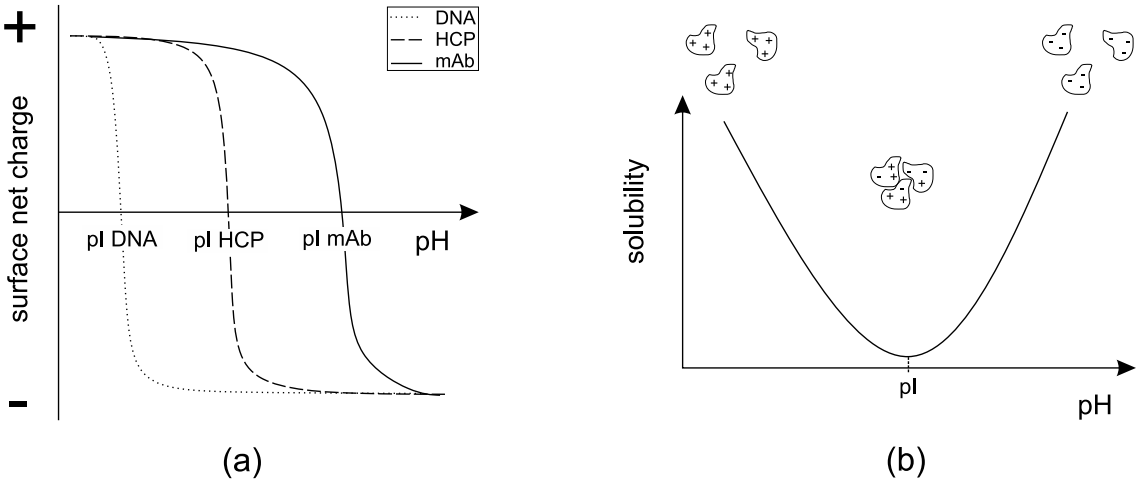

Figure 1.2.: (a) Influence of pH value on the surface net charge of DNA, HCP and mAb. (b) Influence of the surface net charge on the solubility of biomolecules.

of molecules due to electrostatic repulsion occurs mainly at low salt concentrations. At higher salt concentrations the electrostatic double layer is completely shielded and specific salt effects become important.

1.2.3. Influence of Inorganic Salts on Protein Phase Behavior

As unit operation in biotechnological downstream processes, precipitation, or crystallization of proteins is intentionally caused. In order to avoid harming the protein, it is important that native protein phase transition takes place. Native precipitation means that the protein does not unfold before, during or after the precipitation process and thus retains its tertiary structure. The use of inorganic salts, as precipitants, is one of the oldest ways to purify proteins [55]. In 1931 Green reported on an approach of selective salt-induced precipitation of hemoglobin from a complex solution [56]. For a long time it has been assumed, that during precipitation phase separation between a liquid, salt saturated phase, and a solid protein phase takes place. More recent studies describe protein precipitation as separation between two liquid phases with different protein concentrations [57]. Shih *et al.* investigated the composition of these two phases and found, that the dense protein phase still contains a considerable amount of water and salts [58]. They also showed that for certain proteins, the initial protein concentration has an influence on the amount of soluble protein in equilibrium after the precipitation.

The influence of salts on the phase behavior of proteins is complex. By dissolving salts, they dissociate into their charged ions, and thus, influence the electrostatic interactions between the proteins. Irrespective of the type of ion, shielding of the equally charged groups on the protein surface can lead to precipitation, or crystallization. The absence of

long-range repulsive electrostatic interactions can lead to protein-protein attraction, which is caused by short-range interactions, such as VdW forces, or hydrophobic interactions.

In addition to the influence of salts on electrostatic interactions, specific ion effects are known as well. At low salt concentrations, a stabilizing "salting-in" effect is reported. Tanford explained this observation with unspecific interactions depending on the ionic strength of the medium [59]. In a series of articles, Timasheff and coworkers explained this behavior in more detail with the preferential interaction theory [60–63]. According to this theory, a preferential interaction of the ions with the protein leads to a stabilization of the protein. In contrast, preferential hydration of the water, and thus, preferential exclusion of the protein, has a destabilizing "salting-out" effect. Specific ion effects were first mentioned by Franz Hofmeister in 1888 [64]. Accordingly, the influence of anions on the precipitation, and crystallization behavior of proteins is more pronounced than that of cations. The empirically ordered anions, which are related to their ability to precipitate proteins, are shown in Fig. 1.3.. Anions on the left side of Cl^- are called kosmotropes, and are known

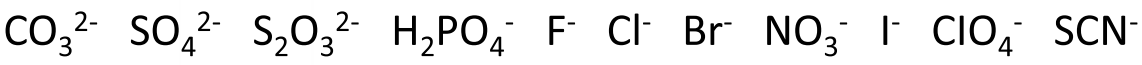

Figure 1.3.: Empirical order of anions ranked after their ability of precipitating proteins.

to strengthen hydrophobic interactions. This can lead to protein aggregation, but can also stabilize the tertiary structure of proteins, by strengthening their hydrophobic core. Anions on the right side of Cl^- are called chaotropes. They weaken hydrophobic interactions, which can prevent proteins from aggregation, but can also lead to protein unfolding. The effect of the Hofmeister series has been extensively investigated, but the nature of these effects is not completely understood. Originally, it was assumed, that the ions affect the water structure both, in the bulk, and around the hydrophobic patches of the protein [65]. Omta and coworkers found out, that only the first hydration shell of the protein and not the bulk water is affected by the ions [66]. Zhang and Cremer postulated, that the specific ion effects can be explained by direct interactions between ions, and the protein [67].

1.2.4. Influence of Polymers on the Protein Phase Behavior

Polymer-induced precipitation shows similar effects compared to salt-induced precipitation, but it is of different nature. The influence on the protein phase behavior of polymer-induced precipitation in general, and polyethylene glycol (PEG) induced precipitation in particular, can be explained by two different theories. According to the theory of excluded volume, introduced by Atha and Ingham, the reduction of protein solubility, in the presence of PEG, can be explained by steric exclusion of the proteins from the surrounding media [68, 69]. According to Arakawa and Timasheff [70] polymers, like PEG, preferentially interact with water molecules and are excluded from the surface of the protein. Hence, it is assumed, that

the polymers trap the solvent and sterically exclude it from the solved proteins. Since this is a steric effect, proteins with a larger hydrodynamic radius tend to precipitate at lower PEG concentrations, compared to proteins with a smaller hydrodynamic radius. A schematic representation of the volume exclusion effect is shown in Fig. 1.4. The theory of attractive

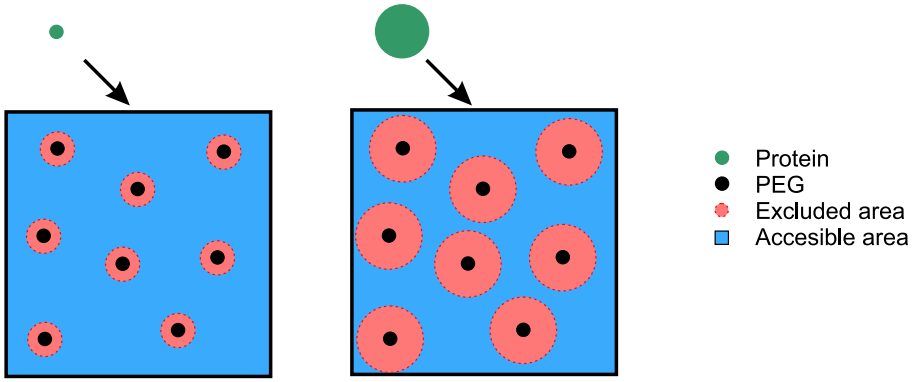

Figure 1.4.: Schematic representation of the accessible and excluded area of a PEG solution for proteins with different sizes, described by the theory of volume exclusion.

depletion introduced osmotic pressure as additional force to the PEG-induced precipitation process [71, 72]. According to this theory, each dissolved protein has a depletion zone, which can not be entered by PEG molecules. If the PEG, or protein concentration is raising, and two depletion zones are overlapping, a PEG free area is created, and a gradient towards the bulk is formed. This gradient leads to an attractive force of the order of osmotic pressure. A schematic representation is shown in Fig. 1.5.. In both theories no

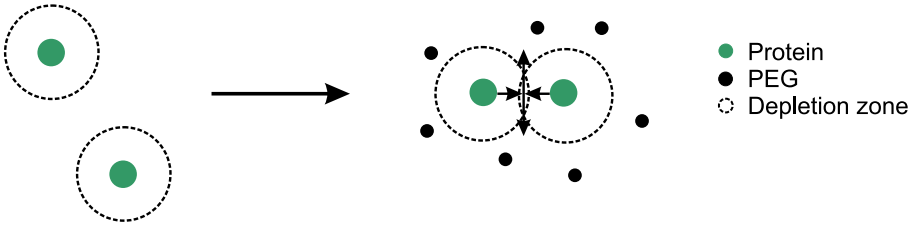

Figure 1.5.: Schematic representation of two proteins in PEG solution and the influence on the depletion zones, described by the theory of attractive depletion.

direct interaction between the proteins and the polymers is assumed. Consequently, all other forces between the particles, described in the previous chapters, are still valid, and must be taken into account.

1.2.5. Protein Phase Diagrams

A protein phase diagram displays the phase state of a protein as a function of the environmental conditions. The most common method, in the biopharmaceutical industry, is to plot variations in protein concentration as a function of another parameter, e.g. precipitant concentration, while keeping all other variables constant [73].

As shown in Fig. 1.6., a schematic protein phase diagram is displayed as a function of the precipitant and protein concentration. At low precipitant and protein concentrations the protein is completely dissolved. In the area called the undersaturated zone the repulsion forces between the proteins dominate and no phase transition occurs [74]. Once the solubility line is exceeded phase transition takes place. Depending on the underlying mechanism, crystallization, gelation, precipitation, or liquid liquid phase separation can occur [75]. In the metastable region of the phase diagram no spontaneous phase transition in form of crystallization takes place, but crystals can grow if a nucleus is present. In the region of moderate supersaturation spontaneous nucleation can occur, which can lead to protein crystallization. In the area of high supersaturation, attraction forces between the proteins are predominant, and the proteins precipitate. In contrast to amorphous precipitate, crystals have an ordered structure that depends on specific interactions between the proteins [76]. To create a protein phase diagram, a large number of data points are

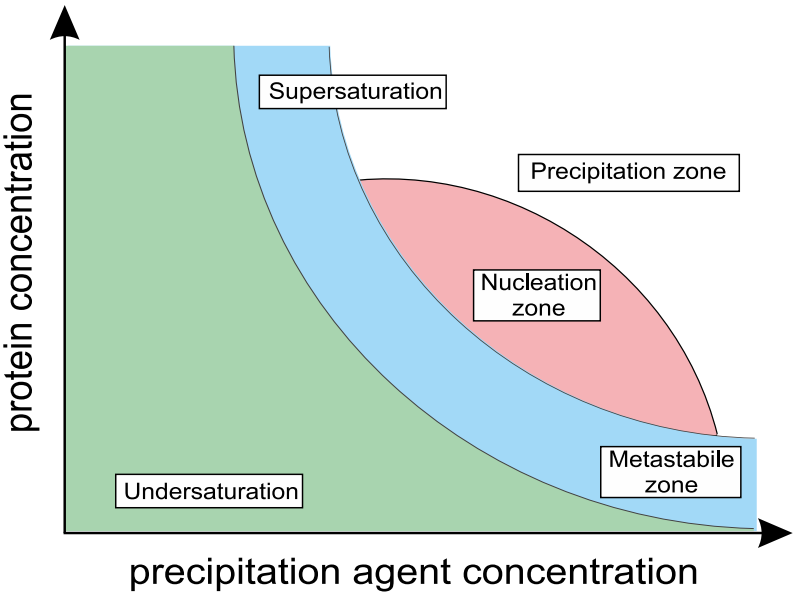

Figure 1.6.: Schematic representation of a protein phase diagram. Shown is the phase state of a protein in dependency of the protein and precipitant concentration. The phase diagram is divided into four areas: An undersaturated area, a metastable zone, a nucleation zone, and a precipitation zone.

required. Therefore, the use of high-throughput experiments (HTE) is very useful. Two different approaches are commonly used, both in 96-well format. Either sitting, or hanging drop vapor diffusion, or microbatch experiments [77]. In vapor diffusion experiments, a protein solution is equilibrated against a reservoir, containing a solution with a higher precipitant concentration. Over time, this leads to a reduction of the drop volume, and thus, to a concentration of the protein. At a certain point this can lead to phase transition, and probably crystallisation [78]. The disadvantage of this methodology is that it is difficult to define the exact concentrations of the components, at which the phase transition takes place. In microbatch experiments, different stock solutions containing buffer, precipitant,

or protein are mixed and subsequently covered with oil, or sealed [51, 79]. This allows a precise definition of the experimental conditions, but higher amounts of protein are required, compared to vapor diffusion experiments.

1.3. Downstream Process Development

The following chapters outline fundamentals of biopharmaceutical downstream process development. In this thesis the chapters 4, 5, and 6 focus on the development of a monoclonal antibody (mAB) downstream process employing preparative protein precipitation as capture step. Furthermore, the integration of this step into the further purification strategy based on chromatographic separation is investigated. Therefore, chapter 1.3.1 gives an introduction to preparative protein precipitation and chapter 1.3.2 to liquid chromatography for proteins. For the purification process developed in this thesis, an exploration of the transfer to a continuous process has been examined. Therefore, chapter 1.3.3 presents the current state of continuous manufacturing in the biopharmaceutical industry. Chapter 1.3.4, 1.3.5, and 1.3.6 present the different development strategies currently used, i.e. knowledge-based process development, high-throughput process development (HTPD) and mechanistic chromatography modeling.

1.3.1. Fundamentals of Industrial Protein Precipitation and Crystallization

Since Cohn developed the first industrial fractionation process in 1941 to recover albumin from blood plasma, precipitation has been used in biotechnological processes as a downstream operation [80]. Precipitation, or related operations, such as flocculation, or crystallization, can be used at any step of the downstream process. While flocculation is mainly used for the clarification of cell debris, precipitation is used for capture, or intermediate steps. Crystallization is mostly applied during polishing, or formulation.

For most unit operations, two different approaches are conceivable: Either precipitation of the product itself, or the precipitation of the impurities while the product remains soluble. The precipitation of the impurities has the advantage that a phase transition of the product is avoided, and thus, the risk of damaging the product is also avoided. On the other hand, native precipitation of the product makes it possible to combine, and integrate three unit operations: Purification, stabilization, and concentration [81].

In any case, a phase transition is induced by changing the solvent conditions. This induces a change in the product solubility, or in the solubility of the impurities [82]. Even if a change of temperature, pH-value of the solution, or concentration of the product would be conceivable,

the most common way to induce the phase transition is the addition of precipitants [83]. In the biopharmaceutical industry, ethanol is used to extract immunoglobulin G (IgG) from human plasma, similar to the original approach of Cohn [84]. Besides organic solvents, chaotropic agents such as inorganic salts, or non-ionic polymers, such as PEG, are possible alternatives to ethanol. [68, 85]. As an industrial application viruses, or virus-like particles (VLP) are precipitated, or concentrated, with the precipitants ammonium sulfate, or PEG [86–88]. For mAbs, one of the most important classes of biopharmaceutical drugs, there is currently no large-scale industrial process on the market. And this despite the fact that many academic studies dealt with ethanol-, salt-, or PEG-induced mAb precipitation [21, 27, 89]. In particular, the use of PEG showed promising potential as it is inexpensive, commonly available, non-toxic, non-flammable, and has a low vapor pressure [90]. In addition to the classical precipitation approaches, recent studies deal with new methods, such as, affinity precipitation, or the use of salt-tolerant copolymers. These studies aim to achieve higher selectivities, compared to classical approaches [91, 92].

In order to increase the acceptance of protein precipitation, and crystallization, simple and fast process development needs to be ensured. Since the mechanism of protein precipitation is not fully understood, the majority of process development is done empirically. High-throughput methods, and Design of Experiment (DoE) can contribute to faster and more material saving process development. These methods can also help to increase the acceptance of phase separation techniques in the biopharmaceutical industry. In the case of polishing steps, however, separations based on chromatographic modes is probably irreplaceable, as these techniques are associated with very high selectivities.

1.3.2. Fundamentals of Liquid Protein Chromatography

Chromatographic purification of biopharmaceuticals is widely used and of great importance because of its high resolution, leading to a high purity of the product. Hence, it is common practice to perform protein separation using liquid chromatography (LC). Thereby, the proteins, solved in the mobile phase, are separated by selective interaction with the stationary phase [93]. Different modes are established for analytical as well as for preparative chromatography. They differ by the interaction mode of the proteins with the ligands. A schematic overview of the most commonly used chromatographic modes, size exclusion chromatography (SEC), affinity chromatography (AC), ion exchange chromatography (IEX), and hydrophobic interaction chromatography (HIC) is presented in Fig. 1.7. SEC separates the molecules depending on their hydrodynamic radii. In an ideal case, no interaction between the stationary phase and the mobile phase takes place. Separation is possible, as particles of different size have different pathways through the porous stationary phase and, therefore, a different residence time. Smaller particles can enter the pores more easily and accordingly have a higher retention time compared to larger ones [95].

AC is potentially the most selective method for protein purification. During an AC step,

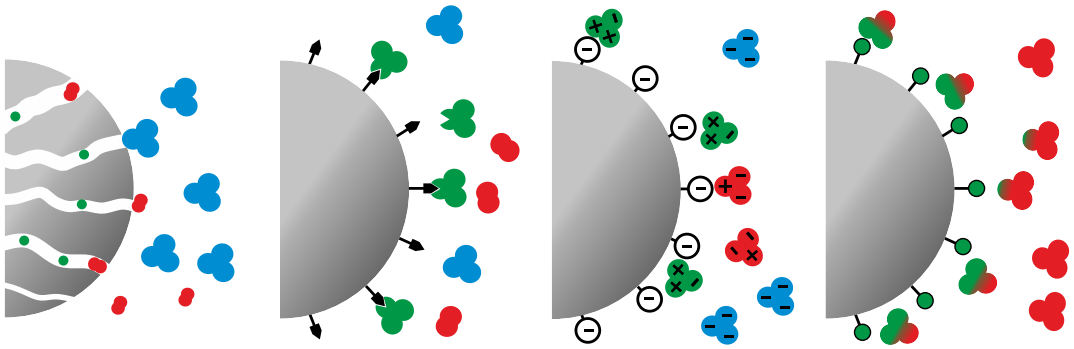

Figure 1.7.: Schematic representation of the most commonly used chromatographic modes. Shown from left to right: Size exclusion chromatography (SEC), affinity chromatography (AC), ion exchange chromatography (IEX), and hydrophobic interaction chromatography (HIC). Illustration adapted from [94].

specific interaction between the protein in the mobile phase and the ligand takes place. In theory only the product should bind to the resin. As a matter of fact, also contaminants are found in the pool after elution [96]. Hence, also for AC additional purification steps are necessary. Nevertheless, AC can lead to high yields and simultaneously a high purity. Unfortunately the drawbacks of affinity resins are the high price and the poor ligand stability [97]. Protein A affinity chromatography for the purification of mAbs is among the most prominent usage of AC. Other examples are the use of specific tags like histidin (HIS) or glutathione S-transferase (GST)-fusion proteins to enable the affinity chromatography for the purification of proteins [98, 99].

IEX uses the interaction of the proteins with the immobilized charged groups onto the porous beads of the stationary phase. Depending on the charge of the ligands, it is distinguished between cation exchange chromatography (CEX) with negatively charged ligands and anion exchange chromatography (AEX) with positively charged ligands. Protein-ligand interaction is not only influenced by the stationary phase, but also by the mobile phase. Changes in the pH of the utilized buffer solution can affect the surface net charge of the protein, and influence the binding (Chapter 1.2.2.). Far away from the pI of the proteins a stronger binding occurs if the charges of protein and ligand are opposite. The conductivity of the mobile phase can prevent the protein from binding to the ligand, by shielding the charged groups of the protein and the ligand. This can be used for selective elution by applying a salt gradient. On the other hand, the conductivity can be a significant issue for protein loading. Binding is usually performed in a conductivity range of 1-4 mS/cm equivalent to an ionic strength of 10-100 mM [100]. Because of high salt concentrations during fermentation, it can be necessary to dilute the clarified feedstock prior loading onto IEX column.

During HIC, or reversed phase chromatography (RP), hydrophobic interaction between the hydrophobic patches on the protein surface and the hydrophobic ligands takes place. The nature of protein-ligand interaction can be influenced by changes in the mobile phase.

During HIC, inverse to IEX, the adsorption increases with higher salt concentrations and decreases at lower ones. Thereby, the mechanism is not depending on the conductivity, but related to specific salt effects which strengthen or weaken hydrophobic interactions [101]. Furthermore, changes in the adsorption characteristics of proteins towards the ligands can be achieved by variations of the ligand type, ligand chain length, ligand density, or the material of the matrix [102]. Through the utilization of ligands with a higher hydrophobicity a stronger binding can be achieved. However this can also lead to a reduction of the selectivity. The retention mechanism during HIC is widely studied but none of those theories has reached general acceptance [102]. Melander and Horvath proposed a mechanism based on the solvophobic theory, and the formation of cavity during the solvation process [103]. Thereby, the specific salt effects contribute to the different changes of the surface tension. Arakawa presented an hydration model based on preferential interaction between the protein and salts [104]. According to this theory the free energy of the protein is increased by the addition of salts, which is thermodynamic unfavorable. As the surface area is reduced during binding to the HIC ligand, preferential binding of salt would transfer the protein to a more stable state. Tanford explained the hydrophobic effect with reorganization of the water structure on the hydrophobic surface of the ligand and the protein prior adsorption [105]. The higher order of water molecules around hydrophobic patches could be proven by Shiraga *et al.* which carried out terahertz spectroscopy of biomolecules [106].

1.3.3. Continuous Manufacturing of Biopharmaceuticals

According to the U.S. Food and Drug Administration (FDA), the transfer of a process to continuous production should bring a number of advantages. For the development of a continuous process, the first step is always a process integration, which ideally leads to a reduction of the required purification steps. This has the advantage of shorter process times, higher efficiency, and increased safety through fewer manual manipulations. Continuous production also leads to a reduction in equipment size and thus to a smaller production facilities. Additionally, continuous manufacturing is associated with the need for on-line monitoring strategies. By applying real-time process monitoring and control, product quality can be improved [107].

The key operation in downstream processes is the capture step, often performed as affinity chromatography. For capture steps performed in bind and elute mode, continuous chromatography can be run in periodic counter-current chromatography (PCCC) mode. Thereby, multiple columns are run in parallel and concurrently [108]. This allows an overloading of the columns without the risk of losing product, as the flow-through is collected by a second interconnected column. Due to this mode the whole column capacity can be used, and the number of elution steps, related to the amount of loaded material onto the column, is reduced. Therefore, continuous chromatography can solve the problem of high resin costs and poor resin lifetimes. Beside the improvement of the resin utilization,

increase in productivity and reduction of the buffer consumption can be achieved by using PCCC [109]. Angarita and coworkers presented an approach were only two columns were used to perform a continuous process [110]. Anyhow, to allow a continuous flow, often additional columns are used. These columns are not interconnected, but eluted and equilibrated during the other ones are used for loading.

During the polishing steps, product-related contaminants are removed. These contaminants only have slightly different surface characteristics, compared to the product, resulting in similar elution behavior. Hence, using chromatography separation often leads to an overlapping of the contaminants with the product during the elution. Flatten the gradient can sometimes solve this problem, but consequently leads to a reduction of the productivity. Therefore, in most of the cases purification will lead to a yield-purity trade-off, depending on the pooling decision, i.e. the fractionation of the eluted material. In a continuous mode this problem can be solved by loading the overlapping regions of the chromatogram onto a second column. This recycling strategy differs from that during capture chromatography. During a continuous capture step recycling of the breakthrough occurs during loading, while during a continuous polishing step recycling is performed during the elution [111].

Different approaches are possible to turn a precipitation or a crystallization process into a continuous one. By using a mixed suspension mixed product removal reactor (MSMPR) the growth of the particles can be controlled depending on the residence time. This is a simple approach as a MSMPR works similar as a continuous stirred tank reactor (CSTR), which is already established for continuous protein refolding [112]. As an alternative, tubular reactors are used for continuous precipitation. Thereby, mixing is ensured by static mixers. The size of the reactor, respectively the tube length is defined by the kinetic of the precipitation in combination with the flow velocity. This design allows a simple integration into a fully continuous process. The variation of the tube length allows a process integration without the necessity of changing the flow rate, and therefore the possibility to forego to hold tanks [113]. Beside the precipitation, resolubilisation of the precipitated product was shown to be challenging for a continuous manufacturing. To achieve acceptable yields, the precipitated product has to be separated from the liquid and resolubilisized completely. The phase separation can be carried out by centrifugation or filtration using depth filter or tangential flow filtration (TFF). Thereby, centrifugation is commonly used in lab-scale, but has the huge disadvantage that the precipitate flocks are compacted during the separation, which makes it more difficult to resolubilise them afterwards [114]. In continuous mode, depth filtration can be realized through parallelisation and sequential backflush of the filters. However, this comes with the disadvantage of high investment costs through the fast blocking of the depth filters. Kuczewski and coworker presented an approach where the precipitate was captured and resolved using TFF [115]. In a first step the precipitate was concentrated and washed using an $0.22\,\mu m$ membrane, which is capable of retaining the precipitated flocks. In a second step the precipitate was resolubilised using precipitant free buffer. This method avoids a complete phase separation and consequently allows the precipitate to stay in solution. Following, higher yields in combination with a concentration of the product can be achieved.

1.3.4. Platform Process for Monoclonal Antibodies - A Heuristic Approach

MAbs are among the most important class of biopharmaceutical products. Each mAb is composed out of two heavy and two light chains held together by intra-molecular disulfide bonds. Each heavy and light chain can be divided into a constant and a variable domain. While the variable part is acting as antigen binding region, the constant domain contains the fragment crystallizable (Fc) region [116]. This high similarity among different mAb species and in particularly the presence of the Fc-region in each mAb enables the use of a platform process with a sequence of equal or similar process steps.

Expression of mAbs usually takes place in mammalian cell culture suspensions. The most common and dominantly used cell lines are chinese hamster ovary (CHO) cells. The upstream processing is usually performed in Batch/Fed-Batch cultivation. For Fed-Batch processes essential nutritions are feeded after inoculation during the cultivation [117]. The first purification step of a generic antibody process is the clarification of the cell culture media using centrifugation and/or depth filtration. For the capture step the clarified cell culture media (HCCF) is loaded onto a Protein A affinity chromatography column. After loading, the elution is performed by applying a low pH step, following by an hold step at low pH to ensure virus inactivation. Afterwards, polishing is carried out by two additional chromatographic steps. Often a CEX in bind-and-elute mode is followed by an AEX step in flow-through mode. Finally, the product is concentrated and transferred into the formulation buffer using ultra- and diafiltration (UF/DF). Since the first introduction of a mAb to the market in 1986 this sequence of unit operations was consequently developed further, and became the basis for a platform process. Only minor changes and adjustments have to be performed, resulting from the variations between the different mAb species [14].

The basis of this process is the Protein A affinity chromatography step, which combines high selectivity with high yields in a generic process step [118]. Anyhow, the key disadvantages of this step are the high resin costs in combination with the low stability of the resin. Especially, the low pH elution can lead to leaching of the Protein A ligands, and hence reduce the lifetime of the affinity resin [119]. Therefore, different approaches are currently under investigation either to reduce the cost of an affinity based purification process or to replace chromatography as unit operation for the capture step. Replacing Protein A chromatography comes with the disadvantage of renouncing the platform process. Therefore, alternative process development strategies are necessary.

1.3.5. High-Throughput Process Development

The biopharmaceutical industry is operating under constant pressure, to lower the cost for process development and ensuring a fast and save process development. High-throughput

process development (HTPD) can help to fulfill these needs. HTPD is thereby characterized by three principles: miniaturization, automation, and parallelization [120]. The large number of experiments, enabled through the low amount of material, requires the use of robotic based high-throughput screenings (HTS). While HTPD was first implemented in the analytical sector and for lead discovery in the 1990s, it is today widely applied for downstream process development [121]. The applications include methods for membrane processes, chromatography operations, solubility screenings, or protein folding studies [122–124].

HTS is applied for the optimization of a varity of alternative purification methodologies. Bensch and coworkers showed an approach using HTS for the development of aqueous two-phase systems (ATPS) [125]. Kevelman and coworkers developed an HTS approach for the screening of PEG based precipitation [26]. For precipitation processes the high amount of influencing parameters, like pH value, conductivity, feed concentration, contaminant profile, or different precipitation agents, leads to the necessity of HTS. The possibility to scale by volume, makes this process step an ideal approach for HTS.

To reduce the number of single experiments it can be useful to combine HTS with DoE. A DoE can help to investigate the influence of different parameters on a system. In a classical one-factor-at-a-time (OFAT) experiment, one factor is varied while the other variables are kept constant. This can be very time consuming and inefficient. However, sometimes this is unavoidable, when the influence of each parameter towards the others can not be described mathematically. In contrast, during a factorial experiment different factors a varied together. Thereby, a well designed experiment can provide answers to the question which parameter influences the investigated system and to which output the parameter yields. Following, DoE can lead to an empirical model which characterizes the system performance [126].

Especially in early development phases, HTS can provide useful information for chromatography process development. Traditionally, several dozen column experiments have to be performed to optimize the conditions for one chromatography step [127]. HTS can help to optimize different parameters and lower the time and material consumption significantly. It allows to screen a huge variety of resins, which might differ in particle size, ligand type, or the pressure flow characteristics. Resin screening can be performed in 96-well format using so called PreDictor plates, or specially designed Robocolumns. Another process parameter which can be optimized, using HTS, is the binding capacity of the target protein. This, among others, changes strongly in relation to the buffer conditions [128, 129]. Further, HTS can be used to determine parameters needed for mechanistic modeling of chromatography processes. Therefore, the combination of HTS and mechanistic modeling has shown huge potential for the future of chromatography process development [130].

1.3.6. Mechanistic Modeling of Ion Exchange Chromatography

Mechanistic chromatography modeling and numerical simulation can help to reduce the number of wet laboratory experiments during chromatography process development. This can help to save time, material, and process development costs [131]. In this thesis, a CEX chromatography step is optimized for aggregate removing using mechanistic modeling. Therefore, in the present chapter the theoretical basis of chromatography modeling is discussed exemplarily on the CEX.

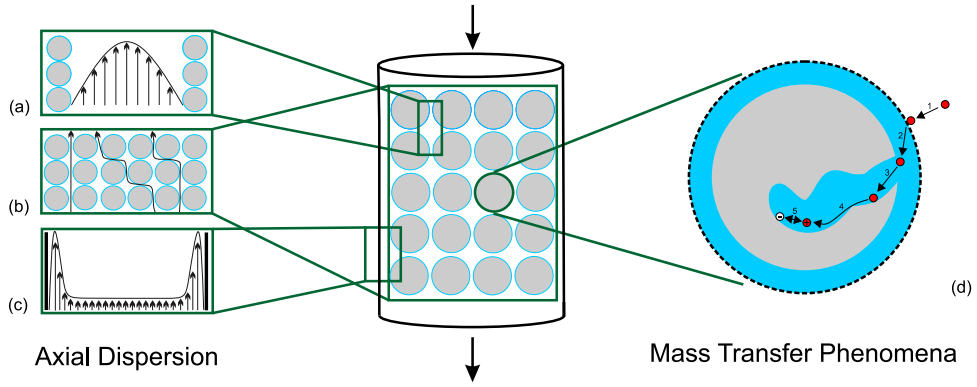

Figure 1.8.: Schematic representation of column phenomena leading to peak broadening. Axial dispersion is a result of (a) fluid dynamic adhersion between the particles, (b) Eddy-diffusion, or (c) wall effects. (d) Mass transfer phenomena occur because of 1. convection and diffusion transport, 2. film diffusion, 3. pore diffusion, 4. surface diffusion, and 5. adsorption and desorption.

During chromatographic separation in an ideal case a rectangular signal would be the answer of a pulse injection. In reality, non-idealties of fluid distribution occur, resulting in peak broadening. A schematic representation is shown in Fig. 1.8.. Hydrodynamic effects are summarized in the axial dispersion. The rest of the peak broadening is a result of mass transfer phenomena.

Axial dispersion occurs due to extra column effects, owning the presence of pumps, tubing or valves. To minimize these effects, especially for analytical chromatography systems, death volumes and tubing lengths should be held at a minimum. For larger columns the critical point for axial dispersion is the column head and the fluid collection at the column outlet. In the column non-ideal fluid distribution can occur too (Fig 1.8. (a, c)). Fluid dynamic adhesion between the macroscopic channels of the packed bed results in a non-uniform flow profile (Fig. 1.8. (a)). Additionally, local inhomogeneity of the packed bed can result in different microscopic fluid distribution of the molecules, the so called Eddy-diffusion (Fig. 1.8 (b).). Finally, wall effects caused by interaction of the fluid with the column wall, and the material lead to a broadening of the peak (Fig. 1.8. (c)) [93].

Mass transfer phenomena are the second aspect contributing to the peak broadening. For enlarging the capacity of the utilized chromatography media, particles with a porous

structure are used. Depending on the mode of chromatography, specific ligands are bound to the porous particles. Resulting from this structure several mass transfer parameters have to be considered (Fig. 1.8. (d)). These parameters describe convective and diffusive transport towards the particles, film diffusion in the laminar boundary layer around the particles, and pore and surface diffusion in the particles. The actual separation takes place through interaction with the adsorbers, described with adsorption and desorption kinetics [93].

To describe the behavior of proteins during a chromatographic process, a description of the convection and diffusion in the chromatography column and a description of the adsorption behavior is necessary. In this thesis, the general rate model (GRM) was employed to cover the convection and diffusion in the column of the length L and the adsorber beads of the radius r_p [93]. In the GRM two mass balances, Eq. 1.5 and Eq. 1.6, describe the mass transfer of the component i from the bulk phase towards the stationary phase during a chromatographic separation.

$$\begin{aligned}\frac{\partial c_i(x,t)}{\partial t} &= \underbrace{-u(t)\frac{\partial c_i(x,t)}{\partial x}}_{convection} + \underbrace{D_{ax}\frac{\partial^2 c_i(x,t)}{\partial x^2}}_{axial\,dispersion} \\ &\quad \underbrace{-\frac{1-\epsilon_b}{\epsilon_b}k_{film,i}\frac{3}{r_p}\left(c_i(x,t)-c_{p,i}(x,r_p,t)\right)}_{mass\,transfer} \end{aligned} \tag{1.5}$$

$$\frac{\partial c_{p,i}(x,r,t)}{\partial t} = \begin{cases} \frac{1}{r^2}\frac{\partial}{\partial r}\left(r^2 D_{p,i}\frac{\partial c_{p,i}(x,r,t)}{\partial r}\right) - \frac{1-\epsilon_p}{\epsilon_p}\frac{\partial q_i(x,r,t)}{\partial t} & \text{for } r \in (0,r_p), \\ \frac{k_{film,i}}{\epsilon_p D_{p,i}}\left(c_i(x,t)-c_{p,i}(x,r_p,t)\right) & \text{for } r = r_p, \\ 0 & \text{for } r = 0. \end{cases} \tag{1.6}$$

Eq. 1.5 describes the transfer between the mobile phase with the concentration $c_i(x,t)$ and the pore phase, depending on the position x in the column, and the time t. Thereby, the first term of Eq. 1.5 describes the convection in the column depending on the flow velocity of the mobile phase u. The second term describes the axial dispersion by the axial dispersive coefficient D_{ax}. The last term describes the transfer from the bulk phase towards the pores with the concentration $c_{p,i}(x,r,t)$. This term is influenced by the film transfer coefficient $k_{film,i}$, and the voidage of the adsorber bed ϵ_b. Eq 1.6 describes the mass transfer from the pore volume with the concentration $c_{p,i}(x,r,t)$ to the stationary phase q_i and vice versa, depending on the adsorber particle voidage ϵ_p, the component-specific pore diffusion coefficient $D_{p,i}$, and the radial pore position r within the particle.

Adsorption and desorption processes of the particles on the adsorbers during a CEX step can be described with the steric mass action (SMA) isotherm, developed by Brooks and Cramer [132]. Velayudan and Horvath developed the theory, that during CEX salt ions and proteins compete for available binding sites[133]. Nilsson and coworker assumed that

this was a first order reaction and developed the kinetic formulation shown in Eq. 1.7 [134].

$$k_{kin,i}\frac{\partial q_i(x,t)}{\partial t} = \underbrace{k_{eq,i}(\Lambda - \sum_{j=1}^{k}(\theta_i + \sigma_i)q_j(x,t))^{\theta_i}c_{p,i}(x,t)}_{adsorption} \underbrace{-c_{p,salt}(x,t)^{\theta_i}q_i(x,t)}_{desorption} \quad \forall i \neq salt \tag{1.7}$$

The fist part of the kinetic SMA isotherm describes the adsorption of the protein in the stationary phase with the concentration q_i. It depends on the protein concentration itself, the ionic binding capacity Λ , the pore phase concentration of the protein c_p and the characteristic charge of the directly involved binding sites θ. σ is a shielding factor, taking into respective that not all binding sides are accessible for the protein, because of steric effects. The second part of the kinetic SMA isotherm represents the desorption term depending on the the pore phase salt concentration $c_{p,salt}$ and the stationary phase protein concentration q_i. For numerical stability and to separate the parameter effects on the retention time and height of the chromatogram, respectively, the equilibrium coefficient and the kinetic coefficient were used instead of k_{ads} and k_{des} [135]. The salt concentration in the stationary phase q_{salt} is described with Eq 1.8.

$$q_{salt}(x,t) = \Lambda - \sum_{j=1}^{k}\theta_j q_j(x,t) \tag{1.8}$$

The combination of GRM and SMA, together with numerical methods for parameter estimation allows the modeling and *in silico* optimization of the CEX processes, developed in this thesis.

1.4. Process Analytical Technology

Production processes for pharmaceutical and biopharmaceutical products are traditionally monitored by offline analytics after the batch has been produced. However, in 2002 the FDA has introduced process analytical technologies (PAT) as a key element of good manufacturing practice (GMP) [136]. In 2004 the FDA has introduced a guidance for the implementation of PAT in biopharmaceutical industry with the goal to improve process development, manufacturing, and quality assurance [137]. PAT describes a broad field of tools and principles which allow real time analytic of process components, as well as process understanding. This real time analytics can lead to a better process understanding, enable real time process control, and help to make real time risk-based decisions [138].

In the past the focus was set on on-line and at-line high-performance liquid chromatography (HPLC). Recently, the implementation of spectroscopic methods has shown great potential. As opposed to HPLC methods, spectroscopic methods are faster and can often be performed in-line, without the necessity of removing samples out of the process steam. Furthermore, they avoid the risk of harming the product. However, spectroscopic, or chemometric methods come with the drawback of a limited selectivity for different components. To overcome this drawback, not only selected wavelength are used, but the information contained in the hole spectra is recorded. That in a turn leads to great amount of data. To overcome this challenge, multivariate data analysis (MVDA) is applied to extract information out of the complex spectra [34]. In this thesis in-line FTIR spectroscopy is investigated as process analytical technology. Therefore, chapters 1.4.1 and 1.4.2 describe the fundamentals of the applied MVDAs and chapter 1.12 the fundamentals of the investigated FTIR sensor.

1.4.1. Principle Component Analysis

Principle component analysis (PCA) is often the basis for data and noise reduction, outlier detection, or classification during MVDA. During a PCA, a transformation of possibly correlating variables into a smaller number of uncorrelated variables, the principle components or factors, is performed. The original data are described as linear combination of different weighted principle components. A graphic illustration of how PCA is calculated can be seen in fig 1.9. Thereby X represents a matrix of the original data with the dimension

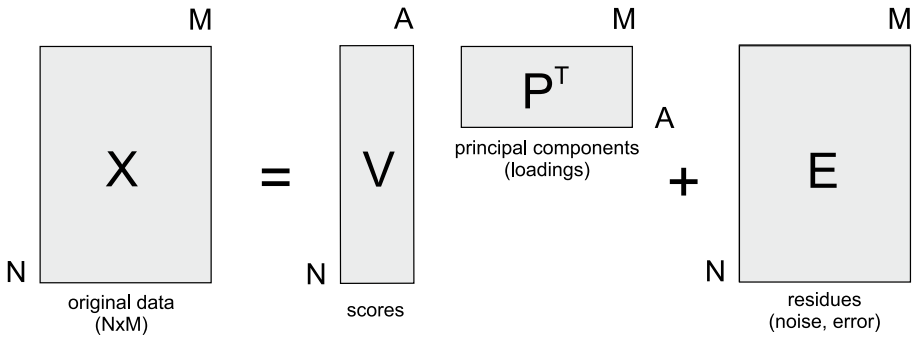

Figure 1.9.: Schematic representation of how PCA is calculated, adapted from [139].

NxM. To carry out a data reduction principle components have to be found. The most common way is to use the mathematical nonlinear iterative partial least square (NIPALS) algorithm. The first principle component is that one, which points in the direction of the highest variance. The first principle component defines a new coordination system with one dimension. The second principle component is orthogonal to the first one, and so on. Finally, a data reduction is reached, if the dimension of the new generated system is lower than the original one. All principle components build the matrix P^T with the dimension AxM. Each column of P^T is represented by one principle component, and the number of rows is defined by the number of variables in the original matrix X. After finding

the principle components the transformation of the original data in the new coordination system is performed. For each new factor a score or weighting is calculated. The scores build the matrix V with the dimension NxA, which has as many rows as the original data and the number of columns is equal to the number of applied principle components. Data reduction is achieved by projecting the original data to a number of principal components smaller than the original dimensions of the data. The variance in the data, that is not explained by the projection, is described in the matrix E as residual or noise [139]. The mathematical representation of Fig. 1.9 is shown in Eq.1.9

$$X = VP^T + E \tag{1.9}$$

1.4.2. Partial Least Square Regression

Partial least square regression (PLS) is a multivariate regression method that correlates a set of Y-variables with a set of X-variables (Eq.1.10).

$$Y = XB + E \tag{1.10}$$

By calibrating a PLS model with known Y and X data, it can be applied to estimate unknown Y-data. In this thesis, PLS is employed to determine the concentration of proteins and process contaminants in combination with Fourier-transform infrared (FTIR) spectroscopy. Hence, the FITR spectra are utilized as X-data for PLS regression. Thereby, the $(N\,x\,M)$ X matrix is composed of N objects with M properties, in the present case different spectral data. The corresponding protein or contaminant concentrations build the matrix Y. The PLS model correlates Y-values to the X-data with the help of a regression matrix B. The residues are summed up in the matrix E [139]. A schematic representation of a PLS model is shown in Fig. 1.10.

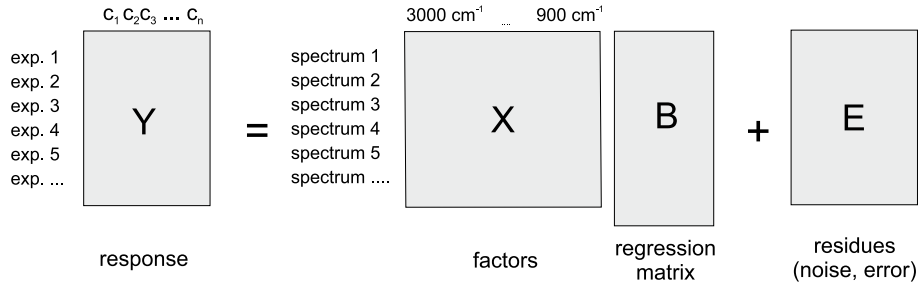

Figure 1.10.: Schematic representation of a PLS regression model, adapted from [139].

To calibrate a PLS model, spectral data are generated and the corresponding response values are determined with the help of offline analytic. In a second step, the model is validated with data not included in the model building, to prove the assurance and predictability

of the model. In the last step the model can be used to estimate the concentrations in samples associated with new spectral data.

The idea of a PLS is to perform a kind of PCA for the X-data (Eq. 1.11), as well as for the Y-data (Eq. 1.12). The matrix X is separated in the score matrix V and the principle components P^T, while the Y-matrix is described by the score matrix W and the principle components Q^T. The residues are described by the matrices E_1, respectively E_2 [139].

$$X = VP^T + E_1 \tag{1.11}$$

$$Y = WQ^T + E_2 \tag{1.12}$$

In opposite to classical PCA a PLS does not aim to find the highest variance of X and Y, but rather to find the highest correlation between the scores of X and Y. Hence, a model is developed in such a way that the different score values W have a maximum covariance to the associated score values V. The linear correlation between both scores is described in the regression matrix B. Finally, by describing W in dependency of V, it is possible to determine the responses in matrix Y out of the initial detected spectral data matrix X. A graphic illustration of the procedure of calibrating PLS is shown Fig. 1.9.

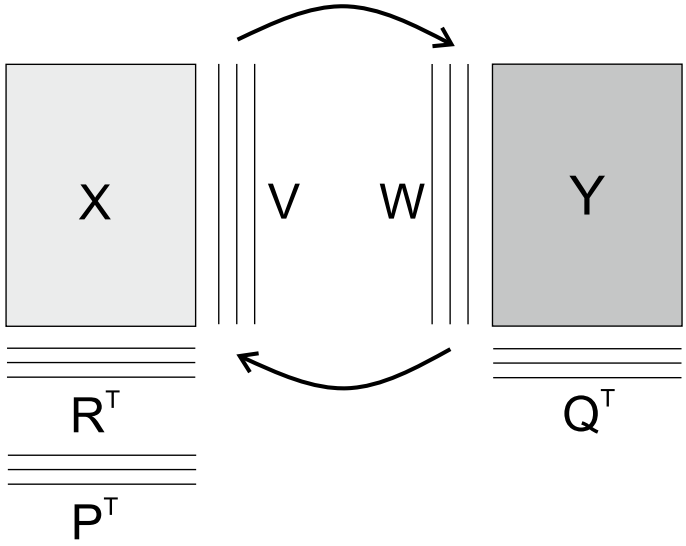

Figure 1.11.: Schematic representation of the procedure for performing PLS regression, adapted from [139].

1.4.3. Fourier-Transform Infrared Spectroscopy

In this thesis FTIR was applied as in-line analytical tool, for the monitoring of downstream process steps. FTIR is a non-invasive analytical technique, and can be used for a wide range of sample types. In particular it allows to investigate proteins in their natural environment.

Thereby, it is possible to determine concentrations, but also to get information about the protein structure [140].

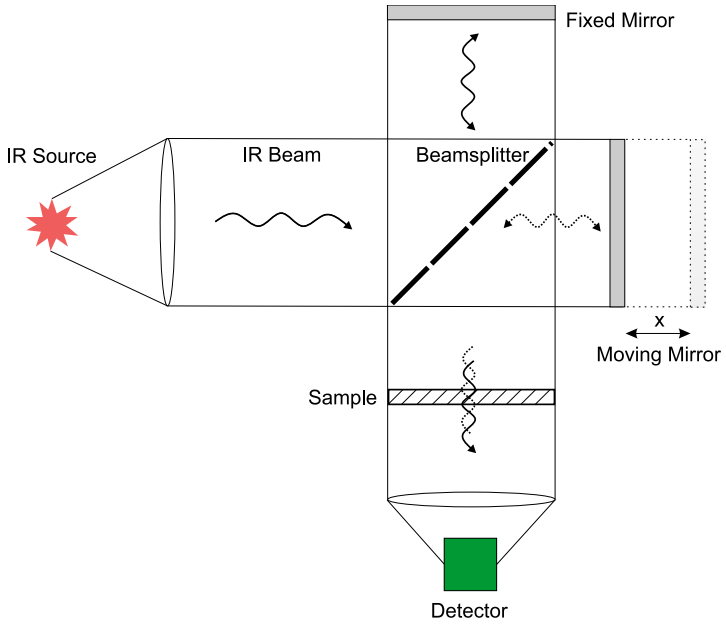

Figure 1.12.: Schematic representation of Michelson-Interferometer. Illustration adapted from [141].

FTIR is a vibrational spectroscopy. Hence, molecular vibrations or rotations are measured to detect and distinguish between different molecules. In general all atoms oscillate around an equilibrium position. This also influences the bond length. As the resonance frequency of these motions is in the infrared region, it can be excited by IR-light [141]. However, only changes in the vibration mode which influence a dipole moment of a molecule show up in an IR-spectrum. In other words, only asymmetric molecules can be detected. When a mid-infrared spectroscopy is used, the functional groups of the molecules get excited, with light in the region between $4000\,cm^{-1}$ and $400\,cm^{-1}$. For proteins, especially vibrations in the amid I band between $1700\,cm^{-1}$ and $1600\,cm^{-1}$ and amid II band between $1580\,cm^{-1}$ and $1510\,cm^{-1}$ are of high importance. Vibrations of the amid I band mainly result from C=O stretching while the amid II band can be correlated to N–H and C–H stretching. Both bands are directly related to the backbone of the proteins. The region between $1400\,cm^{-1}$ and $400\,cm^{-1}$, is called the finger print region, and is highly specific for the configuration and physical state of the protein [140].

Spectrometers equipped with an interferometer are often used to detect mid-infrared spectra. In Fig. 1.12. a schematic representation of a Michelson-Interferometer is presented. The polychromatic light is emitted by a thermal source such as a globar and divided into

two parts by a beamsplitter. One part of the light hits a fixed mirror after the distance L, is reflected, and meets the beamsplitter a second time after the distance $2L$. The other part of the light is reflected by a movable mirror of the distance x, and therefore the distance to the beamsplitter $2(L + x)$ correlates to the position of the mirror. The reunion of the two beams after different path lengths causes interference, leading to different amplitudes of the resulting beam. The modulated light passes the sample and hits the detector, were the interferogram is recorded. In this interferogram the intensity is correlated to the position x of the movable mirror. Fourier transformation is used as mathematical transformation of the deflection amplitude domain into a frequency amplitude domain. The resulting spectrum shows the intensity of each wavenumber [141].

2. Thesis Outline

2.1. Research Proposal

The pharmaceutical market continues to grow and the group of biopharmaceuticals has the highest growth rate by comparison. This opens up the opportunity for biopharmaceuticals to become the core of the industry in the future. That not only requires new products, but also higher production capacities and more efficient processes. Progress in upstream process development (USP) has already, at least partially, met these challenges, and shifted the bottleneck towards downstream process development (DSP). In DSP chromatographic separation is still the workhorse. High resin, and operating costs, combined with a slow volumetric throughput demand new approaches based on Anything but Chromatography (ABC) methodologies. Preparative protein precipitation is one of the most promising techniques among these unit operations. In particular, it is known as a cost-effective alternative for small scale production. For monoclonal antibodies (mAb), polyethylene glycol (PEG) induced precipitation has been presented as an easy-to-use alternative, especially for continuous production. However, there is no large-scale mAb precipitation process on the market yet. The focus of this thesis is to identify the main obstacles that prevent preparative protein precipitation from being applied in industry and to overcome them.

A major challenge in the development of a precipitation process is the high complexity of the underlying processes. Understanding the different forces, acting between the different particles involved, can help to overcome this complexity. Protein phase behavior is influenced by a combination of molecular and process-related factors. Molecular factors are mainly defined by the amino acid composition of the protein. The different residues, of the amino acids lead to different protein structures and influence its charge distribution, as well as the formation of hydrophobic patches on the protein surface. Process-related factors such as ionic strength, pH value, buffer composition, or impurities can change these surface attributes, depending on the process conditions. Understanding the acting forces is a prerequisite for the understanding of protein phase behavior. In particular, the role of hydrophobic interactions still requires the attention of academic research. Therefore, the first part of this thesis will focus on the role and the mechanism of hydrophobic interactions. In order to gain a deeper understanding of the acting forces and the underlying mechanism, a first study will need to investigate similarities between hydrophobic interaction

chromatography (HIC) and protein phase behavior [1]. Based on this data, it will be evaluated whether these findings can be used to predict protein phase behavior and/or serve as a basis for a mathematical description of the precipitation process [2]. The results will provide the framework for an *in silico* process development of a precipitation-based process. A study will be carried out to develop a mechanistic precipitation model and to determine whether the model enables simpler and faster process development. In addition, it will be evaluated whether the model can serve as a basis for further model extensions. The study will also investigate how the model can contribute to a deeper understanding of the process.

Often the process development of a precipitation step is still purely empirical and concentrates on the individual unit operation itself. In contrast, traditional mAb process development is based on an integrated platform process, using Protein A affinity chromatography as capture step. The use of a generic capture step enables simple, and fast process development. In order to establish a precipitation-based process as appropriate alternative, two studies will be conducted. The first study will investigate the influence of the upstream conditions on the subsequent precipitation step [3]. It will be analyzed whether the contaminant composition influences the purification outcome and, consequently, which parameters have to be considered for successful process development. A further study will concentrate on the optimization of the precipitation step itself and the integration of the subsequent polishing steps [4]. Thereby, it is important to consider the mutual influences of precipitation, resolubilisation, and further polishing steps. It will be investigated whether the combination of high-throughput screening (HTS), empirical, and mechanistic modeling can contribute to the establishment of a fast, simple, and material-saving development strategy. In addition, it will be examined whether the resulting process meets the requirements of a fast, flexible and robust purification strategy. In order to meet the current trends in the biopharmaceutical industry, it will also be investigated whether the development platform is suitable for the development of both, a classical batch process, and a continuous one.

In addition to the complexity of the process, and the mutual influences of different parameters on the purification outcome, the monitoring of PEG-induced precipitation is a limiting factor for an industrial application of a precipitation-based purification process. Precipitation leads to a turbidity of the solution, which makes it impossible to monitor the precipitation step itself. This makes it even more important to accurately monitor the following polishing steps. Although PEG is an approved excipient, successful depletion must be ensured during the subsequent purification steps. The challenge in detecting PEG is that it is a component that cannot be detected by conductivity or UV/Vis measurements. Both are currently the standard methods used as in-line process analytical technologies (PAT). For these reasons, the last part of this thesis is dedicated to the development of new technologies and measurement setups for monitoring the subsequent chromatographic polishing step [5]. In particular, the potential of in-line Fourier-transform infrared (FTIR) spectroscopy will be investigated. It will be examined whether the combination of FTIR spectroscopic data with a partial least square regression (PLS) model allows differentiation between different proteins. In addition, it will be tested whether the developed setup is

capable of quantifying other process-relevant impurities including PEG.

2.2. Outline and author statement

In several of the following chapters, first authorship was shared (contributed equally) among colleagues and me. This was undertaken to elevate the quality of our common publication. A detailed listing of author contributions signed by the respective authors is given in Appendix D of the examination copy. In general, work connected to Preparative Protein Precipitation as put forward in Abstract and Research Proposal has been performed by myself. Fundamentals for techniques concerning hydrophobic interaction chromatography, mechanistic chromatography modeling as well as process analytical technology used throughout the study, have been laid by the thesis of a) Baumgartner, K. (2015) Development of a methodology linking protein phase behavior and Hydrophobic Interaction Chromatography, b) Wang, G. (2018) Advancing Downstream Process Development Mechanistic Modeling and Artificial Intelligence and c) Rüdt, M. (2018) Spectroscopy as process analytical technology for preparative protein purification.

Chapter 3: Prediction of salt effects on protein phase behavior by HIC retention and thermal stability

K. Baumgartner*, S. Großhans*, J. Schütz*, J. Hubbuch (*contributed equally)

Journal of Pharmaceutical and Biomedical Analysis (2016) Volume 128, Pages 216–225

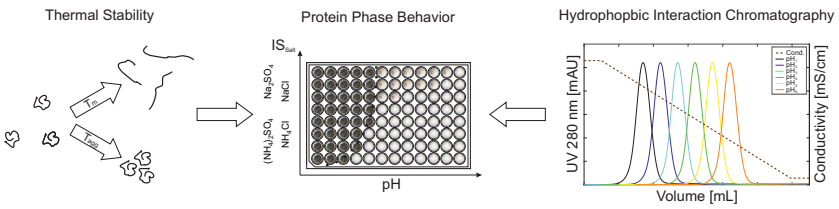

In chapter three, hydrophobic effects occurring during aggregation and influencing protein phase behavior were investigated. Retention times during hydrophobic interaction chromatography (HIC) in combination with measurements of the thermal stability were used as estimation tools for protein stability. In particular, HIC retention times, of the model protein glucose isomerase, were correlated to crystal size and form at varying salt concentrations, salt types, pH values, and protein concentrations. The focus in chapter three was the development of the HIC and temperature stability analytics, the generation of the data, and the comparison and evaluation of the received results. Using HIC a deeper understanding of appearing hydrophobic effects during protein-protein interaction was generated.

Chapter 4: Water on hydrobobic surfaces: Mechanistic modeling of polyethylene glycol induced protein precipitation

S. Großhans*, G. Wang*, J. Hubbuch (*contributed equally)

Bioprocess and Biosystems Engineering (2018) Volume 42, Issue 4, pp 513–520.

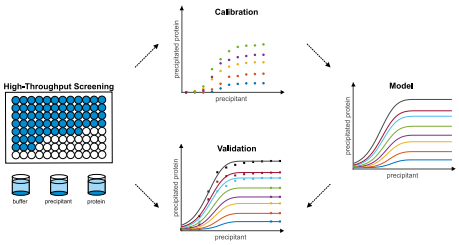

In this chapter, similarities between HIC and protein phase behavior were used to derive a mechanistic model for polyethylene glycol (PEG) induced protein precipitation. The presented approach proposes an equilibrium between well-ordered and bulk-like ordered water molecules on the hydrophobic surfaces of the protein, as driving force for the precipitation process. The model predictability was proven with the help of high-throughput precipitation experiments. Model parameters were estimated for the model proteins lysozyme, myoglobin, bovine serum albumin (BSA), and a monoclonal antibody (mAb) at two different pH values. The model is capable to predict the amount of precipitated protein, depending on the initial protein and PEG concentration. Following, the model was validated with a data set not included into the model building, and beyond the calibration range. The main task in chapter four was the establishment of the screening platform with the corresponding analytics, the generation of the data, model calibration and validation, the transfer of the theoretical assumption to a mathematical model, and the interpretation of the results and model parameters.

Chapter 5: Precipitation of complex antibody solutions - Influence of contaminant composition and fermentation media on the precipitation behavior

S. Großhans, S. Suhm, J. Hubbuch

Bioprocess and Biosystems Engineering (2019) Volume 42, Issue 6, pp 1039–1051.

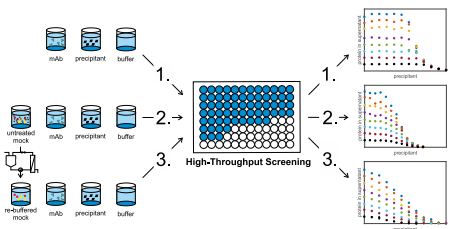

In chapter five, the influence of upstream conditions, and contaminant composition on the PEG-induced precipitation behavior of a complex mAb solution was investigated. A destabilization of the mAb, induced through the addition of contaminants, could be shown, compared to a pure mAb solution. By re-buffering the contaminants solution, prior to the mixing step, the observed destabilization could be correlated to

mAb-macromolecular interactions. Furthermore, also a destabilization of the contaminants was observed. In contrast, for molecules with a size smaller than 10 kDa a stabilizing effect could be shown. This effect could be related to molecules present in the cell culture medium. Hence, the chapter points out the importance of integrating up- and downstream process development. The key tasks in chapter five were the design of the study, the selection of screening parameters, and the preparation of protein and contaminant solutions, so that variations in the precipitation efficiency could be attributed to individual factors.

Chapter 6: An integrated precipitation and ion-exchange chromatography process for antibody manufacturing: Process development strategy and continuous chromatography exploration

S. Großhans*, G. Wang*, C. Fischer, J. Hubbuch (*contributed equally)

Journal of Chromatography A (2018) Volume 1533, Pages 66–76.

This chapter presents a fast and material saving-process development platform, for an integrated precipitation and ion-exchange chromatography mAb process. By combining high-throughput screening, Design of Experiment (DoE), and mechanistic chromatography modeling a promising strategy was presented, which has shown the potential to replace Protein A as affinity chromatography step.

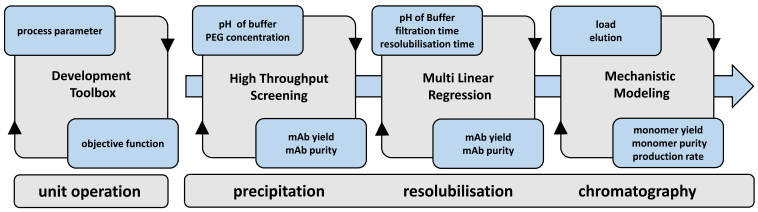

Process-related contaminants like host cell proteins (HCP) and DNA were successfully removed during the precipitation and resolubilisation steps. Cation-exchange chromatography (CEX) was used to remove aggregates. Finally, the capability of a continuous chromatography process was explored theoretically, with the help of *in silico* simulations. The main task in chapter six was the development of the HTS platform with corresponding analytics, the implementation of the DoE, the process integration of the various steps and the execution of the case study, to enable an efficient purification process.

Chapter 7: In-line Fourier-transform infrared spectroscopy as a versatile process analytical technology for preparative protein chromatography

S. Großhans*, M. Rüdt*, A. Sanden*, N. Brestrich, J. Morgenstern, S. Heissler, J. Hubbuch (*contributed equally)

Journal of Chromatography A A (2018) Volume 1547, Pages 37-44

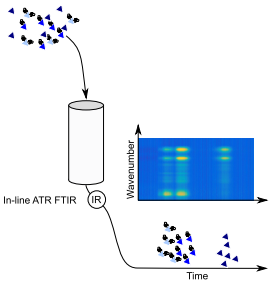

In chapter seven FTIR spectroscopy was implemented as in-line process analytical technology (PAT) tool for chromatographic purification steps. With the help of FTIR spectroscopy, the possibility to distinguish, and selectively quantify different proteins, based on variations in their secondary structure, was shown. Furthermore, it was demonstrated, that in-line FTIR spectroscopy is a powerful tool to detect non UV/Vis active molecules. In a case study the PEGylation degree of proteins could be measured in-line, based on selective in-line quantification. Additionally, selective mass balancing was performed for the process-related contaminant Triton X-100. The main challenge in chapter seven was the transfer of the knowledge gained from offline analysis using FTIR spectroscopy to the requirements of an in-line sensor, the implementation of the sensor and the required offline analytical methods, as well as the interpretation of the data.

Overview of Selected Proteins and Model Systems

In order to investigate the process development, integration, and monitoring of a preparative protein precipitation process, different systems were selected which were adapted to the requirements of the five studies carried out. The preparative protein precipitation process was optimized for a monoclonal antibody (mAb). The antibody was provided by an industrial partner and used in chapter four, five, six, and seven. In order to gain a deeper and more generalized knowledge of the effects of hydrophobicity, appropriate model proteins were selected in chapters three and four. In chapter three, glucose isomerase proved to be the most suitable model protein, since precipitation, crystallization, and denaturation of the protein could be detected, depending on the chosen parameters. In chapter four, the model proteins lysozyme, myoglobin, bovine serum albumin (BSA), and one mAb, were selected as they show a variety in properties such as size, charge, or hydrophobicity. In order to investigate the influence of the feed solution on precipitation behavior, two different mAbs, one IgG1 and one IgG2, were investigated in Chapter five. To demonstrate the ability to monitor and distinguish different proteins using in-line FTIR, a system of mAb and lysozyme was chosen in Chapter seven. In addition, PEGylated lysozyme was chosen as the model protein to demonstrate the ability to differentiate between a

protein and polyethylene glycol.

3. Prediction of Salt Effects on Protein Phase Behavior by HIC Retention and Thermal Stability*

Understanding and controlling protein phase behavior is of great importance in the biopharmaceutical industry. A stable protein solution is crucial to avoid product loss during processing and storage. Furthermore, understanding of the acting forces between all involved particles, like proteins, salts, or contaminants, is mandatory to achieve a better control of intentionally induced preparative precipitation. In the last decades a lot of research has been conducted in this field [49, 75]. However, the role of hydrophobic interactions in particular is not yet fully understood and therefore, requires further academic investigation [45]. In this chapter, which can be viewed as full manuscript in the appendix A, the correlation between protein phase behavior, hydrophobic interaction chromatography (HIC), and thermal stability was investigated. The goal of the study was to investigate new analytical technologies, to reach a deeper knowledge of the role of hydrophobic interaction, and to develop a method to predict the effect of salts on the protein phase behavior.

To do so, the model protein glucose isomerase was used, as it showed a large variation in its morphologies at different pH values and different ionic strengths. In order to detect these different morphologies, a high-throughput screening (HTS) was developed. This HTS enables the visualization of the protein phase behavior at constant protein concentration by simultaneous variation of pH and ionic strength. In order to investigate the influence of different salt ions, the phase behavior of glucose isomerase with addition of sodium chloride, sodium sulfate, ammonium chloride, and ammonium sulfate was examined. For glucose isomerase, the metastable zone showed the occurrence of protein crystallization or the formation of precipitate in combination with skin formation, depending on the salt that was used as precipitant.

* A full version of this publication is given in Appendix A and [1]. In the following the major findings relevant for this thesis are summarized.

Both phenomena occurred over time. This was of particular interest as it allowed to investigate the retention volume during the HIC and the thermal stability of these conditions. The retention volume during HIC was investigated as it allows to detect variations of the hydrophobic effect without considering charge induced attraction or repulsion. The HIC analysis was supplemented by the measurement of the thermal stability, in order to differentiate between conformational and colloidal stability of the protein. The aggregation temperature is an indicator for the colloidal stability, while the melting temperature gives information about the conformational stability of the investigated protein. The information from all applied analytics was compared to the phase state of the protein and the result was used to explain and predict the effects of the different salt ions.

Comparing the different investigated salts a stronger influence of the anions compared to that of the cations was seen. The formation of protein crystals could only be observed in systems with sulfate ions. In comparison, the addition of salts with chloride led to precipitation and skin formation of the protein. This indicates that the addition of salts with sulfate, compared to those with chloride, led to a stabilization of the native conformation of glucose isomerase. These assumptions could be confirmed with measurements of the thermal stability. Systems with chloride showed lower aggregation temperatures and a tendency to melt at lower temperatures, compared to systems with sulfate ions. Measurements of the retention behavior of glucose isomerase showed the importance to consider the hydrophobic effect in the process of precipitation and aggregation. The retention volume during HIC depended strongly on the used salts and the pH value of the solution. While HIC experiments with salts containing chloride led to an isoelectric elution of the proteins, systems with salts containing sulfate led to an immobilized of the proteins on the HIC column. Subsequently, these samples could be eluted with a decreasing salt gradient. In the presence of sulfate different retention volumes could be detected depending on the composition of the solution (Fig. 3.1).

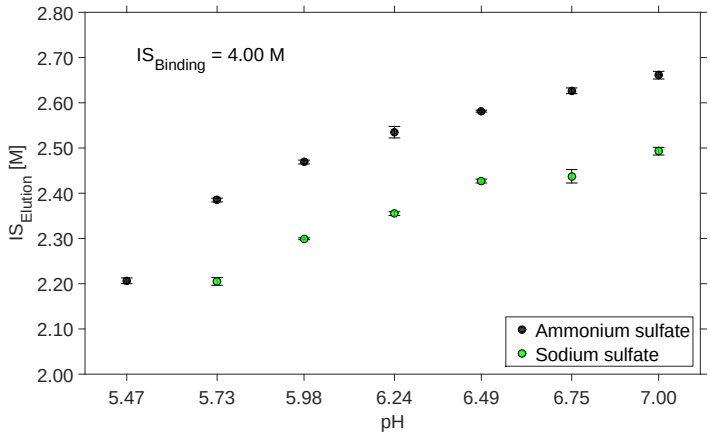

Figure 3.1.: Hydrophobic interaction chromatography elution ionic strength ($IS_{Elution}$) of glucose isomerase at 4.00 M binding ionic strength ($IS_{Binding}$) of sodium sulfate (green) and ammonium sulfate (black) in dependence of the pH value.

The retention volume could be correlated with the pH value of the solution. Higher retention volumes could be measured close to the pI of the protein. These results indicate that the charge of the protein has an important influence on the hydrophobic effect as well. In addition, the retention volumes were higher for systems with salts containing sodium ions compared to salts containing ammonium ions. This in turn could be correlated with the crystal shape. Strong hydrophobic interactions led to small needle-shaped crystals, while moderate attraction led to large tetragonal crystals (Fig. 3.2).

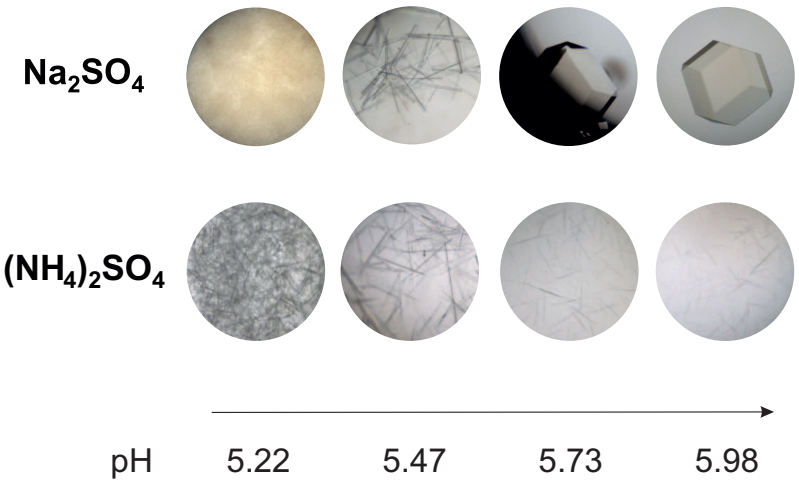

Figure 3.2.: Determined crystal size and form of 10 mg/mL glucose isomerase at an ionic strength of 4.00 M sodium sulfate and ammonium sulfate in the pH range from pH 5.22 to pH 5.98.

The results of this study show how important it is to consider different specific salt effects, to understand the observed protein phase behaviour. The influence of different salt ions and salt concentrations is of great importance, as the purification processes always take place on the background of specific salts from buffers or earlier production steps. In particular, the capture step, after the fermentation of the product, often has to cope with a high salt load. Changing the salt type or ionic strength during the fermentation can be a critical factor for a robust purification strategy. This topic is further discussed in the chapter 5 of this thesis. The different investigated analytical technologies in this study can help to estimate the influence of different salt ions without having to perform long-term storage tests. In addition, this study demonstrates the importance of considering hydrophobic interactions to explain protein phase behavior. The correlation between HIC and protein phase behavior gives the possibility to obtain a mechanistic understanding of the precipitation process. In chapter 4 this correlation was used to derive a mechanistic precipitation isotherm, based on an isotherm previous developed to describe the interaction between a hydrophobic patch and a protein.

4. Water on Hydrophobic Surfaces: Mechanistic Modeling of Polyethylene Glycol-induced Protein Precipitation

Steffen Großhans*, Gang Wang*, Jürgen Hubbuch**

Karlsruhe Institute of Technology (KIT), Institute of Process Engineering in Life Sciences, Section IV: Biomolecular Separation Engineering, Karlsruhe, Germany
* These authors contributed equally to this work
** Corresponding author

Abstract

For the purification of biopharmaceutical proteins, liquid chromatography is still the gold standard. Especially with increasing product titers, drawbacks like slow volumetric throughput and high resin costs lead to an intensifying need for alternative technologies. Selective preparative protein precipitation is one promising alternative technique. Although the capability has been proven, there has been no precipitation process realized for large-scale monoclonal antibody (mAb) production yet. One reason might be that the mechanism behind protein phase behavior is not completely understood and the precipitation process development is still empirical.

Mechanistic modeling can be a means for faster, material-saving process development and a better process understanding at the same time. In preparative chromatography, mechanistic modeling was successfully shown for a variety of applications. Lately, a new isotherm for hydrophobic interaction chromatography (HIC) under consideration

of water molecules as participants was proposed, enabling an accurate description of HIC.

In this work, based on similarities between protein precipitation and HIC, a new precipitation model was derived. In the proposed model, the formation of protein-protein interfaces is thought to be driven by hydrophobic effects, involving a reorganization of the well-ordered water structure on the hydrophobic surfaces of the protein-protein complex. To demonstrate model capability, high-throughput precipitation experiments with pure or prior to the experiments purified proteins lysozyme, myoglobin, bovine serum albumin, and one mAb were conducted at various pH values. Polyethylene glycol (PEG) 6000 was used as precipitant. The precipitant concentration as well as the initial protein concentration was varied systematically. For all investigated proteins, the initial protein concentrations were varied between $1.5\,mg/mL$ and $12\,mg/mL$. The calibrated models were successfully validated with experimental data. This mechanistic description of protein precipitation process offers mathematical explanation of the precipitation behavior of proteins at PEG concentration, protein concentration, protein size, and pH.

4.1. Introduction

Biologics represent a growing share of the pharmaceutical market, reaching global sales of USD 228 billion in 2016 [142]. Among them, monoclonal antibodies (mAb) are the most important family of products [143]. The fact that many mAbs have a relatively low potency requiring high doses makes mAbs among the most expensive drugs [144]. In 2015, the patent of first-generation mAbs began to expire, resulting in a number of biosimilars approved in the USA and Europe [145]. Together with an increasing pressure on healthcare budgets, cost savings are desired [146]. Therefore, improvements in downstream processes such as alternative methods or novel development strategies are necessary [147].

Selective protein precipitation has been known as a cost-efficient alternative purification step for a long time [113]. Phase separation is carried out by adding precipitation agents, such as inorganic salts, organic solvents, or nonionic polymers to the protein solution [57, 89, 148, 149]. Especially, the use of polyethylene glycol (PEG) is favorable as it is not reported to harm the protein by, for example, causing denaturation [68]. For some biopharmaceutical products, precipitation is already well established. For example, ethanol, or PEG precipitation is the basis of the extraction of immunoglobulin G from human plasma [84]. Viral vaccines and virus-like particles (VLP) are purified or concentrated through PEG or salt precipitation [87,

88]. Although there are a lot of studies on precipitation of recombinant mAbs as well, it has not been implemented for large-scale mAb production yet [21, 150, 151].

For downstream process development (DSP), mechanistic understanding is needed to meet the demands of the quality by design (QbD) approach suggested by the US Food and Drug Administration (FDA) [152]. For precipitation, the understanding of protein phase behavior is mandatory [153]. Although protein phase behavior has been well investigated experimentally, the mechanism behind precipitation has not been completely understood. This leads to many degrees of freedom in process development and makes it challenging.

Modeling can reduce the number of experiments and lead to a more thorough process understanding [20]. Cohn *et al.* derived an equation to describe protein precipitation [154]. This equation is a useful empirical expression, but not much of a mechanistic description [155]. Its parameters were specified for salt precipitation and its application to precipitation using polymers was shown [69, 156]. Sim *et al.* generalized the model on the basis of hydrodynamic radii [90]. Quantitative structure-activity relationship (QSAR) modeling was used to estimate the parameters of the Cohn equation [157]. Anyhow, all these models have difficulty dealing with small molecular weight proteins and are not capable to cover variations in the initial protein concentration.

PEG-induced precipitation can be described by the theory of excluded volume [158–160]. According to this theory, adding a certain amount of PEG to a protein solution results in a phase transition of the proteins. The polymers are reported to trap the solvent and, atherefore, sterically exclude proteins from solvent regions occupied by the polymers. In other words, the polymers and proteins compete for the solvent which they are solved in. The theory of attractive depletion introduces osmotic pressure as additional force in the process of PEG-induced protein precipitation [71, 72]. According to this theory, the polymer is sterically excluded from the surface of the protein, the depletion zone. The overlapping of two depletion zones causes a concentration gradient which leads to the described osmotic pressure. In both theories, there is no interaction between PEG and the proteins described; hence, all other forces between particles are still valid. Electrostatic interaction is known to have mainly repulsive influence on protein-protein interaction, so that attractive forces can be reduced to hydrophobic effects [161]. On the molecular level, water molecules next to hydrophobic surfaces are thought to have a well-ordered structure, as opposed to the bulk-like ordered water in free solution [106, 162, 163]. During precipitation, a rearrangement of the protein occurs and the solvent-accessible hydrophobic surface area is reduced. Simultaneously, the water structure has to be reorganized. A new equilibrium between well-ordered and bulk-like water is reached, resulting in an increased entropy [105, 164]. The hydrophobic effect described above is thought to

occur between two proteins in precipitation, as well as between protein and ligand in hydrophobic interaction chromatography (HIC). This means that the mechanism which causes a protein to be retained on an HIC column is analogous to the mechanism that causes proteins to stick together and precipitate. Similarities between HIC and precipitation have been already shown. Melander and Horváth investigated the salt influence on the hydrophobic effect in precipitation and HIC [101]; Nfor and coworkers studied the interrelation between the number of released water molecules in protein precipitation and HIC [165]; Baumgartner and coworkers investigated the retention behavior during HIC and its correlation to protein-protein interaction [1]. The mechanistic effects of HIC are well-investigated [166–168].

In this study, a mechanistic protein precipitation isotherm model was derived, inspired by recent results in HIC modeling [169]. Based on existing precipitation theories, water was introduced as an additional component for the model building. With the help of high-throughput precipitation experiments, data for lysozyme, myoglobin, bovine serum albumin (BSA), and a mAb were generated. For each protein, 50 data points were used to calibrate the model. The three highest protein and the two highest PEG concentrations were excluded and afterward used as validation set (Fig. 4.1.). The model predictability for a wide range of properties such as size, hydrophobicity, and the isoelectric point (pI) was shown.

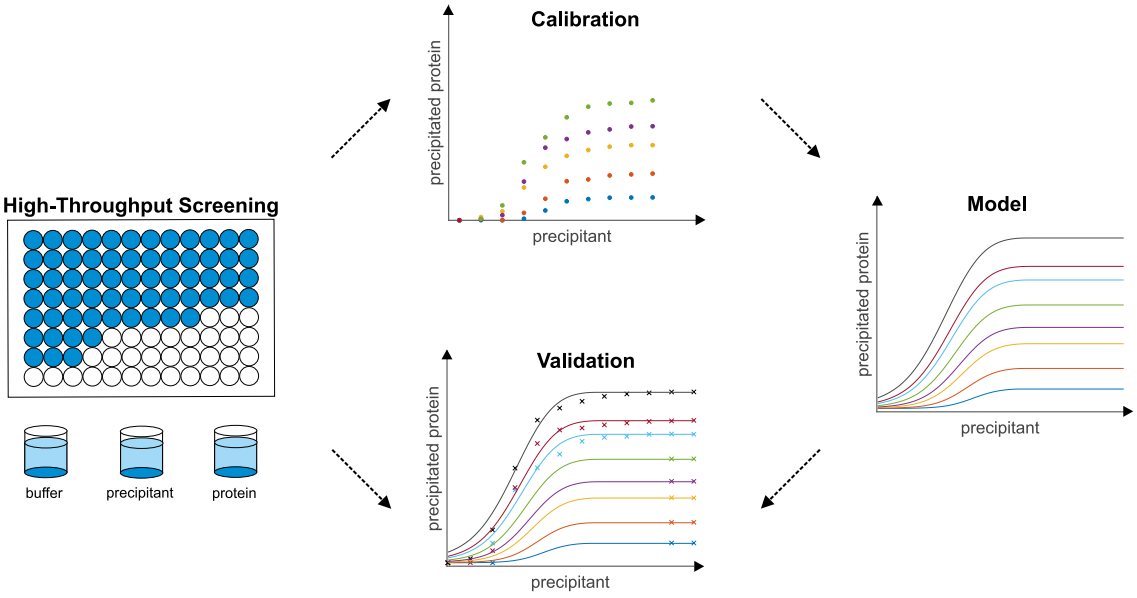

Figure 4.1.: Mechanistic protein precipitation modeling. By varying the amount of buffer, protein and precipitant stock solutions, the precipitant and protein concentration were varied in high-throughput experiments. After phase separation, the protein concentration was detected using UV 280 measurement. 50 Data points were used as calibration set. With this data, the parameters of the model were estimated. The so generated model was validated with the other 46 data points of the experimental data.

4.2. Theory

In 1925, Cohn and coworkers introduced an afterward widely accepted semi-logarithmic equation for modeling protein precipitation:

$$log(C) = C_0 - m\alpha. \tag{4.1}$$

The useful empirical equation describes the protein solubility C in mg/mL in the presence of m PEG in $\%\,(w/w)$. Here, the phase behavior of a constant protein concentration depends on the precipitation efficiency α and the protein solubility in the absence of PEG C_0. This equation represents a summary of a macroscopic observation of the precipitation behavior.

In the present work, the focus is placed on a mechanistic level, especially on the behavior of water molecules during protein precipitation. In the model assumption, the precipitation mechanism of n protein molecules P by a PEG molecule PEG forming the precipitate P_p is considered. The hydrophobic surfaces of proteins are thought to be stabilized by well-ordered water molecules. The precipitate P_p is assumed to be stabilized by β bulk-like ordered water molecules W_B:

$$nP + PEG \rightleftharpoons P_p + n\beta W_B. \tag{4.2}$$

Precipitation using PEG is known to be a fast process [114]. Investigations by Atha and Ingham showed that longer incubation times did not have an influence on the precipitation behavior [69]. Thus, the following equilibrium was considered:

$$\Delta\mu = \mu_{P_p} + n\beta\mu_{W_B} - n\mu_P - \mu_{PEG}. \tag{4.3}$$

The chemical potentials μ are deduced to apply this constraint. It was assumed that the protein surface charges can be considered negligible in the present hydrophobically driven mechanism.

Considering the equilibrium $\Delta\mu = 0$ at constant temperature and pressure, it is

$$\begin{aligned} RT\ln x_{P_p}\gamma_{P_p} \;+\; & n\beta RT\ln x_{W_B}\gamma_{W_B} - nRT\ln x_P\gamma_P - RT\ln x_{PEG}\gamma_{PEG} && (4.4)\\ = \; & -\mu^0_{P_p} - n\beta\mu^0_{W_B} + n\mu^0_P + \mu^0_{PEG} && (4.5)\\ = \; & -\Delta G^0 = RT\ln K. && (4.6) \end{aligned}$$

To simplify the model equation, the activity coefficients of protein, PEG, and

precipitate are assumed to be a constant. The equilibrium constant K is derived

$$K = \frac{x_{P_p} x_{W_B}^{n\beta}}{x_P^n x_{PEG}} \Rightarrow K = \frac{q a_{W_B}^{n\beta}}{c_P^n c_{PEG}} \tag{4.7}$$

with q and c_P being the precipitated protein and protein in solution, respectively. c_{PEG} depicts the concentration of PEG in solution, and a_{W_B} the activity of the bulk-like ordered water molecules. In the following step, parameterizations for a_{W_B} and β have to be found. According to stoichiometric considerations, the number of water molecules involved is linearly correlated to the precipitated protein q. Thus, a linear correlation is proposed to substitute a_{W_B}:

$$a_{W_B}^{n\beta} \cong \nu q^{n\beta}. \tag{4.8}$$

The stoichiometric constant ν is assumed to be independent of the PEG concentration. Inserting Eq. 4.8 into Eq. 4.7, and collecting all constants on the left-hand side, the following isotherm equation is obtained:

$$K = \frac{\nu q^{1+n\beta}}{c_p^n c_{PEG}} \tag{4.9}$$

$$\overset{\cdot\frac{1}{\nu}}{\Longleftrightarrow}: k_{eq} = \frac{q^{1+n\beta}}{c_p^n c_{PEG}}. \tag{4.10}$$

Finally, the PEG and protein dependency of the bulk-like ordered water molecules β is modeled. Since hydration of PEG, protein, and salt ions has high similarities, e.g., attracting water molecules to form a hydration shell, the model originally describing the hydration number of the salt ions h is employed [170]:

$$h = h_0 \exp(-k c_s) \tag{4.11}$$

where h_0 is the ionic hydration number at infinite dilution and k the constant that accounts for the dependency of the hydration number on the ionic concentration c_s. β and h are assumed to be reciprocal, so that the model parameter β can be approximated by the exponential term:

$$\beta = \beta_0 \exp(\beta_1 c_{PEG} + \beta_2 c_{p_0}) \tag{4.12}$$

where β_0 is the hydration number at infinite dilution of PEG and protein, whereas β_1 and β_2 are the constants that account for the dependency of the hydration number on PEG and initial protein concentration, respectively. This completes the derivation of the equilibrium formulation of the precipitation isotherm model.

4.3. Materials and Methods

4.3.1. Disposables

All precipitation experiments were carried out in 350 μL polypropylene flat bottom 96-well micro plates (Greiner Bio-One, Kremsmünster, Austria). For spectroscopic measurements, samples were diluted into Greiner UV-Star® micro plates (Greiner Bio-One, Kremsmünster, Austria).

4.3.2. Chemicals and stock solutions

As buffer substances, sodium hydrogen carbonate and tris(hydroxymethyl)-aminomethane (both Merck KGaA, Darmstadt, Germany) were used. Tris hydrochloride was obtained from PanReac AppliChem (Darmstadt, Germany). Sodium carbonate was obtained from Sigma Aldrich (St. Louis, MO, USA). The PEG with a median molecular mass of 6000 was obtained from Merck KGaA (Darmstadt, Germany). All buffers were prepared with a concentration of 50 mM. For this, the appropriate amounts of associated buffer components were weighed and dissolved in ddH_2O. The desired pH was achieved by varying the amount of acid and basic component for each buffer. For the 40 % (w/w) PEG 6000 and 50 % (w/w) PEG 6000 stock solution, the buffer components were first dissolved in ddH_2O followed by adding the appropriate amount of PEG 6000.

4.3.3. Preparation of protein stock solutions

Lysozyme from chicken egg white was purchased from Hampton Research (Aliso Viejo, CA, USA). Myoglobin and BSA were purchased from Sigma Aldrich (St. Louis, MO, USA). The mAb was provided as purified mAb from LEK d.d. (Ljubljana, Slovenia). Lysozyme, myoglobin, and BSA were provided as lyophilized powder and, therefore, first dissolved in the appropriate buffer. Afterward, all proteins including the mAb were filtered using 0.2 μm cellulose acetate syringe filters (Satorius, Göttingen, Germany). Following the filtration, proteins were rebuffered and desalted into the associated buffer using PD 10 desalting columns (GE Healthcare, Little Chalfont, UK).

4.3.4. Generation of precipitation curves

All precipitation experiments were carried out on a Tecan Freedom Evo 200 System liquid handling station (Tecan, Männedorf, Switzerland). The liquid handling station was equipped with an 8-tip liquid handling arm, a robotic manipulator arm, a Te-Shake orbital shaker, an Infinite® 200 UV-Vis spectrophotometer (all Tecan, Männedorf, Switzerland), and a Rotanta 46RSC centrifuge (Hettlich GmbH & Co. KG, Tuttlingen, Germany). The system was controlled by Evoware 2.5 (Tecan, Männedorf, Switzerland). Excel 2016 (Microsoft, Redmond, WA, USA) was used as data import format and for data storage. All calculations were done using Matlab® R2016a (The Mathworks, Natick, MA, USA). All experiments were carried out at $20°C$, controlled by air-conditioning. Systems with a total volume of $250\,\mu L$ containing varying protein and PEG concentrations were prepared. The PEG concentration was varied in 12 equidistant steps. The protein concentration was varied from $1.5\,mg/mL$ to $12.0\,mg/mL$ in 12 steps. The position for each system on the 96-well micro plate was randomized. After adding the protein stock solution, the system was incubated for $15\,min$ on the orbital shaker at $1000\,rpm$, and followed by $15\,min$ without shaking. To analyze the amount of precipitated protein, the microplate was centrifuged for $30\,min$ at $3400\,g$. Then, the supernatant was sampled and diluted at a ratio of 1:6 for lysozyme, 1:3 for BSA, and 1:4 for myoglobin and the mAb. Subsequently, UV-Vis absorption at $280\,nm$ was measured. The protein concentration was calculated based on a linear calibration curve. For data pretreatment the percentage standard error for each triplicate was calculated. In case of deviations larger than 5 % possible outliers were eliminated.

4.3.5. Numerical procedures

The equilibrium precipitation isotherm model Eqs. 4.10 and 4.12 proposed in the previous section contain unknown parameters, which cannot be determined directly. Model calibration and simulation were carried out in Matlab® R2018a (The Mathworks, Natick, MA, USA). To solve the nonlinear equation, *fsolve* was used. The heuristic algorithm simulated annealing *simulannealbnd* was employed to deliver the parameter estimates for k_{eq}, n, β_0, β_1, and β_2.

The data generated in high-throughput experimentation were split into calibration data and validation data. For model calibration, the three highest protein and the two highest PEG concentrations were excluded. The remaining 50 data points were used to prove the descriptive capability and accuracy of the suggested model. The other 46 data points, used as validation set, were compared with the model prediction to back up the model's accuracy. This data were out of calibration range

and therefore also showed the potential of the model to expand the predictability of the model.

4.4. Results and Discussion

4.4.1. Model calibration

All precipitation data from high-throughput experimentation were divided into two data sets. The calibration data sets contained the five lowest protein and the ten lowest PEG concentrations. With the selection of the calibration data sets the model predictability out of the calibration range should be proved. For paramter estimation simulated annealing with the calibration data sets was used. The equilibrium coefficient k_{eq}, the number of proteins affected by one PEG molecule n, the hydration number at infinite dilution β_0, and the constants accounting for the dependency of hydration number on PEG concentration β_1 and protein concentration β_2 for lysozyme, myoglobin, BSA, and mAb at pH 7.5 and pH 8.5 are given in Table 4.1. Here, the natural logarithm of the k_{eq} is presented for a better overview.

Table 4.1.: Parameters of the precipitation model estimated from the calibration high-throughput experimental data. The natural logarithm of the equilibrium coefficient k_{eq} is presented for a better overview.

parameter	lysozyme	myoglobin	BSA	mAb 7.5	mAb 8.5
$\ln k_{eq}\,[-]$	34.71	15.41	9.78	22.53	19.83
$n\,[-]$	5.55	3.06	2.60	3.65	3.22
$\beta_0\,[-]$	$6.92{\cdot}10^{-3}$	$4.30{\cdot}10^{-4}$	$2.74{\cdot}10^{-3}$	$1.46{\cdot}10^{-2}$	$3.77{\cdot}10^{-2}$
$\beta_1\,[L/mol]$	$9.29{\cdot}10^{1}$	$1.18{\cdot}10^{2}$	$1.40{\cdot}10^{2}$	$2.37{\cdot}10^{2}$	$2.50{\cdot}10^{2}$
$\beta_2\,[L/mol]$	$2.06{\cdot}10^{3}$	$1.51{\cdot}10^{3}$	$1.58{\cdot}10^{3}$	$1.05{\cdot}10^{4}$	$6.61{\cdot}10^{3}$

Fig. 4.2. shows the model simulation as solid curves and the experimental data used for model calibration as dots for lysozyme (Fig. 4.2. (a)), myoglobin (Fig. 4.2. (b)), BSA (Fig. 4.2. (c)), mAb at pH 7.5 (Fig. 4.2. (d)), and pH 8.5 (Fig. 4.2. (e)). In all cases, the results cover eight protein concentrations between $1.5\,mg/mL$ and $12\,mg/mL$ with equidistant steps of $1.5\,mg/mL$. The investigated range of PEG concentrations varies according to the precipitation behavior of each protein. For lysozyme, myoglobin, and BSA, PEG concentrations of up to $0.056\,mol/L$ are shown. The mAb precipitated at lower PEG concentration, so that PEG concentrations of up to $0.02\,mol/L$ are presented.

Despite the very different protein characteristics such as size, hydrophobicity, and surface charge distribution, the calibration data sets are described by the precipitation model accurately in all cases. Regardless of the differences in experimental conditions such as PEG concentration and pH value, a good identifiability of precipitation model parameters is observed. As the smallest protein investigated, lysozyme ($14.6\,kDa$) shows the highest number of proteins affected by one PEG molecule with $n = 5.55$. The slightly larger protein myoglobin ($17.0\,kDa$) shows lower n with 3.06. For all other proteins, the n values were similar to those of myoglobin.

The hydration number constants β_0, β_1, and β_2 of each protein influence the β function in the same order of magnitude. β_1 accounts for the hydration of PEG. Consequently, the behavior can be reconciled with the theory of excluded volume. By adding PEG, the accessible water for the protein is reduced. As this exclusion is caused by a steric phenomenon, the influence can be attributed to protein size, when the PEG species is kept the same. A linear correlation between β_1 and the molecular weight is observed in accordance with the linear correlation of precipitation behavior and the hydrodynamic radius of the protein for PEG as precipitant reported by Sim *et al.* [90]. The similarity of the β_1 values determined for the mAb at pH 7.5 and pH 8.5 supports this assumption. Furthermore, Hämmerling *et al.* confirmed this assumption, but pointed out the influence of additional factors, such as protein shape and other surface characteristics [157].

In the case of mAb, shifting the experimental conditions closer to their pI (pH 8.3-8.5) to pH 8.5 from pH 7.5 leads to decrease of n, and k_{eq} and an increase of β_0, resulting in precipitation of mAb at lower PEG concentrations. At the same time, a decrease in β_2 was observed. While β_1 could be assigned to the protein size, the nature of β_0 and β_2 appears to be more complex. The pH dependence of these parameters suggests a correlation to the surface characteristics of protein. The pH dependency of the hydration number β_0 is consistent with the results delivered by Xia and coworkers [171] suggesting that the water release increases as the buffer pH approaches the protein's pI in HIC. The hydration number parameter β_2 is attributed to the influence of the protein concentration. Closer to the pI, this influence appears to be less important. In the absence of electrostatic interactions, the well-ordered water conformation is reported to be less stable and, therefore, it is favored to set free well-ordered water molecules [172].

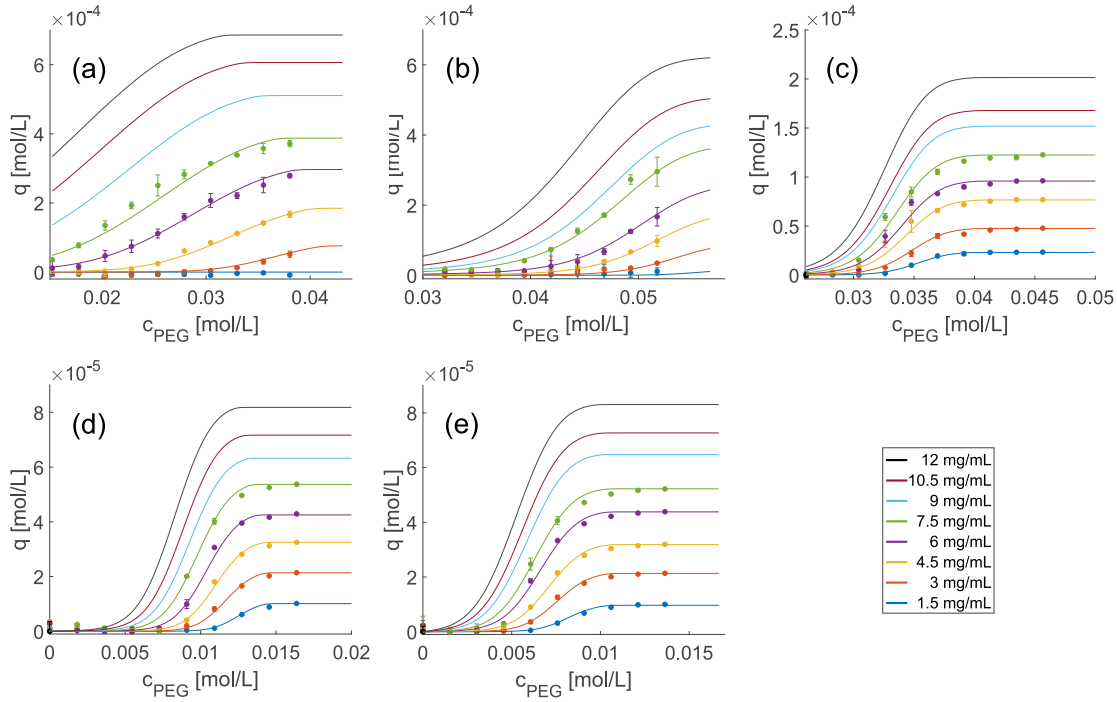

Figure 4.2.: Comparison of model prediction (solid lines) and high-throughput experimental data used for model calibration (dots). Data points represent mean values of at least triplicates. (a) represents lysozyme, (b) myoglobin, (c) BSA, (d) mAb at pH 7.5, and (e) mAb at pH 8.5.

4.4.2. Model validation

To assess the predictive power of the calibrated precipitation models, the validation data sets were used. Precipitation processes using PEG as precipitation agent come with the drawback of highly viscous PEG solution, especially if PEG has to be added as liquid stock solution. In contast to labratory-scale process development or production, the addition of solid PEG is no option for high-throughput screenings. Furthermore, the availability of highly concentrated protein stock solutions is not always given. Hence, using a calibration set containing of low protein and PEG concentration and using the model for expanding the response in both directions can simplify process development and give new options to the production process.

Fig. 4.3. shows the model prediction as solid curves and the experimental data excluded from model calibration as crosses for lysozyme (Fig. 4.3. (a)), myoglobin (Fig. 4.3. (b)), BSA (Fig. 4.3. (c)), mAb at pH 7.5 (Fig. 4.3. (d)), and pH 8.5 (Fig. 4.3. (e)). A very good prediction can be found especially for myoglobin, BSA, mAb at both pH values, and for lysozyme at low protein and, respectively, or at high PEG concentration. For lower PEG concentrations however, the models tend to overestimate the

amount of precipitated protein for all tested proteins. For 12 mg/mL lysozyme the model overestimated the precipitation behavior over the examined PEG range. The root mean square errors of prediction (RMSEP) were $3.22{\cdot}10^{-5}\,mol/L$ for lysozyme, $3.02{\cdot}10^{-5}\,mol/L$ for myoglobin, $7.51{\cdot}10^{-6}\,mol/L$ for BSA, $3.62{\cdot}10^{-6}\,mol/L$ for mAb at pH 7.5, and $2.71{\cdot}10^{-6}\,mol/L$ for mAb at pH 8.5.

Although simplifications and assumptions were made during the precipitation model derivation to balance accuracy with ease of use, predictability and validity are backed up by high-throughput experimental data of very different proteins under diverse operating conditions. The main difference between the widely used models, such as Cohn equation and models related to it, and the proposed precipitation model is its mechanistic nature and capability to describe the protein precipitation process dependent on both PEG and protein concentration.

The validation data showed the predictability of the model even out of the calibration range. This allows a easier and faster model calibration. Furthermore, it opens the possibility using the model for prediction and control of processes with variations in the protein feed concentration.

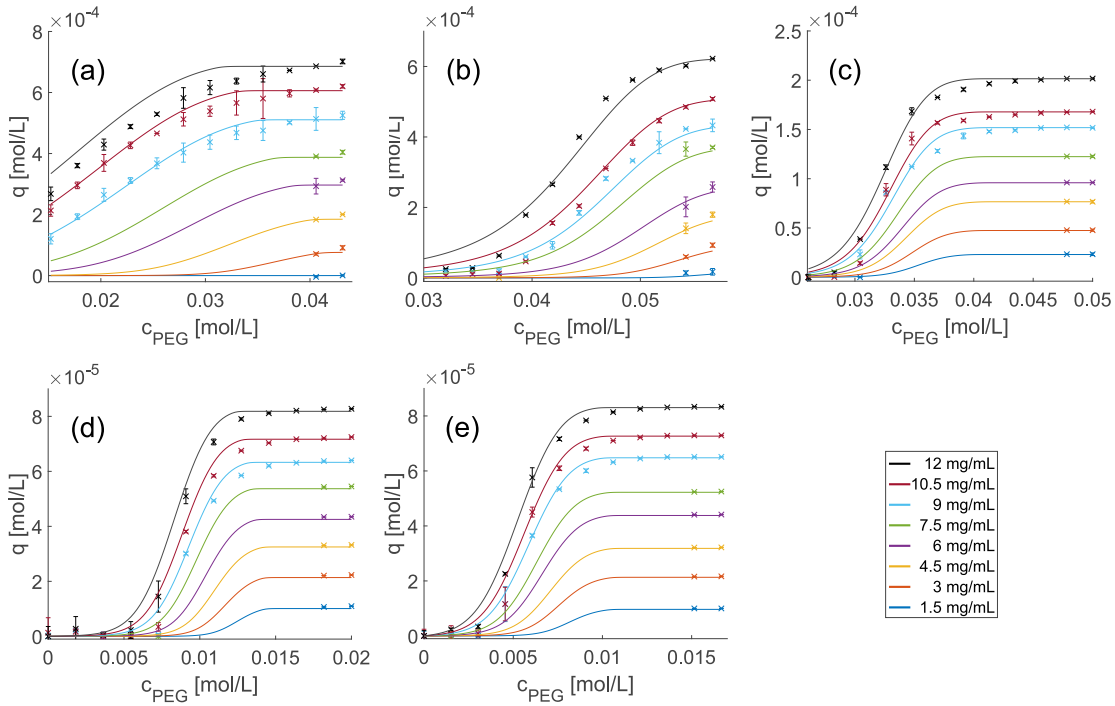

Figure 4.3.: Comparison of model prediction (solid lines) and high-throughput experimental data used for model validation (crosses). Data points represent mean values of at least triplicates. (a) represents lysozyme, (b) myoglobin, (c) BSA, (d) mAb at pH 7.5, and (e) mAb at pH 8.5. The solid lines are identical with Fig. 4.2. and are shown here for comparability.

4.5. Conclusion

In the presented work, a mechanistic model for protein precipitation behavior with PEG was introduced by considering the insights into the water structure on a hydrophobic surface. The present approach proposes the equilibrium between well-ordered and bulk-like ordered water molecules on the hydrophobic surfaces of protein as the driving force for the precipitation process. This equilibrium is described for a constant buffer composition, in particular without change in pH and PEG type.

The model predictability could be proven for the proteins lysozyme, myoglobin, BSA, and mAb at pH 7.5, and the same mAb at pH 8.5 using validation data. The validation data were not included into the model building and beyond the calibration space. The model predictability could be found to be reasonable for proteins investigated despite of their differences in properties such as size, hydrophobicity or charge of the proteins. Th estimated model parameters lead to insights into the precipitation process itself, i.e., the mathematical explanation of proteins' precipitation behavior dependent on their size, pH, and hydration.

In further studies, the dependency of model parameters on changes in pH and PEG type should be investigated to enhance the mechanistic understanding of protein precipitation with PEG. The applicability of the suggested model to protein precipitation with salt-induced precipitation could be tested in a systematic manner. Multi-component systems such as harvested cell culture fluid should be described to enable model-based optimization of selective precipitation processes.

4.6. Acknowledgements

The authors declare no conflict of interest. This project has received funding from the European Union's Horizon 2020 Research and Innovation Programme under grant agreement no. 635557. We thank kindly Frank Hämmerling and Adrian Sanden for the fruitful scientific discussion, and Lek Pharmaceuticals d.d (Menges, Slovenia) for providing the mAb.

5. Precipitation of Complex Antibody Solutions: Influence of Contaminant Composition and Cell Culture Medium on the Precipitation Behavior

Steffen Großhans, Susanna Suhm, Jürgen Hubbuch*

Karlsruhe Institute of Technology (KIT), Institute of Process Engineering in Life Sciences, Section IV: Biomolecular Separation Engineering, Karlsruhe, Germany
* Corresponding author

Abstract

Preparative protein precipitation is known as a cost-efficient and easy-to-use alternative to chromatographic purification steps. This said, at the moment, there is no process for monoclonal antibodies (mAb) on the market, although especially polyethylene glycol-induced precipitation has shown great potential. One reason might be the highly complex behavior of each component of a crude feedstock during the precipitation process. For different investigated mAbs, significant variations in the host cell protein (HCP) reduction are observed. In contrast to the precipitation behavior of single components, the interactions and interplay in a complex feedstock are not fully understood yet.

This work discusses the influence of contaminants on the precipitation behavior of two different mAbs, an IgG1, and an IgG2. By spiking the mAbs with mock solution, a complex feedstock could successfully be mimicked. Spiking contaminants

influenced the yield and purity of the mAbs after the precipitation step, compared to the precipitation behavior of the single components. The mixture showed a decrease in the contaminant and mAb solubility. By re-buffering the mock solution prior to spiking, special salts, small molecules like amino acids, vitamins, or sugars could be depleted while larger ones like HCP or DNA were still present. Therefore, it was possible to distinguish the influence of small molecules and larger ones. Hence, mAb-macromolecular interaction could be identified as a possible reason for the observed higher precipitation propensity, while small molecules of the cell culture medium were identified as solubilisation factors during the precipitation process.

5.1. Introduction

Since the development of the first recombinant biopharmaceuticals, like insulin or monoclonal antibodies (mAb) in the 1980s, the industry has been growing rapidly [173]. The relative low potency of mAbs in combination with the treatment of chronic diseases and cancer currently leads to a high amount for each dose and, consequently, a considerable amount of total mAbs produced. Their success made mAbs one of the most expensive drug classes on the market [144]. In the past, the focus was set on bringing innovative products fast to the market and less on developing cost-efficient processes. Additionally, there was hardly a link between manufacturing costs and the cost of the final product [14]. Restricted healthcare budgets and the development of bio-similars, the first monoclonal antibody having been approved in 2013 by the European Medicines Agency (EMA), however, raised the need for a more economic production [174, 175].

Currently, mAbs are mostly manufactured using platform processes, consisting of batch/fed-batch or perfusion cell cultures, followed by the respective downstream process. The downstream process is mainly a combination of chromatography steps. For the capture step, Protein A affinity chromatography is still the most common technique. High resin costs and slow volumetric throughput make this step an easy-to-use, but expensive unit operation [176]. In upstream process development (USP), higher cell densities and cell culture titers led to an increase in process efficiency [177]. With perfusion cell cultures, titers up to $25\,mg/mL$ were reported [147]. These efforts lead to a demand for new and cost-efficient alternative techniques for downstream process development (DSP). These methodologies need to be comparable to the purification performance of the chromatography step.

Selective protein precipitation has shown promising results such as cost-efficient alternatives. Particularly for small-scale production, PEG as precipitation agent has

shown its potential as easily scalable and simple technique [23, 178]. At best, the mAb is selectively precipitated while the contaminants stay in solution. New techniques such as high-throughput process development (HTPD), design of experiment (DoE), or model-based approaches can help to make precipitation process development faster and with less brute force [2, 26, 90]. However, huge variations in the host cell protein (HCP) reduction were seen for different investigated mAbs [21]. Especially for the development of a generic mAb platform process, a better understanding of the precipitation mechanism is mandatory. Most studies, hence, have aimed more at efficient process development of one mAb feedstock and less at a detailed understanding of the complex behavior of components among each other.

For single protein solutions, much effort was put into the understanding of the mechanism of PEG-induced protein precipitation [68, 179, 180]. In general, precipitation using PEG can be described with two theories. According to the theory of excluded volume, the polymers are reported to trap the solvent and sterically exclude proteins from the solvent region occupied by the polymer [158, 159, 181]. Because this is a steric effect, the selectivity of PEG-induced protein precipitation is given by the size of the proteins. Proteins with a larger hydrodynamic radius tend to precipitate at lower PEG concentrations compared to proteins with a smaller hydrodynamic radius. The theory of attractive depletion further introduces osmotic pressure as additional force to the precipitation process [71, 72]. This force is caused by the steric exclusion of the PEG molecules from the ambiance of the proteins, the depletion zone. When two depletion zones overlap, a PEG-free area is created, and a concentration gradient towards the bulk is formed. This gradient leads to the described osmotic pressure. In both theories, there is no direct interaction between the protein and the polymers described. All other forces between particles, such as electrostatic or hydrophobic interactions, are still valid. This fact makes PEG-induced protein precipitation a function of changes in process conditions, such as pH or conductivity.

In opposite to single protein solutions, there is only little research on the precipitation behavior of protein mixtures. Mahadevan and Hall developed a theory describing the precipitation of protein mixtures by nonionic polymers using statistical mechanics [182]. Coen and co-workers investigated the phase behavior of aqueous binary protein mixtures containing either lysozyme-chymotrypsinogen or lysozyme-ovalbumin [183]. Solms *et al.* developed a thermodynamic framework for the description of a phase diagram of a lysozyme-ovalbumin system [184]. Sieberz *et al.* investigated the influence of model proteins as contaminants on the precipitation behavior of mAbs during an polyelectrolyte preciptiation process [185]. All these findings suggest, on the one hand, that the protein-protein interaction influences the protein phase behavior and, on the other, that this influence is not simply a linear or otherwise geometric combination of pure species interaction terms [186].

When developing a preparative precipitation process, not only a binary protein system has to be looked at, but the challenge is rather to purify one protein out of a complex multi-component system. Beside other proteins such as host cell proteins (HCP), small molecules like endotoxins, vitamins, or small cell culture media additives are present as contaminants as well and have to be removed [116]. The influence of small molecules on single proteins, known as osmolytes or co-solutes, is reported in many studies and can be explained by the preferential interaction theory [63, 187, 188]. According to the theory, originally developed by Timasheff *et al.*, the co-solvents either preferentially interact with the protein or with water [62]. A preferential interaction of the co-solvent with the protein, also known as salting-in, leads to an increase in the colloidal stability of the protein. On the contrary, a preferential interaction with water leads to a destabilization of the system, known as salting-out.

Thus, the purification of a mAb out of a complex feed stock might be influenced by a multitude of contaminants and interactions. Changes in USP can lead to variations in pH, conductivity, contaminant profile, or product titer. These variations, in turn, can possibly influence the precipitation efficiency in terms of yield or purity. Especially with a focus on a platform-based approach to processes using precipitation, the focus should not be limited to the optimizing of one unit operation alone. An integrated process development of up- and downstream is necessary [189].

The aim of this study is to investigate the influence of contaminants and their composition on the precipitation behavior on a preparative mAb precipitation. A workflow of the presented study is illustrated in Fig. 5.1.. Precipitation curves of two purified mAbs at varying concentrations were generated using high-throughput experiments. These results were compared with the precipitation behavior of the same mAbs spiked with mock solution from a Chinese hamster ovary (CHO) cell line. Through this experimental setup, a complex feedstock was imitated. This allows to investigate the influence of a complex feedstock on different mAbs as well as different mAb concentrations. To explain the observed differences in the precipitation behavior, the mAbs were also spiked with purified re-buffered mock solution. Thereby, it was possible to exclude the variations caused by different pH values or conductivities and focus on the influence of protein-contaminant interactions. Finally, the re-buffered mock solution was spiked with fresh cell culture media prior to the precipitation to investigate the influence of the small molecules solved in the cell culture media on the observed interactions.

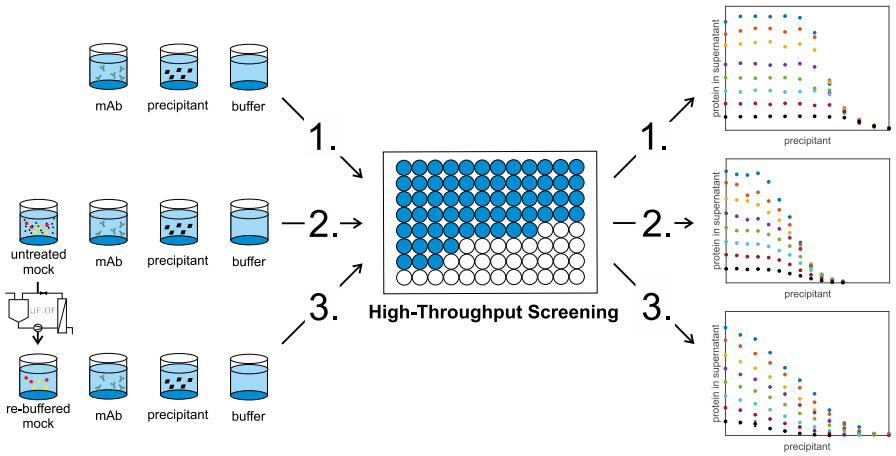

Figure 5.1.: Schematic overview of the workflow for the precipitation experiments carried out in this study. For high-throughput experiments, mAb, mock, precipitant, and buffer stock solutions were mixed on a liquid handling station with varying concentrations. Two different mock solutions were investigated. One was used without pretreatment, the other one was re-buffered prior to use. After phase separation, the supernatant of each system was investigated for mAb and contaminant concentration.

5.2. Materials and Methods

All precipitation experiments were carried out in 350 μL polypropylene flat-bottom 96-well micro plates (Greiner Bio-One, Kremsmünster, Austria). For spectroscopic measurements, samples were diluted into Greiner UV-Star® micro plates (Greiner Bio-One, Kremsmünster, Austria).

5.2.1. Chemicals and stock solutions

All buffer solutions were prepared using water purified by a PURELAB Ultra water purification system (ELGA Labwater, High Wycombe, UK). As buffer substances, tris(hydroxymethyl)-aminomethane (Merck KGaA, Darmstadt, Germany) and tris hydrochloride (PanReac AppliChem, Darmstadt, Germany) were used. The polyethylene glycol (PEG) with a median molecular mass of 6000 g/mol was obtained from Merck KGaA (Darmstadt, Germany). All buffers were prepared with a buffer capacity of 50 mM. The desired pH was achieved by varying the amount of acid and basic component for each buffer. For the 40 % (w/w) PEG stock solution, the buffer components were first dissolved in ddH_2O. Then, the appropriate amount of PEG

was added. RPMI Medium 1640 (1x) + GlutaMAX™ (Thermo Fisher Scientific, Waltham, MA, USA) was used for spiking the samples with cell culture media.

5.2.2. Preparation of protein stock solutions

Two mAbs, A and B, were provided as purified solutions from Novartis (Basel, Switzerland). Additionally, mAbA was provided as harvested cell culture fluid (HCCF). The characteristics of the mAbs are listed in Tab 5.1. Further more, Novartis supplied a mock solution originating from the same cell line used for the mAb fermentation. When mimicking a complex mAb solution, the mock solution was spiked with varying concentrations of purified mAbs. All protein solutions were filtered using $0.2\,\mu m$ cellulose acetate syringe filters (Sartorius AG, Göttingen, Germany) before usage or further pretreatment. All provided protein and feed solutions were stored at $-80\,°C$ for long-term and at $-30\,°C$ for short-term storage, after aliquotation.

Table 5.1.: Characteristics of the utilized protein and contaminant stock solution

Molecule	mAbA purified	mAbA HCCF	mAbB purified	Mock untreated	Mock re-buffered
Type	IgG2	IgG2	IgG1	-	-
Molecular mass $[kDA]$	144.7	144.7	144.2	-	-
pI	8.3-8.5	8.3-8.5	8.3	-	-
mAb $[mg/mL]$	27.3	3.3	22.3	-	-
HCP $[mg/mL]$	< 0.01	1.26	< 0.01	1.04	3.18

5.2.3. Pretreatment of the protein stock solution

After filtration, the purified mAb was re-buffered and desalted into the $50\,mM$ tris buffer pH 7.5 using PD 10 desalting columns (GE Healthcare, Little Chalfont, UK). The mock solution was divided into two parts. One part was spiked later to the mAb without further pretreatment. The other part was re-buffered to $50\,mM$ tris buffer pH 7.5 using a KrosFlow Resarch IIi tangential flow filtration (TFF) system (Spectrum Labs, Breda, Netherlands). To restrain larger contaminants like HCP or DNA and deplete small molecules present in the HCCF, the TFF system was equipped with a $10\,kDa$ modified polyethersulfone (mPES) MicroKros® hollow fiber filter module (Part number: C04-E010-05-S) and an automated back-pressure valve

(both Spectrum Labs, Breda, Netherlands). The process was performed with a flow rate of 27 mL/min, a transmembrane pressure (TMP) of 0.6 bar, and a shear rate of 5800 $1/s$. First, the mock solution was concentrated fivefold in ultrafiltration mode (UF). Subsequently, the mock solution was re-buffered into 50 mM tris buffer over 5 diafiltration volumes (DV). The concentration of both mock stock solutions is listed in Tab. 5.1.

5.2.4. Analytical methods

To determine the component content and size distribution, the UHPLC system ultimate 3000RSLC, controlled with Chromeleon 6.8 (both Thermo Fisher Scientific, Waltham, MA, USA) was used. For mAb concentration and contaminant content, the ultra-high performance chromatography (UHPLC) system was equipped with a Poros analytical Protein A column (Thermo Fisher Scientific, Waltham, MA, USA). The mAb concentrations were calculated by integration of the elution peak area, using calibration curves. The corresponding contaminant content was measured by integration of the flow-through peak. Analytical size exclusion chromatography (SEC) was performed using a TSKgel SuperSW mAb HTP column (TOSOH, Tokio, Japan). For conductivity measurements, a CDM 230 conductivity meter (Radiometer Analytical SAS, Lyon, France) was used. HCP concentration of the mock solutions was determined using a microfluidic CD-based ELISA-like assay on the Gyrolab XPlore station controlled by Gyrolab (Gyros AB, Uppsala, Sweden).

5.2.5. High-throughput method for precipitation screening

Precipitation experiments were carried out on a Tecan Freedom Evo 200 System liquid handling station (Tecan, Männedorf, Switzerland). The liquid handling station was equipped with an 8-tip liquid handling arm, a 96-MultiChannel Arm® (MCA), a robotic manipulator arm, a Te-Shake orbital shaker, an Infinite® 200 UV-VIS spectrophotometer (all Tecan, Männedorf, Switzerland), and a Rotanta 46RSC centrifuge (Hettich GmbH & Co. KG, Tuttlingen, Germany). The system was controlled by Evoware 2.5 (Tecan, Männedorf, Switzerland). Excel 2016 (Microsoft, Redmond, WA, USA) was used as data import format and for data storage. All calculations were done using Matlab® R2018a (The Mathworks, Natick, MA, USA). All experiments were carried out at 22 $°C$, controlled by air conditioning. To avoid evaporation of the systems, the microplates were capped prior to each incubation or centrifugation step. Systems with a total volume of 200 μL containing varying mAb, mock, and PEG concentrations were prepared. The PEG concentration was varied in 12 equidistant steps. For mAbA, the PEG concentration was varied from 0 % (w/w)

to 10% (w/w), for mAbB from 0% (w/w) to 14% (w/w). The mAb concentration was varied from 1 mg/mL to 8 mg/mL in 8 equidistant steps in the case of mAbA, and from 1 mg/mL to 5 mg/mL in 5 equidistant steps for mAbB. For systems containing mock solution, the mock concentration was adjusted referring to a HCP concentration of 0.5 mg/mL, in each system. When cell culture medium was added to the samples, the added volume was kept equal to that of the mock solution. To avoid systematic errors due to automated pipetting, the position for each system on the 96-well micro plate was randomized. After adding the protein stock solution, the system was incubated for 15 min on the orbital shaker at 1000 rpm to ensure complete mixing of the system. Following the system was incubated for additional 15 min incubation time without shaking. To analyze the amount of precipitated protein, the microplate was centrifuged for 30 min at 3400 $times\, g$. Then, the supernatant was sampled and diluted at a ratio of 1:2 or 1:3, depending on the initial mAb concentration to avoid detector saturation. Subsequently, analytics of the generated samples were performed using either UV-VIS spectroscopy for systems containing only mAb, or UHPLC for complex mAb solutions.

5.3. Results

In this study, the precipitation behaviors of two mAb species using PEG as precipitation agent were investigated. Particularly, the focus was set on the influence of contaminants on the phase behavior of the mAbs and vice versa, as well as on the influence of the mAb on the co-precipitation of the contaminants. In a process based on preparative precipitation, the yield of the precipitation step is defined by the precipitation behaviour of the mAb, while the purity is influenced by the precipitation behavior of the contaminants.

To identify variations in the precipitation behavior through the presence of contaminants in mAb solutions and to determine critical process parameters, three sets of experiments were conducted. Precipitation curves of pure mAb solutions were compared to precipitation curves of mAb spiked with untreated and re-buffed mock solution. To imitate a complex mAb feed and, therefore, to investigate the influence of all present contaminants in a cell culture fluid, the mAb was spiked with untreated mock solution. To distinguish between small molecules and molecules larger than 10 kDa, like HCP or DNA, the mAb was spiked with re-buffered mock solution. At the same time, a defined environment could be created, and influencing factors like pH, or buffer components were excluded.

To identify critical process conditions, the influence of conductivity and the cell culture media on the precipitation behavior was investigated in further experiments.

5.3.1. Solubility of the mAbs

To investigate the precipitation behavior of mAbs, the concentrations of two pure mAb species in supernatant after phase separation were measured. Therefore, the initial mAb and the PEG concentration were varied. The results were compared to the solubility of the same initial mAb concentrations spiked with two different mock solutions (Fig. 5.2.). Solubility data of the two pure mAb species in the supernatant after precipitation at varying initial mAb and PEG concentrations is shown in Fig. 5.2. (a), (b). For all investigated mAbA concentrations (Fig. 5.2. (a)), the mAb was completely soluble at PEG concentrations below 4.5 %(w/w). Above this concentration, the solubility was depending on the initial mAb concentrations. Anyhow, all investigated mAbA concentrations approach to the same solubility line. At 10 %(w/w) PEG, mAbA was completely precipitated for all examined mAb concentrations. Compared to these results, mAbB showed a higher solubility and was completely soluble at PEG concentrations below 7.64 %(w/w) (Fig. 5.2. (b)). Independent of the initial mAb concentration, mAbB was completely precipitated at 14 %(w/w) PEG.

To investigate the influence of contaminants on the precipitation behavior, the mAb solutions were spiked with two different mock stock solutions. The added mock solution volume was normalized to a HCP concentration of 0.5 mg/mL. To study the influence of all contaminants present in the cell culture fluid, small ones like sugars, amino acids but also larger ones like HCP or DNA, the mAb solutions were spiked with untreated mock solution. The results are shown in Fig. 5.2. (c), (d). To distinguish between the influence of an entire cell culture fluid and components with a size larger than 10 kDa, like HCP, or DNA, the mock solution was re-buffered prior to spiking. The results are shown in Fig. 5.2. (e), (f). Adding contaminants to the mAbs lowered the solubility at each PEG concentration for both investigated mAbs. Thus, the PEG concentration needed for causing precipitation, was lower comparing pure mAb systems with both spiked ones. For systems with re-buffered mock solution, the solubility decrease was even more pronounced. For a concentration of 8 mg/mL mAbA, the initial PEG concentration needed to precipitate the mAb dropped from 4.5 % (w/w) PEG for the pure mAb solution to 2.7 % (w/w) PEG for the mAb solution spiked with untreated mock solution. For mAbA spiked with re-buffered mock solution, precipitation started at 0.9 % (w/w) PEG. For 5 mg/ml mAbB, initial precipitation was observed at 5.09 % (w/w) PEG when the solution was spiked with untreated mock solution. Spiking mAbB with re-buffered mock solution led to precipitation at 1.29 % (w/w) PEG. Furthermore, there was no approach to the same solubility line detectable for the spiked samples, comparing different initial mAb concentrations. Comparing the precipitation behavior of the same initial mAb concentrations, the spiked samples showed a higher precipitation propensity overall and a flattened solubility line.

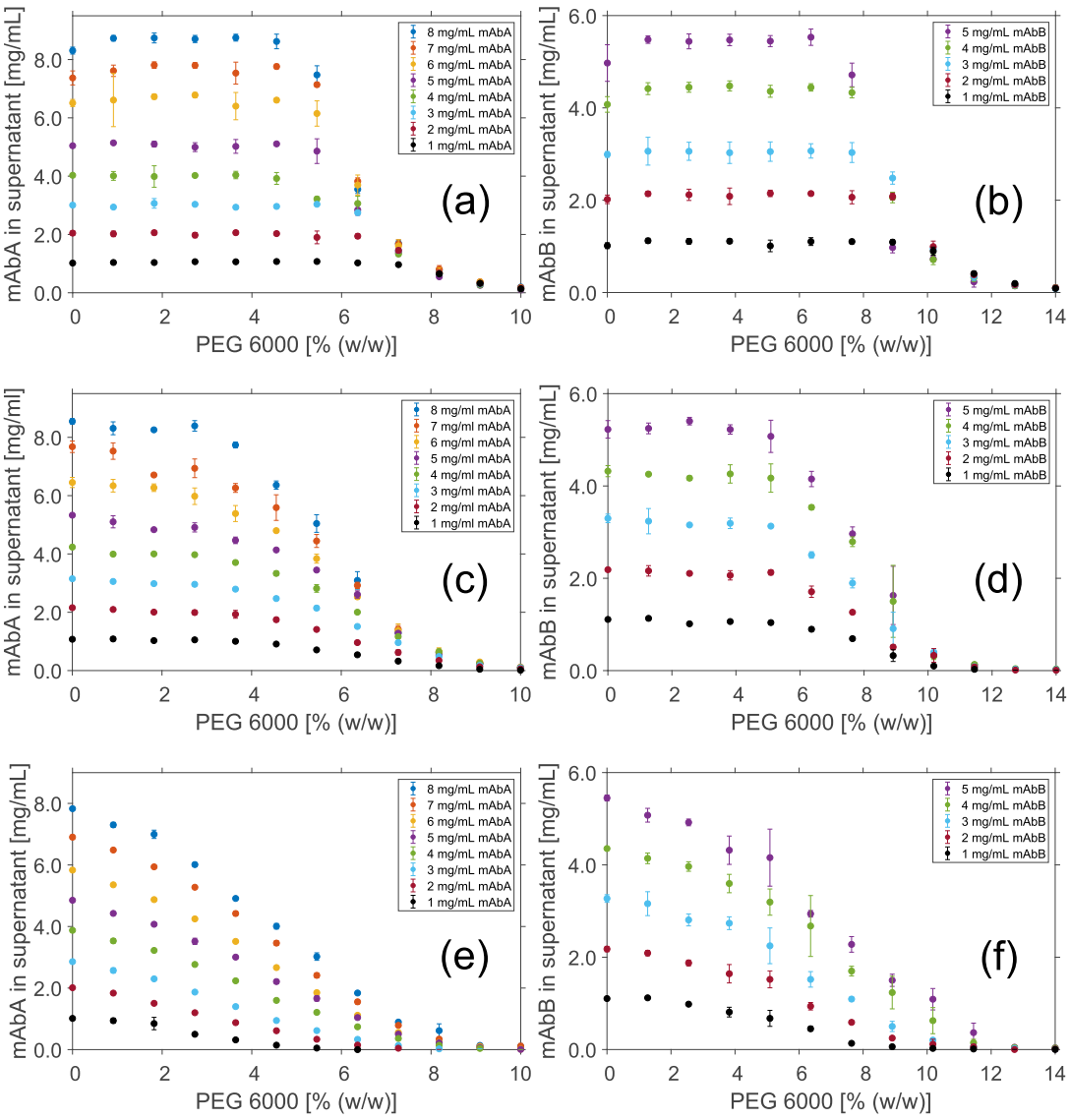

Figure 5.2.: Solubility data of mAbA (a, c, e) and mAbB (b, d, f) in the supernatant after phase separation at varying mAb and PEG concentrations. Data points represent the mean value of triplicates. All experiments were conducted using 50 mM tris buffer at pH 7.5. (a) and (b) Purified mAb was precipitated. (c) and (d) The mAb was spiked with untreated mock solution containing 0.5 mg/mL HCP each. (e) and (f) The mAb was spiked with re-buffered mock solution containing 0.5 mg/mL HCP each. The mock solution was re-buffered to 50 mM tris pH 7.5.

Developing a preparative precipitation process, the precipitation propensity of the mAb can be linked directly to the yield of the purification step. For all investigated conditions mAb yield after the precipitation did depend on the initial mAb concentration, as well as on the contaminant composition. For an initial mAbA concentration of $1\,mg/mL$ the highest yield for samples containing pure mAb solution was reached at $10\,\%\,(w/w)$ PEG with a value of $86\,\%$. However, previous studies have shown that a yield of up to $98\,\%$ can be achieved after precipitation [4]. In this work, this value was reached for $1\,mg/mL$ mAb concentrations at $10\,\%\,(w/w)$ PEG when untreated mock solution was spiked before. For solutions containing re-buffered mock solution $98\,\%$ yield were reached at $6.36\,\%\,(w/w)$ PEG. At an initial mAbA concentration of $8\,mg/mL$ the maximum yield for the pure mAb solution was $97.6\,\%$. For solutions containing untreated mock solution the $98\,\%$ yield was reached at $10\,\%\,(w/w)$ PEG. For samples containing re-buffered mock solution $9.08\,\%\,(w/w)$ PEG were therefore necessary. For mAbB trends were comparable to that of mAbA. At $1\,mg/mL$ initial concentration of mAbB a maximum yield of $92\,\%$, and for $5\,mg/mL$ mAbB a maximum yield of $98\,\%$ could be observed at $14\,\%\,(w/w)$ PEG. For mAbB spiked with untreated mock solution $98\,\%$ yield were reached at $12.73\,\%\,(w/w)$ PEG for all investigated initial mAbB concentrations. For an initial mAbB concentration of $1\,mg/mL$, spiked with re-buffered mock solution $98\,\%$ yield were reached at $11.45\,\%\,(w/w)$ PEG. At $5\,mg/mL$ initital concentration of mAbB, $12.73\,\%\,(w/w)$ PEG were necessary to reach the target yield.

While the precipitation propensity of the mAbs determines the yield, the precipitation behavior of the contaminants affects the purity of the process. Therefore, the solubility of the contaminants was measured as well.

5.3.2. Solubility of contaminants

The amount of the contaminants in the supernatant after phase separation is shown in Fig. 5.3.. Prior to the addition of PEG, each system was spiked with one of the two utilized mock solutions, normalized to a HCP concentration of $0.5\,mg/mL$. With increasing PEG concentration, the solubility of the contaminants decreased. This decrease was less pronounced comparing samples spiked with untreated mock solution (Fig. 5.3. (c), (d)) to samples spiked with re-bufferd mock solution (Fig. 5.3. (e), (f)). For systems containing $8\,mg/mL$ mAbA and untreated mock solution, the solubility dropped to $87\,\%$ of the initial amount at $10\,\%\,(w/w)$ PEG. For the same mAbA and PEG concentrations, the amount dropped to $25\,\%$ when re-buffered mock solution was utilized. For mAbB, a higher contaminant solubility and therefore less precipitation was observed in the same PEG range. Like for mAbA, using re-buffered mock solutions led to a higher amount of precipitated contaminants compared to untreated mock solution.

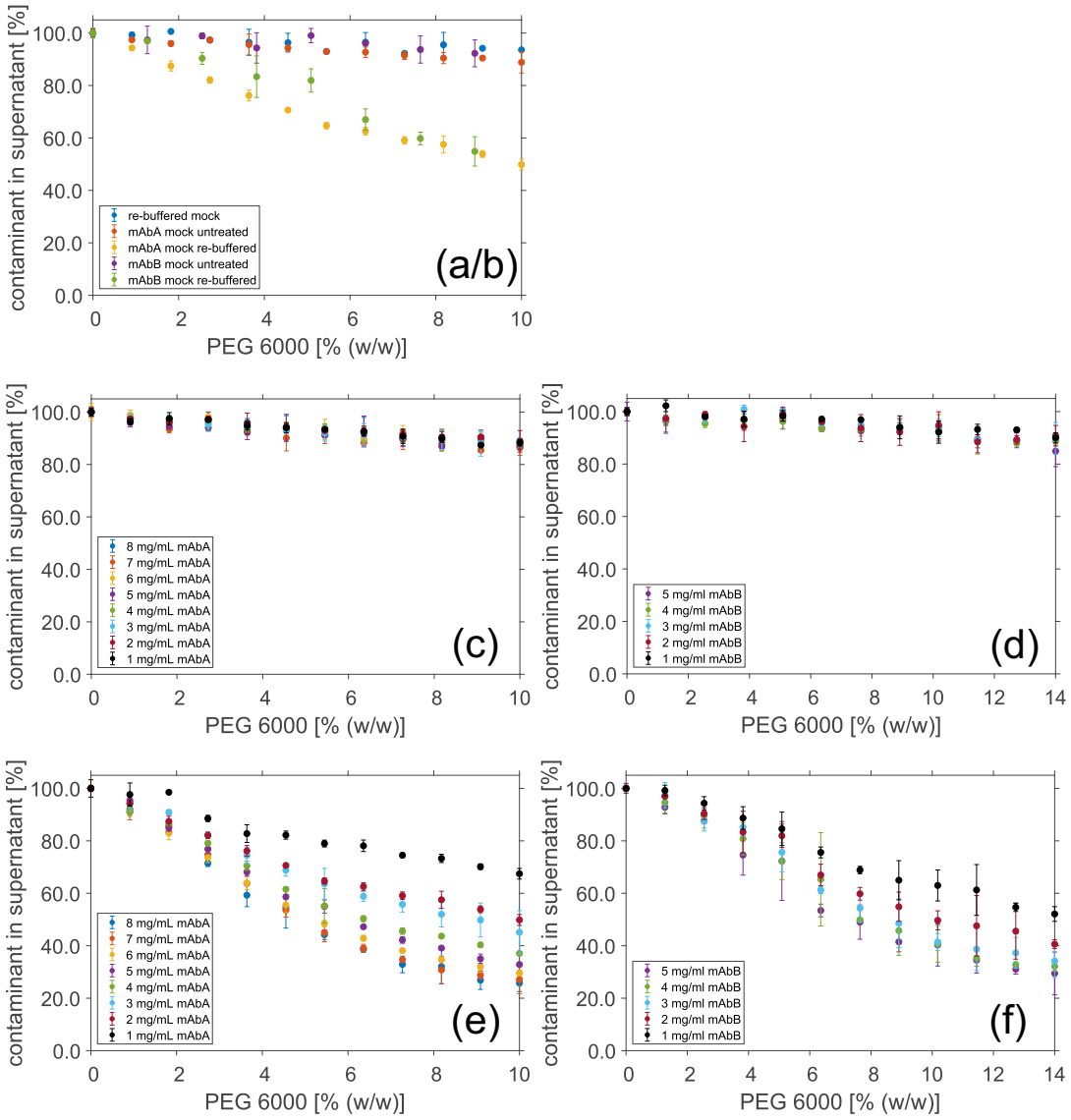

Figure 5.3.: Solubility data of mAbA (a, c, e) and mAbB (b, d, f) in the supernatant after phase separation at varying mAb and PEG concentrations. Data points represent the mean value of triplicates. All experiments were conducted using 50 mM tris buffer at pH 7.5. (a) and (b) Purified mAb was precipitated. (c) and (d) The mAb was spiked with untreated mock solution containing 0.5 mg/mL HCP each. (e) and (f) The mAb was spiked with re-buffered mock solution containing 0.5 mg/mL HCP each. The mock solution was re-buffered to 50 mM tris pH 7.5.

For samples spiked with untreated mock solution, the solubility showed no dependence on the initial mAb concentration. In contrast, the solubility of the re-buffered contaminants could be connected to the initial mAb concentration in each system. With higher mAb concentrations, lower solubility of the contaminants was detected. This behavior was shown for both investigated mAbs.

In Fig. 5.3. (a/b), systems with $2\,mg/mL$ mAbA and mAbB spiked with mock solution are compared to systems containing pure mock solution without addition of mAb. Comparing the samples with mAb and untreated mock solution to pure-mock solution samples, the solubility of the contaminants was lowered by the addition of mAbA. For the pure mock solution samples, a contaminant solubility of 94.6 % of the initial amount was detected at 10 % (w/w) PEG. For the samples of mAbA spiked with untreated mock solution, the residual solubility was 88.9 %, and for samples containing mAbB, the amount was 94.7 %. By comparison, spiking the mAb with re-buffered mock solution lowered the solubility of the contaminants significantly. At 10 % (w/w) PEG, 54.0 % of the initial contaminant amount was detected for samples containing mAbA, and 49.7 % for samples containing mAbB.

Purities after the precipitation step were calculated from the solubility measurements of the impurities and the mAbs. The purity was dependent on the initial mAb concentration, but also on the kind of added mock solution. For the highest investigated PEG concentration and an initial mAbA concentration of $1\,mg/mL$, a purity of 95 % was determined when untreated mock solution was added. At the same initial mAbA concentration, this value dropped to 86 %, when re-buffered mock solution was spiked. For an initial concentration of $8\,mg/mL$ mAbA, the purity was 99 % for samples containing untreated mock solution compared to 94 % for samples containing re-buffered mock solution. Similar trends could also be observed for mAbB. The calculated purities at the highest investigated PEG concentration for samples containing untreated mock solutions were 93 % and 99 % for an initial mAbB concentration of $1\,mg/mL$, respectively $5\,mg/mL$. For samples containing re-buffered mock solution, the purities were 82 %, respectively 96 %, for $1\,mg/mL$, respectively $5\,mg/mL$ mAbB.

The observed differences between untreated and re-buffered mock solution suggest that the differences are caused by small molecules depleted through the UF/DF step. To exclude possible influences of the UF/DF step itself or mixing on the liquid handling station, additional experiments were conducted. Subsequently, the influence of conductivity and fresh cell culture media was examined.

5.3.3. Comparison of the utilized mock solutions

UF/DF of protein solutions can lead to a higher aggregation level, and the protein size is known to be a significant parameter for PEG precipitation [190]. To prove the integrity of the re-buffered mock solution, the size distributions of both mock solution samples were compared using analytical size exclusion chromatography (SEC), displayed in Fig. 5.4.. Until 6.5 min retention time, both chromatograms show a similar peak profile. After this, the UV signal differs, and for the untreated mock solution, an additional peak was detected. Based on the size standard, molecules eluting after this time have a molecular weight smaller than 14 kDa.

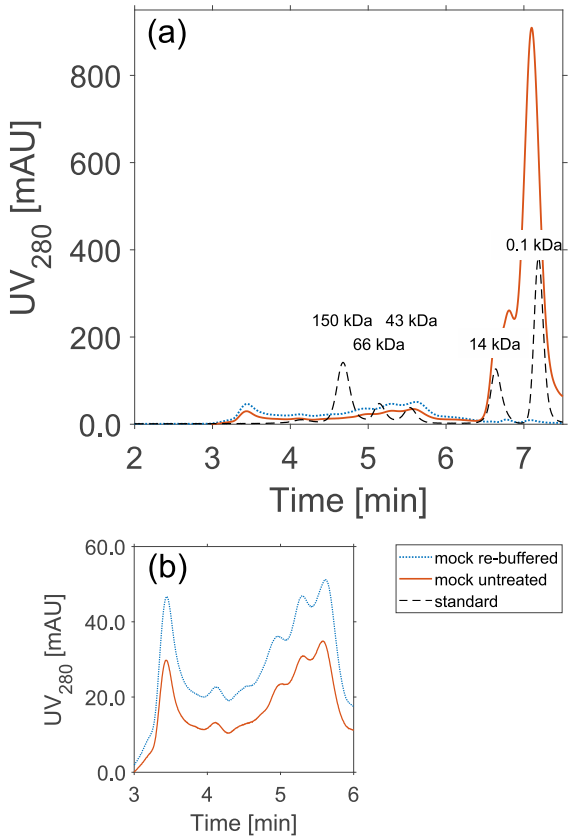

Figure 5.4.: SEC chromatogram of untreated (solid line) and re-buffered (dotted line) mock solution samples. (a) Referred to the size standard (dashed line), molecules above 6.6 min are smaller than 14 kDa. (b) Displays the magnified details of the size distribution of both utilized mAbs.

Beside the UF/DF, mixing the solutions on the liquid handling station is an additional factor in the used experimental setup, which might cause the observed deviations.

Spiking mock solution to the mAb solutions comes along with an additional mixing step of mAb and mock solution, comparing the imitated crude feed stock to the actual HCCF. Hence, the phase behavior of spiked mAbA samples was compared to that of mAbA provided as HCCF (Fig. 5.5.). Comparing the precipitation behavior of the HCCF to that of purified mAbA spiked with untreated mock solution, only minor changes could be detected. Compared to these, the systems with purified mAbA and re-buffered mock solution showed a lower solubility for each investigated PEG concentration.

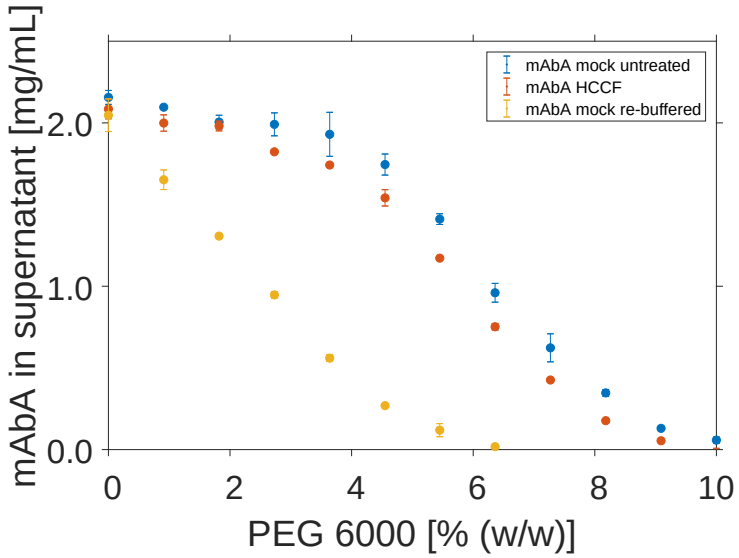

Figure 5.5.: Solubility data of mAbA in the supernatant after phase separation at varying PEG concentrations. Data points represent the mean value of triplicates. Comparison of mAbA provided as HCCF, purified mAbA spiked with untreated mock solution, and purified mAbA spiked with re-buffered mock solution. All experiments were conducted using 50 mM tris buffer at pH 7.5 and a mAbA concentration of 2 mg/mL.

As no influence of the experimental setup could be shown, the different phase behaviors of the mAb and contaminants had to be caused by differences in the composition of untreated and re-buffered mock solution. Due to re-buffering the mock solution, small molecules were depleted. Consequently, the conductivity of the re-buffered solution decreased from 9.91 mS/cm to 3.5 mS/cm. To study this effect on the precipitation behavior, the conductivity of the re-buffered mock solution was adjusted to 9.91 mS/cm again, using a 1 M NaCl solution. Afterwards, the solubility of mAbA and the contaminants was measured at a mAbA concentration of 3 mg/mL. The results were compared to the precipitation behavior of the mAb spiked with unadjusted mock solution (Fig. 5.6.). For the mAb solubility (Fig. 5.6. (a)) as well as for the solubility of the contaminants (Fig. 5.6. (b)), no significant influence of the conductivity was detected.

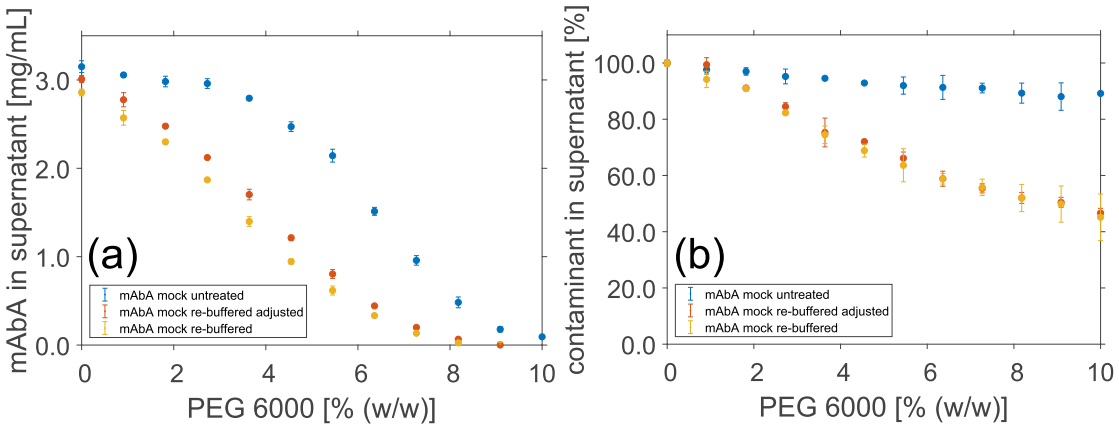

Figure 5.6.: Solubility data of mAbA (a) and contaminants (b) in the supernatant after phase separation at varying PEG concentrations. Data points represent the mean value of triplicates. All experiments were conducted using 50 mM tris buffer at pH 7.5 and mAbA concentration of 3 mg/mL. The mAbA was spiked with untreated mock solution, re-buffered, and conductivity-adjusted re-buffered mock solution. All samples were adjusted to a HCP concentration of 0.5 mg/mL.

By the UF/DF step, not only salts were depleted, but other small molecules like amino acids and vitamins probably as well. Thus, the influence of these small molecules was tested. Therefore, samples containing 3 mg/mL mAb and re-buffered mock solution were spiked with cell culture medium, and afterwards precipitated using PEG (Fig. 5.7.). The used cell culture medium was not identical with the original one used for the fermentation. However, it is composed out of the same group of components: amino acids, vitamins, inorganic salts, and sugars. For mAbA (Fig. 5.7. (a)), as well as for mAbB (Fig. 5.7. (b)), adding cell culture medium led to a comparable precipitation behavior of the samples containing re-buffered mock solution and mAb and the samples containing mAb and untreated mock solution.

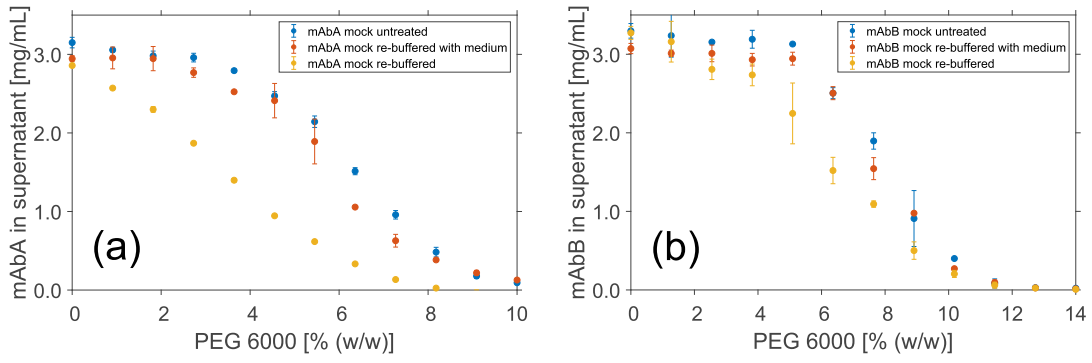

Figure 5.7.: Solubility data of (a) mAbA and (b) mAbB in the supernatant after phase separation at varying PEG concentrations. Data points represent the mean value of triplicates. 3 mg/mL mAb was spiked with untreated mock solution, re-buffered mock solution, or re-buffered mock solution and cell culture medium.

5.4. Discussion

The effect of contaminants on the precipitation behavior of two different mAbs, an IgG1, here named mAbB, and an IgG2, here named mAbA, was investigated. Therefore, the precipitation curves of the mAbs at varying PEG concentrations were determined. Although mAbA and mAbB are similar in size and pI, a different phase behavior was observed. In comparison, higher PEG concentrations were needed to precipitate mAbB. This indicates that the molecular weight, or the overall surface charge of proteins is not the only factor influencing PEG-induced precipitation. This is consistent with the investigation of Haemmerling *et al.* [157]. They showed, with the help of quantitative structure activity relationship models (QSAR), that surface characteristics, such as charge distribution, amount of hydrophobic patches, and their distribution on the surface, might play an important role for the precipitation behavior of proteins as well.

The precipitation behavior of the pure mAb solutions was compared to systems which were spiked with one of two different mock solutions as contaminants. To investigate the influence of the complete cell culture medium, the mAbs were spiked with untreated mock solution. The cell culture fluid includes a variety of small molecular weight contaminants which can briefly be divided into four groups: amino acids, vitamins, inorganic salts, and other components, mainly sugars. Side products like fermentation metabolites, or added antifoam, may be included in the cell culture fluid as well. Furthermore, one finds larger contaminants like HCPs or DNA. To investigate the influence of contaminants with a size larger than $10\,kDa$, the mAbs were spiked with re-buffered mock solution. During the UF/DF step, components with a molecular weight smaller than $10\,kDa$ were removed. The successful removal could be shown with the help of SEC analytic. Additionally, the integrity of the re-buffered mock solution, after the UF/DF step, could be proven. Thereby, changes in the size distribution of the mock solution could be excluded.

To further prove the usability of the developed screening system, the precipitation behavior of mAbA provided as HCCF was compared to systems containing purified mAbA and mock solution. The precipitation behavior of mAbA and the contaminants present in the HCCF could successfully be imitated by mixing purified mAbA with untreated mock solution in a similar proportion. Thus, mixing effects on the liquid handling station could most likely be excluded.

Focusing on the influence of the contaminants on the precipitation behavior of the mAbs, mAbA, and mAbB showed a similar behavior. In both cases, the addition of contaminants led to a decrease in the solubility of the mAbs. When contaminants were added, precipitation started at lower PEG concentrations. Additionally, the

amount of PEG needed for complete precipitation of the antibodies was reduced for both of the mock solutions used. The destabilizing effect could be shown for all investigated mAb concentrations. The higher precipitation propensity was even more pronounced when the mock solution had been re-buffered before. This suggests that, in general, the addition of contaminants destabilizes the antibody, but small molecular contaminants removed through re-buffering the mock solution stabilize the mAb during precipitation. The influence of small molecular contaminants known as osmolytes or co-solutes can be explained with the preferential interaction theory. According to this theory, a preferential binding of co-solutes to the proteins would lead to a stabilization of the system, also known as salting-in [191]. This would mean that the presence of co-solutes either stabilized the mAbs or avoids interaction with larger contaminants present in the re-buffered mock solution. For preparative PEG precipitation, lowering the solubility of the mAb is required. Especially when PEG precipitation is intended to be used as capture step, the amount of required PEG is directly linked to the process costs, as there is no recycling strategy for PEG yet. Therefore, a reduction of the PEG amount is desirable. On the other hand, product loss through incomplete precipitation should be avoided. Changes induced through contaminants are a critical factor for process development, in particular when considering a robust process.

While the amount of precipitated mAb can be linked to the yield, the amount of co-precipitated contaminants influences the purity of the product after the precipitation step. In previous studies it was shown, that the purity can be further increased through selective resolubilisation of the product [4]. However, a lower co-precipitation of the contaminants is advantageous, as it reduces the effort for the next step and the risk that the undissolved impurities lead to filter clogging. In this study, investigation of the contaminant solubility showed a slight decrease, comparing mAb spiked with untreated mock solution to pure mock solution systems. For systems with re-buffered mock solution, the hiring of the precipitation propensity was more pronounced. This is similar to the precipitation behavior of the mAbs. The increase of the precipitation propensity can hence be correlated to the different investigated initial mAb concentrations when re-buffered mock solution was added. An increase in the mAb concentration led to an increase in the precipitated contaminants. This in turn implies a direct or indirect protein-contaminant interaction between the mAbs and the contaminants prior or during the precipitation process.

This leads to a complex problem for process development. Since PEG-induced precipitation of mAbs is mainly used as a capture step, a high yield is of primary significance. For example, for an initial product concentration of $8\,mg/mL$ mAbA, $10\,\%\,(w/w)$ PEG were necessary to achieve a yield of $98\,\%$. This resulted in a purity of $99\,\%$ after the precipitation, when untreated mock solution was spiked as contaminant. If re-buffered mock solution was utilized as contaminant $9\,\%$ less PEG

was required to achieve the same yield. However, this also led to a decrease in the purity of 9.5 %. For an initial product concentration of $1\,mg/mL$ mAbA, the effect was different. When re-buffered mock solutions was added as contaminant, 36.4 % less PEG was required, compared to experiments were untreated mock solution was used, to reach 98 % yield. At the same time, the purity was 2 % higher. For an initial mAB concentration of $1\,mg/mL$, 11 % more PEG was required to achieve 98 % yield when comparing untreated mock to re-buffered mock solution. At the same time, the purity was 21 % higher. The examples illustrate how changes in process conditions, such as different product concentrations, changes in the cell culture medium composition, or a change of the product, can affect the purification outcome.

An indication, that protein-contaminant interaction is the reason for the observed differences in yield and purity, is also provided by other studies investigating variations in the HCP level after Protein A chromatography. Sisodiya *et al.* found that the variation of the HCP level varies between different mAb species and is caused by electrostatic and hydrophobic interactions between the mAb and the HCPs [96]. This confirms the assumption that the presence of large molecular contaminants destabilizes the mAb as well as the contaminant by mAb-contaminant interaction. For systems with untreated mock solution, the correlation between mAb concentration and contaminant precipitation behavior was not possible. Subsequently, modifications during the UF/DF step had to cause the different observed precipitation behaviors.

Two possible explanations for this behavior were investigated. During the UF/DF step, the conductivity was reduced. Beside PEG concentration and pH, the conductivity of the precipitation samples is known to influence the precipitation process [192]. Electrostatic interactions are a conceivable reason for the observed destabilizing effect of added re-buffered mock solution. At the investigated pH of 7.5, both mAbs have a positive net charge while contaminants like HCP, with an average pI of around pH 5.0, are mostly charged negative [52]. Hence, electrostatic attraction might take place and lead to mAb-contaminant interaction and therefore to co-precipitation. However, adjustment of the conductivity did neither show an effect on the phase behavior of mAbA nor on that of the contaminants. This implies either that no electrostatic interaction took place or, more likely, that the higher ionic strength was not the only stabilizing factor.

As changes in the conductivity have not explained the behavior satisfactorily, the other small molecules present in the cell culture fluid, and probably their interplay had to cause the observed variations. By mixing mAb, re-buffered mock solution, and fresh cell culture medium prior to the precipitation, the stabilizing effect of the cell culture media components could be shown. For process development, this is a significant issue, as USP is mostly driven by the needs of higher cell culture,

respectively product titers, and less with respect of the needs for DSP [177]. As side product of USP development, the co-solute composition might change. Furthermore, variations in the HCP profile are reported as a function of the cultivation condition and may be induced during primary clarification [193, 194]. This implies that changes during early production phases are critical for a precipitation process. They can change the precipitation behavior of mAb or contaminants and can, therefore, lead to a variation in yield and purity. Hence, especially for the development of a platform process containing PEG-induced precipitation as the capture step, an integration of up- and downstream steps is of great importance.

5.5. Conclusion

In the present work, the influence of contaminants on the precipitation behavior of mAb and the contaminants during a preparative PEG-induced precipitation step was shown. Higher precipitation propensity could be correlated to the protein-contaminant interaction of the mAb with contaminants larger than $10\,kDA$. Additionally, a stabilizing effect of the mAb as well as of the contaminants could be linked to small molecules contained in the cell culture media. Other factors like size distribution or conductivity were successfully excluded. It was pointed out that variations in the cell culture media during USP may influence the precipitation performance. This study shows that the amount of PEG, required for a successful precipitation step, can vary by up to 36.2 %, depending on the contaminant composition. This theoretically opens up the possibility of reducing the required PEG quantity and thus developing a more economical process. At the same time it helps to estimate the robustness of the process. Also the influence on the purity, after the precipitation step, was found to be a critical factor. Variations of up to 21 % were seen for the various process conditions. Therefore, the knowledge gained in this study can probably be used to increase the product purity. It provides the possibility to use co-solutes for manipulation of the precipitation behavior and increase product purity or yield.

The results demonstrate the importance of integrated up- and downstream process development. Deeper knowledge of the phase behavior of complex protein solutions can simplify empirical precipitation process development. Furthermore, understanding the protein precipitation of complex solutions can help to derive new *in silico*-based models and therefore, make process development faster and less material consuming. During the whole purification process, protein-contaminant interactions play a critical role for the product quality. The results obtained in this study may therefore also be important for other unit operations, like chromatographic separations. Hence,

further studies should focus on the identification of the stabilizing components in the cell culture media.

5.6. Acknowledgments

This project has received funding from the European Union's Horizon 2020 Research and Innovation Programme under Grant agreement no. 635557. We kindly thank Josefine Morgenstern for proofreading the manuscript, Gang Wang for the fruitful scientific discussion, and Novartis (Basel, Switzerland) for providing the mAbs.

5.7. Compliance with ethical standards

Conflict of interest The authors declare no conflict of interest.

6. An Integrated Precipitation and Ion-exchange Chromatography Process for Antibody Manufacturing: Process Development Strategy and Continuous Chromatography Exploration

Steffen Großhans*, Gang Wang*, Christian Fischer, Jürgen Hubbuch**

Karlsruhe Institute of Technology (KIT), Institute of Process Engineering in Life Sciences, Section IV: Biomolecular Separation Engineering, Karlsruhe, Germany
* These authors contributed equally to this work
** Corresponding author

Abstract

In the past decades, research was carried out to find cost-efficient alternatives to Protein A chromatography as a capture step in monoclonal antibody (mAb) purification processes. In this work, polyethylene glycol (PEG) precipitation has shown promising results in the case of mAb yield and purity. Especially with respect to continuous processing, PEG precipitation has many advantages, like low cost of goods, simple setup, easy scalability, and the option to handle perfusion reactors.

Nevertheless, replacing Protein A has the disadvantage of renouncing a platform unit operation as well. Furthermore, PEG precipitation is not capable of reducing high molecular weight impurities (HMW) like aggregates or DNA. To overcome these challenges, an integrated process strategy combining PEG precipitation with cation-exchange chromatography (CEX) for purification of a mAb is presented.

This work discusses the process strategy as well as the associated fast, easy, and material-saving process development platform. These were implemented through the combination of high-throughput methods with empirical and mechanistic modeling. The strategy allows the development of a common batch process. Additionally, it is feasible to develop a continuous process. In the presented case study, a mAb provided from cell culture fluid (HCCF) was purified. The precipitation and resolubilisation conditions as well as the chromatography method were optimized, and the mutual influence of all steps was investigated. A mAb yield of over 95.0 % and a host cell protein (HCP) reduction of over 99.0 % could be shown. At the same time, the aggregate level was reduced from 3.12 % to 1.20 % and the DNA level was reduced by five orders of magnitude. Furthermore, the mAb was concentrated three times to a final concentration of 11.9 mg/mL.

6.1. Introduction

From 1992 to 2015, 47 monoclonal antibodies (mAbs) have been approved either by the US Food and Drug Administration (FDA), or the European Medicines Agency (EMA) [195]; until January 11, 2017, the number of approved therapeutic mAbs by FDA has increased to 68 [196]. Currently, 230 and 52 mAbs have been reported to undergo the phase 2 and phase 3 clinical studies, respectively. Compared to early 2010 (26 mAbs in late-stage studies), a 100 % increase has been achieved, delivering the evidence for a continuing strong growth of the mAb market [197]. The global mAb market was currently expected to reach almost $ 125 billion by 2020 [198].

Based on recent advances in upstream processing, a titer increase at commercial scale up to approximately 20 % from 2014 to 2019 has been predicted, whereas improvements in downstream processing have been adopted more slowly [199]. In 2016, FDA has approved the first mAb biosimilar infliximab-dyyb for the US market, which will be sold with an estimated discount at 20-30 % to its originator. The game-changing biosimilars, along with the increasing demand for mAbs, and achievements in upstream processing have placed downward pressure on downstream processing.

As Protein A chromatography provides highly specific binding to the Fc-region of a variety of mAb types, resulting in high product yield and purity in a single step, it

has become the golden standard for the capture step in the platform process [176, 200, 201]. However, its disadvantages such as slow volumetric throughput and high resin costs have become even more pronounced under the circumstances mentioned above. As a result, a growing interest in the development of non-chromatographic mAb purification processes could be observed [92, 150, 202–206]. Especially precipitation methods based on polyethylene glycol (PEG) showed promising results as alternative capture step [26, 114]. Hammerschmidt *et al.* [207] investigated the economics of precipitation in comparison to the actual platform process. The results showed cost reduction for the precipitation process during clinical as well as in the commercial phase. Especially in the clinical phases and in small scale production replacing Protein A resins showed economical benefit.

Additionally, a trend from conventional single column batch chromatography towards multi-column chromatography has been reported [110, 208–213]. While operating in semi-continuous fashion, the overall operating time can be reduced. Furthermore, higher resin utilization per cycle leads to columns with reduced volume. Thus, an increased productivity may be achieved.

On the process side, Protein A chromatography has been established as an expensive but easy-to-use technique for mAb capturing, which does not require high development effort. In comparison, the process development for both precipitation and multi-column chromatography, however, is much more complicated, which contradicts the desire for shorter development timelines in the biopharmaceutical industry. Thus, the necessity of simplification of process development while maintaining product quality is a major challenge.

In this work, a case study on industrial mAb purification from a harvested cell culture fluid (HCCF) by integrating PEG precipitation and cation-exchange chromatography (CEX) is presented. The occurring difficulties by renouncing Protein A chromatography are addressed. A combined process development strategy minimizing the amount of feedstock needed and experimental effort is suggested. In particular, high-throughput experimentation, design of experiments (DoE), and mechanistic chromatography modeling were employed to develop the precipitation, resolubilisation, and CEX chromatography step. The developed toolbox and the process scheme of the case study are illustrated in Fig 6.1.. Additionally, based on mechanistic modeling, the optimized single-column batch chromatography process was transferred to a three-column CEX periodic counter-current chromatography (3C-PCCC) mode to investigate the advantages and potential of multi-column chromatography in the considered case.

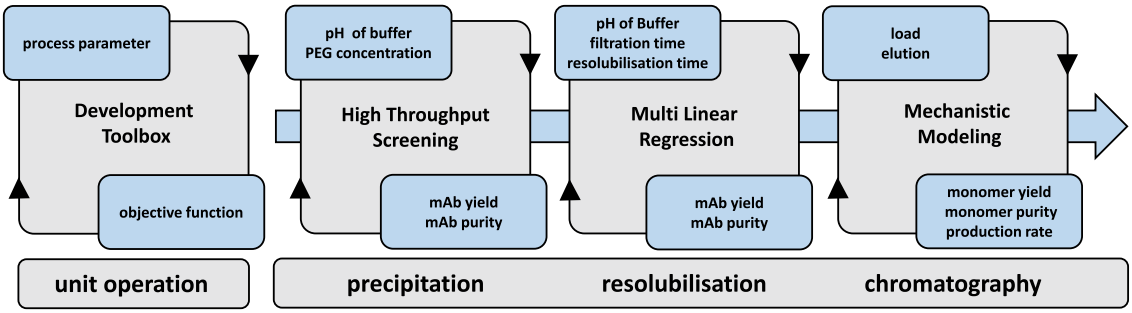

Figure 6.1.: Flowchart of the development toolbox and the integrated process which combines precipitation, resolubilisation and cation-exchange chromatography.

6.2. Theory

6.2.1. Fundamentals of precipitation

Protein precipitation has been known for a long time as a separation method for the purification of complex protein solutions [56]. Phase separation is carried out by adding precipitation agents, like inorganic salts, organic solvents, or nonionic polymers to the protein solution [57, 89, 148, 149]. For the precipitation of a complex mAb solution, in particular the use of polyethylene glycol (PEG) with an average molecular weight of 6000 DA as precipitation agent has shown promising results [68]. Although this phenomenon is well investigated and there are several models describing the behavior of proteins in PEG solution, the mechanism is not completely understood [90, 154, 157]. The two theories which describe the mechanism of PEG-induced precipitation are, on the one hand, the theory of excluded volume [158–160] and on the other hand the theory of attractive depletion [71, 72]. The theory of excluded volume is based on the assumption that PEG traps the solvent in the coiled structure and the folded filament of the solved molecules. This results in the steric exclusion of proteins from the solvent regions occupied by the polymers. Molecules with a larger hydrodynamic radius are more strongly excluded compared to molecules with a smaller one. According to this view, the sterically excluded proteins are concentrated until their solubility is exceeded and precipitation occurs [69]. In contrast to this assumption, the theory of attractive depletion describes a force of the order of osmotic pressure which leads to protein precipitation. This force is caused by mainly steric exclusion of the PEG molecules from the ambience of the proteins, described as depletion zone. If two depletion zones are overlapping, a PEG-free area is created and, therefore, a concentration gradient is formed. This gradient leads to an osmotic pressure which further leads to precipitation of the proteins.

Both theories describe the mechanism of PEG-induced precipitation but additionally other factors which influence the colloidal stability of protein solutions like protein concentration, pH or ionic strength, have to be considered [26].

6.2.2. Ion exchange chromatography modeling

The following theoretical background was used to carry out mechanistic chromatography modeling for the subsequent CEX step. The general rate model (GRM) is employedf to cover the convection and diffusion in a chromatography column of length L and adsorber beads of radius r_p [214]:

$$\begin{aligned}\frac{\partial c_i(x,t)}{\partial t} &= -u(t)\frac{\partial c_i(x,t)}{\partial x} + D_{ax}\frac{\partial^2 c_i(x,t)}{\partial x^2} \\ &\quad -\frac{1-\epsilon_b}{\epsilon_b}k_{film,i}\frac{3}{r_p}\left(c_i(x,t) - c_{p,i}(x,r_p,t)\right) \qquad (6.1)\end{aligned}$$

$$\frac{\partial c_{p,i}(x,r,t)}{\partial t} = \begin{cases} \frac{1}{r^2}\frac{\partial}{\partial r}\left(r^2 D_{p,i}\frac{\partial c_{p,i}(x,r,t)}{\partial r}\right) - \frac{1-\epsilon_p}{\epsilon_p}\frac{\partial q_i(x,r,t)}{\partial t} & \text{for } r \in (0,r_p), \\ \frac{k_{film,i}}{\epsilon_p D_{p,i}}\left(c_i(x,t) - c_{p,i}(x,r_p,t)\right) & \text{for } r = r_p, \\ 0 & \text{for } r = 0. \end{cases} \qquad (6.2)$$

$$\frac{\partial c_i(0,t)}{\partial x} = -\frac{u(t)}{D_{ax}}\left(c_i(0,t) - c_{in,i}(t)\right) \qquad (6.3)$$

$$\frac{\partial c_i(L,t)}{\partial x} = 0 \qquad (6.4)$$

Within the mobile phase $c_i(x,t)$, the mass transfer between the pore volume $c_{p,i}(x,r,t)$ and the interstitial volume is described by Eq. (6.1). The voidage of the adsorber bed ϵ_b, the axial dipersive coefficient D_{ax}, and the film transfer coefficient $k_{film,i}$ describe the peak-broadening effects in the interstitial volume. The mass transfer is from the pore volume concentration $c_{p,i}$ to the stationary phase q_i and vise versa. ϵ_p is the adsorber particle voidage and $D_{p,i}$ the component-specific pore diffusion coefficient. Eqs. (6.3) and (6.4) are the Danckwerts boundary conditions.

The widely accepted steric mass action (SMA) isotherm model introduced by Brooks and Cramer describes adsorption and desorption processes on adsorber surfaces [132]. The kinetic formulation suggested by Nilsson *et al.* is shown in Eq. 6.5 [134]. Here, the stationary phase protein concentration q depends on q itself, pore phase protein concentration c_p, and pore phase salt concentration $c_{p,salt}$. ν is the characteristic charge representing the binding sites number involved in binding directly. σ is the number of binding sites on the adsorber surface sterically hindered by protein binding.

Λ is the ionic binding capacity of the column related to adsorber skeleton.

$$k_{kin,i}\frac{\partial q_i(x,t)}{\partial t} = k_{eq,i}(\Lambda - \sum_{j=1}^{k}(\nu_i + \sigma i)q_j(x,t))^{\nu_i}c_{p,i}(x,t) - c_{p,salt}(x,t)^{\nu_i}q_i(x,t) \quad \forall i \neq salt \tag{6.5}$$

The salt concentration in the stationary phase is described in Eq. 6.6.

$$q_{salt}(x,t) = \Lambda - \sum_{j=1}^{k}\nu_j q_j(x,t) \tag{6.6}$$

The adsorption rate coefficient k_{ads} and the desorption rate coefficient k_{des} were replaced by the equilibrium coefficient k_{eq}=k_{ads}/k_{des} and the kinetic coefficient $k_{kin} = 1/k_{des}$ to simplify parameter estimation, as k_{eq} and k_{kin} correlate mainly with the retention time and peak height, respectively [135]. Out of several reasons, the kinetic formulation has been chosen. Because of limitations in the binding kinetics, protein adsorption is often slow as reported by Carta and Jungbauer. Additionally, true adsorption equilibrium may not be established in column chromatography. The hydroxylated methacrylic polymer-based and polymer-grafted adsorber (Toyopearl GigaCap S-650M) provides high ligand density, resulting in limited access to binding sites with increasing protein binding due to steric crowding and electrostatic repulsion [215, 216].

Combining both GRM and SMA, the presented CEX chromatography process can be modeled using numerical methods.

6.2.3. 3C-PCCC

Periodic counter-current chromatography is a simulated moving-bed process patented by GE Healthcare as a semi-continuous purification process [217]. Usually, it is operated in three- or four-column configurations.

Since PCCC allows the loading of columns much closer to their static binding capacity, it has the potential to reduce resin volume, buffer consumption, and process time in comparison to conventional batch chromatography [208–210, 218]. Economical simulation of a Protein A capture step in 3C-PCCC and 4C-PCCC mode has demonstrated that PCCC can reduce manufacturing costs particularly in early clinical phases [218]. Compared to traditional batch single-column chromatography, where the process steps of a chromatography cycle are conducted consecutively, in PCCC, multiple steps are performed simultaneously but distributed along several

columns. In 3C-PCCC, the process consists of two interconnected columns and one short-circuited column. The columns are shifted only periodically after two out of four process steps. In the first stage, column 3 is interconnected with column 2. In steady-state, column 3 was fed with feed material in the previous steps and is now fully saturated. Wash buffer is passed through this column to remove unbound and weakly bound proteins. The wash effluent is directed to the equilibrated column 2 to recover leached product. In the meantime, feed material is loaded onto column 1. The flow-through is discarded until the first product breaks through. As soon as the first product breaks through, column 1 is switched into the interconnected lane and the outflow is loaded directly onto column 2. Since the load step is now performed with two columns in series, resin capacity utilization can be increased by loading column 1 beyond 1 % product breakthrough [217].

While column loading is continued in the interconnected lane, column 3 is short-circuited and the product is eluted. The short circuit allows the application of arbitrary elution gradients and center-cut separation. After product elution, column 3 is regenerated and equilibrated. Column 1 and column 2 remain in the interconnected lane and continue to receive feed material without product breaking through column 2. The procedure is repeated several times, so that each column is loaded, washed, eluted, and regenerated several times in the process. In addition to column regeneration, it might also be necessary to integrate a CIP step. This step can be carried out after a certain number of process cycles, or, alternatively, as a part of each regeneration step [217].

6.3. Materials and Methods

6.3.1. Feed stock

The mAb used in this work was provided as HCCF from LEK d.d. (Ljubljana, Slovenia). The HCCF was stored at -80°C for long-term and at -30°C for short-term storage. All samples were filtered through 0.2 μm syringe filters (Satorius, Göttingen, Germany) directly before use.

6.3.2. Disposables

All precipitation experiments were carried out in 350 μL polypropylene flat bottom 96-well micro plates (Grainer Bio-One, Kremsmünster Austria). For all resolubilisation

studies, 350 μL AcroPrep filter plates with a 0.2 μm GH polypro membrane (Pall Corporation, Port Washington, NY, USA) were used. For DNA quantification, black 96-well polystyrene microplates (Thermo Fisher Scientific, Waltham, MA, USA) were used. Before loading onto the CEX column, pH of the mAb samples was adjusted using pD 10 desalting columns (GE Healthcare, Little Chalfont, UK).

6.3.3. Chemicals and stock solutions

As buffer substance, acetic acid, sodium acetate trihydrate, sodium chloride, sodium hydrogen carbonate, and tris(hydroxymethyl)-aminomethane (all Merck KGaA, Darmstadt, Germany) were used. Tris hydrodochloride was obtained from PanReac AppliChem (Darmstadt, Germany). Sodium carbonate was obtained from Sigma Aldrich (St. Louis, MO, USA). The PEG with an average molecular mass of 6000 was obtained from Merck KGaA (Darmstadt, Germany). All buffers were prepared with a concentration of 100 mM. For this, the appropriate amounts of associated buffer components were weighted and dissolved in ddH_2O. The desired pH was reached by varying the amount of acid and basic component for each buffer. For the 40 % (w/w) PEG 6000 stock solution, the buffer components were first dissolved in ddH_2O followed by adding the appropriate amount of PEG 6000.

6.3.4. Liquid handling station

All precipitation experiments were carried out on a Tecan Freedom Evo 200 System liquid handling station (Tecan, Männedorf, Switzerland). The liquid handling station was equipped with an 8-tips liquid handling arm, a Te-VacS vacuum separation module, a Te-Shake orbital shaker (all Männedorf, Switzerland), and a Rotanta 46RSC centrifuge (Hettlich GmbH & Co. KG, Tuttlingen, Germany). The system was controlled by Evoware 2.5 (Tecan, Männedorf, Switzerland). Excel 2013 (Microsoft, Redmond, WA, USA) was used as data import format and for data storage. All calculations were done using Matlab R2015a (The Mathworks, Natick, MA, USA). For reproducible HTS, the 8-tips liquid handling arm was calibrated. A separate liquid class for each buffer, precipitant, and protein solution was created. The calibration procedure was described earlier by Oelmeier *et al.* [219] in detail. By variation of air gaps and the adjustment of the aspiration, dispensing and beakeoff speed accuracy pipetting, even for viscous solutions, could be ensured.

6.3.5. Liquid chromatography system

The chromatographic experiments for mechanistic model calibration were performed using an Ettan liquid chromatography (LC) system equipped with a pump module P-905, a dynamic single chamber mixer M-925 (90 μL mixer volume), an autosampler A-905, and a fraction collector Frac-950. The LC system was additionally equipped with an UV monitor UV-900 (3 mm optical path length) and a pH and conductivity monitor pH/C-900 (all GE Healthcare, Little Chalfont, Buckinghamshire, UK). The LC system was controlled with UNICORN™ 5.31.

As chromatography resin, the strong cation exchanger TOYOPEARL™ GigaCap S-650M (TOSOH, Stuttgart, Germany) was applied. The resin beads are comprised of a polymethacrylate backbone with a mean particle size of 75 μm. The resin was prepacked by TOSOH in three 1 mL ToyoScreen™ columns with dimensions of 6.4 $mm\,x\,3\,cm$.

6.3.6. Analytical methods

To determine mAb concentration and aggregate content, the UltraHPLC system Ultimate 3000RSLC, controlled with Chromeleon 6.8 (both Thermo Fisher Scientific, Waltham, MA, USA) was used. For mAb concentration, a POROS analytical Protein A column (Thermo Fisher Scientific, Waltham, MA, USA) was connected to a UHPLC system. Analytical size exclusion chromatography (SEC) was performed using a TSKgel SuperSW mAb HTP column (TOSOH, Stuttgart, Germany). Host cell protein (HCP) concentrations of all samples were determined using a microfluidic CD-based ELISA-like assay on the Gyrolab XPlore station controlled by Gyrolab (Gyros AB, Uppsala, Sweden). DNA was quantified using a Quant-iT dsDNA assay kit (Thermo Fisher Scientific, Waltham, MA, USA). The fluorescence intensity was measured using a Tecan Infinity 200 UV-Vis spectrometer (Tecan, Männedorf, Switzerland).

6.3.7. High-throughput method for precipitation screening

The precipitation procedure on the automated liquid handling station was described in detail by Oelmeier *et al.* [23]. All experiments were carried out at 20°C, controlled by air conditioning. Systems with a total volume of 250 μl containing an mAb concentration of 1.5 mg/mL were prepared. For finding the optimal precipitation conditions, the PEG concentration was varied in 24 steps from 0 % (w/w) to 13.8 % (w/w) PEG

6000. Additionally, the pH was varied in four steps from pH 7.5 to pH 10.5. After adding the complex protein stock solution, the system was incubated for 15 min on the orbital shaker at 1000 rpm, and afterwards 15 min without shaking. To analyze the amount of precipitated protein, the microplate was centrifuged for 30 min at 4000 rpm. Then, 100 μl of the supernatant was sampled and diluted at a ratio of 1:2. Subsequently, mAb and HCP concentration of the samples were analyzed.

6.3.8. Optimization of the resolubilisation using empirical modeling

To find optimal resolubilisation process parameters, a DoE was established using the software Modde 10.1.1 (Umetrics, Umeå, Sweden). As design space, a full factorial design with three factors was chosen. In preliminary experiments, the mAb showed instabilities below pH 4.0 during resolublisation (data not shown). Therefore, the pH value of the resolubilisation buffer was varied between pH 4.0 and pH 6.0. The filtration time after precipitation and resolubilisation was varied between 150 s and 600 s, and the incubation time of the resolubilisation was varied between 75 min and 150 min. As response, mAb yield and the mAb purity were investigated. The experiments for resolubilisation were carried out on the liquid-handling station with a method similar to the one described before. Instead of mixing the systems in 96-well microplates, 96-well filterplates were used. After incubation, phase separation was carried out applying three times 700 $mbar$ pressure difference for various times. Subsequently, 240 μl of resolubilisation buffer were added to each system. Afterwards, the filterplates were incubated on the orbital shaker for various times. After the incubation, a second filtration step was carried out using the vacuum separation module three times at 700 $mbar$ pressure difference for various times.

6.3.9. Chromatography system characterization

The ÄKTA™ system and chromatography column were characterized using tracer pulse injections at constant flow rates of 0.33 mL/min. 25 μL of 10 g/L non-interacting, non-pore-penetrating tracer blue dextran 2000 kDa (Sigma-Aldrich, St. Louis, MO, USA) and 25 μL of 1 %(v/v) pore-penetrating, non-interacting tracer acetone (Merck, Darmstadt, Germany) in ultra-pure water were used to determine the system voidage, interstitial volume and total voidage of the column. Here, the UV signals at 260 nm were used and corrected due to system dead volumes. The ionic capacity Λ of GigaCap S-650M was determined by applying acid-base titration suggested by Huuk *et al.* [130].

6.3.10. Bind-and-elute experiments

After the precipitation and resolubilisation steps, linear gradient elution (LGE) experiments were carried out by means of model calibration. To determine the model parameters in the linear region of the adsorption isotherm, a $0.5\,mL$ loop was used. Post-loading wash steps of $1\,CV$ binding buffer were carried out, followed by an elution step by increasing the salt gradient from $0\,M$to $1.0\,M$ NaCl with gradient lengths of $10\,CV$, $15\,CV$, and $20\,CV$. For the nonlinear region, $23.16\,mL$ protein solution was injected via $50\,mL$ superloop before a wash step of $5\,CV$ binding buffer. Subsequently, the elution was carried out by increasing the salt gradient from $0\,M$ to $1.0\,M$ NaCl with a gradient length of $25\,CV$. After elution, the column was stripped over $3\,CV$ at an NaCl concentration of $1.0\,M$ and re-equilibrated for $5\,CV$ binding buffer. All experiments were conducted at $0.33\,mL/min$.

6.3.11. Model calibration

The chromatograms from LGE in both linear and nonlinear region of the adsorption isotherm were used to carry out the parameter estimation via the inverse method [220]. The first guess was delivered using adaptive simulated annealing (ASA) [221]. For fine adjustment, the Levenberg-Marquardt (LM) algorithm [222] was used. Discretization in space on a grid with equidistant nodes was carried out using the finite element method. The θ-scheme discretization in time was conducted using the fractional step [223]. The solution of the non-linear equation system was approximated via the Picard iteration [224].

6.3.12. *In silico* optimization and model validation

Pareto optimization of the batch single-column chromatography was performed using ChromX. As objective functions, monomer yield, purity, and production rate were chosen. Optimization parameters are the injection volume and sodium chloride concentration in elution step. The salt concentrations of the binding buffer and strip buffer were kept constant to ensure maximal binding and a complete regeneration of the columns. The OpenBeagleMultiObjective algorithm was employed for the *in silico* optimization. One of the Pareto optima that provided monomer yield and purity above 90 % and 99 %, respectively, and the maximal production rate were chosen to be validated in the laboratory. *In silico* screening was carried out to approximate the Pareto optima of the 3C-PCCC process. Here, 1000 simulations of the 3C-PCCC process were generated by varying the protein injection volume and

the optimal salt elution concentration. The fractionation was chosen to start and end at 300 mAU.

6.4. Results

6.4.1. Investigation of precipitation conditions

In this work, PEG precipitation of the mAb was performed as alternative capture step for an mAb purification process. In specific, the goal was to find optimal process conditions for selective precipitation of the mAb. On the one hand, the precipitant concentration and, on the other hand, the pH value of the buffer used was varied. As target parameters, mAb yield and HCP reduction were considered.

The mAb as well as the HCP concentration in the supernatant, after phase separation through centrifugation, are shown in Fig 6.2.. All values shown are mean values of at least triple determinations and refer to conditions at 0 % PEG. 98.5 % yield was chosen as target parameter for the precipitation, as this was the maximum reached yield in this study.

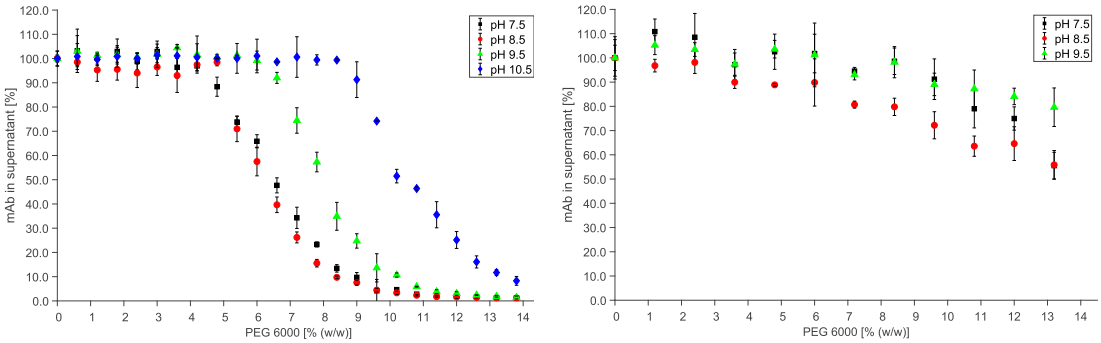

Figure 6.2.: Selected results of the precipitation screening. Data points represent the mean values of at least triplicates. As feedstock HCCF was used. Precipitation was carried out using PEG 6000, varied from 0 % (w/w) to 13.8 % (w/w) PEG, as precipitant. Additionally the pH of the utilized buffer was varied. The relative amount refereed to conditions with 0 % (w/w) PEG of (a) mAb and (b) HCP in the supernatant after centrifugation are displayed.

With increasing PEG concentration, a decrease in the mAb concentration in the supernatant could be observed (Fig. 6.2. (a)). This correlates to an increase in mAb precipitation. For all pH values, the mAb stayed stable in solution for PEG concentrations below 4.2 % (w/w) PEG. With the exception of pH 10.5, all other conditions led to yields above 98.5 %. Therefor, no further investigations were carried out at

pH 10.5. The shape of all curves of the different pH values differed in the initial PEG concentration where the precipitation of the mAb began. For conditions with pH 7.5, pH 8.5, and for pH 9.5, PEG concentrations of 12.6 % (w/w) PEG, 13.2 % (w/w) PEG, respectively 13.8 % (w/w) PEG were required to reach the predetermined yield.

All examined systems with pH values except for pH 10.5 were investigated on HCP concentration in the supernatant after phase separation (Fig. 6.2. (b)). For all conditions, a decrease in HCP concentration in the supernatant could be observed with increasing PEG concentration. This correlates to a decrease in the theoretical purity of the precipitated mAb referred to HCP. Precipitation of HCP was not detectable for conditions with PEG concentrations less than 7.2 % (w/w) PEG. For all conditions with pH 8.5, a stronger reduction in the HCP concentration could be observed compared to pH 7.5 and pH 9.5. Furthermore, for PEG concentrations above 11.8 % (w/w) PEG, less HCP reduction could be observed for systems with pH 9.5 compared to pH 7.5. For conditions with the predetermined yield being greater than 98.5 % and pH 8.5, HCP reduction over 60 % could be reached. For systems with pH 7.5, 70 %, and for systems with pH 9.5, over 79 % HCP reduction could be detected.

6.4.2. Investigation of resolubilisation conditions

For precipitation, with the exception of pH 10.5, all other investigated pH values achieved satisfying results in the case of mAb yield. One precipitation condition for each investigated pH value with an mAb yield over 98.5 % and with the least amount of PEG was chosen for further process optimization. For these conditions, the resolubilisation was investigated. In detail, for pH 7.5 at least 13.2 % (w/w) PEG, for pH 8.5 12.6 % (w/w) PEG, and for pH 9.5 13.8 % (w/w) PEG were needed to reach the predetermined yield. To optimize the resolubilisation, three factors were taken into account. The pH of the resolubilisation buffer, the filtration time of the phase separation through vacuum filtration, and the incubation time of the resolubilisation. The screenings were carried out as DoE. From the results, a multiple linear regression model (MLR) was built.

For all three precipitation conditions, a similar behavior of the responses, mAb yield and purity, could be observed. No significant influence of the filtration time could be measured and, therefore, this factor was not considered for the model (Fig. 6.3.). This results allow the reduction of the parameter set for further investigations. By reducing the filtration time an overall time saving for the HTS could be reached. No influence of the pH of the resolubilisation could be observed in the case of mAb yield. The only factor which had a significant influence on the mAb yield was the resolubilisation time (Fig. 6.3. (a)). With longer resolubilisation times, higher yields

were detected. At 150 *min* incubation, yields from up to 100 % could be measured (Fig. 6.4. (a)). For the mAb purity, the only factor which had a significant influence was the pH of the resolubilisation buffer (Fig. 6.3. (b)). With lower pH values, a higher mAb purity could be observed for all precipitation conditions. Purity of mAb up to 97 % could be detected under conditions with pH 4.0 (Fig. 6.4 .(b)).

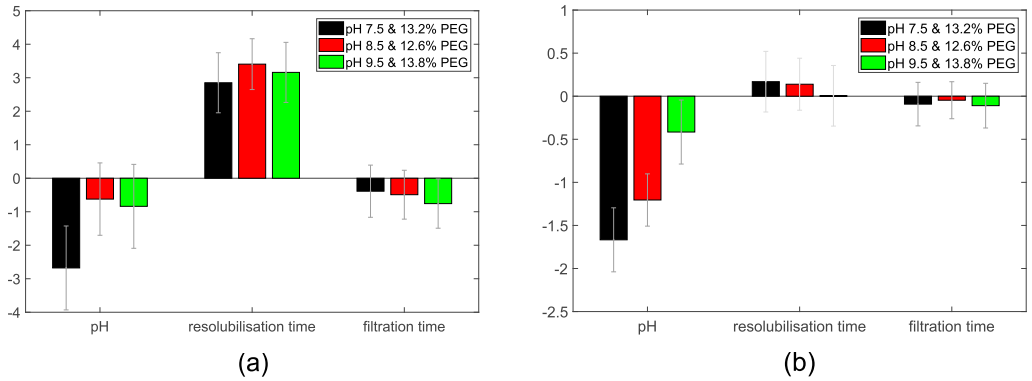

Figure 6.3.: Factors of the MLR model of mAb yield and mAb purity after resolubilisation. HCCF was precipitated at pH 7.5 and 13.2 % (w/w) PEG, pH 8.5 and 12.6 % (w/w) PEG and pH 9.5 and 13.8 % (w/w) PEG. Afterward the precipitated mAb was resolubilisation for incubation times varying from 75 *min* to 150 *min*. Additionally the pH of the resolubilisation buffer was varied from pH 4.0 to pH 6.0. Furthermore the filtration time of the phase separation by vacuum filtration was varied from 150 *s* to 600 *s*. For further investigation only the resolubilisation time in case of yield and the pH of the resolubilisation buffer in case of the mAb purity were taken into account for the MLR.

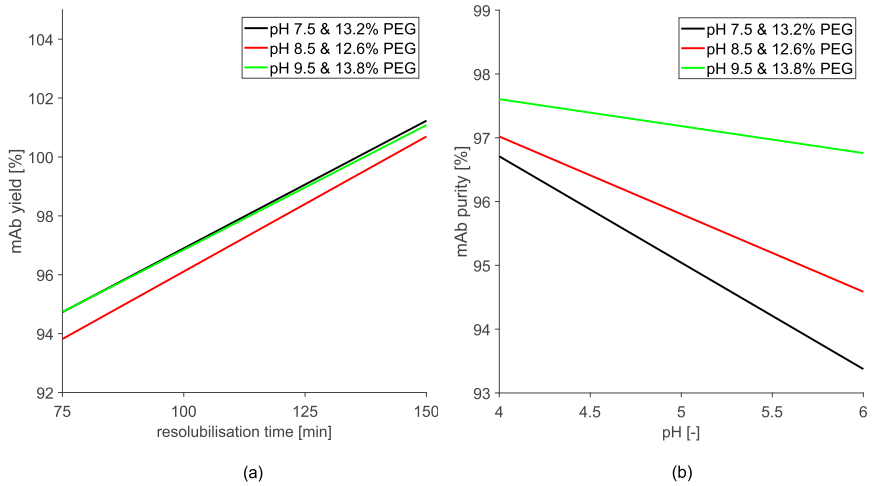

Figure 6.4.: MLR model of mAb yield (a) and mAb purity (b) after resolubilisation. HCCF was precipitated at pH 7.5 and 13.2 % (w/w) PEG, pH 8.5 and 12.6 % (w/w) PEG, and pH 9.5 and 13.8 % (w/w) PEG. Afterwards the precipitated mAb was resolubilised. For the MLR model of the mAb yield the influence of the incubation time was considered. For the MLR model of the purity the pH influence of the resolubilisation buffer was considered.

6.4.3. CEX system characterization

By conducting tracer experiments without a column attached, the LC system dead volume of 280 μl was determined, which was subtracted from all other data from the LC. Based on the results of the tracer injections with a column attached, bed and particle voidage, and axial dispersion were calculated. The acid-basic titration was conducted to determine the ionic capacity. The results are listed in Tab. 6.1.

Table 6.1.: The voidages and axial dispersion are calculated based on tracer experiments. The ionic capacity is determined via acid-base titration.

		GigaCap S-650M
Bed voidage	ϵ_b	0.414
Particle voidage	ϵ_p	0.779
Total voidage	ϵ_t	0.870
Axial dispersion $[mm^2 \cdot s^{-1}]$	D_{ax}	0.067
Ionic capacity $[M]$	Λ	1.383

6.4.4. *In silico* CEX process development

Three linear gradient experiments with gradient lengths of 10 CV, 15 CV, 20 CV, and 25 CV in linear and one with 25 CV in nonlinear region of the adsorption isotherm were used to estimate the chromatography model parameters k_{film}, D_{pore}, k_{eq}, ν, and σ via inverse method by employing ASA and LM algorithm. Non-binding impurities were lumped to one component. The estimated parameter for monomer, aggregate, and lumped impurity are given in Tab. 6.2. k_{kin} was found to be not necessary for the description of the system, since the equilibria of the components considered were reached immediately.

Table 6.2.: The mass transfer model and adsorption isotherm parameters are estimated using the inverse method.

Parameter	mAb	Aggregate	Lumped impurity
k_{film} $[mm \cdot s^{-1}]$	0.086	0.049	0.100
D_{pore} $[mm^2 \cdot s^{-1}]$	$3.508 \cdot 10^{-5}$	$2.788 \cdot 10^{-5}$	$1.648 \cdot 10^{-5}$
k_{eq} [-]	$2.724 \cdot 10^{-7}$	$6.832 \cdot 10^{-9}$	$3.995 \cdot 10^{-12}$
ν [-]	8.899	11.340	-
σ [-]	101.380	98.262	-

Figs. 6.5. (a)-(d) shows the simulated and experimental chromatograms used for the model calibration. The lumped impurity broke through during the wash step. The mAb and aggregate show similar behavior and peak overlapping during gradient elution, whereas the latter shows a slightly stronger binding. Fig. 6.5. (e) shows the magnified simulated and measured signals of the same process as in Fig. 6.5. (d).

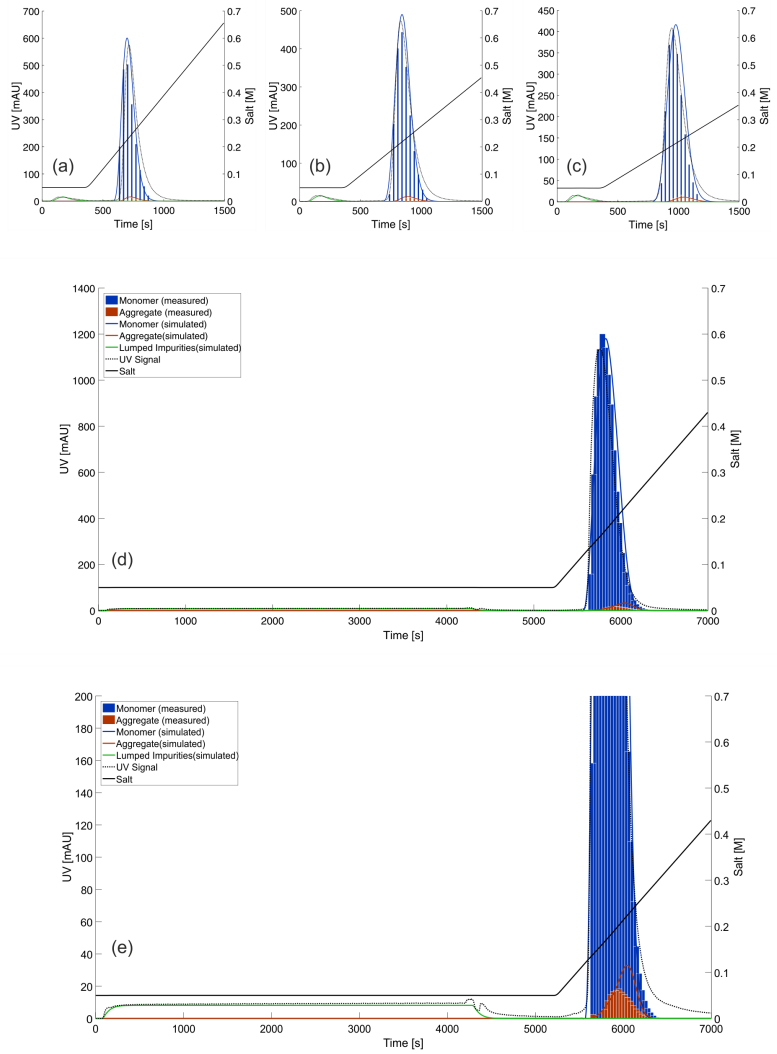

Figure 6.5.: Plots of UV signals over process run time for the bind-and-elute chromatography experiments. Dashed lines display the UV signal measured at column outlet. Black solid lines represent the adjusted salt gradients with elution gradient lengths of 10 CV (a), 15 CV (b), 20 CV (c), and 25 CV (d). Blue solid lines and bars represent the simulation of monomer and offline analytical result, respectively. Red and green are the aggregate and lumped impurity. (e) displays the magnified details of the breakthrough of lumped impurity and the elution of aggregate in the same process as shown in (d).

Knowledge of mass transfer and SMA parameters eventually enabled identification of the optimal step-wise gradient process for the considered separation problem. To find the optimal protein loading volume and elution salt concentration with respect to maximizing monomer yield, purity, and production rate, a multi-objective *in silico* process optimization was performed. The resulting Pareto-optimal points can be seen in Fig. 6.6..

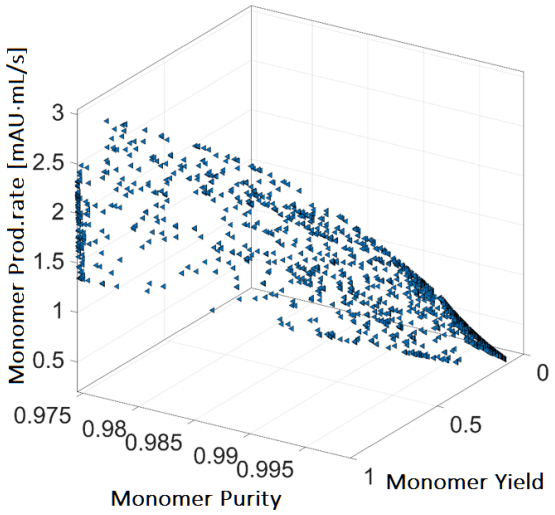

Figure 6.6.: Pareto-optimal operating points for the batch single column chromatography process represent the maximal monomer yield, purity, and production rate by varying protein loading volume and elution salt concentration.

Constraints for monomer yield and purity were set to be above 90 % and 99 %, respectively, whilst the maximal production rate was chosen. The optimal protein injection volume and elution NaCl concentration were predicted to be 35.98 mL and 0.161 M. The validation experiment conducted in the laboratory is compared to the model prediction in Figs. 6.7. (a)-(c). It can be seen that the behavior of lumped impurity, mAb monomer, and aggregate are predicted accurately. As magnified details of Fig. 6.7 (a), Fig. 6.7. (b) and (c) show the simulated and measured signal of lumped impurities and the aggregate, respectively. Small deviations, such as the slight underestimation of the aggregate level in the main peak and the tailing of mAb monomer, are shown. The *in silico* predicted and experimentally determined monomer purity, yield, and concentration in the product fraction are compared in Tab. 6.3. The monomer purity has a deviation of 0.3 %, yields a prediction error of 8.4 %, and the monomer concentration in pooled fraction is underestimated by 8.5 %.

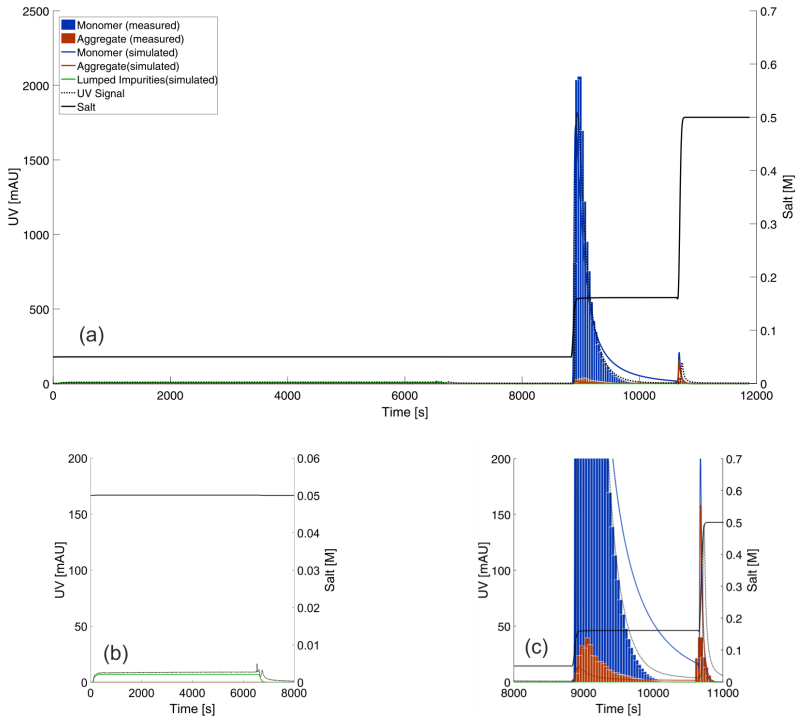

Figure 6.7.: Plot of UV signal over process run time for the validation experiment. Dashed lines display the UV signal measured at column outlet. Black solid lines represent the adjusted step-wise salt gradient. Blue solid lines and bars represent the simulation of monomer and offline analytical result, respectively. Red and green are the aggregate and lumped impurity. (b) and (c) display the magnified details of the breakthrough of lumped impurity and the elution of aggregate in the same process as shown in (a), respectively.

Table 6.3.: Comparison between the *in silico* predicted and experimentally determined objectives.

Objective	Model	Experiment	Deviation
Monomer purity [%]	99.00	98.70	0.30
Monomer yield [%]	91.10	98.75	8.40
c(monomer) pooled $[mg/mL]$	10.94	11.87	8.50

To investigate the potential of a 3C-PCCC process in the considered case, an *in silico* screening was carried out to approximate the Pareto optimal points with respect to maximizing monomer purity and yield simultaneously. Overall, the optimal protein injection volumes were found to be greater and the optimal salt elution concentrations were lower than the ones in the batch single-column process. Improvements of both monomer purity and yield were found as shown in Fig. 6.8..

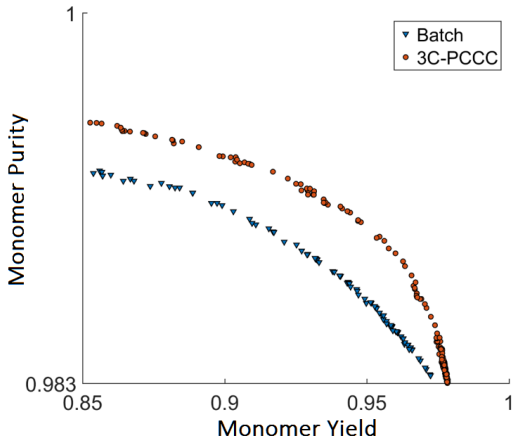

Figure 6.8.: Comparison of the Pareto-optimal operating proteins for the batch (blue triangles) and 3C-PCCC process (orange circles).

6.4.5. Batch process validation

After optimization of each process step, a validation run with the optimal process parameters was performed. The precipitation was performed at pH 8.50 with a PEG concentration of 12.6 % (w/w) PEG. Afterwards, the samples were resolubilised at pH 4.00 for 150 min with a filtration time of 150 s. Before the CEX step, the pH of the sample was adjusted to pH 5.00. The subsequent CEX step was conducted at a loading volume of 35.98 mL, and elution NaCl concentration of 0.161 M, as predicted by the mechanistic chromatography model. At the beginning and after each step, the mAb, HCP and DNA concentration as well as the aggregate content were measured. In Tab. 6.4, these results are compared to a common purification run. The values for Protein A are provided from Lek d.d. and were measured directly after Protein A elution. During the integrated process, HCP and DNA reduction were mainly reached during the precpitation and resolubilisation step. Aggregate reduction and concentration of the product were reached during CEX. Compared to Protein A, mAb yield, HCP reduction, and aggregate content reached similar values. The mAb concentration of the integrated process was 63% lower in comparison to Protein A chromatography, the DNA reduction was four magnitudes higher.

Table 6.4.: Case study validation run after optimisation of the integrated process. Monomer concentration, yield, and purity were detected after each step and compared to a common Protein A process.

Objectives	HCCF	Precipitation	CEX	Protein A
c(monomer) $[mg/ml]$	3.30	1.69	11.87	32.20
Monomer yield [%]	-	96.47	95.41	> 95.00
HCP reduction [%]	-	98.23	99.28	99.99
Aggregate content [%]	3.12	3.96	1.30	1.20
DNA $[ng/ml]$	8.09e+07	2.3 e+03	2.48e+02	1.90e+06

6.5. Discussion

A process strategy for mAb processes was successfully developed. The integration of PEG precipitation and CEX showed the potential of replacing Protein A as capture step in an mAb process.

Through the replacement of Protein A, the necessity of establishing an alternative development platform was given. Furthermore, in comparison to Protein A chromatography, PEG precipitation alone is not capable of reducing high molecular weight impurities (HMW) like aggregates or DNA. The integrated process and the development platform presented in this work can solve both problems. The PEG precipitation showed promising results based on mAb yield and HCP reduction. Resolubilisation at low pH values led to high mAb yields and a high amount of HCP reduction. The results were comparable to common Protein A steps [116]. Furthermore, it allowed a direct loading onto CEX column. Resolubilisation in combination with concentration is reported as being time-consuming and might end up with low yields though incomplete resolubilisation [114]. Using CEX in bind-and-elude mode combined a reduction of HMW with a volume reduction at the same time.

For this integrated process, a process development platform was designed. It combines high-throughput methods with empirical and mechanistic modeling. For the precipitation, a high-throughput method on a liquid handling station was successfully generated. The PEG concentration and the pH of the surrounding buffer showed significant influence on the precipitation behavior. Although PEG is a cheap raw material, recycling is currently not an issue. Therefore, the amount of PEG is one of the driving costs of the process and consequently at least possible PEG should be used. Studies by Hammerschmidt *et al.* have shown that precipitation results, like yield or purity, are independent of the operation mode [225]. This indicates that development strategy presented here could be used for batch and continuous process

development. After the precipitation, the resolubilisation was optimized using a DoE and a MLR model, avoiding brute-force methodology. Afterwards, critical process parameters could be detected and optimized in a goal-driven manner. The mechanistic chromatography modeling reduced the number of experiments needed to be carried out in the laboratory. Thus, the material and time required for the development of precipitation, resolubilisation, and chromatography processes could be reduced. Furthermore, based on the mechanistic understanding gained, the potential of a 3C-PCCC process could be explored.

The development strategy was used to purify an mAb, provided as HCCF. The highest observed mAb yield after precipitation was 98.5%. Comparing different pH values, under conditions with pH 8.5, the least amount of PEG was needed to attend this objective. Conditions with pH 7.5 and pH 9.5 reached this yield at slightly higher PEG concentrations as well. Altogether, the lowest colloidal phase stability of the mAb was observed near its isoelectric point (pI). This is equal to least electrostatic repulsion. However, for these conditions, no more than 79.0% HCP reduction were detected. Co-precipitation of HCP following the mAb could be a reason for this partial reduction. Higher purities were detected under conditions with minor colloidal phase stability of the mAb.

As the precipitation alone was not sufficient enough, the resolubilisation was optimized as second purification step. The DoE showed the pH value to be a critical process parameter for the reduction of HCP. The resolubilisation was carried out at pH values near the pI of most of the HCP. This is reported to be around pH 5.0 [52]. A selective resolubilisation was observed, and HCP reductions of over 98.0% were detected. This suggests that most of the HCP were not resolubilised and remained on the filter. Simultaneously, the investigated pH values were at least 2.5 pH steps below the pI of the mAb. This was probably the reason for a complete resolubilisation of the mAb. Shifting the pH to even lower values could be a possibility to combine virus inactivation with the resolublisation step. The resolubilisation time was detected as the second significant process parameter. Higher yields were detected at longer resolubilisation times. This implies a slow resolubilisation kinetics. The formation of a filter cake is reported as reason for this phenomenon [225]. No reduction of molecules with a hydrodynamic radius bigger than that of the mAb was expected. The aggregate level stayed constant. However, a DNA reduction of over 5 magnitudes could be seen. This might be due to the incubation conditions, as DNA is reported to be sensitive towards low pH values [226].

Because the mAb showed instabilities at high salt concentrations (data not shown), the pH was adjusted from pH 4.0 to pH 5.0 before the CEX step. For the CEX step, the predicted Pareto-optimal process could be validated successfully. Here, the chromatogram predicted showed good agreement with the validation experiment

carried out in the laboratory. The elution of aggregate in the first step was slightly underestimated, leading to a monomer purity overestimated by 0.3 %. The tailing of monomer was predicted to be more pronounced by the model, resulting in a yield deviation of 8.4 %. The reason of these deviations might be the simplification of the protein system by neglecting different binding orientations and charge variants. In the case of the 3C-PCCC process, an *in silico* screening predicted higher monomer purity and yield, whereas the optimal protein injection volumes were found to be greater and the optimal salt elution concentrations were lower than the ones in the batch single-column process. This observation can be explained by the nature of the 3C-PCCC mode i.e., by the fact, that a column can be loaded with more protein. For for the monomers, a more nonlinear region of the adsorption isotherm could be reached. This resulted in a lower elution salt concentration required. The aggregates, however, bind in the linear region of the adsorption isotherm due to their low concentration and tend to retain in the column during the elution step. Hence, 3C-PCCC shows a great potential to be combined with a continuous precipitation capture process.

6.6. Conclusion

This work has shown a fast and material saving-process development method for an mAb process. By integrating a PEG precipitation and CEX chromatography, a feasible alternative to Protein A chromatography as capture step was demonstrated. For process development, a strategy combining high-throughput methods with empirical and mechanistic modeling has shown promising results which might overcome the drawback of replacing an affinity step.

Precipitating under conditions with pH 8.5 and 12.6 % (w/w) PEG and resolubilisation at pH 4.0 led to a significant reduction in HCP level in combination with a yield of over 96.4%. Additionally, loading onto a CEX column with only minor pH adjustments was enabled. Using a step gradient, an aggregate reduction in combination with product concentration to 11.9 mg/mL was demonstrated. All in all, a flexible time-and material-saving method was demonstrated which allows screening of even more parameters than shown in this case study. Furthermore, the capability of a continuous chromatography process was explored theoretically based on the calibrated mechanistic chromatography model.

In further studies, the upscale of these results should be demonstrated. The execution of a fully continuous process including continuous PEG precipitation in combination with CEX-PCCC at a larger scale would be desirable.

6.7. Acknowledgment

The authors declare no conflict of interest. This project has received funding from the European Union's Horizon 2020 Research and Innovation Programme under grant agreement no. 635557. We kindly thank Lek Pharmaceuticals d.d (Menges, Slovenia) for providing the mAb.

7. In-line Fourier-Transform Infrared Spectroscopy as a Versatile Process Analytical Technology for Preparative Protein Chromatography*

Developing new biopharmaceutical purification technologies and process strategies leads consequently also to an increased demand for advanced analytical technologies, that can meet the requirements of such processes. On the one hand the change from well established and proven platform processes to alternative purification strategies raises the need for enhanced monitoring of the process. On the other hand, the monitoring strategy faces the challenge of identifying different molecules. Usually, biopharmaceutical processes are monitored with the help of univariate signals such as pH, conductivity, pressure, and UV/Vis absorption at a single wavelength [214, 227]. Especially single wavelength UV/Vis adsorption measurements are most commonly used for in-line process monitoring and control. However, this technology is limited in some respects. For example, it is possible to detect multiple proteins in solution, but it is not possible to destingiuish between them. The similarity of the signal prevents the identification of these molecules. Additionally there are many molecules that may be encountered in a purification process that are not UV active at all. For example, PEG-induced protein precipitation involves the addition of a non UV/Vis active precipitant, whose subsequent depletion must be ensured and monitored. The overall objective of the seventh chapter of this work, added as full manuscript in the appendix B, was to develop an in-line sensor capable of distinguishing between different proteins while at the same time being sensitive to a wide range of commonly used molecules in a downstream biopharmaceutical process.

Fourier-Transform Infrared Spectroscopy (FTIR) is a promising technology to fulfill

* A full version of this publication is given in Appendix B and [5]. In the following the major findings relevant for this thesis are summarized.

this demand. This spectroscopy method is non-invasive, quantitative, fast, and has the potential to be performed in-line [228–230]. FTIR spectroscopy measures the vibrational modes of samples and provides a spectroscopic fingerprint of the different measured organic molecules [140, 231, 232]. By measuring the backbone vibrations of proteins, FTIR can be used to detect, quantify and identify proteins. Therefore, FTIR is a widely used method for detecting and distinguishing the integrity of proteins [140]. In this work, in-line FTIR was implemented as process analytical technology (PAT) for preparative protein purification. For this purpose, the FTIR spectrometer was coupled to a preparative chromatography system on laboratory scale. The implementation of the sensor included enabling communication between the devices and thus enabling automated FTIR measurements in the context of chromatography runs. After the implementation, three case studies were conducted, to demonstrate the versatility of the PAT sensor.

To demonstrate the ability to distinguish between different protein species, a mixture composed of lysozyme and a monoclonal antibody (mAb) was purified using cation exchange chromatography (CEX). The effluent of four runs, with a variation in the gradient elution length, were monitored in-line using FTIR spectroscopy. Three of the runs were used to calibrate a partial least squares regression model (PLS), the forth run was used as validation run. Both proteins show a significant difference in their secondary structure. Therefore, the PLS model was able to successfully distinguish between both proteins, although their elution profiles were overlapping (Fig. 7.1).

In the second case study lysozyme molecules with different PEGylation degrees were purified using CEX. Because PEG shows a prominent band at $1090\,cm^{-1}$ with multiple shoulders, FTIR spectroscopy is able to detect and quantify PEG. However, since proteins are also in the solution and have their fingerprint region at this wavenumbers, it is not possible to quantify the PEG by simply applying an adsorption coefficient. In order to distinguish between PEG and protein, a PLS model was calibrated and applied. Hence, it was possible to quantify the amount of PEG, the protein concentration, and finally calculate the PEGylation degree of the lysozyme during elution (Fig. 7.2).

In a third case study the potential to monitor further process related impurities was demonstrated by the detection and quantification of Triton X-100 in the flow through of a CEX chromatography run. Triton X-100 is used as viral inactivation agent and needs to be below a minimal level after the purification. With the help of a linear regression it was possible to detect and quantify Triton X-100 in the flow through and during the elution.

The results of the case studies show the potential of FTIR spectroscopy as an in-

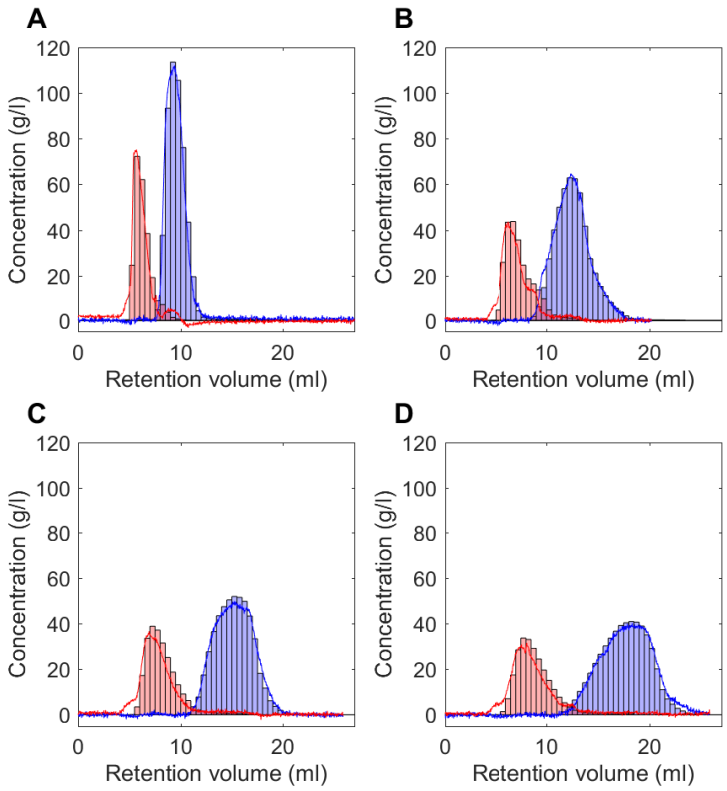

Figure 7.1.: Four chromatographic runs are shown for in-line FTIR measurements and selective quantification of mAb and lysozyme. The red bars and lines refer to the mAb off-line measurement and mAb PLS prediction, respectively. The blue bars and lines refer to the lysozyme off-line measurement and lysozyme PLS prediction, respectively. The different subplots show different gradient lengths: A $1\,CV$, B $2\,CV$, C $3\,CV$, D $4\,CV$.

line sensor for preparative protein purification. The applied monitoring and signal processing strategies allow the monitoring of the process, but also has the potential of active process control. This would, for example, allow active real-time decision making during peak cutting. It was shown that FTIR spectroscopy has the great advantage of being able to detect proteins as well as other small organic components. For the integrated precipitation and IEX process, presented in chapter 6, this sensor is an ideal solution for monitoring the CEX step. Thereby, two applications are feasible. Either monitoring the resolubilized protein solution and thus, the loading onto the CEX column or monitoring the elution of the protein during the CEX. In both cases, in addition to the detection of the mAb concentration, the complete depletion of the PEG, which was added during the precipitation step, can be verified. For the precipitation process itself, the implementation of an in-line FITR sensor probably opens up the possibility to monitor the precipitation and resolubilisation process itself. FTIR spectroscopy has the option of using an attenuated total reflection (ATR)

cell instead of measuring in transmission mode. As ATR has a very low penetration depth into the sample, it might be possible to distinguish between precipitated and soluble protein. Therefore, with ATR FITR only the soluble protein might be detected. Further investigations have to show whether ATR FTIR can be a promising technique for monitoring processes with turbid solutions.

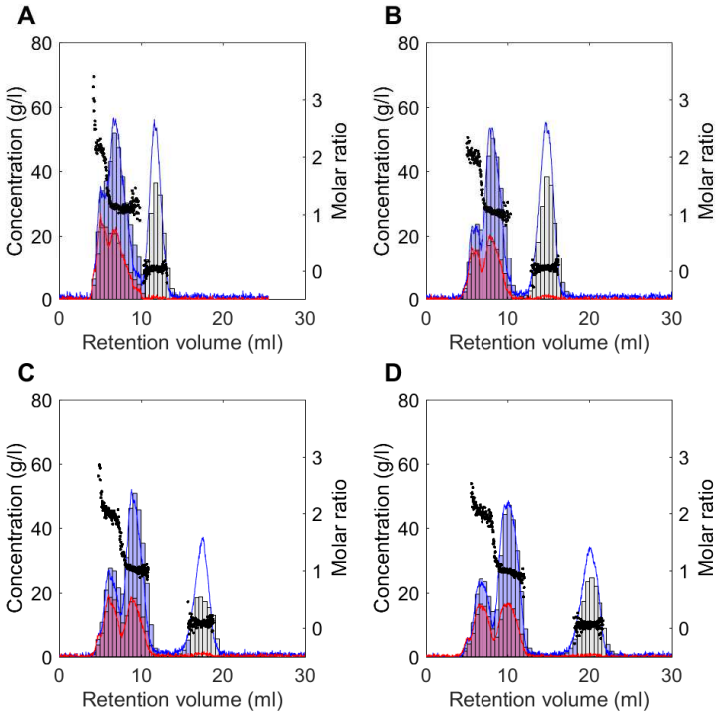

Figure 7.2.: Four chromatographic runs are shown for in-line FTIR measurements and selective quantification of PEG and lysozyme. The red bars and lines refer to the PEG off-line measurement and PEG PLS prediction, respectively. The blue bars and lines refer to the lysozyme off-line measurement and lysozyme PLS prediction, respectively. Grey bars correspond to measured protein concentrations on partially precipitated samples. Black dots show the molar ratio between PEG and lysozyme, i.e. the current mean PEGylation degree. The different subplots show different gradient lengths: A $2\,CV$, B $3\,CV$, C $4\,CV$, D $5\,CV$.

8. Conclusion and Outlook

The present PhD thesis addresses issues, currently preventing preparative protein precipitation to be implemented into a biopharmaceutical production process for proteins. In academia, such precipitation processes have already proven applicability. Compared to chromatographic based processes, they have shown the potential to make process development easier, more flexible, and more cost-efficient. However, for an industrial utilization there are still several challenges present. This includes a deeper process understanding, a faster and easier process development, and an enhanced monitoring of all included molecules. In these three fields challenges of particular interest were defined. Among the acting forces between proteins, hydrophobic interactions are of great importance, but the underlying mechanism is not fully understood. The gained knowledge of the precipitation mechanism can be used for better process understanding and was further applied to derive a mechanistic precipitation model, for PEG-induced precipitation. The model showed the possibility to make process development easier and less time consuming. Additionally, a new process development strategy was presented, with the focus on integrated up- and downstream process development. The influence of previous production steps was considered, as well as following polishing steps. In addition, new monitoring strategies, incorporating in-line FTIR spectroscopy as PAT tool, were investigated. The applicability for chromatography was shown in three different case studies.

In the first part of this thesis, measurements of the protein hydrophobicity and thermal stability were applied, to explain and estimate the protein phase state. In combination, both techniques could successfully be used to describe the crystallization behavior of glucose isomerase, at varying salt types, salt concentrations, and pH values. The different observed crystal structures could be described and explained with differences in the protein surface hydrophobicity, and following estimated by HIC. With the help of HIC, a deeper understanding of the influence of hydrophobic interactions during protein-protein interaction was generated.

Consequently, the similarities between HIC and protein-protein interaction could be dedicated to the same hydrophobic driven mechanism. By introducing water as additional component into the precipitation process, it was possible to derive

an isotherm, which is capable to describe the precipitation behavior of proteins at varying initial protein and PEG concentrations. Thereby, an equilibrium between a well-ordered, and a bulk-like ordered water structure was assumed. The developed mechanistic precipitation model allowed to predict the precipitation behavior over the entire precipitation curve. Together with the capability to describe accurately the precipitation behavior of small proteins the model is superior to other commonly applied models. With the help of high-throughput experiments the model predictability was validated with data beyond the calibration range.

The second part of this thesis focused on the process development of a purification step for a complex mAb feedstock. The influence of upstream conditions on a PEG-induced precipitation step was investigated. Thereby, a destabilizing effect of the contaminants was detected, compared to pure mAb solutions. The destabilization could be assigned to the occurrence of interactions between the mAb and macromolecules like HCP, or DNA. On the other hand, a stabilizing effect of components present in the cell culture medium could be shown. These molecules most likely prevent mAb-macromolecule interactions, and therefore, lead to higher purities after the precipitation step. The presented study pointed out the importance of considering the needs of a precipitation step already during the development of the USP.

Considering the following purification strategies a development platform was evolved. The platform combines HTS for the precipitation step, empiric modeling for the resolubilisation step, and mechanistic modeling for the optimization of the following CEX step. The developed process showed the potential to replace Protein A affinity chromatography as capture step during a mAb process. Thereby, process-related contaminants were purified mainly during the precipitation and resolubilisation step. Product-related contaminants were depleted using CEX. By performing the resolubilisation at low pH values, a direct binding of the product onto the CEX column was enabled. Process integration was further considered as during CEX, purification, and concentration of the product were performed simultaneously. The development platform can be used to optimize a classical batch process, but is also capable for the development of a continuous one.

The last part of the thesis was contributed to the development of in-line monitoring strategies for chromatography, taking into account the requirements of a polishing step after precipitation. A sensor setup was developed, combining in-line FTIR spectroscopy with PLS regression modeling, for the monitoring of a chromatographic separation step. Based on differences in their secondary structure, it was possible to distinguish between different proteins. The strength of FTIR spectroscopy lies in the ability to detect also non UV/Vis active molecules, for example PEG. This was successfully shown in a case study, where different PEGylated lysozyme species were detected during CEX elution. In another case study, the variety of FTIR

spectroscopy was shown by performing selective mass balancing with the process-related contaminant Triton X-100.

In summary, this thesis contributes to a better understanding of the acting forces between proteins, and the mechanism of preparative protein precipitation. The developed mechanistic precipitation model can build the basis for further model extensions. An additional description of the behavior of multi-component solutions, would enable *in silico* process development. The knowledge, obtained through the study of the precipitation behavior of complex protein solutions, can build a good basis for that. Model based optimization of the precipitation step would fit perfectly in the presented development strategy. With the extension of the development toolbox, a further reduction of necessary wet laboratory experiments, and material consumption could be achieved. At the same time, meta modeling would be enabled, to describe the influence of each purification step towards the whole production process. This can lead to a reduction of uncertainties, a more robust process, and probably help protein precipitation to be used as alternative purification step. While for classical blockbuster mAb products the currently used platform based strategy might be more comfortable, new drug, or biosimilar products will raise the necessity for cheaper, and more flexible processes, including the corresponding development strategies. Especially, with the transfer to continuous manufacturing, the necessity of simple and easy adaptable processes could make protein precipitation more attractive to the biopharmaceutical industry. The developed in-line monitoring strategy can help to ensure constant product quality over long term productions. Especially, the lack of an in-line sensor for monitoring the precipitation step itself, shows the need for further research. The developed methods of this work could potentially be transferred to different sensors and help to meet these requirements. Additionally, combination with other in-line sensors would probably help to detect more, at the moment hidden, information about the product, the contaminants, or the composition. As a result, in-line process monitoring in combination with process modeling could help to perform route cause investigations, and consequently active process control.

Bibliography

1. Baumgartner, K., Großhans, S., Schütz, J., Suhm, S. & Hubbuch, J. Prediction of salt effects on protein phase behavior by HIC retention and thermal stability. *J. Pharmaceut. biomed.* **128**. 216–225 https://doi.org/10.1016/j.jpba.2016.04.040 (2016) (cit. on pp. vii, xii, 28, 35, 42).
2. Großhans, S., Wang, G. & Hubbuch, J. Water on hydrophobic surfaces: mechanistic modeling of polyethylene glycol-induced protein precipitation. *Bioproc. Biosyst. Eng.* 1–8 https://doi.org/10.1007/s00449-018-2054-5 (2018) (cit. on pp. vii, xiii, 28, 55).
3. Großhans, S., Suhm, S. & Hubbuch, J. Precipitation of complex antibody solutions: influence of contaminant composition and cell culture medium on the precipitation behavior. *Bioproc. Biosyst. Eng.* 1–13 https://doi.org/10.1007/s00449-019-02103-y (2019) (cit. on pp. viii, xiii, 28).
4. Großhans, S., Wang, G., Fischer, C. & Hubbuch, J. An integrated precipitation and ion-exchange chromatography process for antibody manufacturing: Process development strategy and continuous chromatography exploration. *J. Chromatogr. A* **1533**. 66–76 https://doi.org/10.1016/j.chroma.2017.12.013 (2018) (cit. on pp. viii, xiv, 28, 63, 70).
5. Großhans, S., Rüdt, M., Sanden, A., Brestrich, N., Morgenstern, J., Heissler, S. & Hubbuch, J. In-line Fourier-transform infrared spectroscopy as a versatile process analytical technology for preparative protein chromatography. *J. Chromatogr. A* **1547**. 37–44 https://doi.org/10.1016/j.chroma.2018.03.005 (2018) (cit. on pp. viii, xiv, 28, 99).
6. Thomas, J. A. & Fuchs, R. L. *Biotechnology and safety assessment* (Elsevier, 2002) (cit. on p. 1).
7. Watson, J. D., Crick, F. H., *et al.* Molecular structure of nucleic acids. *Nature* **171**, 737–738 (1953) (cit. on p. 1).
8. Chmiel, H. *Bioprozesstechnik* (Springer, 2011) (cit. on p. 1).
9. Rader, R. A. (Re) defining biopharmaceutical. *Nat. Biotechnol.* **26**, 743 (2008) (cit. on p. 1).
10. Craik, D. J., Fairlie, D. P., Liras, S. & Price, D. The future of peptide-based drugs. *Chem. Biol. Drug Des.* **81**, 136–147 (2013) (cit. on pp. 1, 2).
11. Kesik-Brodacka, M. Progress in biopharmaceutical development. *Biotechnol. Applied Bioc.* **65**, 306–322 (2018) (cit. on p. 1).

12. Dimitrov, D. S. in *Therapeutic Proteins* 1–26 (Springer, 2012) (cit. on p. 1).
13. Sauerborn, M., Brinks, V., Jiskoot, W. & Schellekens, H. Immunological mechanism underlying the immune response to recombinant human protein therapeutics. *Trends Pharmacol. Sci.* **31**, 53–59 (2010) (cit. on p. 1).
14. Kelley, B. *Industrialization of mAb production technology: the bioprocessing industry at a crossroads* in *Mabs* **1** (2009), 443–452 (cit. on pp. 2, 17, 54).
15. Lines, S. Drug patent expirations and the patent cliff. *US Pharm.* **37**, 12–20 (2012) (cit. on p. 2).
16. Gagnon, P. Technology trends in antibody purification. *J. Chromatogr. A* **1221**, 57–70 (2012) (cit. on p. 2).
17. Walsh, G. Biopharmaceutical benchmarks 2014. *Nat. Biotechnol.* **32**, 992 (2014) (cit. on p. 2).
18. Beck, A. *Biosimilar, biobetter and next generation therapeutic antibodies* in *Mabs* **3** (2011), 107–110 (cit. on p. 2).
19. Jain, K. K. *et al. Textbook of personalized medicine* (Springer, 2009) (cit. on p. 2).
20. Baumann, P. & Hubbuch, J. Downstream process development strategies for effective bioprocesses: Trends, progress, and combinatorial approaches. *Eng. Life Sci.* **17**, 1142–1158 (2017) (cit. on pp. 2, 41).
21. Sommer, R., Satzer, P., Tscheliessnig, A., Schulz, H., Helk, B. & Jungbauer, A. Combined polyethylene glycol and CaCl2 precipitation for the capture and purification of recombinant antibodies. *Proc. Biochem.* **49**, 2001–2009 (2014) (cit. on pp. 2, 13, 41, 55).
22. Hubbuch, J., Kind, M. & Nirschl, H. Preparative Protein Crystallization. *Chem. Eng. Technol.* (2019) (cit. on p. 2).
23. Oelmeier, S. A., Ladd-Effio, C. & Hubbuch, J. Alternative separation steps for monoclonal antibody purification: Combination of centrifugal partitioning chromatography and precipitation. *J. Chromatogr. A* **1319**, 118–126 (2013) (cit. on pp. 2, 55, 83).
24. Charcosset, C. Purification of proteins by membrane chromatography. *J Chem. Technol. Biot.* **71**, 95–110 (1998) (cit. on p. 2).
25. Ladisch, M. *Bioseparations Engineering: Principles, Practice and Economics. 2001* (cit. on p. 2).
26. Knevelman, C., Davies, J., Allen, L. & Titchener-Hooker, N. J. High-throughput screening techniques for rapid PEG-based precipitation of IgG4 mAb from clarified cell culture supernatant. *Biotechnol. Prog.* **26**, 697–705 (2010) (cit. on pp. 2, 18, 55, 77, 79).
27. Tscheliessnig, A., Satzer, P., Hammerschmidt, N., Schulz, H., Helk, B. & Jungbauer, A. Ethanol precipitation for purification of recombinant antibodies. *J. Biotechnol.* **188**, 17–28 (2014) (cit. on pp. 2, 13).

28. Hubbuch, J. High-throughput process development. *Biotechnol. J.* **7**, 1185–1185 (2012) (cit. on p. 2).

29. Osberghaus, A., Drechsel, K., Hansen, S., Hepbildikler, S., Nath, S., Haindl, M., von Lieres, E. & Hubbuch, J. Model-integrated process development demonstrated on the optimization of a robotic cation exchange step. *Chem. Eng. Sci.* **76**, 129–139 (2012) (cit. on p. 2).

30. Nfor, B. K., Ahamed, T., van Dedem, G. W., Verhaert, P. D., van der Wielen, L. A., Eppink, M. H., van de Sandt, E. J. & Ottens, M. Model-based rational methodology for protein purification process synthesis. *Chem. Eng. Sci.* **89**, 185–195 (2013) (cit. on p. 2).

31. Huuk, T. C., Hahn, T., Osberghaus, A. & Hubbuch, J. Model-based integrated optimization and evaluation of a multi-step ion exchange chromatography. *Sep. Purifi Technol.* **136**, 207–222 (2014) (cit. on p. 2).

32. Rathore, A. S., Agarwal, H., Sharma, A. K., Pathak, M. & Muthukumar, S. Continuous processing for production of biopharmaceuticals. *Prep. Biochem. Biotech.* **45**, 836–849 (2015) (cit. on p. 3).

33. Glassey, J., Gernaey, K. V., Clemens, C., Schulz, T. W., Oliveira, R., Striedner, G. & Mandenius, C.-F. Process analytical technology (PAT) for biopharmaceuticals. *Biotechnol. J.* **6**, 369–377 (2011) (cit. on p. 3).

34. Rüdt, M., Briskot, T. & Hubbuch, J. Advances in downstream processing of biologics–Spectroscopy: An emerging process analytical technology. *J. Chromatogr. A* **1490**, 2–9 (2017) (cit. on pp. 3, 22, 164, 165).

35. Latscha, H. P., Kazmaier, U. & Klein, H. A. *Chemie für Biologen* (Springer, 2008) (cit. on p. 4).

36. Roth, C. M., Neal, B. L. & Lenhoff, A. M. Van der Waals interactions involving proteins. *Biophys. J.* **70**, 977–987 (1996) (cit. on p. 4).

37. Dill, K. A. Dominant forces in protein folding. *Biochemistry-US* **29**, 7133–7155 (1990) (cit. on p. 4).

38. Von Stockar, U. & van der Wielen, L. A. *Biothermodynamics: The Role of Thermodynamics in Biochemical Engineering* (EPFL Press, 2013) (cit. on pp. 4, 5).

39. Verwey, E. J. W., Overbeek, J. T. G. & Overbeek, J. T. G. *Theory of the stability of lyophobic colloids* (Courier Corporation, 1999) (cit. on p. 5).

40. Ninham, B. W. On progress in forces since the DLVO theory. *Adv. Colloid Interfac.* **83**, 1–17 (1999) (cit. on p. 5).

41. Hoinkis, J. *Chemie für Ingenieure* (John Wiley & Sons, 2015) (cit. on p. 5).

42. Kauzmann, W. Some Factors in the Interpretation of Protein Denauration. *Adv. Protein Chem.* **29**, 1–63 (1959) (cit. on p. 6).

43. Israelachvili, J. & Pashley, R. The hydrophobic interaction is long range, decaying exponentially with distance. *Nature* **300**, 341–342 (1982) (cit. on p. 6).

44. Tanford, C. The hydrophobic effect and the organization of living matter. *Science* **200**, 1012–1018 (1978) (cit. on p. 6).

45. Sun, Q. The physical origin of hydrophobic effects. *Chem. Phys. Lett.* **672**, 21–25 (2017) (cit. on pp. 6, 35).

46. Huang, D. M., Geissler, P. L. & Chandler, D. Scaling of hydrophobic solvation free energies. *J. Phys. Chem. B* **105**, 6704–6709 (2001) (cit. on p. 6).

47. Crommelin, D. J., Sindelar, R. D. & Meibohm, B. *Pharmaceutical biotechnology: fundamentals and applications* (Springer Science & Business Media, 2013) (cit. on p. 7).

48. Lodish, H. F. Post-translational modification of proteins. *Enzyme Microb. Tech.* **3**, 178–188 (1981) (cit. on p. 7).

49. Wang, W., Nema, S. & Teagarden, D. Protein aggregationPathways and influencing factors. *Int. J. Pharm.* **390**, 89–99 (2010) (cit. on pp. 7, 35, 140).

50. Malamud, D. & Drysdale, J. W. Isoelectric points of proteins: a table. *Anal. Biochem.* **86**, 620–647 (1978) (cit. on p. 7).

51. Baumgartner, K., Galm, L., Nötzold, J., Sigloch, H., Morgenstern, J., Schleining, K., Suhm, S., Oelmeier, S. A. & Hubbuch, J. Determination of protein phase diagrams by microbatch experiments: Exploring the influence of precipitants and pH. *Int. J. Pharm.* **479**, 28–40 (2015) (cit. on pp. 7, 12, 141, 142, 144, 145, 154, 169).

52. Valente, K. N., Schaefer, A. K., Kempton, H. R., Lenhoff, A. M. & Lee, K. H. Recovery of Chinese hamster ovary host cell proteins for proteomic analysis. *Biotechnol. J.* **9**, 87–99 (2014) (cit. on pp. 7, 71, 95).

53. Neal, B., Asthagiri, D, Velev, O., Lenhoff, A. & Kaler, E. Why is the osmotic second virial coefficient related to protein crystallization? *J. Cryst. Growth* **196**, 377–387 (1999) (cit. on pp. 7, 140).

54. Gey, M. H. *Instrumentelle Analytik und Bioanalytik: Biosubstanzen, Trennmethoden, Strukturanalytik, Applikationen* (Springer-Verlag, 2015) (cit. on p. 7).

55. Kim, S. G., Bae, Y. C. & Ryu, S. O. Salt-induced protein precipitation in aqueous solution: The effect of pre-aggregation. *Korean J. Chem. Eng.* **17**, 638–642 (2000) (cit. on p. 8).

56. Green, A. A. Studies in the physical chemistry of the proteins VIII. The solubility of hemoglobin in concentrated salt solutions. A study of the salting out of proteins. *J. Biol. Chem.* **93**, 495–516 (1931) (cit. on pp. 8, 78).

57. Kuehner, D. E., Blanch, H. W. & Prausnitz, J. M. Salt-induced protein precipitation: Phase equilibria from an equation of state. *Fluid Phase Equilibr.* **116**, 140–147 (1996) (cit. on pp. 8, 40, 78).

58. Shih, Y.-C., Prausnitz, J. M. & Blanch, H. W. Some characteristics of protein precipitation by salts. *Biotechnol. Bioeng.* **40**, 1155–1164 (1992) (cit. on p. 8).

59. Tanford, C. *et al. Physical chemistry of macromolecules* (Wiley, 1961) (cit. on p. 9).

60. Timasheff, S. N., Lee, J. C., Pittz, E. P. & Tweedy, N. The interaction of tubulin and other proteins with structure-stabilizing solvents. *J. Colloid Interf. Sci.* **55**, 658–663 (1976) (cit. on p. 9).

61. Pittz, E. P. & Timasheff, S. N. Interaction of ribonuclease A with aqueous 2-methyl-2, 4-pentanediol at pH 5.8. *Biochemistry-US* **17**, 615–623 (1978) (cit. on p. 9).

62. Lee, J. C. & Timasheff, S. N. The stabilization of proteins by sucrose. *J. Biol. Chem.* **256**, 7193–7201 (1981) (cit. on pp. 9, 56).

63. Arakawa, T. & Timasheff, S. N. Preferential interactions of proteins with salts in concentrated solutions. *Biochemistry-US* **21**, 6545–6552 (1982) (cit. on pp. 9, 56, 157).

64. Hofmeister, F. Zur lehre von der wirkung der salze. *Arch. Exp. Pathol. Phar.* **25**, 1–30 (1888) (cit. on p. 9).

65. Collins, K. D. & Washabaugh, M. W. The Hofmeister effect and the behaviour of water at interfaces. *Q. Rev. Biophys.* **18**, 323–422 (1985) (cit. on p. 9).

66. Omta, A. W., Kropman, M. F., Woutersen, S. & Bakker, H. J. Negligible effect of ions on the hydrogen-bond structure in liquid water. *Science* **301**, 347–349 (2003) (cit. on p. 9).

67. Zhang, Y. & Cremer, P. S. Interactions between macromolecules and ions: the Hofmeister series. *Curr. Opin. Chem. Biol.* **10**, 658–663 (2006) (cit. on pp. 9, 155, 156, 159, 160).

68. Polson, A, Potgieter, G., Largier, J., Mears, G. & Joubert, F. The fractionation of protein mixtures by linear polymers of high molecular weight. *BBA-Gen. Subjects* **82**, 463–475 (1964) (cit. on pp. 9, 13, 40, 55, 78).

69. Atha, D. H. & Ingham, K. C. Mechanism of precipitation of proteins by polyethylene glycols. Analysis in terms of excluded volume. *J. Biol. Chem.* **256**, 12108–12117 (1981) (cit. on pp. 9, 41, 43, 78).

70. Arakawa, T. & Timasheff, S. N. Mechanism of polyethylene glycol interaction with proteins. *Biochemistry-US* **24**, 6756–6762 (1985) (cit. on p. 9).

71. Asakura, S. & Oosawa, F. Interaction between particles suspended in solutions of macromolecules. *J. Polym. Sci.* **33**, 183–192 (1958) (cit. on pp. 10, 41, 55, 78).

72. Odijk, T. Depletion theory and the precipitation of protein by polymer. *J. Phys. Chem. B* **113**, 3941–3946 (2009) (cit. on pp. 10, 41, 55, 78).

73. Asherie, N. Protein crystallization and phase diagrams. *Methods* **34**, 266–272 (2004) (cit. on pp. 10, 155).

74. Chayen, N., Boggon, T., Cassetta, A, Deacon, A, Gleichmann, T, Habash, J, Harrop, S., Helliwell, J., Nieh, Y., Peterson, M., *et al.* Trends and challenges in experimental macromolecular crystallography. *Q. Rev. Biophys.* **29**, 227–278 (1996) (cit. on p. 11).

75. Ahamed, T., Esteban, B. N. A., Ottens, M., van Dedem, G. W. K., van der Wielen, L. A. M., Bisschops, M. A. T., Lee, A., Pham, C. & Thömmes, J. Phase behavior of an intact monoclonal antibody. *Biophys. J.* **93**, 610–619 (July 2007) (cit. on pp. 11, 35, 140, 155).

76. Finet, S., Vivarès, D., Bonneté, F. & Tardieu, A. in *Method. Enzymol.* 105–129 (Elsevier, 2003) (cit. on p. 11).

77. Stevens, R. C. High-throughput protein crystallization. *Curr. Opin. Struc. Biol.* **10**, 558–563 (2000) (cit. on p. 11).

78. Chayen, N. E. & Saridakis, E. Protein crystallization: from purified protein to diffraction-quality crystal. *Nat. Methods* **5**, 147–153 (2008) (cit. on p. 11).

79. Chayen, N. E. Comparative studies of protein crystallization by vapour-diffusion and microbatch techniques. *Acta Crystallogr. D* **54**, 8–15 (1998) (cit. on p. 12).

80. Cohn, E. J. The Properties and Functions of the Plasma Proteins, with a Consideration of the Methods for their Separation and Purification. *Chem. Rev.* **28**, 395–417 (1941) (cit. on p. 12).

81. Dos Santos, R., Carvalho, A. L. & Roque, A. C. A. Renaissance of protein crystallization and precipitation in biopharmaceuticals purification. *Biotechnol. Adv.* **35**, 41–50 (2017) (cit. on p. 12).

82. Schaffner, W & Weissmann, C. A rapid, sensitive, and specific method for the determination of protein in dilute solution. *Anal. Biochem.* **56**, 502–514 (1973) (cit. on p. 12).

83. Groß, M. & Kind, M. Bulk Crystallization of Proteins by Low-Pressure Water Evaporation. *Chem. Eng. Technol.* **39**, 1483–1489 (2016) (cit. on p. 13).

84. Buchacher, A. & Iberer, G. Purification of intravenous immunoglobulin G from human plasma–aspects of yield and virus safety. *Biotechnol. J.* **1**, 148–163 (2006) (cit. on pp. 13, 40).

85. Narhi, L. O., Caughey, D., Horan, T. P., Kita, Y., Chang, D. & Arakawa, T. Fractionation and characterization of polyclonal antibodies using three progressively more chaotropic solvents. *Anal. Biochem.* **253**, 246–252 (1997) (cit. on p. 13).

86. Juckles, I. Fractionation of proteins and viruses with polyethylene glycol. *Biochimi. Biophys. Acta* **229**, 535–546 (1971) (cit. on p. 13).

87. Tsoka, S., Ciniawskyj, O. C., Thomas, O. R., Titchener-Hooker, N. J. & Hoare, M. Selective flocculation and precipitation for the improvement of virus-like particle recovery from yeast homogenate. *Biotechnol. Progr.* **16**, 661–667 (2000) (cit. on pp. 13, 40).

88. Zeltins, A. Construction and characterization of virus-like particles: a review. *Mol. Biotechnol.* **53**, 92–107 (2013) (cit. on pp. 13, 40).

89. Ghosh, R. Separation of human albumin and IgG by a membrane-based integrated bioseparation technique involving simultaneous precipitation, microfiltration and membrane adsorption. *J. Membrane Sci.* **237**, 109–117 (2004) (cit. on pp. 13, 40, 78).

90. Sim, S.-L., He, T., Tscheliessnig, A., Mueller, M., Tan, R. B. & Jungbauer, A. Protein precipitation by polyethylene glycol: A generalized model based on hydrodynamic radius. *J. Biotechnol.* **157**, 315–319 (2012) (cit. on pp. 13, 41, 48, 55, 78).

91. Sheth, R. D., Madan, B., Chen, W. & Cramer, S. M. High-throughput screening for the development of a monoclonal antibody affinity precipitation step using ELP-z stimuli responsive biopolymers. *Biotechnol. Bioeng.* **110**, 2664–2676 (2013) (cit. on p. 13).

92. Capito, F., Bauer, J., Rapp, A., Schroter, C., Kolmar, H. & Stanislawski, B. Feasibility study of semi-selective protein precipitation with salt-tolerant copolymers for industrial purificiation of therapeutic antibodies. *Biotechnol. Bioeng.* **110**, 2915–2927 (2013) (cit. on pp. 13, 77).

93. Schmidt-Traub, H., Schulte, M. & Seidel-Morgenster, A. *Preparative Chromatography* (Wiley-VCH, 2013) (cit. on pp. 13, 19, 20).

94. Healthcare, G. Ion Exchange Chromatography & Chromatofocusing: Principles and Methods. *GE HealtCare Handbooks*, 170 (2016) (cit. on p. 14).

95. Wu, C.-S. *Handbook of size exclusion chromatography and related techniques: revised and expanded* (CRC Press, 2003) (cit. on p. 13).

96. Sisodiya, V. N., Lequieu, J., Rodriguez, M., McDonald, P. & Lazzareschi, K. P. Studying host cell protein interactions with monoclonal antibodies using high throughput protein A chromatography. *Biotechnol. J.* **7**, 1233–1241 (2012) (cit. on pp. 14, 71).

97. Labrou, N. Design and selection of ligands for affinity chromatography. *J. Chromatogr. B* **790**, 67–78 (2003) (cit. on p. 14).

98. Hochuli, E, Döbeli, H & Schacher, A. New metal chelate adsorbent selective for proteins and peptides containing neighbouring histidine residues. *J. Chromatogr. A* **411**, 177–184 (1987) (cit. on p. 14).

99. Smith, D. B. & Johnson, K. S. Single-step purification of polypeptides expressed in Escherichia coli as fusions with glutathione S-transferase. *Gene* **67**, 31–40 (1988) (cit. on p. 14).

100. Jungbauer, A. & Hahn, R. in *Method. Enzymol.* 349–371 (Elsevier, 2009) (cit. on p. 14).

101. Melander, W. & Horváth, C. Salt effects on hydrophobic interactions in precipitation and chromatography of proteins: an interpretation of the lyotropic series. *Arch. Biochem. Biophys.* **183**, 200–215 (1977) (cit. on pp. 15, 42).

102. Queiroz, J., Tomaz, C. & Cabral, J. Hydrophobic interaction chromatography of proteins. *J. Biotechnol.* **87**, 143–159 (2001) (cit. on p. 15).

103. Melander, W., Corradini, D. & Horváth, C. Salt-mediated retention of proteins in hydrophobic-interaction chromatography: application of solvophobic theory. *J. Chromatogr. A* **317**, 67–85 (1984) (cit. on p. 15).

104. Arakawa, T. Thermodynamic analysis of the effect of concentrated salts on protein interaction with hydrophobic and polysaccharide columns. *Arch. Biochem. Biophys.* **248**, 101–105 (1986) (cit. on p. 15).

105. Tanford, C. *The hydrophobic effect: formation of micelles and biological membranes 2d ed* (J. Wiley., 1980) (cit. on pp. 15, 41).

106. Shiraga, K, Suzuki, T, Kondo, N & Ogawa, Y. Hydration and hydrogen bond network of water around hydrophobic surface investigated by terahertz spectroscopy. *J. Chem. Phys.* **141**, 12B647_1 (2014) (cit. on pp. 15, 41).

107. Chatterjee, S. *FDA perspective on continuous manufacturing* in *IFPAC Annual Meeting, Baltimore, MD* **26** (2012), 34–42 (cit. on p. 15).

108. Jungbauer, A. Preparative chromatography of biomolecules. *J. Chromatogr. A* **639**, 3–16 (1993) (cit. on p. 15).

109. Carta, G. & Perez-Almodovar, E. X. Productivity considerations and design charts for biomolecule capture with periodic countercurrent adsorption systems. *Sep. Sci. Technol.* **45**, 149–154 (2010) (cit. on p. 16).

110. Angarita, M., Müller-Späth, T., Baur, D., Lievrouw, R., Lissens, G. & Morbidelli, M. Twin-column CaptureSMB: a novel cyclic process for protein A affinity chromatography. *J. Chromatogr. A* **1389**, 85–95 (2015) (cit. on pp. 16, 77).

111. Steinebach, F., Müller-Späth, T. & Morbidelli, M. Continuous counter-current chromatography for capture and polishing steps in biopharmaceutical production. *Biotechnol. J.* **11**, 1126–1141 (2016) (cit. on p. 16).

112. Schlegl, R., Tscheliessnig, A., Necina, R., Wandl, R. & Jungbauer, A. Refolding of proteins in a CSTR. *Chem. Eng. Sci.* **60**, 5770–5780 (2005) (cit. on p. 16).

113. Jungbauer, A. Continuous downstream processing of biopharmaceuticals. *Trends Biotechnol.* **31**, 479–492 (2013) (cit. on pp. 16, 40).

114. Hammerschmidt, N., Hobiger, S. & Jungbauer, A. Continuous polyethylene glycol precipitation of recombinant antibodies: Sequential precipitation and resolubilization. *Proc. Biochem.* **51**, 325–332 (2016) (cit. on pp. 16, 43, 77, 94).

115. Kuczewski, M., Schirmer, E., Lain, B. & Zarbis-Papastoitsis, G. A single-use purification process for the production of a monoclonal antibody produced in a PER. C6 human cell line. *Biotechnol. J.* **6**, 56–65 (2011) (cit. on p. 16).

116. Shukla, A. A., Hubbard, B., Tressel, T., Guhan, S. & Low, D. Downstream processing of monoclonal antibodies application of platform approaches. *J. Chromatogr. B* **848**, 28–39 (2007) (cit. on pp. 17, 56, 94).

117. Wurm, F. M. Production of recombinant protein therapeutics in cultivated mammalian cells. *Nat. Biotechnol.* **22**, 1393 (2004) (cit. on p. 17).

118. Follman, D. K. & Fahrner, R. L. Factorial screening of antibody purification processes using three chromatography steps without protein A. *J. Chromatogr. A* **1024**, 79–85 (2004) (cit. on p. 17).

119. Hale, G, Drumm, A, Harrison, P & Phillips, J. Repeated cleaning of protein A affinity column with sodium hydroxide. *J. Immunol. Methods* **171**, 15–21 (1994) (cit. on p. 17).

120. Hong, J., Edel, J. B., *et al.* Micro-and nanofluidic systems for high-throughput biological screening. *Drug discov. Today* **14**, 134–146 (2009) (cit. on p. 18).

121. Hertzberg, R. P. & Pope, A. J. High-throughput screening: new technology for the 21st century. *Curr. Opin. Chem. Biol.* **4**, 445–451 (2000) (cit. on p. 18).

122. Chandler, M. & Zydney, A. High throughput screening for membrane process development. *J. Membrane Sci.* **237**, 181–188 (2004) (cit. on p. 18).

123. Łącki, K. M. High-throughput process development of chromatography steps: Advantages and limitations of different formats used. *Biotechnol. J.* **7**, 1192–1202 (2012) (cit. on p. 18).

124. Gregoire, S. & Kwon, I. A revisited folding reporter for quantitative assay of protein misfolding and aggregation in mammalian cells. *Biotechnol. J.* **7**, 1297–1307 (2012) (cit. on p. 18).

125. Bensch, M., Selbach, B. & Hubbuch, J. High throughput screening techniques in downstream processing: preparation, characterization and optimization of aqueous two-phase systems. *Chem. Eng. Sci.* **62**, 2011–2021 (2007) (cit. on p. 18).

126. Montgomery, D. C. *Design and analysis of experiments* (John wiley & sons, 2017) (cit. on p. 18).

127. Coffman, J. L., Kramarczyk, J. F. & Kelley, B. D. High-throughput screening of chromatographic separations: I. Method development and column modeling. *Biotechnol. Bioeng.* **100**, 605–618 (2008) (cit. on p. 18).

128. Carta, G. Predicting protein dynamic binding capacity from batch adsorption tests. *Biotechnol. J.* **7**, 1216–20 (2012) (cit. on p. 18).

129. Pirrung, S. M. & Ottens, M. *High-Throughput Process Development - Preparative Chromatography for Separation of Proteins* (John Wiley & Sons, 2017) (cit. on p. 18).

130. Huuk, T. C., Briskot, T., Hahn, T. & Hubbuch, J. A versatile noninvasive method for adsorber quantification in batch and column chromatography based on the ionic capacity. *Biotechnol. Progr.* **32**, 666–677 (2016) (cit. on pp. 18, 84).

131. Nfor, B. K., Verhaert, P. D., van der Wielen, L. A., Hubbuch, J. & Ottens, M. Rational and systematic protein purification process development: the next generation. *Trends Biotechnol.* **27**, 673–679 (2009) (cit. on p. 19).

132. Brooks, C. A. & Cramer, S. M. Steric mass-action ion exchange: Displacement profiles and induced salt gradients. *Fluid Phase Equilibr.* **38**, 1969–1978 (1992) (cit. on pp. 20, 79).

133. Velayudhan, A. & Horváth, C. Preparative chromatography of proteins: Analysis of the multivalent ion-exchange formalism. *J. Chromatogr. A* **443**, 13–29 (1988) (cit. on p. 20).

134. Jakobsson, N., Karlsson, D., Axelsson, J. P., Zacchi, G. & Nilsson, B. Using computer simulation to assist in the robustness analysis of an ion-exchange chromatography step. *J. Chromatogr. A* **1063**, 99–109 (2005) (cit. on pp. 21, 79).

135. Hahn, T., Huuk, T., Heuveline, V. & Hubbuch, J. Simulating and optimizing preparative protein chromatography with ChromX. *J. Chem. Educ.* **92**, 1497–1502 (2015) (cit. on pp. 21, 80).

136. Group, E.-E. R. *et al.* Good Manufacturing Practices (GMPs) for the 21st century–Food processing. *Final Report prepared for US Food and Drug Administration* (2004) (cit. on p. 21).

137. Food, Administration, D., *et al.* Guidance for industry, PAT-A Framework for Innovative Pharmaceutical Development, Manufacturing and Quality Assurance. *http://www. fda. gov/cder/guidance/published. html* (2004) (cit. on p. 21).

138. Bakeev, K. A. *Process analytical technology: spectroscopic tools and implementation strategies for the chemical and pharmaceutical industries* (John Wiley & Sons, 2010) (cit. on p. 21).

139. Kessler, W. *Multivariate datenanalyse: für die pharma, bio-und Prozessanalytik* (John Wiley & Sons, 2007) (cit. on pp. 22–24).

140. Jiskoot, W. & Crommelin, D. *Methods for structural analysis of protein pharmaceuticals* (Springer Science & Business Media, 2005) (cit. on pp. 25, 100, 165, 172).

141. Günzler, H., Böck, H. & Günzler-Böck... *IR-Spektroskopie: Eine Einführung* (Wiley Online Library, 1975) (cit. on pp. 25, 26).

142. Moorkens, E., Meuwissen, N., Huys, I., Declerck, P., Vulto, A. G. & Simoens, S. The market of biopharmaceutical medicines: a snapshot of a diverse industrial landscape. *Front Pharmacol.* **8**, 314 (2017) (cit. on p. 40).

143. Marichal-Gallardo, P. & Alvarez, M. State-of-the-art in downstream processing of monoclonal antibodies: Process trends in design and validation. *Biotechnol. Progr.* **28**, 899–916 (2012) (cit. on p. 40).

144. Farid, S. S. Process economics of industrial monoclonal antibody manufacture. *J. Chromatogr. B.* **848**, 8–18 (2007) (cit. on pp. 40, 54).

145. Mestre-Ferrandiz, J., Towse, A. & Berdud, M. Biosimilars: how can payers get long-term savings? *Pharmacoeconomics* **34**, 609–616 (2016) (cit. on p. 40).

146. Sekhon, B. S. & Saluja, V. Biosimilars: an overview. *Biosimilars* **1**, 1–11 (2011) (cit. on p. 40).

147. Chon, J. H. & Zarbis-Papastoitsis, G. Advances in the production and downstream processing of antibodies. *New Biotechnol.* **28**, 458–463 (2011) (cit. on pp. 40, 54).

148. Cohn, E. J., Strong, L. E., Hughes, W., Mulford, D., Ashworth, J., Melin, M. e. & Taylor, H. Preparation and Properties of Serum and Plasma Proteins. IV. A System for the Separation into Fractions of the Protein and Lipoprotein Components of Biological Tissues and Fluids1a, b, c, d. *J. Am. Chem. Soc.* **68**, 459–475 (1946) (cit. on pp. 40, 78).

149. Brooks, D., Bradford, T. & Hopwood, J. An improved method for the purification of IgG monoclonal antibodies from culture supernatants. *J. Immunol. Methods* **155**, 129–132 (1992) (cit. on pp. 40, 78).

150. McDonald, P., Victa, C., Carter-Franklin, J. N. & Fahrner, R. Selective antibody precipitation using polyelectrolytes: A novel approach to the purification of monoclonal antibodies. *Biotechnol. Bioeng.* **102**, 1141–1151 (2009) (cit. on pp. 41, 77).

151. Cramer, S. M. & Holstein, M. A. Downstream bioprocessing: recent advances and future promise. *Curr. Opin. in Chem. Eng.* **1**, 27–37 (2011) (cit. on p. 41).

152. Chhatre, S., Farid, S. S., Coffman, J., Bird, P., Newcombe, A. R. & Titchener-Hooker, N. J. How implementation of quality by design and advances in biochemical engineering are enabling efficient bioprocess development and manufacture. *J. Chem. Technol. Biot.* **86**, 1125–1129 (2011) (cit. on p. 41).

153. Lewus, R. A., Darcy, P. A., Lenhoff, A. M. & Sandler, S. I. Interactions and phase behavior of a monoclonal antibody. *Biotechnol. Progr.* **27**, 280–289 (2011) (cit. on p. 41).

154. Cohn, E. J. THE PHYSICAL CHEMISTRY OF THE PROTEINS. *Phys. Rev.* **5**, 349–437 (1925) (cit. on pp. 41, 78).

155. Foster, P., Dunnill, P & Lilly, M. The kinetics of protein salting-out: precipitation of yeast enzymes by ammonium sulfate. *Biotechnol. Bioeng.* **18**, 545–580 (1976) (cit. on p. 41).

156. Przybycien, T. M. & Bailey, J. E. Solubility-activity relationships in the inorganic salt-induced precipitation of α-chymotrypsin. *Enzyme Microb. Tech.* **11**, 264–276 (1989) (cit. on p. 41).

157. Hämmerling, F., Effio, C. L., Andris, S., Kittelmann, J. & Hubbuch, J. Investigation and prediction of protein precipitation by polyethylene glycol using quantitative structure–activity relationship models. *J. Biotechnol.* **241**, 87–97 (2017) (cit. on pp. 41, 48, 69, 78).

158. Laurent, T. The interaction between polysaccharides and other macromolecules. 5. The solubility of proteins in the presence of dextran. *Biochem. J.* **89**, 253 (1963) (cit. on pp. 41, 55, 78).

159. Iverius, P. & Laurent, T. Precipitation of some plasma proteins by the addition of dextran or polyethylene glycol. *BBA-Protein Struct. M.* **133**, 371–373 (1967) (cit. on pp. 41, 55, 78).

160. Polson, A. A theory for the displacement of proteins and viruses with polyethylene glycol. *Prep. Biochem.* **7**, 129–154 (1977) (cit. on pp. 41, 78).

161. De Young, L. R., Fink, A. L. & Dill, K. A. Aggregation of globular proteins. *Accounts Chem. Res.* **26**, 614–620 (1993) (cit. on p. 41).

162. Frank, H. S. & Evans, M. W. Free volume and entropy in condensed systems III. Entropy in binary liquid mixtures; partial molal entropy in dilute solutions; structure and thermodynamics in aqueous electrolytes. *J. Chem. Phys.* **13**, 507–532 (1945) (cit. on p. 41).

163. Head-Gordon, T. Is water structure around hydrophobic groups clathrate-like? *P. Natl. Acad. Sci. USA* **92**, 8308–8312 (1995) (cit. on p. 41).

164. Jungbauer, A., Machold, C. & Hahn, R. Hydrophobic interaction chromatography of proteins: III. Unfolding of proteins upon adsorption. *J. Chromatogr. A* **1079**, 221–228 (2005) (cit. on p. 41).

165. Nfor, B. K., Hylkema, N. N., Wiedhaup, K. R., Verhaert, P. D., Van der Wielen, L. A. & Ottens, M. High-throughput protein precipitation and hydrophobic interaction chromatography: salt effects and thermodynamic interrelation. *J. Chromatogr. A* **1218**, 8958–8973 (2011) (cit. on p. 42).

166. Staby, A. & Mollerup, J. Solute retention of lysozyme in hydrophobic interaction perfusion chromatography. *J. Chromatogr. A* **734**, 205–212 (1996) (cit. on p. 42).

167. Mollerup, J. M. Applied thermodynamics: A new frontier for biotechnology. *Fluid Phase Equilibr.* **241**, 205–215 (2006) (cit. on p. 42).

168. Chen, J. & Cramer, S. M. Protein adsorption isotherm behavior in hydrophobic interaction chromatography. *J. Chromatogr. A* **1165**, 67–77 (2007) (cit. on p. 42).

169. Wang, G., Hahn, T. & Hubbuch, J. Water on hydrophobic surfaces: Mechanistic modeling of hydrophobic interaction chromatography. *J. Chromatogr. A* **1465**, 71–78 (2016) (cit. on p. 42).

170. Afanasiev, V. N., Ustinov, A. N. & Vashurina, I. Y. Acoustic study of solvent coordination in the hydration shells of potassium iodide. *J. Solution Chem.* **35**, 1477–1491 (2006) (cit. on p. 44).

171. Xia, F., Nagrath, D. & Cramer, S. M. Effect of pH changes on water release values in hydrophobic interaction chromatographic systems. *J. Chromatogr. A* **1079**, 229–235 (2005) (cit. on p. 48).

172. Zhou, R., Huang, X., Margulis, C. J. & Berne, B. J. Hydrophobic collapse in multidomain protein folding. *Science* **305**, 1605–1609 (2004) (cit. on p. 48).

173. Walther, J., Godawat, R., Hwang, C., Abe, Y., Sinclair, A. & Konstantinov, K. The business impact of an integrated continuous biomanufacturing platform for recombinant protein production. *J. Biotechnol.* **213**, 3–12 (2015) (cit. on p. 54).

174. Beck, A. & Reichert, J. M. *Approval of the first biosimilar antibodies in Europe: a major landmark for the biopharmaceutical industry* in *mAbs* **5** (2013), 621–623 (cit. on p. 54).

175. Yoo, D. H. The rise of biosimilars: potential benefits and drawbacks in rheumatoid arthritis. *Excpert Rev. Clin. Immu.* **10**. PMID: 24961712, 981–983 (2014) (cit. on p. 54).

176. Huse, K., Böhme, H.-J. & Scholz, G. H. Purification of antibodies by affinity chromatography. *J. Biochem. Biophys. Methods* **51**, 217–231 (2002) (cit. on pp. 54, 77).

177. Gronemeyer, P., Ditz, R. & Strube, J. Trends in upstream and downstream process development for antibody manufacturing. *Bioengineering* **1**, 188–212 (2014) (cit. on pp. 54, 72).

178. Sommer, R., Tscheliessnig, A., Satzer, P., Schulz, H., Helk, B. & Jungbauer, A. Capture and intermediate purification of recombinant antibodies with combined precipitation methods. *Biochem. Eng, J.* **93**, 200–211 (2015) (cit. on p. 55).

179. Mahadevan, H. & Hall, C. K. Experimental analysis of protein precipitation by polyethylene glycol and comparison with theory. *Fluid phase equilibr.* **78**, 297–321 (1992) (cit. on p. 55).

180. Shulgin, I. L. & Ruckenstein, E. Preferential hydration and solubility of proteins in aqueous solutions of polyethylene glycol. *Biophys. Chem.* **120**, 188–198 (2006) (cit. on p. 55).

181. Poison, A. A theory for the displacement of proteins and viruses with polyethylene glycol. *Prep. Biochem.* **7**, 129–154 (1977) (cit. on p. 55).

182. Mahadevan, H. & Hall, C. K. Theory of precipitation of protein mixtures by nonionic polymer. *Aiche. J.* **38**, 573–591 (1992) (cit. on p. 55).

183. Coen, C., Prausnitz, J. & Blanch, H. Protein salting-out: Phase equilibria in two-protein systems. *Biotechnol. Bioeng.* **53**, 567–574 (1997) (cit. on p. 55).

184. Von Solms, N., Anderson, C. O., Blanch, H. W. & Prausnitz, J. M. Molecular thermodynamics for fluid-phase equilibria in aqueous two-protein systems. *Aiche. J.* **48**, 1292–1300 (2002) (cit. on p. 55).

185. Sieberz, J., Cinar, E., Wohlgemuth, K. & Schembecker, G. Clarification of a monoclonal antibody with cationic polyelectrolytes: Analysis of influencing parameters. *Biochem. Eng. J.* **122**, 60–70 (2017) (cit. on p. 55).

186. Przybycien, T. M. Protein-protein interactions as a means of purification. *Curr. Opin. Biotech.* **9**, 164–170 (1998) (cit. on p. 55).

187. Singh, L., Poddar, N., Dar, T., Rahman, S, Kumar, R & Ahmad, F. Forty years of research on osmolyte-induced protein folding and stability. *J. Iran. Chem. Soc.* **8**, 1–23 (2011) (cit. on p. 56).

188. Barnett, G. V., Razinkov, V. I., Kerwin, B. A., Blake, S., Qi, W., Curtis, R. A. & Roberts, C. J. Osmolyte effects on monoclonal antibody stability and concentration-dependent protein interactions with water and common osmolytes. *J. Phys. Chem. B* **120**, 3318–3330 (2016) (cit. on p. 56).

189. Baumann, P., Hahn, T. & Hubbuch, J. High-throughput micro-scale cultivations and chromatography modeling: Powerful tools for integrated process development. *Biotechnol. Bioeng.* **112**, 2123–2133 (2015) (cit. on p. 56).

190. Cromwell, M. E., Hilario, E. & Jacobson, F. Protein aggregation and bioprocessing. *AAPS J.* **8**, E572–E579 (2006) (cit. on p. 66).

191. Timasheff, S. N. Protein-solvent preferential interactions, protein hydration, and the modulation of biochemical reactions by solvent components. *P. Natl. Acad. Sci. USA* **99**, 9721–9726 (2002) (cit. on p. 70).

192. Giese, G., Myrold, A., Gorrell, J. & Persson, J. Purification of antibodies by precipitating impurities using Polyethylene Glycol to enable a two chromatography step process. *J. Chromatogr. B* **938**, 14–21 (2013) (cit. on p. 71).

193. Tait, A. S., Hogwood, C. E., Smales, C. M. & Bracewell, D. G. Host cell protein dynamics in the supernatant of a mAb producing CHO cell line. *Biotechnol. Bioeng.* **109**, 971–982 (2012) (cit. on p. 72).

194. Hogwood, C. E., Tait, A. S., Koloteva-Levine, N., Bracewell, D. G. & Smales, C. M. The dynamics of the CHO host cell protein profile during clarification and protein A capture in a platform antibody purification process. *Biotechnol. Bioeng.* **110**, 240–251 (2013) (cit. on p. 72).

195. Gjoka, X., Rogler, K., Martino, R. A., Gantier, R. & Schofield, M. A straightforward methodology for designing continuous monoclonal antibody capture multi-column chromatography processes. *J. Chromatogr. A* **1416**, 38–46 (2015) (cit. on p. 76).

196. Cai, H. H. Therapeutic monoclonal antibodies approved by FDA in 2016. *J. Immunol.* **5**, 1–2 (2017) (cit. on p. 76).

197. Reichert, J. M. Antibodies to watch in 2017. *Mabs* **9**, 167–181 (2017) (cit. on p. 76).

198. Ecker, D. M, Jones, S. D. & Levine, H. L. The therapeutic monoclonal antibody market. *Mabs* **7**, 9–14 (2015) (cit. on p. 76).

199. Rader, R. A. & Langer, E. S. Biopharmaceutical manufacturing: Historical and future trends in titers, yields, and efficiency in commercial-scale bioprocessing. *BioProc. J.* **13**, 47–54 (2015) (cit. on p. 76).

200. *Affinity chromatography* (ed Fassina, G.) (John Wiley & Sons, Ltd, 2001) (cit. on p. 77).

201. Hober, S., Nord, K. & Linhult, M. Protein A chromatography for antibody purification. *J. Chromatogr. B* **848**, 40–47 (2007) (cit. on p. 77).

202. Thömmes, J. & Etzel, M. Alternatives to chromatographic separations. *Biotechnol. Prog.* **23**, 42–45 (2007) (cit. on p. 77).

203. Low, D., O'Leary, R. & Pujar, N. S. Future of antibody purification. *J. Chromatogr. B* **848**, 48–63 (2007) (cit. on p. 77).

204. Venkiteshwaran, A., Heider, P., Teysseyre, L. & Belfort, G. Selective precipitation-assisted recovery of immunoglobulins from bovine serum using controlled fouling crossflow membrane microfiltration. *Biotechnol. Bioeng.* **101**, 957–966 (2008) (cit. on p. 77).

205. Brodsky, Y., Zhang, C., Yigzaw, Y. & Vedantham, G. Caprylic acid precipitation method for impurity reduction: An alternative to conventional chromatography for monoclonal antibody purification. *Biotechnol. Bioeng.* **109**, 2589–2598 (2012) (cit. on p. 77).

206. Sheth, R. D., Jin, M., Bhut, B. V., Li, Z., Chen, W. & Cramer, S. M. Affinity precipitation of a monoclonal antibody from an industrial harvest feedstock using an ELP-Z stimuli responsive biopolymer. *Biotechnol. Bioeng.* **111**, 1595–1603 (2014) (cit. on p. 77).

207. Hammerschmidt, N., Tscheliessnig, A., Sommer, R., Helk, B. & Jungbauer, A. Economics of recombinant antibody production processes at various scales: Industry-standard compared to continuous precipitation. *Biotechnol. J.* **9**, 766–775 (2014) (cit. on p. 77).

208. Warikoo, V. *et al.* Integrated continuous production of recombinant therapeutic proteins. *Biotechnol. Bioeng.* **2012**, 255–296 (2012) (cit. on pp. 77, 80).

209. Mahajan, E., George, A. & Wolk, B. Improving affinity chromatography resin efficiency using semi-continuous chromatography. *J. Chromatogr. A* **1227**, 154–162 (2012) (cit. on pp. 77, 80).

210. Godawat, R., Brower, K., Jain, S., Konstantinov, K., Riske, F. & Warikoo, V. Periodic counter-current chromatography - design and operational considerations for integrated and continuous purification of proteins. *Biotechnol. J.* **7**, 1496–1500 (2012) (cit. on pp. 77, 80).

211. Bisschops, M. & Brower, M. The impact of continuous multicolumn chromatography on biomanufacturing efficiency. *Pharm. Bioprocess.* **1**, 361–372 (2013) (cit. on p. 77).

212. Ng, C. K. S., Rousset, F., Valery, E., Bracewell, D. G. & Sorensen, E. Design of high productivity sequential multi-column chromatography for antibody capture. *Food Bioprod. Process* **92**, 233–241 (2014) (cit. on p. 77).

213. Brower, M., Hou, Y. & Pollard, D. *Monoclonal antibody continuous processing enabled by single use* (John Wiley & Sons, 2014) (cit. on p. 77).

214. *Preparative Chromatography of Fine Chemicals and Pharmaceutical Agents* 2nd (eds Schmidt-Traub, H., Schulte, M. & Seidel-Morgenstern, A.) (Wiley, 2012) (cit. on pp. 79, 99, 164).

215. Lenhoff, A. M. Protein adsorption and transport in polymer-functionalized ion-exchangers. *J. Chromatogr. A* **1218**, 8748–8759 (2011) (cit. on p. 80).

216. Wittemann, A., Haupt, B. & Ballauff, M. Adsorption of proteins on spherical polyelectrolyte brushes in aqueous solution. *Phys. Chem. Chem. Phys.* **5**, 1671–1677 (2003) (cit. on p. 80).

217. Bryntesson, M., Hall, M. & Lacki, K. *Patent* US 7901581 (US) (2011) (cit. on pp. 80, 81).

218. Pollock, J., Bolton, G., Coffman, J., Ho, S. V., Bracewell, D. G. & Farid, S. S. Optimising the design and operation of semi-continuous affinity chromatography for clinical and commercial manufacture. *J. Chromatogr. A* **1284**, 17–27 (2013) (cit. on p. 80).

219. Oelmeier, S. A., Dismer, F. & Hubbuch, J. Application of an aqueous two-phase systems high-throughput screening method to evaluate mAb HCP separation. *Biotechnol. Bioeng.* **108**, 69–81 (2010) (cit. on p. 82).

220. Hahn, T., Baumann, P., Huuk, T., Heuveline, V. & Hubbuch, J. UV absorption-based inverse modeling of protein chromatography. *Eng. Life Sci.* **16**, 99–106 (2016) (cit. on p. 85).

221. Kaczmarski, K. & Antos, D. Use of simulated annealing for optimization of chromatographic separations. *Acta Chromatogr.* **17**, 20–45 (2006) (cit. on p. 85).

222. Devernay, F. *C/C++ Minpack* `http://devernay.free.fr/hacks/cminpack/`. 2007 (cit. on p. 85).

223. Glowinski, R. *Finite element methods for incompressible viscous flow. In Numerical Methods for Fluids (Part 3)* 3–1176 (Elsevier, 2003) (cit. on p. 85).

224. Quarteroni, A. & Vallii, A. *Numerical approximation of partial differential equations* 160 (Springer, 1994) (cit. on p. 85).

225. Hammerschmidt, N., Hintersteiner, B., Lingg, N. & Jungbauer, A. Continuous precipitation of IgG from CHO cell culture supernatant in a tubular reactor. *Biotechnol. J.* **10**, 1196–1205 (2015) (cit. on pp. 94, 95).

226. Sturtevant, J. M., Rice, S. A. & Geiduschek, E. P. The stability of the helical DNA molecule in solution. *Discuss. Faraday Soc.* **25**, 138–149 (1958) (cit. on p. 95).

227. Carta, G. & Jungbauer, A. *Protein chromatography: Process development and scale-up* (John Wiley & Sons, 2010) (cit. on pp. 99, 164).

228. Remsen, E. E. & Freeman, J. J. A Size-Exclusion Chromatography/FT-IR (SEC/FT-IR) Technique for Improved FTIR Spectroscopy of Proteins in D 2 O Solution. *Appl. Spectrosc.* **45**, 868–873 (1991) (cit. on pp. 100, 165).

229. Somsen, G. W., Gooijer, C. & Brinkman, U. A. T. Liquid chromatography-Fourier-transform infrared spectrometry. *J. Chromatogr. A* **856**, 213–242 (1999) (cit. on pp. 100, 165).

230. Kuligowski, J., Quintás, G., de la Guardia, M. & Lendl, B. Analytical potential of mid-infrared detection in capillary electrophoresis and liquid chromatography: A review. *Anal. Chim. Acta* **679**, 31–42 (2010) (cit. on pp. 100, 165).

231. Goormaghtigh, E., Cabiaux, V. & Ruysschaert, J.-M. in *Physicochemical methods in the study of biomembranes* 328–357 (Springer, 1994) (cit. on pp. 100, 165, 172).

232. Schweitzer-Stenner, R. Advances in vibrational spectroscopy as a sensitive probe of peptide and protein structure: A critical review. *Vib. Spectrosc.* **42**, 98–117 (2006) (cit. on pp. 100, 165, 172).

233. Piazza, R. Interactions and phase transitions in protein solutions. *Curr. Opin. Collioid. In.* **5**, 38–43 (2000) (cit. on p. 140).

234. Beretta, S., Chirico, G. & Baldini, G. Short-range interactions of globular proteins at high ionic strengths. *Macromolecules* **33**, 8663–8670 (2000) (cit. on p. 140).

235. Arakawa, T. & Timasheff, S. N. Protein stabilization and destabilization by guanidinium salts. *Biochemistry-US* **23**, 5924–5929 (1984) (cit. on pp. 140, 156).

236. Arakawa, T., Bhat, R. & Timasheff, S. N. Preferential interactions determine protein solubility in 3-component solutions â the MgCl2 system. *Biochemistry-US* **29**, 1914–1923 (1990) (cit. on pp. 140, 157).

237. Arakawa, T. Hydration as a Major Factor in Preferential Solvent–Protein Interactions. *Cryst. Growth Des.* **2**, 549–551 (2002) (cit. on pp. 140, 157).

238. Senisterra, G., Chau, I. & Vedadi, M. Thermal denaturation assays in chemical biology. *Assay Drug Dev. Techn.* **10**, 128–136 (2012) (cit. on p. 141).

239. Goldberg, D. S., Bishop, S. M., Shah, A. U. & Sathish, H. A. Formulation development of therapeutic monoclonal antibodies using high-throughput fluorescence and static light scattering techniques: Role of conformational and colloidal stability. *J. Polym. Sci.* **100**, 1306–1315 (2011) (cit. on p. 141).

240. Mahler, H.-C., Müller, R., Friess, W., Delille, A. & Matheus, S. Induction and analysis of aggregates in a liquid IgG1-antibody formulation. *Eur. J. Pharm. Biopharm.* **5G9**, 407–417 (2005) (cit. on p. 141).

241. Mahler, H.-C., Friess, W., Grauschopf, U. & Kiese, S. Protein aggregation: Pathways, induction factors and analysis. *J. Pharm. Sci.* **98**, 2909–2934 (2009) (cit. on p. 141).

242. Ericsson, U. B., Hallberg, B. M., Detitta, G. T., Dekke, N. & Nordlund, P. Thermofluor-based high-throughput stability optimization of proteins for structural studies. *Anal Biochem.* **357**, 289–298 (2006) (cit. on p. 141).

243. Senisterra, G. A. & Finerty, P. J. J. High throughput methods of assessing protein stability and aggregation. *Mol Biosyst.* **5**, 217–223 (2009) (cit. on p. 141).

244. Kröner, F. & Hubbuch, J. Systematic generation of buffer systems for pH gradient ion exchange chromatography and their application. *J. Chromatogr. A* **1285**, 78–87 (2013) (cit. on pp. 141, 144, 154).

245. Durbin, S. D. & Feher, G. Protein Crystallization. *Annu. Rev. Phys. Chem.* **47**, 171–204 (1996) (cit. on pp. 154, 157).

246. Islam, S. A. & Weaver, D. L. Molecular Interactions in Protein Crystals: Solvent Accessible Surface and Stability. *Proteins* **8**, 1–5 (1990) (cit. on p. 154).

247. Goodenough, P. W. A review of protein engineering for the food industry. *Int. J. Food Sci. Tech.* **30**, 119–139 (1995) (cit. on p. 154).

248. Dumetz, A. C., Chockla, A. M., Kaler, E. W. & Lenhoff, A. M. Effects of pH on proteinâprotein interactions and implications for protein phase behavior. *BBA - Proteins Proteom.* **1784**, 600–610 (2008) (cit. on p. 155).

249. Curtis, R. A., Ulrich, J., Montaser, A., Prausnitz, J. M. & Blanch, H. W. Protein-Protein Interactions in Concentrated Electrolyte Solutions. *Biotechnol. Bioeng.* **79**, 367–380 (2002) (cit. on p. 155).

250. Lin, F.-Y., Chen, W.-Y. & Hearn, M. T. W. Microcalorimetric Studies on the Interaction Mechanism between Proteins and Hydrophobic Solid Surfaces in Hydrophobic Interaction Chromatography: Effects of Salts, Hydrophobicity of the Sorbent, and Structure of the Protein. *Anal. Chem.* **73**, 3875–3883 (2001) (cit. on pp. 155, 156).

251. Collins, K. D. Ions from the Hofmeister series and osmloytes: effects on proteins in solution and in the crystallization process. *Methods* **34**, 300–311 (2004) (cit. on pp. 155, 158–160).

252. Baumann, P., Baumgartner, K. & Hubbuch, J. Influence of Binding pH and Protein Solubility on the Dynamic Binding Capacity in Hydrophobic Interaction Chromatography. *J. Chromatogr. A* **1396**, 77–85 (2015) (cit. on p. 156).

253. Manning, M. C., Chou, D. K., Murphy, B. M., Payne, R. W. & Katayama, D. S. Stability of Protein Pharmaceuticals: An Update. *Pharm. Res.* **27**, 544–575 (2010) (cit. on p. 157).

254. Von Hippel, P. H. & Wong, K.-Y. Neutral Salts: The Generality of Their Effects on the Stability of Macromolecular Conformations. *Science* **145**, 577–580 (1964) (cit. on p. 157).

255. Von Hippel, P. H. & Wong, K.-Y. On the Conformational Stability of Globular Proteins: THE EFFECTS OF VARIOUS ELECTROLYTES AND NONELECTROLYTES ON THE THERMAL RIBONUCLEASE TRANSITION. *J. Biol. Chem.* **240**, 3909–3923 (1965) (cit. on p. 157).

256. Chi, E. Y., Krishnan, S., Kendrick, B. S., Chang, B. S., Carpenter, J. F. & Randolph, T. W. Roles of conformational stability and colloidal stability in the aggregation of recombinant human granulocyte colony-stimulating factor. *Protein Sci.* **12**, 903–913 (2003) (cit. on p. 157).

257. Dupeux, F., Röwer, M., Seroul, G., Blot, D. & Marquez, J. A. A thermal stability assay can help to estimate the crystallization likelihood of biological samples. *Acta Crystallogr. D* **67**, 915–919 (2011) (cit. on p. 157).

258. Zeelen, J. P. in *Protein Cryst.* (ed Bergfors, T. M.) 2nd, 175–194 (Internat'l University Line, 2009) (cit. on p. 158).

259. Arakawa, T. & Timasheff, S. N. Mechanism of protein salting in and salting out by divalent cation salts: Balance between hydration and salt binding. *Biochemistry-US* **23**, 5912–5923 (1984) (cit. on pp. 158–160).

260. *Methods for affinity-based separations of enzymes and proteins* 1st ed. (ed Gupta, M. N.) (Birkhäuser, 2002) (cit. on p. 164).

261. FDA. *Guidance for industry. PAT – A framework for innovative pharmaceutical development, manufacturing, and quality assurance* (cit. on p. 164).

262. Rathore, A. S. & Kapoor, G. Application of process analytical technology for downstream purification of biotherapeutics. *J. Chem. Technol. Biot.* **90**, 228–236 (Feb. 2015) (cit. on p. 164).

263. Fahrner, R. L. & Blank, G. S. Real-time control of antibody loading during protein A affinity chromatography using an on-line assay. *J Chromatogr A* **849**, 191–196 (1999) (cit. on p. 164).

264. Karst, D. J., Steinebach, F., Soos, M. & Morbidelli, M. Process performance and product quality in an integrated continuous antibody production process. *Biotechnol. Bioeng.* **114**, 298–307 (2017) (cit. on p. 164).

265. Williams, A., Read, E. K., Agarabi, C. D., Lute, S. & Brorson, K. A. Automated 2D-HPLC method for characterization of protein aggregation with in-line fraction collection device. *J. Chromatogr. B* **1046**, 122–130 (2017) (cit. on p. 164).

266. Fahrner, R. L., Lester, P. M., Blank, G. S. & Reifsnyder, D. H. Real-time control of purified product collection during chromatography of recombinant human insulin-like growth factor-I using an on-line assay. *J Chromatogr A* **827**, 37–43 (1998) (cit. on p. 164).

267. Rathore, A. S., Yu, M., Yeboah, S. & Sharma, A. Case study and application of process analytical technology (PAT) towards bioprocessing: Use of on-line high-performance liquid chromatography (HPLC) for making real-time pooling decisions for process chromatography. *Biotechnol. Bioeng.* **100**, 306–316 (2008) (cit. on p. 164).

268. Brestrich, N., Briskot, T., Osberghaus, A. & Hubbuch, J. A tool for selective inline quantification of co-eluting proteins in chromatography using spectral analysis and partial least squares regression. *Biotechnol. Bioeng.* **111**, 1365–1373 (2014) (cit. on p. 165).

269. Brestrich, N., Sanden, A., Kraft, A., McCann, K., Bertolini, J. & Hubbuch, J. Advances in inline quantification of co-eluting proteins in chromatography: Process-data-based model calibration and application towards real-life separation issues. *Biotechnol. Bioeng.* **112**, 1406–1416 (2015) (cit. on p. 165).

270. Rüdt, M., Brestrich, N., Rolinger, L. & Hubbuch, J. Real-time monitoring and control of the load phase of a protein A capture step. *Biotechnol. Bioeng.* **114**, 368–373 (2017) (cit. on p. 165).

271. Hansen, S. K., Jamali, B. & Hubbuch, J. Selective high throughput protein quantification based on UV absorption spectra. *Biotechnol. Bioeng.* **110**, 448–460 (2013) (cit. on p. 165).

272. Parkins, D. A. & Lashmar, U. T. The formulation of biopharmaceutical products. *Pharmaceutical Science and Technology Today* **3**, 129–137 (2000) (cit. on p. 165).

273. Morgenstern, J., Busch, M., Baumann, P. & Hubbuch, J. Quantification of PEGylated proteases with varying degree of conjugation in mixtures: An analytical protocol combining protein precipitation and capillary gel electrophoresis. English. *J. Chromatogr. A* **1462**, 153–164 (2016) (cit. on pp. 165, 170, 175, 176).

274. Strancar, A, Raspor, P, Schwinn, H, Schutz, R & Josic, D. Extraction of Triton-X-100 and Its Determination in Virus-Inactivated Human Plasma By the Solvent Detergent Method. *J. Chromatogr. A* **658**, 475–481 (1994) (cit. on pp. 165, 177).

275. Thakkar, S. V., Allegre, K. M., Joshi, S. B., Volkin, D. B. & Middaugh, C. R. An Application of Ultraviolet Spectroscopy to Study Interactions in Proteins Solutions at High Concentrations. *J. Polym. Sci.* **101**, 3051–3061 (2012) (cit. on p. 165).

276. Capito, F., Skudas, R., Kolmar, H. & Stanislawski, B. Host cell protein quantification by fourier transform mid infrared spectroscopy (FT-MIR). *Biotechnol. Bioeng.* **110**, 252–259 (2013) (cit. on p. 165).

277. Capito, F., Skudas, R., Kolmar, H. & Hunzinger, C. At-line mid infrared spectroscopy for monitoring downstream processing unit operations. *Proc. Biochem.* **50**, 997–1005 (2015) (cit. on p. 165).

278. Roberts, P. L. Virus elimination during the purification of monoclonal antibodies by column chromatography and additional steps. *Biotechnol. Progr.* **30**, 1341–1347 (2014) (cit. on pp. 165, 169, 177).

279. Morgenstern, J., Baumann, P., Brunner, C. & Hubbuch, J. Effect of PEG molecular weight and PEGylation degree on the physical stability of PEGylated lysozyme. *Int. J. Pharm.* **519**, 408–417 (2017) (cit. on pp. 168, 169).

280. De Jong, S. SIMPLS: An alternative approach to partial least squares regression. *Chemometr. Intell. Lab.* **18**, 251 –263 (1993) (cit. on p. 170).

281. Savitzky, A. & Golay, M. J. E. Smoothing and differentiation of data by simplified least squares procedures. *Anal. Chem.* **36**, 1627–1639 (1964) (cit. on pp. 170, 173).

282. Wold, S., Sjöström, M. & Eriksson, L. PLS-regression: A basic tool of chemometrics. *Chemometr. Intell. Lab.* **58**, 109–130 (2001) (cit. on pp. 170, 171, 173).

283. Deep, K., Singh, K. P., Kansal, M. & Mohan, C. A real coded genetic algorithm for solving integer and mixed integer optimization problems. *Appl. Math. Comput.* **212**, 505 –518 (2009) (cit. on p. 170).

284. Quintás, G., Lendl, B., Garrigues, S. & de la Guardia, M. Univariate method for background correction in liquid chromatography-Fourier transform infrared spectrometry. *J Chrom A* **1190**, 102–109 (2008) (cit. on p. 172).

285. Pretsch, E., Bühlmann, P., Affolter, C., Pretsch, E., Bhuhlmann, P & Affolter, C. *Structure determination of organic compounds* (Springer, 2009) (cit. on p. 174).

286. Seely, J. E. & Richey, C. W. Use of ion-exchange chromatography and hydrophobic interaction chromatography in the preparation and recovery of polyethylene glycol-linked proteins. *J. Chromatogr. A* **908**, 235–241 (2001) (cit. on p. 175).

287. Yamamoto, S., Fujii, S., Yoshimoto, N. & Akbarzadehlaleh, P. Effects of protein conformational changes on separation performance in electrostatic interaction chromatography: Unfolded proteins and PEGylated proteins. *J. Biotechnol.* **132**, 196–201 (2007) (cit. on p. 175).

288. Hansen, S. K., Maiser, B. & Hubbuch, J. Rapid quantification of protein-polyethylene glycol conjugates by multivariate evaluation of chromatographic data. *J. Chromatogr. A* **1257**, 41–47 (2012) (cit. on p. 176).

List of Figures

List of Tables

A. Full paper - Prediction of Salt Effects on Protein Phase Behavior by HIC Retention and Thermal Stability

Kai Baumgartner*, Steffen Großhans*, Juliane Schütz*, Susanna Suhm, and Jürgen Hubbuch**

Karlsruhe Institute of Technology (KIT), Institute of Process Engineering in Life Sciences, Section IV: Biomolecular Separation Engineering, Karlsruhe, Germany
* These authors contributed equally to this work
** Corresponding author

Abstract

In the biopharmaceutical industry it is mandatory to know and ensure the correct protein phase state as a critical quality attribute in every process step. Unwanted protein precipitation or crystallization can lead to column, pipe or filter blocking. In formulation, the formation of aggregates can even be lethal when injected into the patient. The typical methodology to illustrate protein phase states is the generation of protein phase diagrams. Commonly, protein phase behavior is shown in dependence of protein and precipitant concentration. Despite using high-throughput methods for the generation of phase diagrams, the time necessary to reach equilibrium is the bottleneck. Faster methods to predict protein phase behavior are desirable. In this study, hydrophobic interaction chromatography retention times were correlated to crystal size and form. High-throughput thermal stability measurements (melting and aggregation temperatures), using an Optim®2 system, were successfully correlated to glucose isomerase stability. By using hydrophobic interaction chromatography

and thermal stability determinations, glucose isomerase conformational and colloidal stability were successfully predicted for different salts in a specific pH range.

A.1. Introduction

In biopharmaceutical processes knowledge and control of protein phase behavior is of high importance. Controlling protein phase states - being in most processes a critical quality attribute - is on the one hand essential to avoid protein loss during upstream, downstream, and formulation of biopharmaceutical drugs, on the other hand the application of phase transitions such as precipitation or crystallization can be used as downstream unit operation. The influence of changing protein-solvent and protein-protein interactions due to a change in process parameters - defining these parameters as critical process parameters - on macroscopic protein phase behavior can be displayed in protein phase diagrams as a function of protein concentration and precipitant concentration [49, 75].

On a molecular level, the acting forces include long-range and short-range interactions. In this context, electrostatic interactions are generally defined as long-range forces whereas hydrogen bridges, van-der-Waals forces or hydrophobic interactions are examples for short-range forces [53]. Changing these interactions can influence protein phase behavior and therefore lead to phase transitions. Intermolecular electrostatic repulsive interactions between equally charged protein molecules have a stabilizing effect on protein solutions. Short-range attractive forces are superimposed by these long-range interactions. By increasing the ionic strength of a solution, these electrostatic repulsive effects are shielded and short-range attractive forces are predominant [233, 234].

During purification, biomolecules are often exposed to high-salt conditions. In high-salt conditions additional salt ion effects are induced and are not entirely understood. The preferential interaction theory, first postulated by Arakawa *et al.* [235, 236], is the most promising approach for explaining these effects. They distinguish between preferential binding of co-solutes to protein and preferential exclusion from protein surface. The former type is provoked by chaotropic agents which are found to enhance protein solubility (salting-in) but destabilize the native protein conformation. These agents are nonpolar and therefore weakly hydrated. The latter is induced by polar kosmotropic agents that increase protein stability or lead to salting-out effects due to their strongly hydrated character. Arakawa *et al.* [237] postulated that the hydration of a protein in a concentrated solution of co-solute is at a constant level independently whether this solute shows a preferential interaction or not.

Protein stability comprises conformational and colloidal stability. Conformational stability is important to assess as an indicator for protein unfolding. Exposed hydrophobic surface patches can enhance aggregate formation. Colloidal instability describes the aggregate formation due to clustering of protein molecules. Increased conformational and colloidal stability are believed to enhance overall protein stability [238]. Long-term stability tests under stressed conditions [239–241] are generally used to assess protein stability in pharmaceutical industry. In recent years, high-throughput techniques to evaluate protein stability were established to determine melting temperatures and aggregation temperatures. Differential scanning fluorescence measures protein conformational stability by using extrinsic dyes, such as SYPRO Orange, that bind to hydrophobic protein patches [242]. Differential static light scattering monitors light scattering of protein solutions due to aggregate formation [239, 243]. The combination of both parameters, melting temperature and aggregation temperature, is important to evaluate protein stability [239]. These two parameters have not been investigated in literature in dependence of the kosmotropic and chaotropic character of the salts, their ionic strengths, and pH values in respect to the protein's isoelectric point (pI) so far.

In this study, the impact of pH value and ionic strength of different salts on protein phase behavior was investigated using glucose isomerase as model protein. Sodium sulfate, ammonium sulfate, sodium chloride, and ammonium chloride were used as precipitants to investigate the influence of the two cations - sodium and ammonium - and of the anions - chloride and sodium - on the protein phase behavior. The high-throughput method to obtain protein phase diagrams was established earlier by Baumgartner *et al.* [51]. In the present work, this method was adapted to obtain information about protein phase behavior at varying pH values and different salt ionic strengths at a constant protein concentration. A multi-component buffer system [244] was used to ensure a constant buffer capacity over a defined pH range. By using the same buffer for the whole investigated pH range, buffer effects were excluded. The protein phase states are examined after 40 days of incubation.

Hydrophobic interaction chromatography (HIC) was used to investigate changes in hydrophobicity of glucose isomerase caused by changing salt type and pH values. Applying HIC bind-elute experiments, the diversity of short-range forces is reduced to hydrophobic interactions.Furthermore, correlation of thermal stability measurements to protein phase behavior was investigated measuring the melting and aggregation temperature in the respective solutions. The present work demonstrates the use of HIC bind-elute experiments and thermal stability measurements to predict protein conformational and colloidal stability in fast time and at low sample consumption. A schematic drawing of the used methodologies is shown in Fig. A.1..

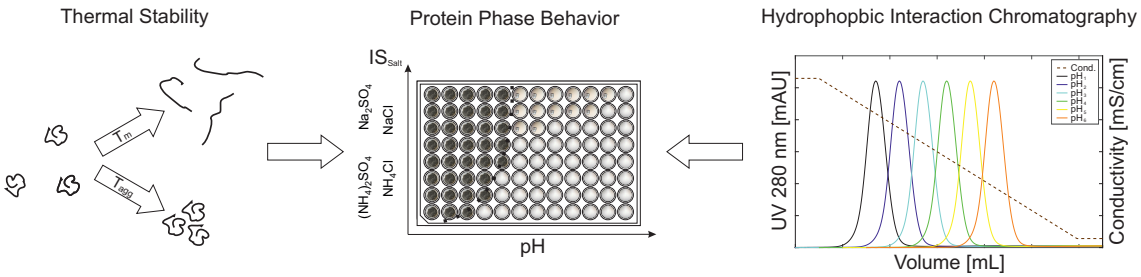

Figure A.1.: Schematic illustration of the experimental setup: Melting temperatures (T_m) and aggregation temperatures (T_{agg}) and retention volumes in hydrophobic interaction chromatography were used to predict protein phase behavior.

A.2. Materials and Methods

A.2.1. Materials

The multicomponent buffer with a linear buffering range from pH 3.5 to pH 11.5 consisted of the organic acids CABS (4-(cyclohexylamino)butane-1-sulfonic acid) (Santa Cruz Biotechnology, USA), AMPSO (2-hydroxy-3-[(1-hydroxy-2-methylpropan-2-yl)amino]propane-1-sulfonic acid) (Sigma-Aldrich, USA), TAPSO (3-[[1,3-dihydroxy-2-(hydroxymethyl)propan-2-yl]amino]-2-hydroxypropane-1-sulfonic acid) (Sigma-Aldrich, USA), MES (2-morpholin-4-ylethanesulfonic acid) (AppliChem, Germany), acetic acid (Merck Millipore, Germany), and formic acid (Merck Millipore, Germany). The investigated salts sodium chloride, sodium sulfate and ammonium chloride were obtained from Merck Millipore (Germany). Ammonium sulfate was purchased from AppliChem (Germany). Sodium hydroxide for pH adjustment was obtained from Merck Millipore (Germany). pH adjustment was performed using a five-point calibrated pH meter (HI-3220, Hanna Instruments, USA) equipped with a SenTix®62 pH electrode (Xylem Inc., USA) or an InLab® Semi-Micro pH electrode (Mettler Toledo, Switzerland) dependent on the application. All buffers were filtered through 0.2 μm, and precipitant solutions through 0.45 μm cellulose acetate filters (Sartorius, Germany). Glucose isomerase (HR7-100) produced in *Streptomyces rubiginosus* (PDB: 3KBS, pI: 4.78 [51]) was supplied by Hampton Research (USA). Protein solutions were filtered through 0.2 μm syringe filters with PTFE membranes (VWR, USA). Size exclusion chromatography was conducted using HiTrap Desalting Columns (GE Healthcare, Sweden) on an AEKTA prime plus system (GE Healthcare, Sweden). A subsequent protein concentration step was performed using Vivaspin centrifugal concentrators (Sartorius, Germany) with PES membranes and molecular weight cutoff of 30 kDa.

Protein phase diagrams were prepared on MRC Under Oil 96-Well Crystallization

Plates (Swissci, Switzerland) in microbatch experiments using a Freedom EVO®100 (Tecan, Switzerland) automated liquid handling station controlled by Evoware 2.5 (Tecan, Switzerland). Calibration of pipetting for liquid handling of buffers, precipitant solutions, and protein solutions were generated using a WXTS205DU analytical balance (Mettler-Toledo, Switzerland). The microbatch plates were covered with HDclear ™sealing tape (ShurTech Brands, USA) to prevent evaporation. A Rock Imager 182/54 (Formulatrix, USA) was used as an automated imaging system for determining protein phase states. Protein concentration measurements were conducted using a NanoDrop2000c UV-Vis spectrophotometer (Thermo Fisher Scientific, USA).

For hydrophobic interaction chromatography runs a $0.5\,mL$ Toyopearl Butyl-650M column (Atoll, Germany) on an AEKTA™purifier (GE Healthcare, Sweden) was applied. The AEKTA™purifier is equipped with an autosampler, UV detector, and a conductivity cell. The operating software package for system control and data analysis was Unicorn 5.1 (GE Healthcare, USA).

For determining protein melting temperatures and aggregation temperatures using Optim®2 (Avacta Analytical, UK), operated with the Optim Client, protein samples were analyzed in multi-cuvette arrays (Avacta Analytical, UK). Static light scattering and intrinsic fluorescence data analysis was performed with the integrated Optim Analysis software to evaluate protein thermal stability.

Data processing and creation of figures was performed in Matlab®R2014b (MathWorks, USA) and CorelDRAW® Graphics Suite X5 (Corel Corporation, Canada).

A.2.2. Methods

Preparation of Stock Solutions

Buffers were prepared by weighing and dissolving all buffer components in ultrapure water to 90% of the final buffer volume. This volume was splitted into three identical batches and pH value was adjusted using $4\,M$ sodium hydroxide solution as titrant. The pH value was adjusted to both ends of the desired pH gradient and an intermediate pH value. After filling up to the final buffer volume all buffers were filtered through $0.2\,\mu m$ cellulose acetate filters. Precipitant stock solutions were filtered through $0.45\,\mu m$ cellulose acetate filters. Buffers and precipitant stock solutions were used at the earliest one day after preparation and after repeated pH verification. The pH value was again adjusted at the day of use with an accuracy of $\pm\,0.05$ pH units. The global buffer capacity of $20\,mM$ was chosen over the buffering

range of pH 3.5 to pH 11.5 . The buffer composition (Tab. A.1) was calculated using a Matlab tool developed by Kröner *et al.* [244].

Table A.1.: Multi-component buffer composition with 20 mM buffer capacitiy in a pH range of pH 3.5 to pH 11.5 based on Kröner *et al.* [244]

Substance	Concentration $[mM]$	pK_a
CABS	32.96	10.70
AMPSO	30.58	9.14
TAPSO	27.93	7.64
MES	29.52	6.10
Acetic acid	25.18	4.76
Formic acid	24.06	3.75

Sodium sulfate, ammonium sulfate, sodium chloride, and ammonium chloride were used as precipitants. Precipitant stock solutions contained an additional ionic strength of 2.5 M and 5.0 M, respectively. The intermediate salt concentration ensured pH stability while mixing (data not shown). Otherwise, by mixing low-salt buffer (buffer without additional salt) with 5.0 M buffer at the same pH value, the pH value would shift [51, 244]. To set up the protein stock solutions the crystal suspension of glucose isomerase was diluted with low-salt buffer at pH 7.0 to redissolve the protein. Centrifugal concentrators were used to reduce the volume. The protein solution then was filtered through 0.2 μm syringe filters to remove particulates and desalted using size exclusion chromatography. Protein concentration was adjusted via centrifugal concentrators to 50 mg/mL.

Generation of Protein Phase Diagrams

Protein phase diagrams were prepared in high-throughput mode using the method described by Baumgartner *et al* [51]. The protein phase diagrams were established on 96-well crystallization plates in microbatch experiments using an automated liquid handling station. For buffer and precipitant solutions a maximum pipetting deviation of below 2 % could be realized [51]. For protein solutions the maximal deviation was below 3 %. The protein phase behavior at constant glucose isomerase concentration of 10 mg/mL was investigated with varying precipitant concentration and pH value (Fig. A.1. center).

The pH value of the precipitant stock solutions of identical ionic strength (0.0 M, 2.5 M, and 5.0 M) was varied in twelve steps from pH 3.5 to pH 7.0 on one sample plate. To ensure a linear pH performance while mixing, an intermediate pH step at

pH 5.5 was included. This has shown to smoothen pH deviations occurring due to high salt contents to an experimentally satisfying extend (data not shown). Further, for each pH step 0.0 M, 2.5 M, and 5.0 M ionic strength were mixed to create eight uniform salt dilution steps on a second sample plate.

The protein phase diagrams were then generated by adding 6 μL of 50 mg/mL protein solution (low-salt buffer at pH 7.0) to 24 μL of the previously mentioned diluted precipitant solution on the crystallization plate. The precipitant concentration was varied per row and pH value was varied per column.

The final phase diagram was investigated at a resulting glucose isomerase concentration of 10 mg/mL in the pH range from pH 4.2 to pH 7.0 and an ionic strength between 0.0 M and 4.0 M for sodium sulfate, ammonium sulfate, sodium chloride, and ammonium chloride. Crystallization plates were then centrifuged for 1 min at 1000 rpm to remove air bubbles and afterwards covered using optically clear and UV compatible sealing film. The sealed plates were stored in the Rock Imager for automated imaging for 40 $days$ at 20°C. The automated imaging was performed as described earlier by Baumgartner *et al.* [51] to visually identify phase states such as clear solution, crystallization, precipitation, and skin formation. With polarized light at 90° crystals can be identified. Exposure to UV light was used to distinguish between protein and salt crystals due to fluorescence of aromatic amino acids.

Hydrophobic Interaction Chromatography Bind-Elute Experiments

Bind-elute experiments in hydrophobic interaction mode were conducted on a 0.5 mL Toyopearl Butyl-650M column. Protein retention was evaluated at different pH values (pH 5.47 - pH 7.00) and salt ionic strengths of 2.86 M, 3.43 M, and 4.00 M. The high salt conditions at protein injection were chosen to match the conditions at the protein phase diagrams. Equilibration was performed with 10 column volumes (CV) desalted water and subsequently 4 CV of low-salt buffer at a flowrate of 1 mL/min. This was followed by high-salt equilibration for 6 CV at 1 mL/min and 4 CV at 0.2 mL/min. After equilibration, 100 μL protein solution with 10 mg/mL, in the respective high-salt buffer, were injected using an autosampler. Elution was conducted in a linear salt gradient of 20 CV at 0.2 mL/min from high-salt to low-salt. Subsequently, a column wash with low-salt buffer was performed for 10 CV. A constant pH value for the entire experiment was ensured. The 280 nm UV signal was used to determine the protein retention time. By using predetermined calibration curves, the conductivity signal was converted into the ionic strength value of the applied salt. These 3^{rd} degree calibration curves were obtained due to reduction of high-salt (5.0 M) to low-salt (0.0 M) condition in 5 % steps.

Determination of Melting and Aggregation Temperature

Melting and aggregation temperatures were determined using an Optim®2 system, which combines intrinsic fluorescence and static light scattering measurements. This device allows simultaneous analysis of the same low-volume sample in high-throughput mode. Intrinsic tryptophan fluorescence is exploited to obtain information about protein folding. The fluorescence spectra shift to red wavelengths due to a change in the vicinity of the tryptophan residues from hydrophobic to hydrophilic environment while protein unfolding. This label-free technique eliminates the possible influence of extrinsic dyes on protein-protein interactions. The simultaneously measured static light scattering evaluates the aggregation formation within the applied thermal shift. Thermal stability was investigated using a temperature gradient from $20°C$ to $90°C$ with a linear slope of $0.25\,K/min$ in the Optim®2 system. Measurements of $9\,\mu$L protein samples, pipetted into multi-cuvette arrays, were investigated in triplicates using static light scattering at $473\,nm$ to determine aggregation temperatures. Further, melting temperatures were determined by simultaneous measuring of intrinsic fluorescence.

A.3. Results

A.3.1. Protein Phase Diagrams

Protein phase diagrams were established in microbatch format to obtain information about protein phase behavior in dependence of pH value and precipitant ionic strength at a constant protein concentration. This high-throughput approach provided a versatile tool to screen protein phase behavior at low protein consumption.
Glucose isomerase phase behavior was investigated in a pH range of pH 4.20 to pH 7.00 with the precipitants sodium sulfate, ammonium sulfate, sodium chloride, and ammonium chloride in microbatch format.

$10\,mg/mL$ glucose isomerase was soluble at low-salt (buffer without additional salt) conditions with a pH value higher than pH 4.45. At pH 4.45 and below precipitation occurred. For the investigated precipitants, phase transitions like precipitation, crystallization, and skin formation were observed. The determined phase diagrams are illustrated in Fig. A.2..

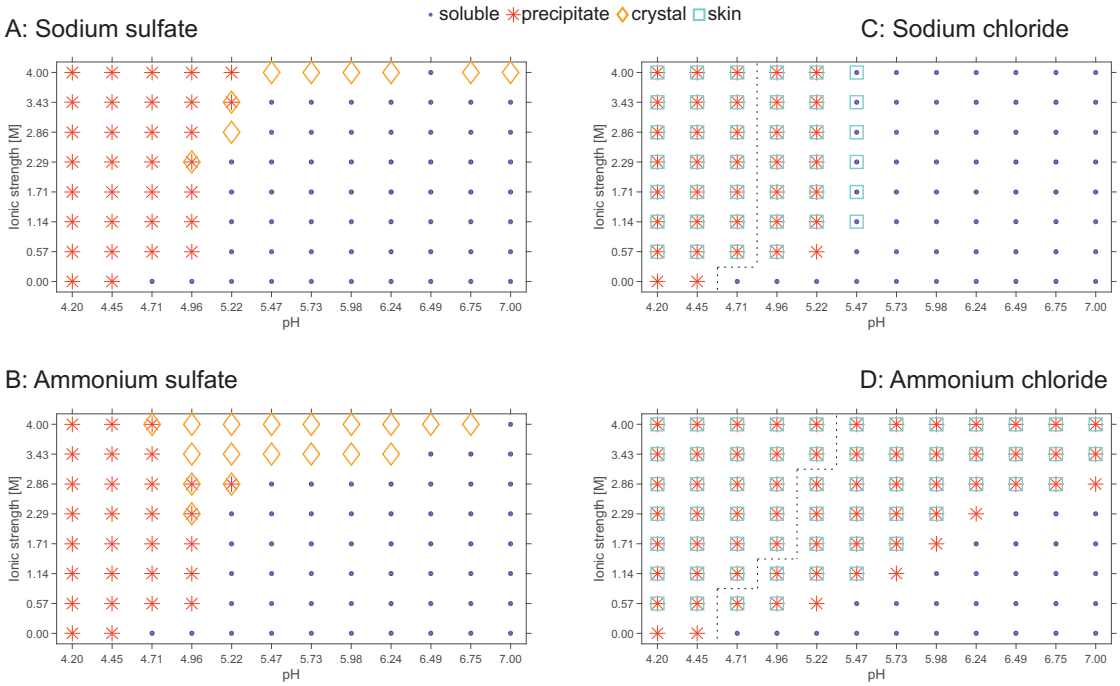

Figure A.2.: Phase diagrams of 10 mg/mL glucose isomerase for an ionic strength range of 0.00 M to 4.00 M of sodium sulfate (A), ammonium sulfate (B), sodium chloride (C), and ammonium chloride (D) in the pH range of pH 4.20 to pH 7.00. Four phase states for glucose isomerase were observed: soluble, precipitate, crystal, skin. The dashed lines in the sodium and ammonium chloride phase diagrams separates immediate and evolving precipitation zones.

Sodium Sulfate as Precipitant

For glucose isomerase with sodium sulfate as precipitant, phase transitions to precipitation and crystallization occurred over the entire investigate pH range (Fig. A.2. (A)). For and below pH 4.96 precipitation occurred independent of ionic strength and additionally for pH 5.22 at the two highest ionic strength conditions (3.43 M and 4.00 M). Crystallization occurred at 4.00 M ionic strength for conditions above pH 5.22 with an exception at pH 6.49. Crystallization was additionally observed for three conditions (pH 4.96 with 2.29 M; pH 5.22 with 2.86 M or 3.43 M) in the transition phase to precipitation. These crystals partially co-existed with precipitation.

All ionic strength conditions below the mentioned crystallizing conditions, from and above pH 5.22, were soluble. Regarding the crystal structure at 4.00 M ionic strength it has to be noted that at higher pH values three-dimensional tetragonal crystal formes were observed. Towards lower pH values (for example pH 5.47) the crystals were more elongated needles (Fig. A.3.).

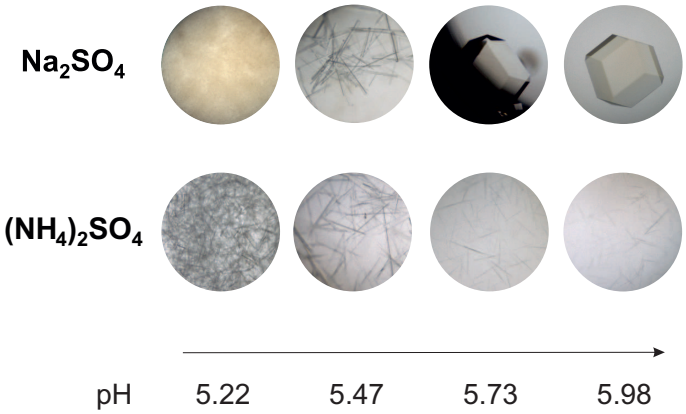

Figure A.3.: Determined crystal size and form of 10 mg/mL glucose isomerase at an ionic strength of 4.00 M sodium sulfate and ammonium sulfate in the pH range from pH 5.22 to pH 5.98.

Ammonium Sulfate as Precipitant

For glucose isomerase with ammonium sulfate as precipitant phase transitions to precipitation and crystallization occurred (Fig. A.2. (B)). Precipitation occurred at all conditions at and below pH 4.96 independent of ionic strength with two exceptions at 3.43 M and 4.00 M ionic strength for pH 4.96. For pH 5.22 and 2.86 M ionic strength an additional precipitated condition was observed. Crystallization was observed for 4.00 M ionic strength in the pH range from pH 4.96 to pH 6.75 and for 3.43 M ionic strength up to pH 6.24. In the transition phase from precipitation to crystallization, co-existent precipitate and crystals were observed (pH 4.71 at 4.00 M ionic strength; pH 4.96 at 2.29 M - 2.86 M ionic strength; pH 5.22 at 2.86 M ionic strength). All observed crystals were needle shaped. At lower pH value and higher ionic strengths the extent of crystallization increased (Fig. A.3.).

Sodium Chloride as Precipitant

For glucose isomerase with sodium chloride as precipitant phase transitions to precipitation and skin formation occurred at conditions with a pH value lower than pH 5.73 (Fig. A.2. (C)). At higher pH values all conditions were soluble. Precipitation occurred for all conditions below pH 5.47. The precipitation can be divided into two zones of different kinetics. At precipitated conditions below pH 4.96, precipitation occurred immediately whereas the precipitation at higher pH values evolved over time. Additional skin formation, which evolved over time, was observed for all precipitated conditions with exception of the condition at pH 5.22 and 0.57 M ionic

strength. Additionally, skin formation was observed for conditions at pH 5.47 and ionic strength higher than 0.57 M although no precipitation was detected.

Ammonium Chloride as Precipitant

For glucose isomerase with ammonium chloride precipitation and skin formation occurred over the entire investigated pH range (Fig A.2. (D)). A soluble region occurred at low precipitant concentrations and high pH values. This region starts at 0.57 M ionic strength for pH values above pH 5.22 up to conditions below 2.86 M ionic strength for pH 6.49 to pH 7.00. The precipitation region at higher precipitant concentrations and lower pH values can be divided in two zones of different kinetics. At conditions below pH 5.47 and 4.00 M ionic strength immediate precipitation occurred. At lower pH values lower ionic strength sufficed for immediate precipitate formation. Between the immediately precipitated and soluble region, slowly evolving precipitation occurred during the 40 days of incubation. At higher pH values and lower ionic strengths precipitation kinetics decelerated. Skin formation evolved over time at and above 0.57 M ionic strength for precipitation conditions excluding the conditions for each ionic strength at the respective highest pH value for 0.57 M to 2.86 M ionic strength.

A.3.2. Hydrophobic Interaction Chromatography Bind-Elute Experiments

Hydrophobic interaction chromatography (HIC) bind-elute experiments of glucose isomerase on a Toyopearl Butyl-650M adsorber were performed on an AEKTA™pu-rifier system. The retention behavior was used as a degree of protein hydrophobicity. In Fig. A.4. the corresponding ionic strengths to the retention volumes of the bind-elute experiments are exemplarily shown at a binding ionic strength of 4.00 M for ammonium sulfate (black) and sodium sulfate (green) in dependence of the respective pH value. For both salts, the retention volumes in dependence of pH value show the same logarithmic progression, seeming to slowly converge to a threshold at higher pH values. With increasing pH value the ionic strength of the retention volumes increased, implying an earlier elution from the HIC column. For ammonium sulfate, the elution ionic strengths were between 2.21 M at pH 5.47 and 2.66 M at pH 7.00. The elution ionic strengths for experiments with sodium sulfate were generally lower with the minimum of 2.20 M at pH 5.73 and the maximum of 2.49 M at pH 7.00. Using sodium sulfate at pH 5.47, glucose isomerase precipitated immediately in this scale and thus no HIC experiment was possible. The bind-elute experiments at varied binding ionic strengths (2.86 M and 3.43 M) showed the same progressions.

For sodium chloride and ammonium chloride no binding of glucose isomerase to the HIC column was feasible at the same ionic strengths.

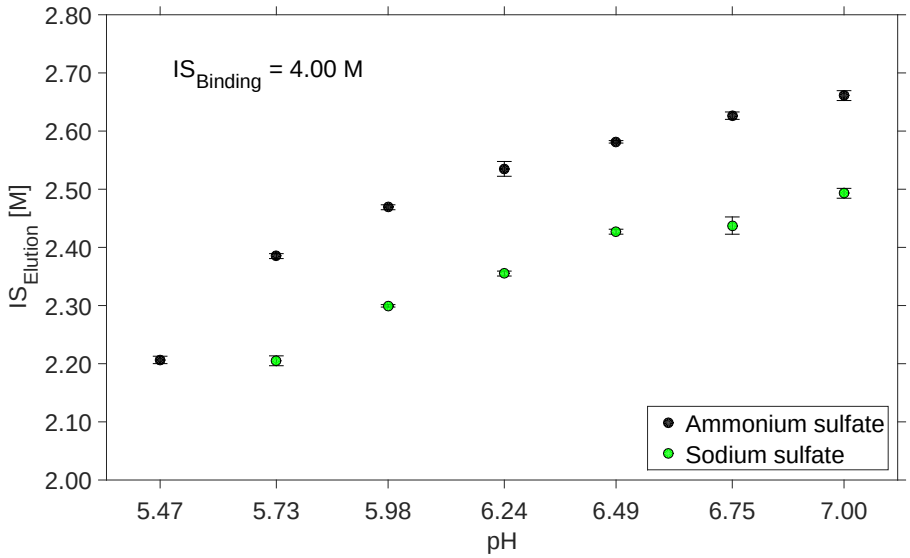

Figure A.4.: Hydrophobic interaction chromatography elution ionic strength ($IS_{Elution}$) of glucose isomerase at 4.00 M binding ionic strength ($IS_{Binding}$) of sodium sulfate (green) and ammonium sulfate (black) in dependence of the pH value.

A.3.3. Thermal Stability

For determining thermal stability of glucose isomerase, melting temperatures and aggregation temperatures were measured using the Optim ®2 system.

Melting Temperature

Melting temperatures of glucose isomerase in dependence of salt type, salt ionic strength and pH value are shown in Fig. A.5. The melting temperatures of 10 mg/mL glucose isomerase at low-salt conditions increased from 71.4°C at pH 5.47 to 84.9°C at pH 7.00. The melting temperatures with precipitant were generally lower regarding the same pH value.

For sodium sulfate as precipitant, melting temperatures varied between 67.0°C at pH 5.47 and 78.9°C at pH 7.00 with an ionic strength of 2.29 M (Fig. A.5. (A)). With an increasing amount of sodium sulfate the melting temperatures are in a similar range.

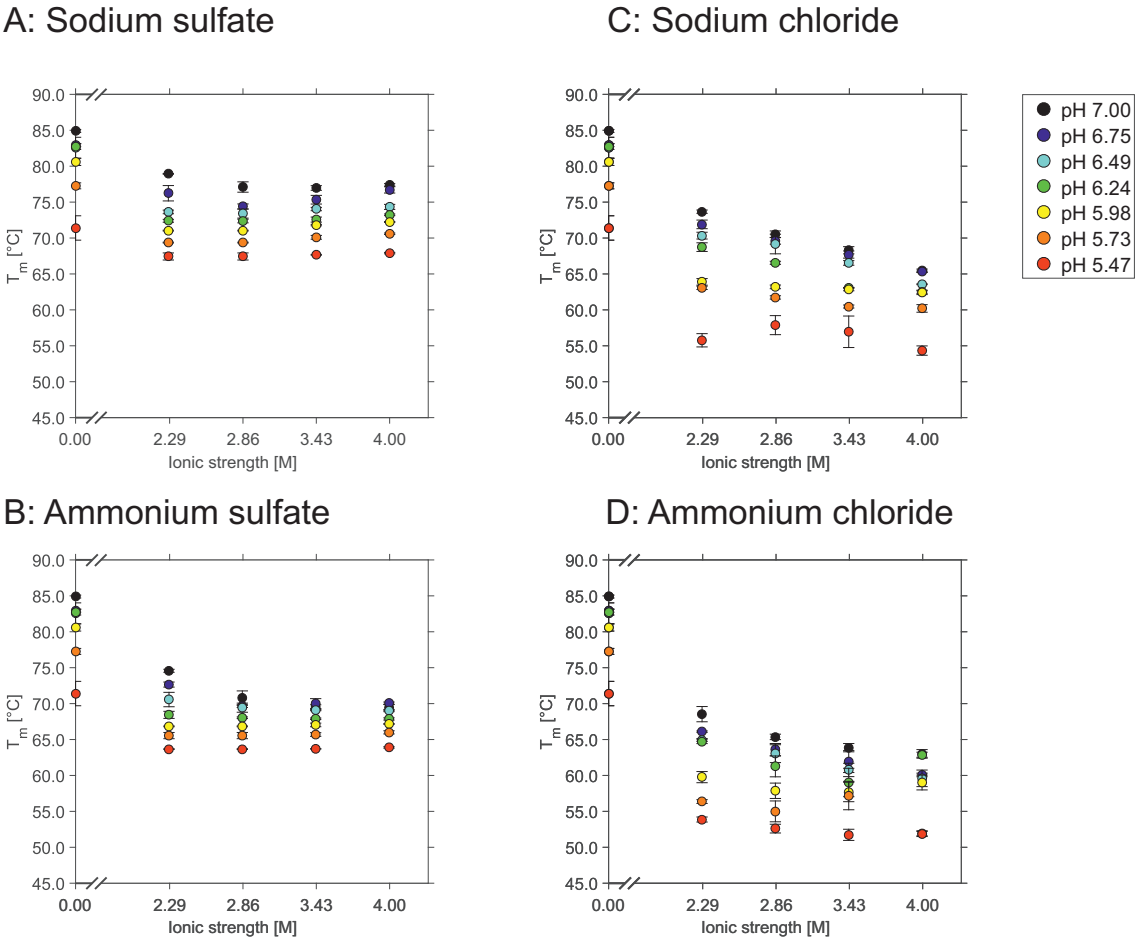

Figure A.5.: Melting temperatures of 10 mg/mL glucose isomerase in dependence of pH value and ionic strength of sodium sulfate (A), ammonium sulfate (B), sodium chloride (C), and ammonium chloride (D).

Using ammonium sulfate as precipitant (Fig. A.5. (B)), melting temperatures were generally lower compared to results determined with precipitant sodium sulfate. At an ammonium sulfate ionic strength of 2.29 M the temperatures varied between 63.4°C at pH 5.47 and 74.6°C at pH 7.00. For 2.86 M to 4.00 M ionic strength of ammonium sulfate, the temperatures stayed constant between ≈64.0°C at pH 5.47 and ≈70.0°C at pH 7.00.

For sodium chloride as precipitant (Fig. A.5. (C)), melting temperatures decrease with increasing ionic strength. At pH 7.00 the melting temperature decreased from 73.7°C at an ionic strength of 2.29 M to 65.5°C at an ionic strength of 4.00 M. The same trend was observed at the other investigated pH values.

Using ammonium chloride as precipitant (Fig. A.5. (D)), the determined melting

temperatures were lowest in comparison to the other applied precipitants with the overall minimum of 51.7°C at pH 5.47 and 3.43 M ionic strength. As already noticed for sodium chloride, the melting temperatures of glucose isomerase decreased with an increasing ionic strength of ammonium chloride. At pH 7.00 the melting temperature decreased from 68.5°C at an ionic strength of 2.29 M to 63.0°C at 4.00 M. The same trend was observed at the other investigated pH values.

When comparing the melting temperatures at a constant ionic strength and different pH values, the temperatures generally decreased with decreasing pH value. For sodium sulfate and ammonium sulfate the differences in melting temperatures at constant ionic strengths and varying pH values were much lower ($\approx \Delta\, 10\, K$) compared to sodium chloride and ammonium chloride ($\approx \Delta\, 20\, K$).

Aggregation Temperature

In Fig. A.6. the aggregation temperatures of 10 mg/mL glucose isomerase are shown in dependence of ionic strength of the applied precipitants at varying pH values. At low-salt conditions the aggregation temperatures were between 60.0°C at pH 7.00 and 39.2°C at pH 5.47. Adding salt to the protein solution generally decreased the determined aggregation temperatures.

At an ionic strength of 2.29 M sodium sulfate aggregation temperatures were between 45.3°C at the highest pH values and 36.2°C at pH 5.47 (Fig. A.6. (A)). With an increasing ionic strength aggregation temperatures increased approximately +3°C.

Using ammonium sulfate as precipitant (Fig. A.6. (B)), aggregation temperatures were lower compared to sodium sulfate as precipitant. At an ionic strength of 2.29 M ammonium sulfate the determined aggregation temperatures were around 38.0°C at all investigated pH values. With increasing ionic strength aggregation temperatures increased up to 45.8°C at pH 7.00 at an ionic strength of 4.00 M.

Aggregation temperatures of glucose isomerase with sodium chloride as precipitant (Fig. A.6. (C)) were in a similar region as determined for the precipitants sodium and ammonium sulfate. However, the progression of aggregation temperatures is different. Starting at aggregation temperatures of 50.0°C at an ionic strength of 2.29 M at pH 7.00 the aggregation temperatures decreased to 44.1°C at an ionic strength of 4.00 M sodium chloride. The aggregation temperatures at lower pH values decreased towards 35.7°C at an ionic strength of 4.00 M.

For ammonium chloride as precipitant large errorbars were observed (data not shown). When comparing aggregation temperatures at different pH values and constant ionic

strengths, aggregation temperatures decreased with decreasing pH value. The observed difference was largest at low-salt conditions. By adding precipitant this distinction reduced.

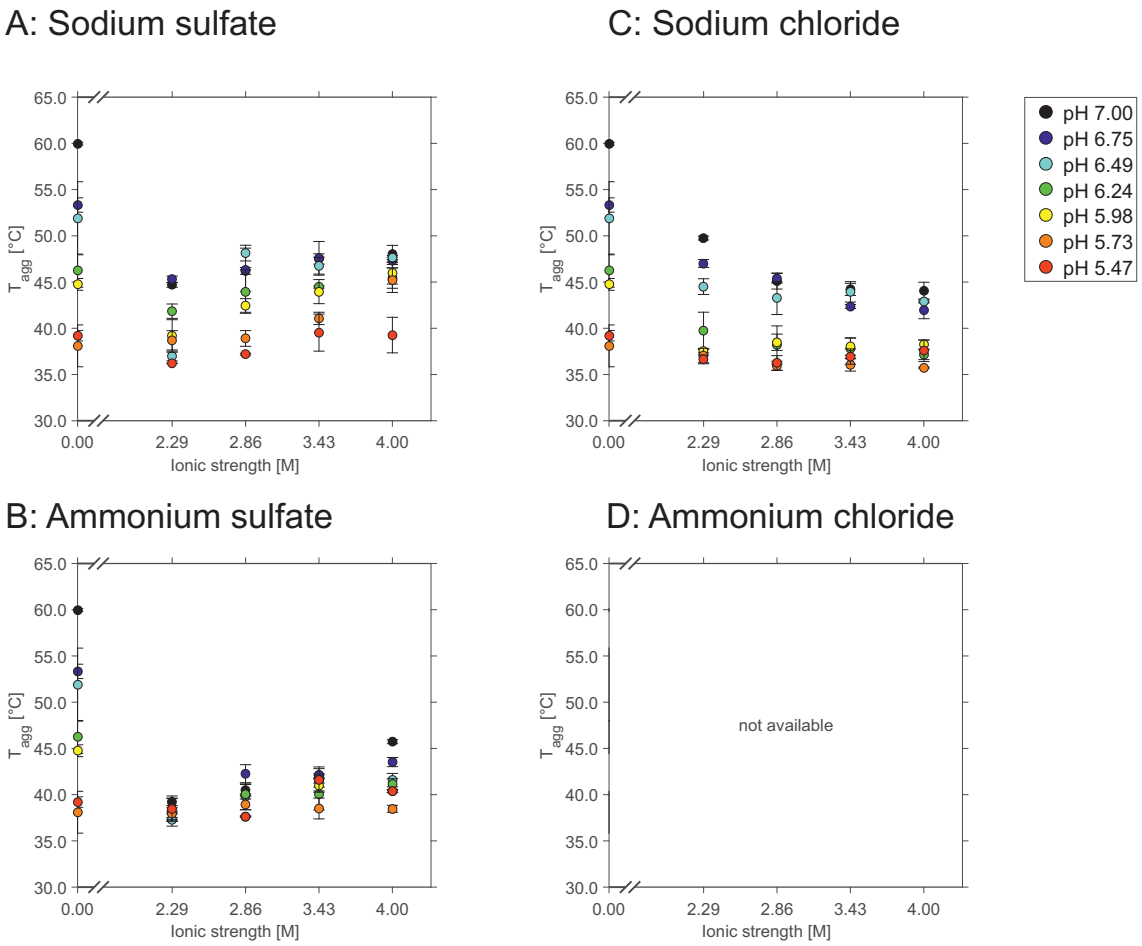

Figure A.6.: Aggregation temperatures of $10\,mg/mL$ glucose isomerase in dependence of pH value and ionic strength of sodium sulfate (A), ammonium sulfate (B), sodium chloride (C), and ammonium chloride (D).

A.4. Discussion

A.4.1. Protein Phase Diagrams

In this paper a method to create protein phase diagrams with variation in pH value and ionic strength at a constant protein concentration is presented. These microbatch

experiments were realized in high-throughput as described earlier by Baumgartner *et al.* [51]. The utilization of a multi-component buffer system, developed by Kröner *et al.* [244], provides the possibility to manipulate pH linearly due to a constant buffer capacity over the whole pH range. The desired pH value was maintained by mixing different starting pH values in microbatch format. One protein phase diagram consists of 96 different conditions with eight equidistant steps of ionic strength and twelve equidistant pH steps at a constant protein concentration.

Phase Behavior of Glucose Isomerase

Glucose isomerase phase behavior at a concentration of $10\,mg/mL$ was investigated in dependence of pH value and ionic strength. The pH value was varied between pH 4.20 and pH 7.00. Precipitant ionic strengths of sodium sulfate, ammonium sulfate, sodium chloride, and ammonium chloride were altered in an range of $0.00\,M$ to $4.00\,M$.

An influence of ionic strength on protein phase transitions was found for all investigated precipitants. For sodium sulfate and ammonium sulfate, precipitation and crystallization zones were observed. Precipitation was observed at lower pH values close to the isoelectric point (pI) and crystallization at higher pH values and high ionic strengths. The crystallization zones were found for sodium sulfate and ammonium sulfate at pH values from and above pH 4.96 and pH 4.71, respectively. In the transition zone from precipitation to crystallization both phase states co-existed. Although the crystallization zone for ammonium sulfate was larger compared to sodium sulfate, the crystal yield was higher for sodium sulfate. Here, at $4.00\,M$ ionic strength three-dimensionally shaped crystals developed whereas for ammonium sulfate needle-shaped crystals were found. The formation of three-dimensional crystals requires a larger number of specific binding sites on the protein surface compared to two-dimensional needle-shaped crystals [245]. Due to shielding of long-range electrostatic forces at high-salt conditions it is assumed that short-range forces on protein surface provoke protein-protein attractive interactions, possibly resulting in crystallization. These short-range interactions like van-der-Waals or hydrophobic interactions contribute to protein crystal stability and formation [245–247]. These short-range interactions have to be higher for sodium sulfate compared to ammonium sulfate. Additionally, the nucleation onset of glucose isomerase was observed much earlier for conditions with sodium sulfate compared to ammonium sulfate.

Further, the pH value had an additional influence on crystal form and size. For sodium sulfate, needle-shaped crystals were found close to the precipitation zone at pH 5.47, whereas three-dimensional crystals were observed at higher pH values. Altering the pH value, salt bridges and hydrogen bonds as well as hydration of

protein are influenced [248]. At lower pH values, close to the pI, glucose isomerase has a lower number of surface charges. This was verified using PDB structure 3kbs using the molecular dynamics simulation tool Yasara (YASARA Biosciences) (data not shown). Resulting, glucose isomerase is less hydrated and attractive hydrophobic forces are higher. Due to this fact faster crystal nucleation and growth leads to many small needle-shaped crystals. In the precipitation zone attractive forces are too high for protein molecules to form structured crystal lattices [249]. For ammonium sulfate as precipitant the extent of crystallization is higher, whereas crystal size is smaller at lower pH values. This can be attributed to higher attractive forces close to the pI. In summary, sodium sulfate had a stronger tendency to induce short-range protein-protein interactions for glucose isomerase, enhancing crystallization, at the investigated pH range from pH 4.20 to pH 7.00, when compared to ammonium sulfate. This is consistent with findings for lysozyme from Lin *et al.* [250].

The phase behavior of glucose isomerase with sodium chloride or ammonium chloride as precipitant, phase transition to precipitation and skin formation occurred. For sodium chloride, no significant influence of ionic strength on precipitation and skin formation was noted. For ammonium chloride, higher ionic strengths led to a broader precipitated area at higher pH values. It can be concluded that ammonium chloride had a more destabilizing effect on glucose isomerase phase behavior compared to sodium chloride.

The impact of pH on phase behavior was clearly distinguishable for sodium chloride and ammonium chloride as precipitants. At low pH values close to the isoelectric point of glucose isomerase precipitation and skin formation was observed for both precipitants. Skin formation is believed to be attributed to protein denaturation [73, 75] and therefore lower conformational stability. For glucose isomerase, higher pH values, implying more charges on the protein surface, resulted in more stable solutions. Ammonium chloride destabilized glucose isomerase more strongly compared to sodium chloride.

The impact on glucose isomerase phase behavior was found to be mainly dependent on the anion [67, 251]. Larger precipitation zones were found for salts containing chloride than for sulfate. Additionally, skin formation and thereby protein denaturation can be attributed to chloride. Sulfate led to crystallization for both investigated salts. The impact of the cations sodium and ammonium was not as distinctively as of the anions. The ammonium cation was found to obtain a more chaotropic character compared to sodium.

A.4.2. Hydrophobic Interaction Chromatography

In this study, retention volumes in hydrophobic interaction chromatography (HIC) were examined to describe protein hydrophobic properties [235] as a component of the short-range interactions mentioned in A.4.1. Due to high ionic strengths used at binding to the adsorber, it can be assumed that electrostatic interactions are shielded and predominantly hydrophobic interactions are decisive. Generally, in HIC lower ionic strengths at elution imply stronger binding to the HIC adsorber. Therefore, lower elution ionic strengths, as determined for sodium sulfate compared to ammonium sulfate, imply stronger hydrophobic interactions of glucose isomerase with the adsorber using sodium sulfate. This observation is compliant with findings made by Lin *et al.* [250], who found sodium sulfate to enhance hydrophobic interactions of lysozyme stronger compared to ammonium sulfate. For sodium chloride and ammonium chloride, no HIC retention experiments were possible under the given conditions. The applied ionic strengths at binding were too low to achieve binding of glucose isomerase to the adsorber. Hence, it was observed that sulfate ions increased hydrophobicity of glucose isomerase more strongly in comparison to chloride ions. This is in accordance with literature [67], where it has been recorded that anions have the main influence on binding in HIC.

The elution ionic strengths of glucose isomerase were lower at lower pH values. This observation can be explained by the proximity to the isoelectric point of glucose isomerase (pI: 4.78). At the isoelectric point protein surface net charge is zero. But also the total amount of surface charges is smaller compared to conditions at higher pH values for glucose isomerase (A.4.1). This weakens the hydration shell and thus, hydrophobic interactions are strengthened. Therefore, elution ionic strengths decrease rapidly with the proximity to the pI. At pH values towards pH 7.00 retention volumes only change slightly. This behavior can be explained by the titration curve. Above the pI, total amount of surface charges decreases rapidly close to the pI, whereas further away the total amount of surface charges approaches a threshold.

Concluding, the pH value has a big influence on protein hydrophobicity. The degree of hydrophobic interactions increase with decreasing distance to the isoelectric point. This observation also correlates with the observations made by Baumann *et al.* [252]. Baumann *et al.* found that binding at pH values close to the proteins' pI increased the binding behavior in HIC.The progression of elution ionic strengths of sodium sulfate and ammonium sulfate are similar in dependence of pH value. The small vertical shift of the two curves can be attributed to the different cations sodium and ammonium. Retention times in HIC were used to describe protein hydrophobic properties. These relative hydrophobicities directly correlate with crystal size and form, determined by the phase diagrams. The yield of protein crystallization was higher for sodium sulfate compared to ammonium sulfate. Additionally, three-dimensional crystals

were found for sodium sulfate implying more specific binding sites. When comparing these two salts at the same pH value, enhanced hydrophobic interactions led to three-dimensionally shaped crystals whereas reduced hydrophobic interactions resulted in two-dimensional crystals. Regarding the pH value, crystal size decreased with decreasing distance to the pI. Here, hydrophobicity is significantly higher, leading to faster crystallization kinetics. The fast kinetics hinders the formation of complex large crystals [245]. The HIC results indicate that hydrophobic interactions can directly be correlated to crystal complexity.

A.4.3. Melting Temperature

In this study, melting temperatures were examined to correlate protein thermal stability to protein phase behavior and bind-elute experiments on hydrophobic interaction chromatography. Glucose isomerase was investigated at low-salt (buffer without additional salt) and high-salt (2.29 - 4.00 M ionic strength) conditions of sodium sulfate, ammonium sulfate, sodium chloride and ammonium chloride. The higher melting temperatures at low-salt conditions for all tested pH values compared to high-salt conditions indicate a higher stability of glucose isomerase. Salt ions influence the protein hydration, which was earlier described as preferential interaction theory [63, 236]. Preferential interaction of ions with the protein weakens protein hydration whereas preferential exclusion sustains hydration and is believed to stabilize the protein in solution [237]. The observed decrease in melting temperature for glucose isomerase indicates a weakening of the protein hydration in the investigated ionic strength range for the analyzed salt types. This observation is in accordance to the preferential interaction theory that all investigated salts should exhibit preferential interaction with the protein, thus destabilizing the native protein conformation and decreasing protein thermal stability [253–256]. The above-mentioned observations are in concert with the observed phase behavior of glucose isomerase. The solubility of glucose isomerase decreased with increasing salt ionic strength. This behavior was mainly noticeable at pH values close to the isoelectric point where the precipitation zone enlarged with addition of salt. Different salt type specific influences on melting temperatures were observed. When comparing the melting temperatures an order of ammonium chloride < sodium chloride < ammonium sulfate < sodium sulfate was found, where ammonium chloride shows the most destabilizing properties and sodium sulfate the most stabilizing. Dupeux *et al.* [257] correlated thermal stability to higher crystallization success rates. This is in agreement with the generated data presented in this manuscript. Higher glucose isomerase melting temperatures were observed for experiments using sodium sulfate and ammonium sulfate whilst leading to crystallization as determined with the phase diagrams. The order of melting temperatures corresponds to protein solubility and stability behavior observed with the phase diagrams.

When comparing the cations sodium and ammonium, higher melting temperatures were found for sodium. Thus, sodium stabilizes glucose isomerase more strongly compared to ammonium. This can be correlated to glucose isomerase solubility and stability phase behavior. For salts with sulfate as anion, sodium leads to bigger crystals compared to ammonium. Hence, the solubility of glucose isomerase is higher in the crystallization zone for ammonium sulfate compared to sodium sulfate. This is in concert with ammonium being a weakly hydrated chaotropic agent [251] known to increase solubility.

For salts with chloride as anion, sodium shows a smaller precipitation area with skin formation compared to ammonium. Ammonium interacts more strongly with the protein inducing destabilization of the native conformation which can be observed by reduced thermal stability and macroscopically as skin formation [258].

The determined results imply higher stabilizing effects for sodium when compared to ammonium which is in agreement with findings from Collins [251]. Sodium is a strongly hydrated ion with kosmotropic properties, whereas ammonium is a weakly hydrated ion with chaotropic properties.

When comparing the anions sulfate and chloride, higher melting temperatures were observed for sulfate compared to chloride. Thus, sulfate stabilizes glucose isomerase more strongly compared to chloride. This is in concert with findings from Arakawa and Timasheff [259] that for sulfate preferential exclusion is higher compared to chloride.

Melting temperatures were successfully correlated to glucose isomerase stability. Sulfate is more stabilizing, leading to crystallization in combination with both investigated cations sodium and ammonium. In contrast, chloride is more destabilizing, inducing larger precipitation zones and skin formation. Regarding the preferential interaction theory, chloride preferentially interacts with the protein and leads to protein destabilization and consequently to lower thermal stability.

Regarding the pH value, with decreasing distance to the proteins' isoelectric point the melting temperatures decreased for all investigated salt ionic strengths. The number of protein surface charges of glucose isomerase decreases with decreasing distance to its pI (A.4.1). Therefore, stabilizing electrostatic interactions between proteins and water molecules are reduced. Hence, the hydration shell around the protein is weakend and the native protein conformation is perturbed leading to lower thermal stability as was found for all ionic strengths. This is also in agreement with the determined macroscopic phase behavior of glucose isomerase.

It can be concluded that the anions and cations have a distinct impact on protein

solubility and stability as investigated using melting temperature. Those findings could successfully be correlated to protein phase behavior. Anions were found to have a stronger effect on protein solubility and stability compared to cations which is in agreement with literature [67, 251, 259]. Concluding from that, this is a comparatively fast method to evaluate protein solubility and stability. Distinctions between native (crystal, soluble, precipitate) and non-native (skin formation) phase behavior can be made. Thus, melting temperatures can help to assess estimations for protein phase behavior.

A.4.4. Aggregation Temperature

The thermal aggregation temperatures were examined to study glucose isomerase stability. Low-salt and high-salt (2.29 M - 4.00 M ionic strength) conditions of sodium sulfate, ammonium sulfate, sodium chloride, and ammonium chloride were investigated for glucose isomerase using the Optim®2. The resolution limit of this method was found to be around 36°C resulting in problems to discriminate conditions close to the isoelectric point of glucose isomerase.

The higher aggregation temperatures at low-salt conditions for all tested pH values compared to high-salt conditions indicate a higher colloidal stability of glucose isomerase. This is in concert with the results for the melting temperatures. Glucose isomerase thermal stability is reduced by the addition of the investigated salts in the given ionic strength and pH range.

The comparison of the cations sodium and ammonium, only possible for sulfate as anion, shows higher aggregation temperatures for sodium compared to ammonium. Thus, sodium cations stabilize glucose isomerase more strongly compared to ammonium cations. This is in accordance to findings for melting temperature and glucose isomerase phase behavior. Sodium, having a kosmotropic character, stabilizes glucose isomerase more and leads to bigger crystals, whereas ammonium is chaotropic and reduces crystal size.

The comparison of the anions sulfate and chloride, only possible for sodium as cation, shows higher aggregation temperatures for sulfate. Thus, sulfate stabilized glucose isomerase more strongly compared to chloride. This in concert with findings for melting temperatures and glucose isomerase phase behavior.

The results for ammonium chloride showed large standard deviations for repeated measurements indicating the existence of light scattering aggregates at the starting conditions (data not shown). The results for ammonium chloride are in accordance

with the observation concerning glucose isomerase phase behavior where ammonium chloride led to evolving precipitation and skin formation in the investigated ionic strength and pH range. Here, thermal aggregation temperatures support the statements made by the evaluation of the melting temperatures.

A.5. Conclusions and Outlook

The present work shows that protein hydrophobicity and thermal stability measurements can be used as tools for estimating protein stability. Protein phase behavior was determined using a high-throughput methodology for generation of protein phase diagrams. Protein phase behavior was investigated at a constant protein concentration in dependence of precipitant ionic strength and pH value. Using for different salt types, the influence of two anions and two cations on glucose isomerase phase behavior was investigated. The results confirmed findings from literature [67, 251, 259], that anions influence protein phase behavior more strongly compared to cations. Using hydrophobic interaction chromatography (HIC) and thermal stability measurements, initially and completely soluble conditions were investigated.

Using retention behavior in HIC a deeper understanding of hydrophobic forces in protein-protein interaction was generated. The differences in crystal form and size, using sodium sulfate and ammonium sulfate, can be described by protein surface hydrophobicity and thus estimated by HIC.

Melting temperatures and aggregation temperatures were measured to characterize glucose isomerase thermal stability. Sulfate was found to have a less destabilizing effect on glucose isomerase compared to chloride regarding conformational and colloidal stability. Thermal stability measurements can be used to distinguish between native (crystal, soluble, precipitate) and non-native (skin formation) phase behavior.

Using HIC experiments and thermal stability measurements, glucose isomerase stability can be estimated in relation to variations of parameter settings. The observed correlations should be verified for other biomolecules and variations of parameters.

A.6. Acknowledgments

The authors are grateful for the financial support by the German Federal Ministry of Education and Research (BMBF) - funding code 0315342B - and by Novo Nordisk.

The authors bear the complete responsibility for the content of the publication. The authors have declared no conflict of interest.

B. Full paper - In-line Fourier-Transform Infrared Spectroscopy as a Versatile Process Analytical Technology for Preparative Protein Chromatography

Steffen Großhans[1*], Matthias Rüdt[1*], Adrian Sanden[1*], Nina Brestrich[1], Josephine Morgenstern[1], Stefan Heissler[2], Jürgen Hubbuch[1,**]

[1] Karlsruhe Institute of Technology (KIT), Institute of Process Engineering in Life Sciences, Section IV: Biomolecular Separation Engineering, Karlsruhe, Germany
[2] Karlsruhe Institute of Technology (KIT), Institute of Functional Interfaces, Eggenstein-Leopoldshafen, Germany
* These authors contributed equally to this work
** Corresponding author

Abstract

Fourier-Transform Infrared Spectroscopy (FTIR) is a well-established spectroscopic method in the analysis of small molecules and protein secondary structure. However, FTIR is not commonly applied for in-line monitoring of protein chromatography. Here, the potential of in-line FTIR as a Process Analytical Technology (PAT) in downstream processing was investigated in three case studies addressing the limits of currently applied spectroscopic PAT methods. A first case study exploited the

secondary structural differences of monoclonal antibodies (mAbs) and lysozyme to selectively quantify the two proteins with Partial Least Squares Regression (PLS) giving Root Mean Square Errors of Cross Validation (RMSECV) of 2.42 g/L and 1.67 g/L, respectively. The corresponding Q^2 values are 0.92, 0.93 and, respectively, 0.99, indicating robust models in the calibration range. Second, a process separating lysozyme and PEGylated lysozyme species was monitored giving an estimate of the PEGylation degree of currently eluting species with RMSECV of 2.35 g/L for lysozyme and 1.24 g/L for PEG with Q^2 of 0.96 and 0.94, respectively. Finally, Triton X-100 was added to a feed of lysozyme as a typical process-related impurity. It was shown that the species could be selectively quantified from the FTIR 3D field without PLS calibration. In summary, the proposed PAT tool has the potential to be used as a versatile option for monitoring protein chromatography. It may help to achieve a more complete implementation of the PAT initiative by mitigating limitations of currently used techniques.

B.1. Introduction

Preparative chromatography of biopharmaceuticals is typically monitored by measuring univariate signals such as pH, conductivity, pressure, and UV/Vis absorbance at a given wavelength [214, 227]. Among these, especially single-wavelength UV/Vis spectroscopy has been a staple for process monitoring of biopharmaceutical chromatography due to its linear response to protein concentration as well as its broad dynamic range, sensitivity, and robustness. In spite of advantages, single-wavelength UV/Vis absorption measurements generally do not allow for selective quantification of multiple co-eluting proteins [260].

Even before the PAT initiative by the FDA in 2004 [261], research towards more selective monitoring methods for preparative chromatography was conducted. But the often small differences between biopharmaceutical product and protein as well as non-protein contaminants make this a nontrivial task [34, 262]. As a possible solution, fast at- or on-line analytical methods, such as analytical chromatography, have been established. Discrete samples are taken from the process stream and analyzed on the spot. This approach has been proposed for controlling capture [263–265] and polishing steps [266, 267]. However, at- or on-line analytical chromatography is complex in terms of equipment requiring a sampling module as well as an analytical chromatography system close to the process stream. Furthermore, the sampling and analysis time may be too long compared to the typical time frame available for taking process decisions.

An alternative approach exploits slight differences in UV/Vis absorption spectra of different components to selectively quantify different species by chemometric methods [34]. The approach yields results quickly enough to allow for real-time process decisions in chromatography [268–270] and works for minute spectral differences [271]. However, in the commonly measured spectral ranges, UV/Vis spectroscopy lacks sensitivity towards relevant aspects of protein structure, notably the secondary structure [140]. Furthermore, organic compounds are often not UV-active (e.g. sugars, polyols, and Polyethylene Glycol (PEG) [272, 273]) or they may obscure the protein signal (e.g. Triton X-100 [274] and benzyl alcohol [140]). Due to the high sensitivity, UV/Vis absorption spectroscopy is also prone to detector saturation [34, 275].

FTIR allows to address several of these short-comings. Like UV/Vis spectroscopy, FTIR is a non-destructive, quantitative, and quick method which can be performed in-line [228–230]. FTIR measures the vibrational modes of samples and thereby provides a spectroscopic fingerprint for different organic molecules. Proteins absorb in the IR spectral range mainly due to vibrations of the polypeptide backbone [140, 231, 232]. Based on the backbone vibrations, FTIR grants insight into the secondary structure of the measured proteins. In consequence, FTIR is a widely used method for assessing the structural integrity of proteins during protein purification and formulation [140]. Furthermore, FTIR was previously used as an at-line PAT tool in downstream processing of biopharmaceuticals for quantifying product content, High Molecular Weight species (HMW), and Host Cell Proteins (HCP) [276, 277].

In this work, in-line FTIR as a PAT tool for preparative protein purification was implemented. An FTIR instrument was coupled to a lab-scale preparative chromatography system to perform the experiments. Three case studies were selected to investigate potential applications of FTIR as a PAT tool. First, a mixture of lysozyme and mAb was chosen due to the significant differences in secondary structure of the two proteins. While lysozyme mainly consists of alpha-helices (PDB ID 193L), mAb largely consists of beta-sheets (PDB ID 1HZH). The expected spectral differences can be used to selectively quantify the two proteins by PLS regression. Four linear-gradient elutions with varying gradient lengths were performed. Based on the results, a PLS model for each protein was optimized. The error of the PLS model was assessed by cross validation. Second, the preparative separation of PEGylated lysozyme was monitored. In contrast to UV/Vis spectroscopy, PEG gives a distinct signal in IR which can be used for quantification by PLS regression. Again, four linear gradient elutions were performed for the calibration of two PLS models. Finally, the potential to monitor process-related impurities using in-line FTIR was demonstrated by adding Triton X-100 to a feed solution of lysozyme. Triton X-100 is employed for virus inactivation in biopharmaceutical production and has to be removed from the product [274, 278]. Based on an off-line calibration curve, mass-balancing of Triton X-100 in the flow-through during product loading was performed.

B.2. Materials and Methods

B.2.1. Experimental Setup

In-line FTIR measurements were performed using a Tensor 27 by Bruker Optics (Ettlingen, Germany) connected to an ÄKTApurifier system by GE Healthcare (Little Chalfort, UK). The chromatography system was equipped with a P-900 pump, a P-960 sample pump, UV-900 UV/Vis cell, and a Frac-950 fraction collector (all GE Healthcare). Unicorn 5.31 (GE Healthcare) was used to control the system. The FTIR was equipped with a liquid nitrogen-cooled Mercury Cadmium Telluride (MCT) detector and a BioATR II (Bruker Optics) with a flow-cell insert and a seven-reflections silicon crystal. The instrument was controlled by OPUS 7.2 (Bruker Optics).

In this setup, the effluent stream from the column outlet was diverted through the FTIR instrument and then back into the UV/Vis cell in the ÄKTApurifier system. The flowpath is illustrated in Fig. B.1.. The delay volume between the FTIR and the fraction collector was determined gravimetrically. As the flow rate was set in the chromatographic methods, the measurement of the delay volume enables the correlation of spectral data from the FTIR to collected fractions.

The interconnection between OPUS and Unicorn was achieved using a software solution developed in-house consisting of a Matlab (The Mathworks, Natrick, MA, United States) script and a VBScript in the built-in visual basic script engine of OPUS. The custom software enables start of a measurement at a time defined by Unicorn by sending a digital signal through the I/O port of the pump of the ÄKTApurifier System. The signal is captured by a USB-6008 data acquisition device (National Instruments, Austin, Tx, United States) controlled by Matlab which in turn triggers the measurement in OPUS.

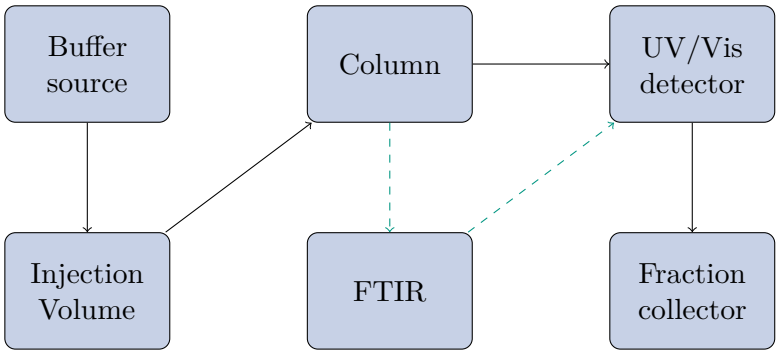

Figure B.1.: Schematic representation of the flow path in the custom chromatography setup, solid lines represent the common flow path in the ÄKTApurifier while the dashed line represents the modification.

B.2.2. Proteins and Buffers

All solutions were prepared using water purified by a PURELAB Ultra water purification system by ELGA Labwater (High Wycombe, United Kingdom). Buffers were filtered using a $0.2\,\mu m$ filter purchased from Sartorius (Göttingen, Germany) and degassed by sonification before use. All buffers were pH-adjusted using 32% HCl (Merck, Darmstadt, Germany).

Lysozyme was purchased from Hampton Research (Aliso Viejo, CA, United States). mAb was provided by Lek Pharmaceuticals d.d. (Mengeš, Slovenia) as a virus-inactivated Protein A eluate pool.

Preparative CEX chromatography runs in case studies I and III were conducted with a $50\,mM$ sodium citrate buffer as equilibration buffer and with an added $500\,mM$ NaCl as elution buffer. Both buffers were adjusted to pH 6.0. Sodium citrate tribasic dihydrate was purchased from Sigma-Aldrich (St. Louis, MO, United States), sodium chloride was purchased from Merck. For the CEX chromatography experiments in case study II, a $25\ mM$ sodium acetate buffer (pH 5.0) was used as equilibration buffer. As elution buffer, a $25\,mM$ sodium acetate buffer with $1\,M$ NaCl (pH 5.0) was used. Sodium acetate trihydrate was purchased from Sigma-Aldrich. Batch-PEGylation of lysozyme was performed in a $25\,mM$ sodium phosphate buffer at pH 7.2 using sodium phosphate monobasic dihydrate (Sigma-Aldrich) and di-sodium hydrogen phosphate dihydrate (Merck).

Analytical cation-exchange chromatography was carried out at pH 8.0 using a $20\,mM$ Tris (Merck) buffer for equilibration and a $20\,mM$ Tris buffer with $700\,mM$ NaCl for elution.

PEGylation of Lysozyme

The PEGylation protocol was adapted from [279]. Briefly, activated $5\,kDA$ PEG was purchased as Methoxy-PEG-propionaldehyde (mPEG-aldehyde, Sunbright ME-050 AL) from NOF Corporation (Tokyo, Japan). Sodium cyanoborohydride (NaCNBH3, Sigma Aldrich) was added to the reaction buffer to a concentration of $20\,mM$ as reducing agent. mPEG-aldehyde was added to a molar PEG-to-protein ratio of 6.67. After $3\,h$, the mixture was diluted volumetrically 7-fold using the acetate equilibration buffer and loaded onto the chromatography column.

B.2.3. Preparative Chromatography Experiments

For all chromatography experiments, FTIR spectra were recorded continuously in the chromatography mode of OPUS with a resolution of $2\,cm^{-1}$ in a range from 4000-$900\,cm^{-1}$ without averaging multiple scans. In the given setup, each measurement took $3.22\,s$. Background measurements at the beginning of chromatographic runs were taken at the same resolution with 400 scans in equilibration buffer. All experiments were conducted twice, once with protein injection and once with buffer only as a blank run. The FTIR spectra from the blank runs were subsequently subtracted from the protein runs to account for spectral effects by the gradient.

Case Study I: Selective Protein Quantification

For case study I, a HiTrap column by GE Healthcare prepacked with SP Sepharose FF resin (Column Volume (CV) $5\,mL$) was used. The column was loaded to a density of $18.75\,g/L$, consisting of $12.5\,g/L$ lysozyme and $6.25\,g/L$ monoclonal antibody. The flow rate for all experiments was set to $0.5\,mL/min$. The column was equilibrated in a low-salt buffer for $5\,CV$ before injection. The $50\,mL$ sample was injected using a $50\,mL$ superloop from GE Healthcare. Elution was carried out with a linear gradient from 0-100% high-salt buffer with gradient lengths of $1\,CV$, $2\,CV$, $3\,CV$, $4\,CV$. After elution, a high-salt wash of $8\,CV$ was performed for column regeneration. The effluent was collected over the complete injection and elution in $500\,\mu L$ fractions for offline analytics.

Case Study II: Separation of PEGylated Lysozyme Species

The experiments with different PEGylated lysozyme species were conducted with Toyopearl Gigacap S-650M resin prepacked in a MiniChrom column (CV $5mL$) by Tosoh (Griesheim, Germany). The column was loaded to a density of $50\,g/L$ of the heterogeneous batch PEGylation. The sample pump was run at $1\,mL/min$ for loading. For the remaining chromatography run, the flow rate was set to $0.5\,mL/min$. The column was first equilibrated for $1\,CV$, followed by an injection of $57.6\,CV$ of sample solution. Linear-gradient elutions from 0-100 % high-salt buffer were conducted with gradients of $2\,CV$, $3\,CV$, $4\,CV$, $5\,CV$ length, followed by a $2\,CV$ high-salt rinse. The effluent was collected from the beginning of the gradient until the end of the high-salt rinse in $500\,\mu L$ fractions for offline analytics.

In some of the collected fractions, unconjugated lysozyme started to precipitate after elution probably due to the low pH, high salt concentration or low temperature [51, 279]. Fractions and the corresponding spectra showing signs of precipitation were excluded from PLS model calibration.

Case Study III: Process-related Impurity

For the simulated process-related impurity experiments, a HiTrap column by GE Healthcare prepacked with SP Sepharose FF resin (CV $5\,mL$) was used. Triton X-100 Biochemica was purchased from AppliChem GmbH (Darmstadt, Germany). The column was loaded with $5\,mL$ of $25\,g/L$ lysozyme and $10\,g/L$ Triton X-100 solution [278]. The elution step was set to $2\,CV$.

Reference samples were generated by diluting defined amounts of Triton X-100 in equilibration buffer at concentrations from $1.25\,g/L$ to $10\,g/L$. To generate a calibration curve, the samples were manually applied onto the ATR crystal. FTIR measurements were performed with 400 scans for background and samples.

B.2.4. Analytical CEX Chromatography

As reference analytics for case study I, analytical CEX chromatography was performed using a Dionex UltiMate 3000 liquid chromatography system by Thermo Fisher Scientific (Waltham, MA, United States). The system was composed of a HPG-3400RS pump, a WPS-3000TFC analytical autosampler, a TCC-3000RS column thermostat, and a DAD3000RS detector. The system was controlled by Chromeleon

6.80 (Thermo Fisher Scientific). Fractions from preparative CEX chromatography were analyzed off-line on a Proswift SCX-1S 4.6x50 mm column by Thermo Fisher Scientific. A flow rate of 1.5 mL/min was used. For each sample, the column was first equilibrated for 1.8 min with equilibration buffer. Next, 20 μL sample was injected into the system and washed for 0.5 min with equilibration buffer. A linear gradient was performed during the next 2 min from 0-50 % followed by a step to 100 % elution buffer which was maintained for 2 min.

For the experiments in case study II, a Vanquish UHPLC system (Thermo Fisher Scientific) was used. The Vanquish UHPLC System consisted of a Diode Array Detector HL, a Split Sampler FT, a Binary Pump F, and a Column Compartment H including a preheater and post-column cooler (all Thermo Fisher Scientific). The same buffers, column, and flow rate were used as for case study I. After injecting 5 μL of sample, the column was washed for 0.5 min. Subsequently, a bilinear gradient was performed from 0-50 % elution buffer over 5 min and 50-100 % elution buffer over 1.75 min. After the elution, a high-salt strip at 100 % was run for 1 min. Calibration was performed by a dilution series of pure lysozyme. Since PEG does not absorb in UV/Vis, solely lysozyme contributes to the absorption signal. Peak identification with respect to the PEGylation degree was conducted using purified samples prepared according to [273]. From the molar concentration of PEGylated lysozyme species, the molar concentration of PEG was calculated.

B.2.5. Data analysis

All data analysis was performed in Matlab. For case studies I and II, the data was first preprocessed and subsequently fitted with PLS-1 models by the SIMPLS algorithm [280]. Preprocessing consisted of linearly interpolating off-line analytics to be on the same time scale as the FTIR spectra. For case studies I and II, spectral data above 2000 cm^{-1} resp. above 3100 cm^{-1} was discarded. Next, a Savitzky-Golay filter with a second-order polynomial was applied on the spectra and optionally, the first or second derivative was taken [281]. Cross-validation was performed by excluding one chromatography run, calibrating a PLS model on the remaining runs, and calculating a residual sum of squares on the excluded run. This procedure was repeated until all runs had been excluded once. All residual sums of squares for the different submodels were subsequently summed yielding the Predictive Residual Sum of Squares (PRESS). The PRESS was scaled according to Wold *et al.* by the number of samples and latent variables used in the PLS model [282]. Based on the scaled PRESS, an optimization was performed using the built-in genetic algorithm of Matlab for integers [283]. The genetic algorithm optimized the window width of the Savitzky-Golay filter, the order of derivative, as well as the number of latent variables for the PLS-1 model. The RMSECV was calculated from the PRESS by

dividing by the total number of samples. The Q^2 values were calculated by dividing the PRESS by the summed squares of the response corrected to the mean [282].

For case study III, spectral data was smoothed both in direction of time and wavenumber using a Savitzky-Golay filter with a second-order polynomial and a frame length of 17 and 51, respectively. A linear baseline was calculated and subtracted for each spectrum individually to account for a non-horizontal non-zero baseline. The baseline subtraction was performed on the reference spectra as well as on the spectra from the chromatography experiment. Based on the area under the spectrum between wavenumbers 1007-1170 cm^{-1}, a mass balance for Triton X-100 was calculated from the spectral data of the chromatography run. The volume represented by each spectrum was calculated from the recording time and the volumetric flow rate of the experiment. Triton X-100 masses in each segment were calculated utilizing the calibration curve and summed up over time.

B.3. Results and Discussion

In-line FTIR measurements were applied as a PAT tool for different preparative chromatographic protein separations. In three different case studies, FTIR was used for selective quantification of different species. First, background correction of the FTIR chromatograms is discussed which was necessary for further data processing. In a first case study, the capability of FTIR to measure differences in secondary structure in-line and utilize the differences for selective quantification of mAb and lysozyme was demonstrated. A second case study made use of the absorption of PEG in IR to monitor the PEGylation degree of eluting PEGylated lysozyme species. Finally, the third case study used the selectivity of FTIR to selectively quantify Triton-X 100, a detergent used for viral inactivation.

B.3.1. Background Subtraction and Spectral Preprocessing

Background subtraction for in-line FTIR measurements is of major importance as water has an absorption band around 1600 cm^{-1} (Fig. B.2. (A)) which coincides with the most prominent protein band amide I. The spectral processing workflow is illustrated in Fig. B.2. using data from case study I. Specifically the elution of mAb and lysozyme using a 4 CV gradient is shown. Most of the water absorption can be eliminated by taking a background with the equilibration buffer at the beginning of each chromatographic run. The water band is, however, also influenced by the salt content of the buffer around 1650 cm^{-1}. Salt gradients therefore cause a change in

absorption over the run (Fig. B.2. (A), (B)). To reduce buffer effects, it is important to find a suitable dynamic background correction. An approach based on reference spectra matrices and chemometric correlations was not implemented due to the overlap of water and protein bands [284]. Instead, an alternative approach was chosen. Based on the retention time, a blank run without protein but including the salt gradient was subtracted from the actual preparative run (Fig. B.2. (C)). The resulting chromatogram provided a smooth baseline over the whole experiment. After baseline correction, additional data preprocessing was performed. The single scan spectra were smoothed by a Savitzky-Golay filter to reduce random noise (Fig. B.2. (D)) and to take derivatives on the spectral data.

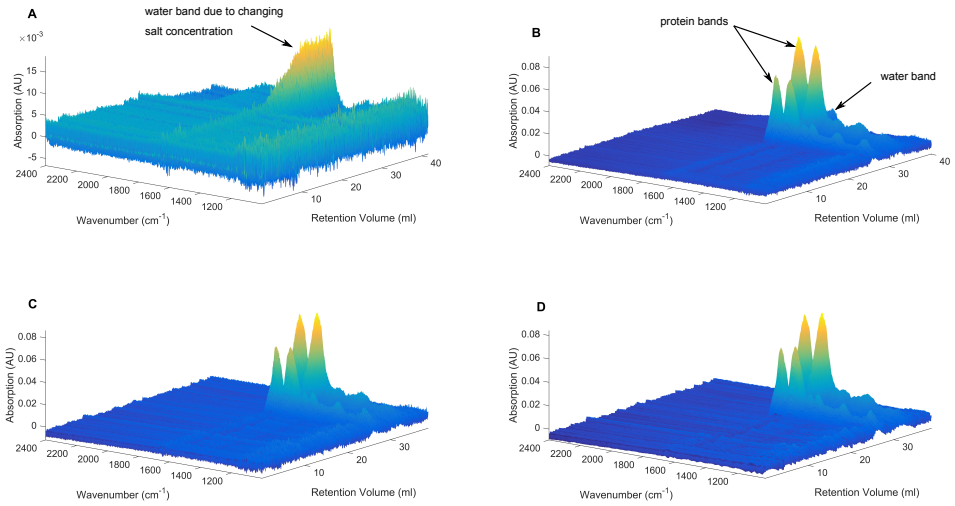

Figure B.2.: Work flow for data treatment of chromatography spectra illustrated with data from case study I, 4 CV run: background run – salt gradient without protein (A); raw spectra of the run with protein (B); spectral data after the background has been subtracted (C); data after smoothing by Savitzky-Golay algorithm (D).

B.3.2. Case Study I: Selective Protein Quantification

mAb and lysozyme feature significant differences in secondary structure. While mAb consists largely of beta-sheets (PDB ID 1HZH), lysozyme mainly contains alpha-helices (PDB ID 193L). These differences make the two proteins simple model components to study the performance of in-line FTIR for selectively quantifying proteins. The bands visible between 1200 cm^{-1} and 1700 cm^{-1} in Fig. B.2. (D) are characteristic amide bands associated with the protein backbone [140, 231, 232]. Especially the amide I band is frequently used for assessing the secondary structure

of proteins. For PLS calibration, all wavenumbers below $2000\,cm^{-1}$ were taken into account to include all protein bands without interference at the boundary due to the Savitzky-Golay filter.

Based on four CEX runs, two PLS-1 models were optimized for selective quantification of mAb and lysozyme, respectively. The resulting model parameters are listed in Tab. B.1. Fig. B.3. shows a comparison from off-line analytics and the prediction of PLS models. Both PLS models match peak maxima and peak widths well and are able to discern the two components. For mAb, a root-mean-square error of cross validation (RMSECV) of $2.42\,g/L$ was reached. For lysozyme, the RMSECV was $1.67\,g/L$. The corresponding Q^2 values were 0.92 and 0.99, respectively. The high Q^2 values show, that a large part of the variation in the off-line concentration measurements could be explained by the PLS model. The differentiation between different proteins may however become more challenging for smaller differences in secondary structure. Interestingly, the combination of Savitzky-Golay filtering and PLS modeling allowed to reduce the measurement noise compared to single-wavelength measurements. As shown by Fig. B.2. (C) and Fig. B.3., the measurement noise in the IR spectra is higher than the noise observed in the PLS prediction. By filtering and projecting the spectra to latent variables, random noise is reduced [281, 282]. Furthermore, $3.23\,s$ measurement time makes FTIR quick enough for monitoring most practical preparative chromatography applications in real-time. In-line FTIR spectroscopy allowed to cover high concentration ranges. The predicted concentration of lysozyme during the $1\,CV$ run reaches $112\,g/L$ without any interference from detector saturation. The measurement setup therefore covers all concentrations typically occurring in preparative protein chromatography.

In summary, the results show that FTIR in conjunction with PLS modeling can differentiate in-line between proteins based on their secondary structure and has the potential to be applied for real-time monitoring and control of preparative chromatography.

Table B.1.: Model parameters for case studies I and II are listed below including the parameters for the Savitzky-Golay filter and the latent variables of the PLS-1 model. Additionally, the RMSECV for each model is listed.

	Case study I		Case study II	
	mAb	lysozyme	lysozyme	PEG
Savitzky-Golay Window	215	21	101	361
Derivative	0	0	2	2
Latent variables	3	7	6	8
RMSECV ($g\,l^{-1}$)	2.41	1.63	2.35	1.24

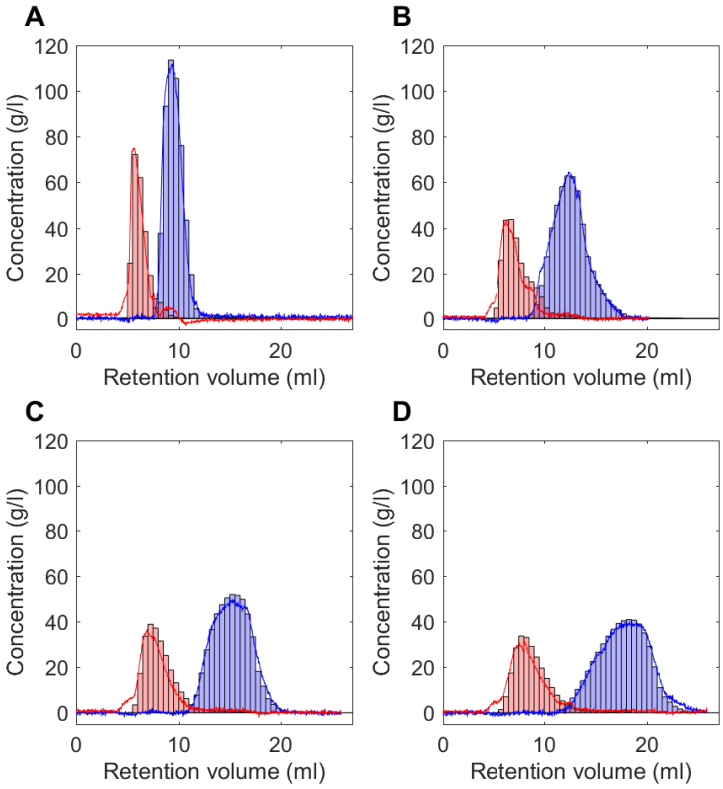

Figure B.3.: Four chromatographic runs are shown for in-line FTIR measurements and selective quantification of mAb and lysozyme. The red bars and lines refer to the mAb off-line measurement and mAb PLS prediction, respectively. The blue bars and lines refer to the lysozyme off-line measurement and lysozyme PLS prediction, respectively. The different subplots show different gradient lengths: A $1\,CV$, B $2\,CV$, C $3\,CV$, D $4\,CV$.

B.3.3. Case Study II: Separation of PEGylated Lysozyme Species

In conventional chromatography systems, the separation of differently PEGylated species cannot be monitored holistically as PEG does not absorb in UV. Contrary to this, PEG produces a number of prominent bands in IR. A strong band around $1090\,cm^{-1}$ with multiple shoulders is characteristic of C-O stretching [285]. Due to symmetric CH2 stretching, PEG furthermore generates a doublet at 2884; $2922\,cm^{-1}$. Bands occurring between $1200\,cm^{-1}$ and $1700\,cm^{-1}$ are related to the protein backbone with some interference from PEG C-H bending.

Fig. B.4. shows a typical chromatographic separation of PEGylated lysozyme species. During the elution, the ratio between PEG and protein bands decreases. First, with a retention volume of $6.8\,mL$, the absorption of the C-O band at $1090\,cm^{-1}$

(denoted as CO1 in Fig. B.4.) exceeds the absorption of amide I band (AI1). For the second peak with a retention volume of 10.3 mL, the absorption of the amide I (AI2) is higher than for the C-O stretching band (CO2). The last peak does not show characteristic PEG bands, i.e. consists of unconjugated lysozyme. The order of elution followed a descending degree of PEGylation which is in line with previous publications [273, 286, 287]. Based on the evaluation of IR absorption

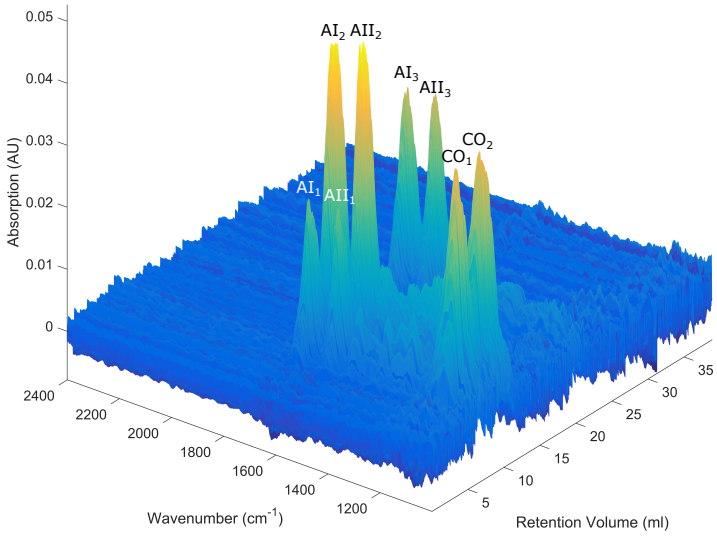

Figure B.4.: Elution of PEGylated lysozyme species from a CEX column with a gradient length of 5 CV. Bands visible between wavenumbers 1200-1700 cm^{-1} are the characteristic amide bands associated with protein. The major protein bands amide I and amide II are marked as AI and AII, respectively. The band at approximately 1100 cm^{-1} is characteristic of PEG (C-O stretching, marked as CO). The subscript numerals refer to the elution order.

bands, it was decided to include all wavenumbers from 900-3100 cm^{-1} into PLS model calibration. Initial PLS calibration on the concentration of the different PEGylated lysozyme species showed that the conjugation did not cause large enough band shifts to allow for selective quantification of the different PEGylated lysozyme species. Instead, two PLS models were fitted on the total PEG resp. lysozyme concentration independently. PEG concentration was calculated by weighting the off-line lysozyme concentration according to the PEGylation degree. In Tab, B.1, the optimization results are summarized. Fig. B.5. compares the PLS prediction with off-line analytics.

RMSECV values of $1.24\,g/L$ and $2.35\,g/L$ were reached for the PEG and lysozyme concentration, respectively. The corresponding Q^2 values were respectively 0.96 and 0.94 showing that the PLS models predicted the responses well. Based on the PEG and lysozyme concentrations, a molar ratio could be calculated corresponding to the current average PEGylation degree. To simplify visual interpretation, the molar ratio was only plotted if the lysozyme concentration exceeded its RMSECV 3-fold.

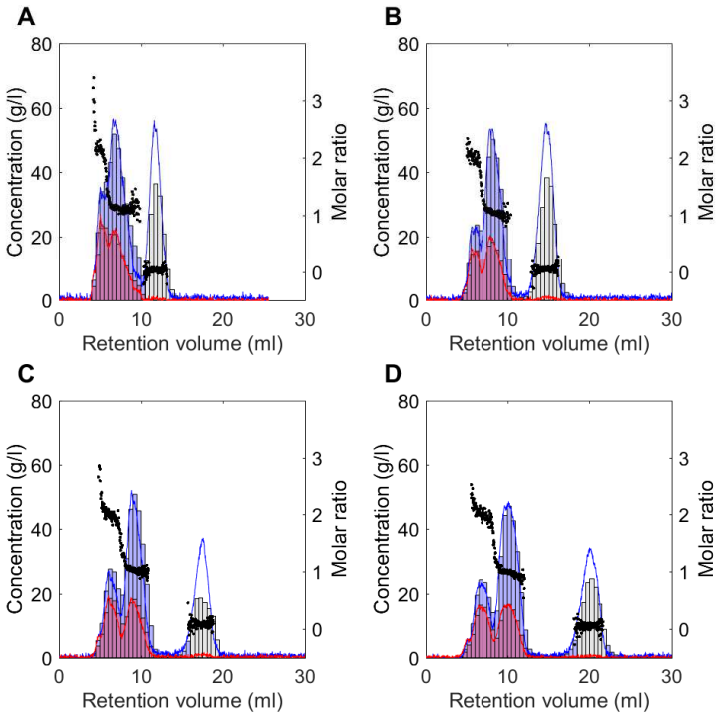

Figure B.5.: Four chromatographic runs are shown for in-line FTIR measurements and selective quantification of PEG and lysozyme. The red bars and lines refer to the PEG off-line measurement and PEG PLS prediction, respectively. The blue bars and lines refer to the lysozyme off-line measurement and lysozyme PLS prediction, respectively. Grey bars correspond to measured protein concentrations on partially precipitated samples. Black dots show the molar ratio between PEG and lysozyme, i.e. the current mean PEGylation degree. The different subplots show different gradient lengths: A $2\,CV$, B $3\,CV$, C $4\,CV$, D $5\,CV$.

The predicted PEG and lysozyme concentrations accurately followed the concentrations measured by off-line analytics. Furthermore, the molar ratio gives a suitable tool for in-line monitoring of the elution of different PEG species. Interestingly, the two PLS models are able to extend their prediction over the calibration range, i.e. to perform a weak extrapolation. This can be seen as the PEG-to-lysozyme ratio exceeds the value of two, which limits the calibration range spanned by off-line analytics. Higher PEGylated species of lysozyme do however occur and could be measured by the FTIR [273, 288].

In summary, FTIR allows to monitor not only the protein and PEG concentration but also the PEGylation degree during chromatographic separations.

B.3.4. Case Study III: Quantification of a Process-related

Triton X-100 is used for viral inactivation of biopharmaceuticals if pH treatment has to be circumvented, e.g. for Factor VIII or pH-sensitive mAbs [274, 278]. To achieve viral inactivation, Triton X-100 concentration needs to be above a minimal level. Typically, a concentration of 1 % (w/V) is used. Here, Triton X-100 concentration of a mock virus inactivation batch was monitored during the subsequent load phase onto a chromatographic column. During the chromatographic run, in-line FTIR measurements were perform (Fig. B.6.).

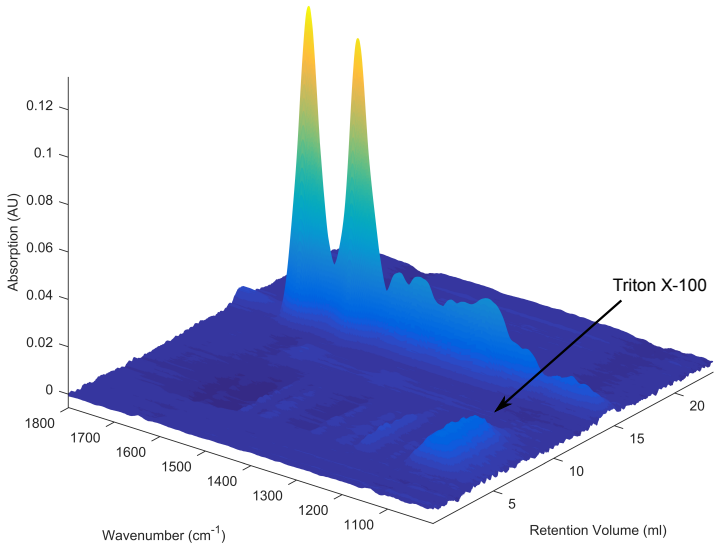

Figure B.6.: Triton X-100 as a process-related impurity can be seen in the flow-through of the cation-exchange experiment from 5.5-11 mL at 1090 cm^{-1}.

In IR, Triton X-100 causes a characteristic band due to C-O stretching at 1090 cm^{-1}. By comparison of the blank run and the actual experiment, it was concluded that Triton X-100 is not retained on the column and is mainly present in the flow-through. The flow-through occurred between 5.5-11 mL. As Triton X-100 and protein spectra only weakly interfere with each other, the Triton X-100 content was measured by simply correlating the band area of C-O stretching from 1007-1170 cm^{-1} to the

Triton X-100 concentration. A linear regression for the calibration curve resulted in a $R^2 > 0.9997$. Based on the calibration curve, in-line mass-balancing could be performed. The mass balance for Triton X-100 showed a recovery rate of 94.12 % in the flow-through. This shows that it is possible to selectively quantify Triton X-100 content during the chromatographic load phase.

B.4. Conclusion and Outlook

FTIR spectroscopy was successfully implemented in-line as a PAT tool for biopharmaceutical purification processes. It was demonstrated that FTIR is able to distinguish and selectively quantify proteins in-line based on their secondary structure. Furthermore, FTIR presents a powerful tool for monitoring different chemical components such as PEG or Triton X-100. Based on selective in-line quantification of PEG and protein, PEGylation degrees could be measured in-line. Selective mass balancing was performed on the process-related contaminant Triton X-100. In summary, FTIR provides orthogonal information to the typically measured UV/Vis spectra. It therefore is potentially interesting for monitoring process attributes which have been previously hidden. FTIR may help to achieve a more complete implementation of the PAT initiative.

Future research should be directed towards making the setup more compatible with the production environment. Challenges include the use of detectors without liquid nitrogen cooling and the application of fiber optics for in-line process probes.

Acknowledgment

This work has received funding from the European Union's Horizon 2020 research and innovation programme under grant agreement No 635557. We are thankful for the mAb protein A pool which we received from Lek Pharmaceuticals, d.d. We would also like to thank Daniel Büchler for his help conducting the experiments.

C. Abbreviations and Symbols

Abbreviations

ABC	Anything But Chromatography
AC	Affinity chromatography
ADC	Antibody drug conjugate
ASA	Adaptive simulated annealing
ATPS	Aqueous two-phase system
ATR	Attenuated total reflection
AEX	Anion exchange chromatography
BSA	Bovine serum albumin
CEX	Cation exchange chromatography
CHO	Chinese hamster ovary
CSTR	Continuous stirred tank reactor
CV	Column volume
DF	Diafiltration
DLVO	Derjaguin, Landau, Verwey, Overbeek
DNA	Deoxyribonucleic acid
DSP	Downstream process development
DoE	Design of experiment
ELISA	Enzyme-linked immunosorbent Assay
EMA	European Medicines Agency
Fc	Fragment crystallizable
FDA	Food and drug administration
FTIR	Fourier-transform infrared spectroscopy
GMP	Good manufacturing practice
GRM	General rate model
GST	Glutathione S-transferase

HCCF	Harvested cell culture fluid
HCP	Host cell proteins
HIC	Hydrophobic interaction chromatography
HIS	Histidine
HMW	High molecular weight impurities
HPLC	High performance liquid chromatography
HT	High-throughput
HTPD	High-throughput process development
HTS	High-throughput screening
IEX	Ion exchange chromatography
IgG	Immunglobulin G
LC	Liquid chromatography
LGE	Linear gradient elution
LM	Levenberg-Marquardt
mAb	Monoclonal antibody
MCA	MultiChannel Arm
MCT	Mercury Cadmium Telluride
MLR	Multi linear regression
mPSE	Modified polyethersulfone
MSMPR	Mixed product removal reactor
MVDA	Multivariate data analysis
NIPALS	Nonlinear iterative partial last square
OFAT	One-factor-at-a-time
PDB	Protein data base
pKa	Acid dissociation constant
PLS	Partial least square
PAT	Process analytical technologies
PCA	Principle component analysis
PCCC	Periodic counter current chromatography
PEG	Polyethylene glycol
pI	Isoelectric point
QbD	Quality by design
QSAR	Quantitative structure-activity relationship
PRESS	Predictive residual sum of square
RMSECV	Root mean square errors of validation

RMSEP	Root mean square errors of prediction
RP	Reversed phase chromatography
SEC	Size exclusion chromatography
SMA	Steric mass action
TMP	Transmembrane pressure
TFF	Tangential flow filtration
UF	Ultrafiltration
UHPLC	Ultra-high performance chromatography
UV	Ultraviolet
USP	Upstream process development
VdW	Van-der-Waals
Vis	Visible
VLP	Virus-like particles

Symbols

a_i	Activity	M
B	Regression matrix	-
c_i	Bulk phase concentration of species i	M
c_p	Protein in solution	M
$c_{p,i}$	Pore phase concentration of species i	M
C	Protein solubility in the Cohen equation	M
C_0	Protein solubility in the absence of PEG in the Cohen equation	-
D_{ax}	Axial dispersion coefficient	$\frac{mm^2}{s}$
D_p	Pore diffusion coefficient	$\frac{mm^2}{s}$
E_i	Residues matrix of a PLS or PCA	
F	Electric force	N
G	Gibbs free energy	J
h	Ionic hydration number	-
k	Constant for hydration dependency of salts	-
k_e	Coulomb constant	$\frac{NM^2}{C^2}$
k_{ads}	Adsorption coefficient	-
k_{des}	Desorption coefficient	-
k_{eq}	Equilibrium coefficient	-
$k_{film,i}$	Film transfer coefficient	$\frac{mm}{s}$
k_{kin}	Kinetic coefficient	-
K	Equilibrium constant	-
L	Distance of the mirror	mm
m	PEG concentration	$\%\,(w/w)$
n	Number of protein molecules	-
P	Protein molecules	-
P_p	Precipitate	-
PEG	One PEG molecule	-
P^T	Principle component matrix	-
pKa	Acid dissociation constant at logarithmic scale	
q	Precipitated protein	M
q_i	Stationary phase concentration of species i	M
q_p	Charge of the species p	C

Q	Principle component matrix	-
r	Radius	mm
r_p	Particle radius of adsorbent	mm
R	Gas constant	$\frac{J}{Kmol}$
S	Entropy	$\frac{J}{K}$
t	Time	s
T	Temperature	K
T_{agg}	Aggregation temperature	$°C$
T_m	Melting temperature	$°C$
u	Flow velocity	$\frac{mm}{s}$
U	Potential energy	J
H	Enthalpy	J
V	Score matrix	-
W	Score matrix	-
W_B	Bulk-like ordered water molecules	-
x	Space dimension	mm
x_i	Amount fraction	mol
X	Matrix with original data during PCA	-
z	Distance between two particles	m
β	Number of bulk-like water molecules	-
β_0	Hydration number at infinite dilution of PEG and protein	-
β_1	Hydration number accounting for PEG	$\frac{L}{mol}$
β_2	Hydration number accounting for protein	$\frac{L}{mol}$
ε	Permittivity	$\frac{F}{m}$
ϵ_b	Particle porosity	-
γ	Activity coefficient	-
θ	Characteristic binding charge	-
Λ	Total ligand density	M
μ_i	Chemical potential	$\frac{J}{mol}$
ν	Stoichiometric coefficient	-
Ψ	Electrostatic potential	V
σ	Shielding factor	-